Functions of the ribose methyltransferase FTSJ1 in regulation of gene expression and neural development

Mira Brazane

Sorbonne Université

École doctorale 515 - Complexité du vivant

Laboratoire de Biologie du développement UMR7622 - Institut de Biologie Paris-Seine

Épigénétique Transgénérationnelle et Biologie des petits ARN

Functions of the ribose methyltransferase FTSJ1 in regulation of gene expression and neural development

---

Thèse de doctorat de Biologie

Par **Mira BRAZANE**

Présentée et soutenue publiquement le 06 octobre 2023

Devant un jury composé de :

Directeur de thèse	
Dr. Clément Carré	Maître de conférences, Sorbonne Université
Président du jury	
Pr. Hubert Becker	Professeur, Sorbonne Université
Rapporteur.ice.s	
Dr. Marc Graille	Directeur de Recherche, Polytechnique
Dr. Francesca Tuorto	Principal investigator - University of Heidelberg
Examinateurs	
Dr. Olivier Namy	Directeur de Recherche, CNRS – Université Paris-Saclay
Pr. Jean-Yves Roignant	Professeur, Université de Lausanne

Acknowledgements

I am grateful for the members of my PhD jury for taking the time to evaluate my work. **Dr. Francesca Tuorto**, **Dr. Marc Graille** for graciously accepting to review my manuscript, **Dr. Olivier Namy**, and **Dr. Jean-Yves Roignant**, for taking part in my jury as examiners, and for your input to the FTSJ1 project. **Pr. Hubert Becker**, thank you for participating in the examination of my PhD, but also for the crucial role you played in my career, when along with Pr. Yannick Andéol to whom I am also grateful, you allowed my admittance to the wonderful RNA Master of Sorbonne Université, and the interest I developed in RNA modifications, and for meeting Dr. Clément Carré, who welcomed me in his lab.

“Thank you” is an understatement for the amount of gratitude I have for you **Clément**. A series of wonderful and difficult adventures led me to your lab, and I was always, and still am convinced I could not have hoped for a better mentor. I am very happy to have learned from you, and worked alongside you for five years, just a blink of an eye! Beyond you opening the way for exciting research, your patience, and kindness definitely helped me reach the finish line, especially at the end when I was too overwhelmed to function. Thanks for being my neuron gardener ;) always teaching me till the end, even when I send you work during weekends, for always trusting and encouraging me, and putting up with me being the worst morning person ever!

Thanks to the members of my thesis committee for their helpful advice and discussions: **Dr. Damien Brégeon**, **Dr. Germano Cecere**, and **Pr. Sébastien Bloyer**. I am grateful to the late **Dr. Hélène Bierne** for being a great supervisor during my M1 internship, and for the support I had while working in her lab. You will not be forgotten.

A big thank you to all of the TerBio lab members, the amazing team that I had the privilege to work with, and to former members, **Dilyana**, **Elise**, **Karine**, **Claudia**, **Ludivine**, **Robin**, **Céline**, **Natacha**, and of course Nai, the former and future member of the lab. Thank you **Céline**, **Natacha**, and **Robin**, the first interns I supervised for the pleasure of working with you, for being dedicated, perseverent, and nice students. Thanks **Laure** and **Stéphane** for your wise advice, and stimulating discussions, and for overall being cool and nice people to be around. **La Boiv’**, thanks for teaching me so much about science, life, and constellations during all these years, for being such a cool and fun person to work with, and talk to. Thank you **Valérie**, and **Bruno**, our great lab engineers, for your support, being it logistic, experimental, or human, your presence made things run smoothly in the lab, and so much fun during the retreat, and all our social gatherings. **Dilyana**, I was lucky to have you as my bench Yoda when I joined the lab, thanks for being a great labmate and friend (pokemon and other :)), and for initiating me in every way to the FTSJ1 project, and I wish you all the best in your career and personal life. **Julie**, thank you for being immensely positive and caring from

day one, for the great movie nights, sharing salads and drinks. I am glad our friendship upgraded from Pokemon GO to real life! (sorry again about that). I have great hope you'll kill it this last year, but still wish you good fortune for the future, professionally and personally. **Zoheir**, Thanks for bringing a touch of art to this unlawful academic world, for being a kind coworker (:P) despite me wondering which day of the week you'll ruin coffee time with another hemicycle debate, I enjoyed dissing you, but also sharing movie nights, and outings in inclined and tilted places. I wish you all the best in your PhD adventure, and for the future. **Hayet**, I had a great time working alongside you, you were always fun and supportive and I wish you a great recovery and a bright future. Thank you to my PhD friends the C5 crew that made my world a better place, **Antoine** (*PhD C5 honoris causa*), **Raphaël**, **Julie**, **Zoheir**, **Hayet**, **Justine**, **Valentine**, **Rémy** and **Cécile** (Also *PhD C5 honoris causa*). You guys definitely made my PhD. For the coffee breaks and movie nights, topoisomerase talks, and overall making the C5 a better place for all of its residents. **Raph**, thanks for being a great qPCR companion and friend. I had a great time working with you, watching movies, cooking bricks, and coriander seasoning. I am grateful to you and **Zoé** for that wonderful hike (never again), and finally, thanks for sharing this wonderful moment with thesis writing! I wish you the bestest to you and Zoé, and for the last time, It wasn't me, I promise! **Juice**, thanks for the great talks with a coffee/tea in hand, I am glad I met you and I'm thankful for your neverending wisdom, *C. elegans* fun facts, and for the bromance we ended up developing ;) **Valoche**, thanks for always being joyful and fun during our coffee time debates on important subjects, also for finding common ground on one word: Boltimbalance!

A big thank you **Julien Pigeon** for your precious help in the immunostainings experiments despite your busy schedule, and for initiating me to NPC culture. Best of luck for the remainder of your PhD. I am grateful to **Dr. Bassem Hassan** for opening his lab to me and contributing to the advancement of our project. Thanks **Chiara Paolantoni** for your immense help with the larvae staining experiments, and to **Dr. Thomas Préat** and his team for the behavior experiments on flies. A big thank you to **Dr. Isabelle Hatin**, **Hugo Arbes**, and **Dr. Olivier Namy** for their strong involvement in the FTSJ1 RiboSeq project, availability for discussion, and active collaboration. Thank you **Fabrice Lejeune, Stéphane Nédélec**, and **Ludovic Tricoire**, for all helpful scientific exchanges, and experimental assistance, and provided materials. To **Dr. Bernard Moss** for providing *FTSJ1* CRISPR-edited cells, and to all collaborators for providing patient-derived cells, especially **Dr. Jozef Gecz**, and **Dr. Amélie Piton**. To all funding agencies that supported my work, especially to the "Fondation pour la Recherche Médicale " for funding my 4th year of PhD. To the Drosophilist teams of the C5, The Gho team, the Peronnet/Gibert team, and the honorary members of the C5, the Rera team. Thanks for being nice, helpful, and overall great people to be around. The positive experience I had alongside you all made me not ever want to leave the world of

model organisms. To **Hélène Thomassin** for being so helpful and kind everytime I come to you with a question. An extended thank you to all the people of the C5 (The Galy team and the Jessus team), I couldn't cite you all by name, but know that I had a great time working and growing alongside you all. Thank you **Enrico** for all the helpful discussions as the expert of protein detection and quantification, but also as a fun colleague. I wish you great personal and professional achievement. Thanks to all the companions of pain during writing: **Ponpon**, **Raph**, **Rémy**, and **Ferdinand**. Thank you to the people of the **UMR7622** for making everything run smoothly, and for all their implication and kindness, especially **Isabelle**, **Hafida**, **Pierre-Yves**, and all the administrative staff, and the laverie staff. Thanks **Laurence** for welcoming me in the cell culture room and for always being helpful. Merci **Viviane** pour ta bienveillance, ta joie de vivre, toutes les plantes offertes au labo, et toute l'aide que tu m'as apportée quand je venais errer au C6, je te souhaite une très belle retraite!

To finish, I am grateful to all my family for their never ending support. To my big sister **Lylia**, where do I start… Well, thanks for always being there since day one, for supporting me through this adventure (and previous ones). It's the end of an era, hopefully one we'll be both happy with! Thanks for always looking out for me and putting up with my messy self, and for always going the extra mile for making things easy for me, I am eternally grateful. To my cousin **Amel**, thanks for being the person that I don't even need to speak to in order to be understood since forever, our interactions made life easier on me. We overcame little and big challenges together through the years, and I'm happy to report, we made it! **Antoine**, huge thank you for supporting me and putting up with the best, but also the worst version of myself (even when I could not put up with her myself), for our crazy trails, brunches, salads, trips, movie sessions, and Pokemon walks were the brightest these last two years, no need to wait for brighter days, these are the best days of our lives, and I am so glad we found each other.

Thank you to all my friends, especially **Nishat** and **Etienne**, **Asma**, **Meriem**, **Ritchy**, and **Liza**. **Nini**, Thanks for the late night coffees that once started on a scorching Madrid evening, I wish you a bright future! **Asma,** thanks for remaining my friend through the years and distance that separates us. I hope to see you again very soon and wish you the best. **Liza**, for being my friend for almost a decade through my best and worst (and yours). You are far but I like to think it will be the same when we meet again, as ridiculous as it can get ;)

Enfin, je dédie ce travail à ma famille, à celle qui est là, loin, ou d'un autre monde, À mes frères **Hamza** et **Idir**, à ma super grande sœur **Sonia**, mes belles-sœurs **Sarah** et **Naima**, mes neveux et nièces **Emma**, **Yanni**, **Ayline** et **Aris**, je vous souhaite le plus brillant des futurs. **À mes grand-mères**, les plus belles et inspirantes personnes que j'ai connu, vous me manquerez toujours. Enfin à **mes parents**, merci de m'avoir toujours poussé à aller plus loin dans mes études, à votre manière et depuis le début, vous aurez toujours cru en moi, même quand moi même j'ai douté, merci pour tout, et je vous souhaite une belle retraite!

Table of contents

Abbreviations

A-site: Ribosomal Aminoacyl site
A: Adenosine
Aars: Aminoacyl-tRNA synthase
ADAR: Adenosine Deaminases Acting on RNAs
Ago: Argonaute
Arg: Arginine
AUB: Aubergine
C: Cytosine
cDNA: Complementary DNA
CDS: Coding DNA sequence
CRISPR: Clustered Regularly Interspaced Short Palindromic Repeats
DNA: Deoxyribo nucleic acid
DNMT2: DNA methyltransferase 2
dNTP: Deoxynucleotide
dsRNA: double-stranded RNA
EDTA: Ethylenediaminetetraacetic acid
Endo-siRNA: Endogenous siRNAs
FTSJ1: FtsJ RNA methyltransferase homolog1
G: Guanine
GAAC: General Amino Acid Control
GAPDH: GlycerAldehyde-3-Phosphate Deshydrogenase
Gln: Glutamine
Glu: Glutamate
Gly: Glycine
GTP: Guanosine triphosphate
hAGO1: Human AGO1
HPLC: High-Performance Liquid Chromatography
ID: Intellectual disability
I : Inosine
IP: Immunoprecipitation
KD: Knock Down
KEOPS: Kinase, putative Endopeptidase and Other Proteins of Small size
LC-MS: Liquid Chromatography coupled to mass spectrometry
LCL: Lymphoblastoid Cell Lines
Leu: Leucine
M^3C: N-3 methylcytosine
M^5C: N-5 methylcytosine
m^6A : N-6 Methyladenosine
m^7G: N-7 methylguanosine
Met: Methionine
miRISC : miRNA-Induced Silencing Complex
miRNA: micro-RNA
Nm: 2'-O-methylation
NSUN2: NOP2/Sun RNA Methyltransferase 2
Nt: Nucleotides
o2yW: Peroxywybutosine
P- Site: Ribosomal Peptidyl site
pAGO: Prokaryotic Argonaute
PAZ: Piwi-Argonaute-Zwille
PBS: Phosphate-Buffered Saline
Phe: Phenylalanine
piRITS: piRNA-Induced Silencing Complex
piRITS: piRNA-Induced Transcriptional Silencing
piRNA: Piwi interacting RNA
Piwi: P-Element Induced Wimpy Testis
pre-tRNA: precursor tRNA

PTGS: Post Transcriptional Gene Silencing
qPCR: Quantitative Polymerase Chain Reaction
RIP: RNA Immunoprecipitation
RISC: RNA Induced Silencing Complex.
RLC: RISC Loading Complex
RNA : Ribo nucleic Acid
RNAi: RNA interference
rRNA: Ribosomal RNA
RT: Reverse transcription
S2 : Schneider 2 cells
SAM: S-AdenosylMethionine
SDS: Sodium Dodecyl Sulfate
Sec: Selenocysteine
siRISC: siRNA-Induced Silencing Complex
siRNA: Small interfering RNA
SNORDs: Box C/D snoRNAs
snoRNA: small Nucleolar RNA
snRNA: small Nuclear RNA
t6A: N-threonylcarbamoyladenosine
TGS: Transcriptional Gene Silencing
tRFs: tRNA derived fragments
Trm7: tRNA methyltransferase 7
tRNA: transfert RNA
tRNAse Z: tRNA endoribonuclease
Trp: Tryptophan
tSEN: tRNA splicing endonuclease
U: Uracil
UPLC: Ultra-Performance Liquid Chromatography
UTR: untranslated region
Val: Valine
WAGO: Worm Argonaute
WT: Wild type
XLID: X-linked intellectual disability
Yw: Wybutosine

Abstract

RNAs of all the domains of life carry chemical modifications. Extensive studies over the last decades linked the loss of RNA modification enzymes to several pathologies, notably, ones related to the nervous system. During my PhD, I contributed to the understanding of the functions of FTSJ1, a Trm7 family enzyme responsible for tRNA ribose methylation of two nucleotides of the anticodon loop including the *Wobble* (34th) position. *FTSJ1* loss of function causes intellectual disability, however, the mechanisms underlying this condition remain elusive. My colleagues previously identified the orthologs of *FTSJ1* in *Drosophila* as regulators of RNA interference pathways. During my PhD, I contributed to the characterization of a new *FTSJ1* pathological variant, and to the study of transcriptomes of patient derived lymphocytes. I also identified morphological defects associated with the loss of FTSJ1 in cultured human immature neurons. Similarly, the *Drosophila* model lacking the orthologs of *FTSJ1* exhibits similar morphological defects in the neuromuscular junctions. Cognitive assessments exhibited drastically reduced long-term memory in all mutant combinations. Given the primary function of tRNAs in translation, I lastly conducted a transcriptome wide profiling of ribosome footprints on patient derived cell lines, together with an RNAseq analysis. A gene ontology analysis revealed a number of deregulated genes at the translational level, primarily involved in vocal and imitative learning. Overall, these results show a substantial regulation of brain morphogenesis genes attributed to FTSJ1, as well as morphological defects altering cultured neural cells, but also in the *Drosophila* model lacking FTSJ1. As a perspective, exploitation of new ribosome profiling datasets, with an emphasis on codon specific signatures on translation efficiency by tRNA substrates of FTSJ1 could lead to a better understanding of the mechanisms underlying FTSJ1-related intellectual disability.

French Abstract

Dans tous les domaines du vivant, la majorité des ARN de toutes les catégories sont chimiquement modifiés. De nombreuses études au cours des dernières décennies ont permis de montrer que la perte des enzymes de modification des ARN sont à l'origine de nombreuses pathologies, notamment liées au système nerveux. Au cours de ma thèse, j'ai contribué à la compréhension des fonctions de FTSJ1, une enzyme de la famille Trm7 responsable de la 2'-O-méthylation des ARNt sur deux nucléotides de la boucle anticodon dont le *Wobble* (nucléotide 34). La perte de fonction de *FTSJ1* est à l'origine d'une déficience intellectuelle, cependant, les mécanismes moléculaires sous-jacents restent incompris. Mes collègues de laboratoire ont précédemment identifié les orthologues de *FTSJ1* chez la drosophile comme régulateurs des voies d'ARN interférence. Au cours de ma thèse, j'ai contribué à la caractérisation d'un nouveau variant pathologique de *FTSJ1* et à l'étude des transcriptomes de lymphocytes dérivés de patients atteints de déficience intellectuelle. J'ai également identifié des défauts morphologiques associés à l'inhibition de FTSJ1 dans des neurones immatures humains en culture. De même, le modèle drosophile dépourvu des orthologues de *FTSJ1* présente des défauts morphologiques similaires au niveau des jonctions neuromusculaires. Des évaluations cognitives ont montré une réduction drastique de la mémoire à long terme chez tous les mutants. Étant donné la fonction principale des ARNt dans la traduction, j'ai enfin réalisé un ribosome *profiling* sur les lignées cellulaires dérivées de patients, ainsi qu'une analyse RNAseq. Une analyse de *gene ontology* a révélé un nombre de gènes dérégulés au niveau traductionnel, principalement impliqués dans l'apprentissage vocal et imitatif. Dans l'ensemble, ces résultats montrent une régulation des gènes de la morphogenèse cérébrale attribués à FTSJ1, ainsi que des défauts morphologiques altérant les cellules neuronales en culture, mais aussi dans le modèle de drosophile muté dans *FTSJ1*. En perspective, il serait utile d'exploiter ces nouveaux jeux de données de ribosome *profiling* chez l'homme et la drosophile, en mettant l'accent sur les codons dépendant des substrats de FTSJ1, et sur l'efficacité de leur traduction. Ces résultats pourraient conduire à une meilleure compréhension des mécanismes à l'origine de la déficience intellectuelle liée à FTSJ1.

Introduction

1- Preface

The central dogma of molecular biology lectured by Francis Crick in 1957 states that there's a single direction for gene expression with DNA as the blueprint, messenger RNA (mRNA) as a disposable copy, and protein is the final gene product (Cobb 2017). Several studies would soon come to challenge this view with ground breaking discoveries like the existence of reverse transcriptase. Decades later during the genomic era, complex eukaryotic genomes, including the human, were found to contain a minor fraction of protein-coding genes and an overwhelming majority of non-coding genes, that is nonetheless transcribed (Green, Watson, and Collins 2015). These findings opened new fields of studies for annotation and functional characterization of these non-protein coding genes and their transcripts, that are often referred to as "junk", or simple products of pervasive transcription. The notion of RNA gene arose, although many of them have been known for a long time, including ribosomal RNA (rRNA), transfer RNA (tRNA) which constitute a vast majority of total RNAs in a cell and essential factors for protein synthesis.

Throughout evolution, several mechanisms for gene expression regulation have been selected and maintained in order to ensure correct development, differentiation and overall function. At the transcriptional level, distal transcription enhancers and repressors control transcription initiation. In this regard, the vast world of epigenetic regulation through DNA and chromatin modifications plays an important role in fine tuning of gene regulation, but remain nonetheless permissive to environmentally-induced epigenetic regulation, that is both crucial for adaptation, but also powerful motor for evolution, especially in complex organisms, with no or little recourse to sequence alteration (Peixoto et al. 2020).

Gene dysregulations are often found to alter organism biology, and cause different alterations and disease. The need to study gene functions and regulation and necessity for new approaches led to the discovery of conserved small regulatory

RNA pathways in almost all eukaryotes, an elegant system not only used for endogenous gene regulation, but also as a unique immune system for protection against invasive nucleic acids (Agrawal et al. 2003).

The epigenome recapitulates the post-translational Histone modifications and DNA modifications that alter chromatin topology. This ensemble is now referred to as the, conditioning the maintenance and protection of the blueprint, but also making it “non-static” and modelable by the environment for the sake of evolution and adaptation. By analogy, the epitranscriptome represents an expanding field of post-transcriptional RNA modifications. Since the discovery of Pseudouridine over 60 years ago, functions for RNA modifications have raised a lot of questions, but limited knowledge has been gained as to the “writer” enzymes, despite the discovery of many novel modifications. A crucial need for new efficient detection and mapping methods, lacked until the mid 1990s where the development of new sequencing techniques, and rapid mutagenesis tools allowed a considerable leap in understanding of RNA modification biology (Summarized by *(Grosjean 2015)*).

With functions spanning from stability to fine tuning of translation, RNA modifications are involved in various physiological functions, and are often found associated with human pathologies in a poorly understood manner, especially in cancer, and neurological disorders. Epitranscriptomic studies also led to interesting observations regarding modified residues’ functions in RNA stability and self *Vs* non-self distinction, which allowed, for instance, the development of efficient RNA vaccines (Polack et al. 2020).

My PhD project was positioned at the interface of gene regulatory functions of RNA modifications in disease context, and involvement of small RNA-mediated silencing in *Drosophila*, then in human cells.

2 - RNA interference: Regulatory systems of RNA, by RNA, and for RNA

RNA interference (RNAi) is a small RNA based system that allows sequence specific regulation of a complementary target. RNAi was gradually discovered from the 1980s to the 1990s, where it was first observed that the introduction of sense and antisense transcripts led to the silencing of the endogenous complementary mRNAs (Izant and Weintraub 1984; Nellen and Lichtenstein 1993; Fire et al. 1991). This phenomenon had been widely observed in plants (van der Krol et al. 1990; Napoli, Lemieux, and Jorgensen 1990), and in the worm *Caenorhabditis elegans* (Fire et al. 1991). At the time, RNAi was used as a tool to perform genetic knockdowns before the involved machinery was even understood or characterized. Further investigation showed that injection of double stranded RNAs (dsRNAs) encoding a given gene would phenocopy a mutant for the considered gene, as well as demonstrate the sequence specific character of this process known as Post Transcriptional Gene Silencing (PTGS) *(Fire et al. 1998)*. Until the discovery of small RNAs as major components of PTGS (Hamilton and Baulcombe 1999) studies of RNAi were quickly expanded to other species. In fact, it was discovered that dsRNAs in flies were processed into 20 to 23 nt small RNAs (Zamore et al. 2000), leading to the progressive uncovering of the proteins involved in these processes (Zamore et al. 2000; Tabara et al. 1999). These discoveries unveiled a tremendous layer of gene expression regulation that was unknown. RNAi later arose as a potent negative regulator of gene expression, selfish nucleic acids, or exogenous elements like viruses and parasites. Small non-coding RNA pathways are remarkably conserved in the majority of eukaryotes including a few yeast species, *Protozoa*, plants, arthropods and vertebrates (Kennerdell and Carthew 1998; Torri et al. 2022). RNAi is a eukaryote specific system but many effectors of these pathways can be found in *Protozoa* and play an important role in RNA independent gene regulation and genome defense (Zaremba et al. 2022; Koopal, Mutte, and Swarts 2023).

Small RNA regulation naturally occurs at a transcriptional gene silencing level (TGS) but also at a post transcriptional gene silencing level (PTGS). It can target protein coding transcripts, but also mobile genetic elements, or non-coding RNAs. For instance, silencing of retrotransposons and other mobile elements is mediated by small RNAs in the *Drosophila* germline (Aravin et al. 2001; Saito et al. 2006).

The common features of small non-coding RNA pathways

2A- Small non-coding RNAs

Small RNAs spanning from 20-30 nucleotides serve as guides for the specificity of silencing with partial or complete sequence complementarity with the target to regulate (Reviewed by (Ghildiyal and Zamore 2009)). Small RNA-mediated silencing requires the action of different catalytic components for their biogenesis, export and silencing activity. The most conserved proteins of these pathways are Argonaute proteins (AGO) that directly bind small RNAs and repress gene expression, and Dicer proteins which are involved in the biogenesis and loading of small RNAs in the effector AGO protein thus forming a complex called the RNA Induced Silencing Complex (RISC) (Ghildiyal and Zamore 2009; Pratt and MacRae 2009).

Following the genomic era and the development of high throughput sequencing techniques, different sources of endogenous small non-coding RNAs were described (Reviewed by (X. Chen 2010)). Based on the genetic origin of small RNAs, their biogenesis, and the RISC components involved in the silencing they mediate, small regulatory RNAs were separated into three distinct classes: the microRNAs (miRNA), small interfering RNAs (siRNA) and Piwi-interacting RNAs (piRNA) (Reviewed in (Ghildiyal and Zamore 2009)). These regulatory pathways differ in small RNA biogenesis and AGO preferential loading, but a few features are very common in most metazoans which are the RISC activity and the silencing mechanisms (TGS and PTGS).

2B- Argonaute proteins

The first discovered gene of the Argonaute family was AGO1 in *Arabidopsis Thaliana*, whose loss of function led to misshapen leaves reminiscent of the shape of an octopus of the *Argonauta* genus (Bohmert et al. 1998). Retrospectively, this was one of the first clues of small RNAs as key regulators during development, which was also observed in *C. elegans* whose developmental stages are punctuated by miRNAs *lin-4* and *Let-7* (R. C. Lee, Feinbaum, and Ambros 1993; Reinhart et al. 2000; Ambros 2000).

AGOs are the main effectors of small non-coding RNA pathways in eukaryotes. They represent the active, and sometimes, catalytic component of the RISC, which directly binds small RNAs (Hutvagner and Simard 2008). Argonautes are highly conserved in eukaryotes with homologs from unicellular species to vertebrates. AGOs are also found in Prokaryotes (pAGOs). Despite the absence of RNA interference systems in this domain, pAGOs rather serve functions in DNA-mediated DNA silencing (Also called DNA interference) and genome stability (Makarova et al. 2009; Swarts, Jore, et al. 2014; Kuzmenko et al. 2020). In ciliates, AGO proteins are involved in DNA elimination with a Piwi-like pathway during somatic genome rearrangements (Chalker and Yao 2011).

Functional domains of Argonaute proteins

Argonaute proteins possess four highly conserved domains with varying degrees of homology: The N domain (N-terminal), the PAZ domain (Piwi-Argonaute-Zwille), the MID domain (middle), and the PIWI domain (Figure 1) (Willkomm et al. 2015).

Prokaryotic AGOs are divided into two categories based on the presence or absence of a PAZ domain, with PAZ-less AGOs no longer carrying nuclease activity (Makarova et al. 2009). Eukaryotic AGOs are divided into four main subfamilies

based on domain architecture: The AGO subfamily, the PIWI-like subfamily, WAGO (Worm Argonautes), and Trypanosoma subfamily (Swarts, Makarova, et al. 2014).

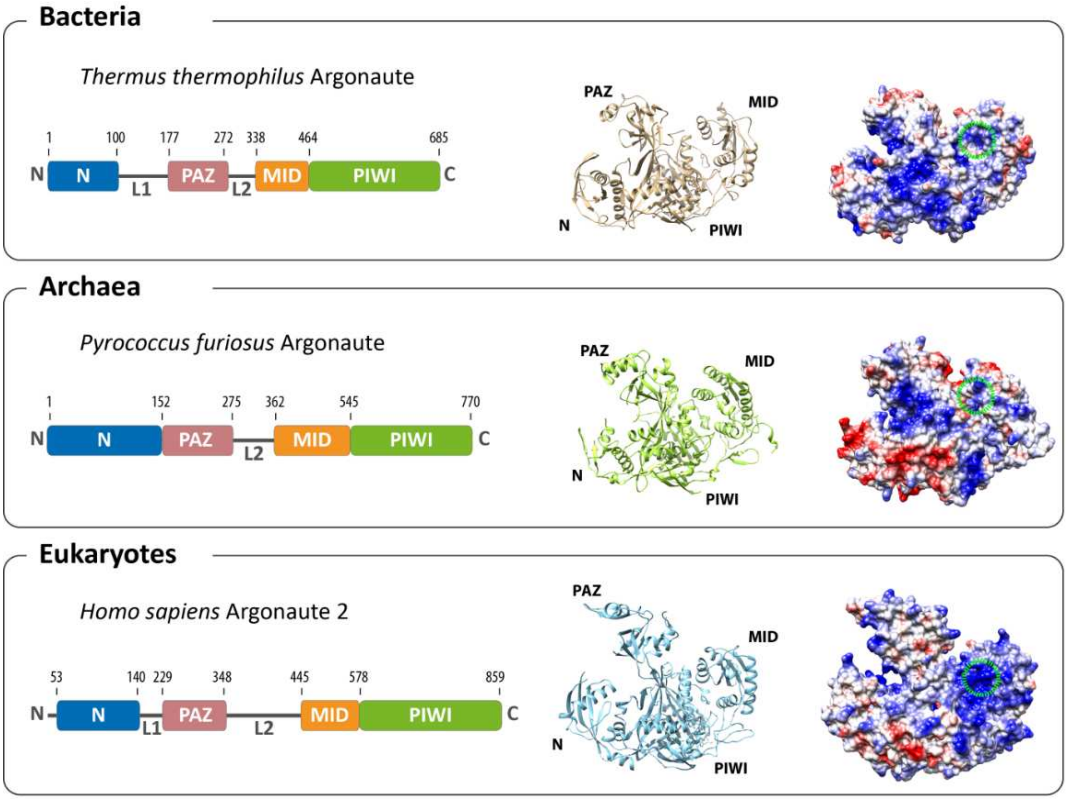

Figure 1. Structure and functional domains of Argonaute proteins from the three domains of life. The different AGO domains for each example of species of the three taxons reveal high conservation of AGO functional domains. Example of Bacterial AGO is based on *Thermus thermophilus*, the archaeal AGO is based on *Pyrococcus furiosus*, and the eukaryotic AGO is based on human Argonaute 2. Positive charges are depicted in blue, and negative ones in red. The positively-charged binding pocket in the MID domain for the 5'-end of the small RNA is indicated in green (Adapted from (Willkomm et al. 2015)).

One fundamental intrinsic difference between the AGO subfamily and the Piwi subfamily is their capacity to bind small RNA duplexes or single stranded small RNAs respectively (Cenik and Zamore 2011). However, all AGOs use small RNAs as guides to target a completely or partially complementary target RNA, with few notable examples, like siRNA-directed DNA methylation in plants (M. Xie and Yu 2015). The RNA silencing is mediated by target cleavage, or inhibition of its translation (PTGS) or epigenetic regulation like chromatin modifications and DNA methylation.

Slicer Argonautes: the example of *Drosophila* AGO2

The AGO subfamily in *Drosophila* consists of AGO1 and AGO2 involved mainly but not exclusively in the miRNA and siRNA pathways respectively (Refer to mi- and siRNA sub-chapters in page 27) (Okamura et al. 2004; Förstemann et al. 2007). In order for the small RNA to be loaded in the AGO protein a RISC Loading complex (RLC) is required, and is different depending on intrinsic properties of the small RNA (Refer to pathways chapter below). The RISC loading complex of the siRNA pathway is composed of R2D2 and DCR2. The latter is also required for the biogenesis of the siRNA through processing of dsRNA precursors (see siRNA pathway below) (Figure 3) (X. Liu et al. 2006). Studies of the human AGO2 showed that the PIWI domain and the MID domain serve as anchors to accommodate the less thermodynamically stable 5' end of the RNA duplex, while the 3' end is positioned in the PAZ domain (Elkayam et al. 2012; Schirle and MacRae 2012). The accommodated single strand is called the guide strand, that will mediate sequence specific silencing. The PIWI domain of AGO2 first exerts its endonuclease activity to cleave the passenger strand, releasing, and therefore allowing RISC activation. Target binding is made possible by the N domain necessary for target cleavage by correctly positioning the small RNA and target (Elkayam et al. 2012).

Many metazoans Argonautes lost the endonucleolytic activity, even with retained catalytic tetrad (Table 1) (Höck and Meister 2008). The catalytic tetrad (DEDH/D) allows the formation of the RNAse H-like fold necessary for the endonuclease activity of AGOs. However, the PIWI domain is retained in non-slicer AGOs and remain central to the repressive functions of miRISCs as it permits interactions with the Glycine Tryptophan repeats of the GW182 anchor protein responsible for the recruitment of canonical RNA decay machineries (Behm-Ansmant et al. 2006; J. E. Braun et al. 2011). Human AGO2 is the only member of the human Argonaute subfamily to retain its slicer activity (Meister et al. 2004; J. Liu et al. 2004).

Drosophila melanogaster encodes five AGO proteins, two of whom part of the AGO-like subfamily and are ubiquitously expressed, while the three others are part of the Piwi subfamily bind piRNAs and are mostly expressed in the germline to protect from transposition of mobile elements (Saito et al. 2006; Vagin et al. 2006). Ubiquitous *Drosophila* AGOs are AGO1 and AGO2, and germline AGOs are PIWI, AUBERGINE (AUB) and Argonaute 3 (AGO3). The human genome encodes four AGO subfamily proteins and four Piwi subfamily proteins. Human AGO subfamily consists of AGO1, AGO2, AGO3 and AGO4, which bind miRNAs and siRNAs similarly to *Drosophila* somatic (or rather ubiquitous) AGOs (Nakanishi 2022). Human Piwi subfamily comprises HIWI (or PIWIL1), HILI (or PIWIL2), HIWI3 (or PIWIL3) and HIWI2 (or PIWIL4) (Peters and Meister 2007; Ender and Meister 2010). *Drosophila* AGO1, mainly involved in the miRNA pathway, shows high levels of sequence identity with the four human ubiquitous AGOs, consistently with their common functions in miRNA binding and silencing through translation inhibition (J. E. Braun et al. 2011). The highest levels of homology are exhibited by mice and human Argonautes (Figure 2).

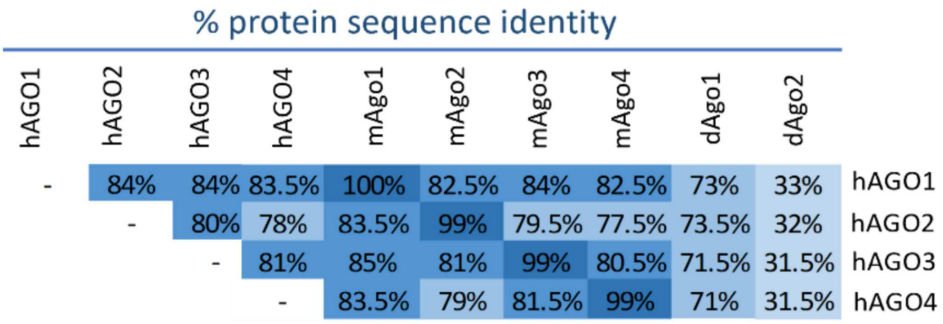

Figure 2. Sequence homology between AGO orthologs. Percentages of protein sequence identity between human AGO (hAGO), mouse Ago (mAgo) and *Drosophila* Ago (dAgo) are depicted above (Source: *pAgoDE* ANR #2023 project, A. Piton- *Personal communication*).

Silencing activity

Two levels of silencing are performed after RISC assembly: TGS and PTGS. At the transcriptional level, the RISC complex translocates to the nucleus. A known example is the pi-RNA Induced Transcriptional Silencing (piRITS) complexes carrying piRNAs targeting in most cases euchromatic copies of transposable elements in *Drosophila* germline (Saito et al. 2006; Aravin et al. 2001; Brennecke et al. 2007). A piRITS complex is guided by a piRNA to the euchromatic copy with sequence complementarity and recruit a dedicated heterochromatinization machinery at the vicinity of the nascent RNA (Komarov et al. 2020). In contrast, PTGS targets transcripts for AGO-mediated endonucleolytic cleavage or translation inhibition. PTGS choice between the degradation or inhibition is defined by the effector AGO protein, however, small RNAs are not randomly assigned to any AGO protein. In fact, the choice of an AGO protein is highly dependant on the self complementarity level of the small RNA duplex, as well as the RISC Loading complex involved (Förstemann et al. 2007; Tomari, Du, and Zamore 2007) (Figure 3 - Refer to mi- siRNA pathways below).

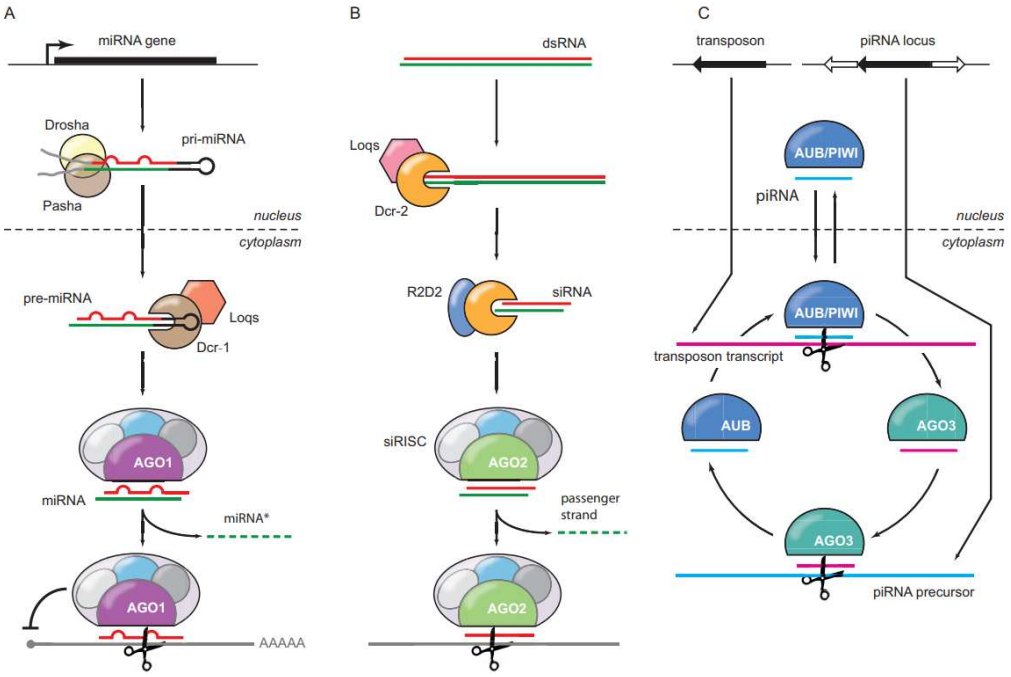

Figure 3. Small RNA pathways in *Drosophila*. (A) miRNAs originate from Primary miRNA (pri- miRNA) transcripts of genomic origin (miRNA genes, introns (mirtrons) or dedicated loci). pri-miRNAs are processed in the nucleus by Drosha/Pasha complex and later exported to the cytoplasm as pre-miRNAs. Dcr-1 and loquacious (loqs) further cleave the precursor to produce a mature miRNA, and load the duplex into AGO1 forming a miRISC. The * strand (or passenger) is excluded, and the guide strand base pairs to the target to ensure translational repression or endonucleolytic cleavage. **(B)** The siRNA pathway involves processing of long dsRNAs (from exogenous or endogenous or genomic origin) into siRNAs by Dcr-2 and R2D2. The siRNA duplex of 21 nucleotides is loaded by Dcr-2 and R2D2 into AGO2 resulting in a siRISC. The passenger strand is cleaved by AGO2, and remaining siRNA guides AGO2-mediated endonucleolytic cleavage. **(C)** The piRNA pathway is mediated by maternally inherited piRNAs originating from dedicated piRNA clusters. piRNA precursors are processed into 23-29 nucleotides primary piRNAs. An amplification loop ensures production of secondary piRNAs involving sense and antisense RNAs, as well as the germline specific Argonautes AGO3 and AUB. Mature piRNAs carry out gene silencing at the transcriptional level with chromatin modifications, and post transcriptional gene silencing through target cleavage. Adapted from (Vodovar and Saleh 2012)).

Small non-coding RNA pathways in *Drosophila*

A- microRNAs (miRNAs):

miRNAs originate from different genomic regions including dedicated miRNA loci (Y. Lee et al. 2002; Lagos-Quintana et al. 2003), and intronic regions of protein coding genes (Rodriguez et al. 2004; Bhaskaran and Mohan 2014).

A primary miRNA (pri-miRNA) reaching several Kilobases-long is transcribed from the genomic locus by RNA Polymerase II and undergoes two successive processing steps in the nucleus and later in the cytoplasm (Denli et al. 2004). Pri-miRNAs fold into a stem-loop secondary structure with a 33 nt self complementary stretch and two single stranded unstructured regions (Figure 3) (Vodovar and Saleh 2012). The pri-miRNA is recognized by the Microprocessor complex composed of DROSHA and PASHA (in flies, DGCR8 in humans) in the nucleus and a first cleavage is introduced close to the stem through the RNase III activity of DROSHA in the nucleus resulting in a premature (pre-) miRNA (Y. Lee et al. 2003; Denli et al. 2004). A second cleavage by DICER RNAse III family enzyme (Dicer 1 in flies) occurs after export of the pre-miRNA to the cytoplasm by EXPORTIN-5 (Yi et al. 2003). There is an alternative biogenesis pathway that is DROSHA-independent when miRNAs are generated from spliced out introns called Mirtrons, which mimic the structure of pre-miRNAs (Ruby, Jan, and Bartel 2007).

After cytoplasmic export, the pre-miRNA is processed by DICER-1 (Dcr-1) and LOQUACIOUS (Loqs) into a 22 nt miRNA duplex through DICER's Ribonuclease III activity (Hutvágner et al. 2001; Ketting et al. 2001). In *Drosophila*, Dcr-1 is responsible for generating mature miRNAs from pre-miRNA. Dcr-1 is part of the RISC Loading complex that is responsible for the loading of the miRNA into AGO1 or AGO2, thus forming the miRISC. The RISC is active when the passenger strand (for miRNA called star: *) is excluded and the mature guide miRNA is available to base

pair with the target mRNA. miRNAs are able to bind their target despite incomplete complementarity, provided that the 5' end of the miRNA (nucleotides 2-8) called "seed" is highly complementary to the target mRNA (Lewis et al. 2003; Brennecke et al. 2005), thus making it still today difficult to predict miRNA targets.

To achieve PTGS in metazoans, miRISC containing miRNAs with very high or perfect target complementarity induce target cleavage through the ribonuclease activity of AGO2 (Förstemann et al. 2007). Whereas miRNAs with partial target complementarity loaded in AGO1 induce mRNA destabilization by interacting with GW182 to recruit canonical deadenylation and/or decapping enzymes leading to mRNA decay or storage in p bodies (J. E. Braun et al. 2011; Rehwinkel et al. 2005; Tat et al. 2016). A few PTGS strategies are depicted in Figure 4 below.

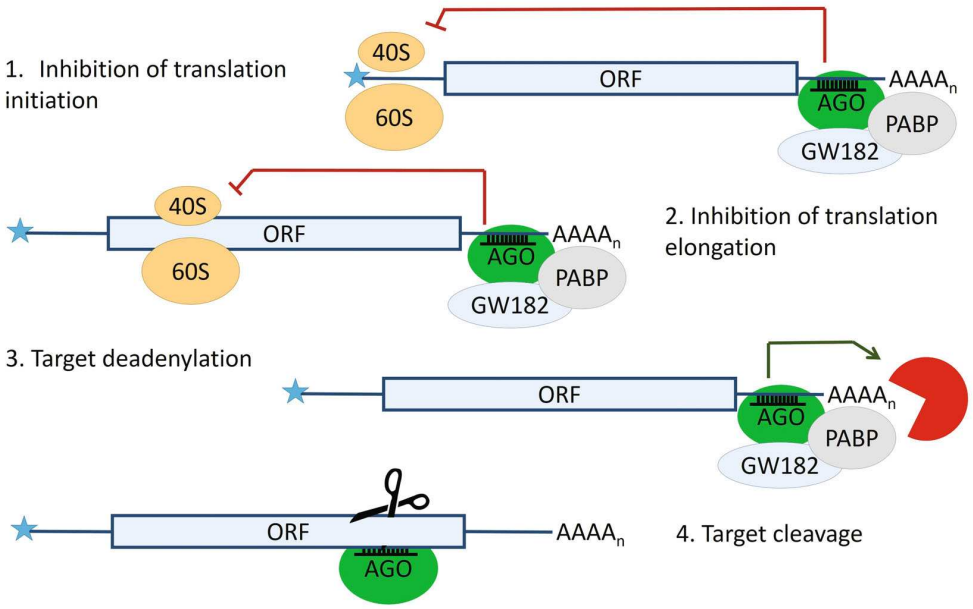

Figure 4. Post transcriptional gene silencing by miRISC. (1) Translation initiation blocking through recruitment of GW182 by the miRISC **(2)** Translation Elongation inhibition through miRISC GW182 binding **(3)** mRNA deadenylation **(4)** mRNA endonucleolytic cleavage. (Adapted from (Olina et al. 2018)).

B- Small interfering RNAs (siRNAs) pathway

The siRNA pathway was originally termed as the canonical RNAi pathway (as described by Fire et al in 1998), thus a pathway activated by the presence of long dsRNAs that induce PTGS. As opposed to miRNAs, siRNAs originate from long dsRNAs of both endogenous (endo-siRNAs) and exogenous origin (exo-siRNAs). In *Drosophila*, endosiRNAs are a product of dual strand transcription from different genomic regions like certain protein coding genes, or retrotransposons (Czech et al. 2008; Ghildiyal et al. 2008). Exo-siRNAs on the other hand are processed from infectious RNA viruses. Long dsRNAs are processed into duplexes of siRNAs of 21 nucleotides by the ribonuclease III activity of DICER2 (Dcr-2) (Bernstein et al. 2001; Elbashir, Lendeckel, and Tuschl 2001). When loaded in AGO proteins, *Drosophila* siRNAs, same as piRNAs, undergo a post transcriptional ribose methylation deposited by HEN1 (also called piMet) on the 3' end, which prevents polyuridylation guided exonucleolytic degradation (Horwich et al. 2007).

The si-RISC loading complex composed of Dcr-2 and R2D2 is responsible for loading of the siRNA duplex in AGO2 (X. Liu et al. 2006), which first, exerts its ribonuclease activity to cleave the passenger strand (Matranga et al. 2005; Preall and Sontheimer 2005). The release of the passenger strand induces the preRISC activation and allows base pairing of the guide strand to the target RNA to induce endonucleolytic cleavage through AGO2's nuclease activity (Zamore et al. 2000; Okamura et al. 2004; Förstemann et al. 2007).

Either by regulating endogenous mobile elements in *Drosophila* somatic tissues, or exogenous viral infections, the siRNA pathway is the main immune system in arthropods and plants that do not possess a vertebrate's innate immune system. It was long thought that siRNA pathways were absent in mammals, thus replaced by an elaborate system based on interferon responses that is sensitive to the presence of dsRNAs, despite the presence of the whole machinery of the siRNA pathway.

Surprisingly, a study showed that mouse cells infected with encephalomyocarditis virus accumulate cognate siRNAs. These small RNAs are Dicer dependent, and are able to bind AGO2 (Maillard et al. 2013). Supporting these findings, a novel Dicer isoform called *AviD* (Antiviral DICER) was described in mice and humans, and directs sequence-specific cleavage of viral RNAs (Zika virus and SARS-Cov-2) thus protecting tissue stem cells from viruses (Poirier et al. 2021). These results support the existence of antiviral RNAi in mammals.

C- Piwi interacting RNAs (piRNAs)

Piwi interacting RNAs are, namely, a category of small RNAs specifically loaded in the Piwi subfamily of Argonaute proteins. In *Drosophila*, piRNAs originate from specific loci called piRNA clusters and are maternally inherited (Brennecke et al. 2007). Despite the heterochromatic nature of piRNA clusters, they are nonetheless transcribed in the germline using a specific machinery involving the Rhino, Deadlock and Cutoff complex (Mohn et al. 2014). piRNA precursors are then exported to the cytoplasm through the intervention of several export factors including Nxf2-Nxt1, as part of the SFiNX complex (Batki et al. 2019). piRNA precursors are processed as single strands by the endoribonuclease activity of ZUCCHINI (Nishimasu et al. 2012) to produce what is called primary piRNAs.

In the *Drosophila* germline: dual strand piRNA clusters produce primary piRNAs that undergo a feed forward amplification loop called the Ping-Pong cycle, in order to allow efficient and sustainable silencing of detrimental genetic mobile elements. Secondary piRNAs are processed by AUB using complementary piRNA precursors, as well as target transposable element transcripts to feed the amplification cycle (Figure 5). The amplification step is crucial for the maintenance of transposable element silencing for germline preservation, but also for sustainability of the silencing to the next generation through maternal inheritance of piRNAs (de Vanssay et al. 2012; Fabry et al. 2021).

Other organisms like worms use alternative amplification mechanisms based on RNA Dependent RNA Polymerases (Smardon et al. 2000).

In ovarian somatic cells: *Drosophila* ovarian chambers are surrounded by a layer of follicular cells of somatic nature. Ovarian follicular cells use a somatic piRNA pathway to regulate retrotransposons. For instance the *Gypsy* retro element is regulated by the *Flamenco* piRNA cluster (Sarot et al. 2004).

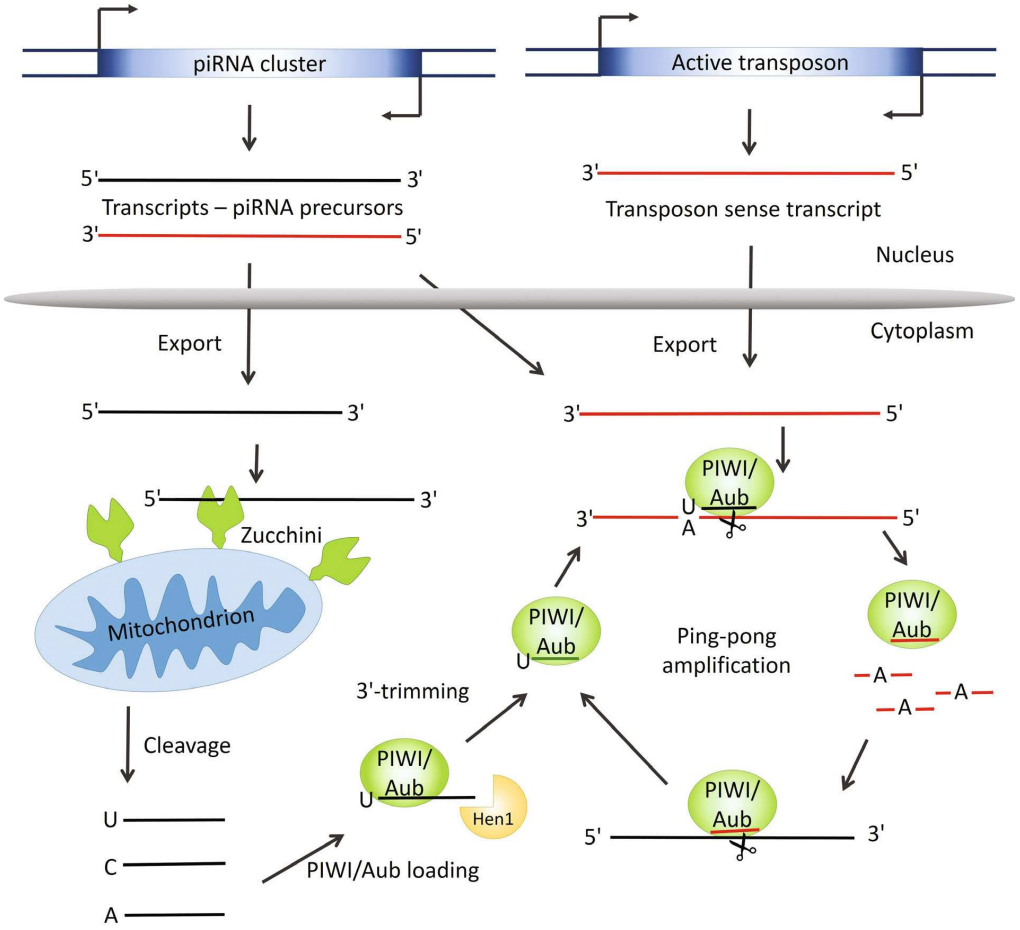

Figure 5. Ping-pong amplification loop in the *Drosophila* germline. piRNA precursors originating from piRNA clusters are processed by Zuc at the mitochondrial surface. Aubergine is loaded with a piRNA that guides towards complementary transposable elements or mRNAs or primary piRNA precursors transcribed from the opposite strand of the same piRNA cluster. This cleavage results in a secondary piRNA that is subsequently loaded in Ago3 and in turn can induce cleavage of antisense precursors or TE transcripts, thus feeding the cycle. (Adapted from (Olina et al. 2018)).

PiRNAs carry out gene regulatory functions at two possible levels. At the post transcriptional level, piRNAs form a piRISC complex in association with an Argonaute

of the Piwi subfamily to target complementary transcripts of transposable elements. piRNAs can also mediate transcriptional gene silencing (TGS) in the nucleus. PiRITS complexes containing PIWI are translocated to the nucleus. The loaded PIWI protein is guided to a target nascent transcript to recruit heterochromatinization factors, such as HP1 (Heterochromatin Protein 1), at the active transposable element locus (Brennecke et al. 2007; Batki et al. 2019; Casier et al. 2023).

Interconnexions of small non-coding RNA pathways

These pathways are found to interact with one another rather than being separate networks. For example, it is found in *Drosophila* that miRNAs (processed by Dicer 1) can be loaded into AGO2, a component of the siRNA pathway, thus inducing target cleavage (Förstemann et al. 2007; Tomari, Du, and Zamore 2007). Another notable example is an interesting entanglement of the si- and piRNA pathways in *Drosophila* germline, potentially leading to initiation of piRNA production in the offspring through maternally inherited siRNAs (Y. Luo et al. 2022).

Context leading to PhD project

During my PhD, I had the opportunity to learn about RNA interference in *Drosophila melanogaster*, a powerful model organism where these pathways were extensively studied since the early days of RNAi discoveries. Before I joined the lab as a Master student, and later as a PhD student, my supervisor, Dr. Clément Carré and his team at the time (*Drosophila* Genetics and Epigenetics team led by Dr. Christophe Antoniewski) conducted a transcriptome wide RNAi screen in order to identify regulators of the small non-coding RNA pathways in the *Drosophila* model using the previously described *automiG* sensor (Carré et al. 2013). This screen would soon link RNA interference to a whole new layer of gene regulation through RNA chemical modifications, a field that is already known in small RNA biology as *Drosophila* piRNAs and siRNAs carry a 3’ terminal ribose methylation (Nm). Unbeknownst to us,

a gene uncovered in this screen would be found to alter another category of small non-coding RNAs, transfer RNAs, and would open a new field of investigation in the lab, new models, as well as implications in human disease.

3- The tRNA biology and modifications

The Epitranscriptome

Most classes of RNAs were found to carry different nucleotide derivatives since the discovery of Pseudouridine (ψ) in the 1950s (Cohn and Volkin 1951; Davis and Allen 1957). RNAs undergo post transcriptional chemical modifications catalyzed by genetically encoded RNA modifying enzymes on different ribonucleotide components, but most of them are carried by the nitrogen base (Boccaletto et al. 2022). Extensive studies over the last two decades widened the scope of known RNA modifications to over 170 different RNA modifications described and indexed in the modomics database as of today (Boccaletto et al. 2022). Despite the description of abundant RNA modification a long time ago, most synthesis pathways remained poorly understood, for a long time until the first genomes were sequenced, and novel technologies provided tremendous mutagenesis tools to study RNA modifying enzymes (Grosjean 2015).

From simple methyl groups to complex chemical residues requiring multiple enzymes and metabolic pathways for their addition, RNA modifications diversify the chemical properties of RNA molecules beyond the capabilities of the four canonical ribonucleotides (Ontiveros, Stoute, and Liu 2019; Boccaletto et al. 2022).

RNA modifications are highly responsive to environmental stress, similarly to epigenetic modifications altering chromatin and DNA, RNA modifications are permissive to epigenetic changes. A nice example of environmentally modelable RNA modification is Queuosine, a tRNA wobble modification, requiring queuine, which cannot be synthesized by eukaryotic organisms, making it only available through nutrient supply or microbiota (Farkas 1980; Reyniers et al. 1981). The versatility, universality and dynamics of RNA modifications and their different functions is now referred to as the epitranscriptome.

It is noteworthy to evoke the difficulties faced in the field of epitranscriptomics regarding the accurate mapping of RNA modifications, as well as the assignment of enzymes to each modification. A crucial task when dealing with disease related RNA modifications. In fact, one of the biggest challenges in the field is to identify and characterize the function of each modification, as impairments in these pathways are often linked to neurological disorders and cancers (Dimitrova, Teysset, and Carré 2019; Angelova et al. 2018; Suzuki 2021).

RNA modifications are deposited co-or post transcriptionally. For instance, rRNA modification machinery is located in the nucleolus, and proceeds to the deposition of modified residues before cytoplasmic export and maturation (Sloan et al. 2017). Nucleotide derivatives determine the chemical properties and structural conformations at the basis of RNA function, but some modifications evolved to act as part of complex pathways necessitating reader proteins in order to carry out their functions similarly to some epigenetic marks, making their functions dynamic and dependant on writer and eraser enzymes. It is the case of N-6-Methyladenosine (m^6A) and N-3-methylcytosine (m^3C) with diverse functions depending on their localization and RNA class (Hailing Shi, Wei, and He 2019; Ontiveros, Stoute, and Liu 2019). Some RNA modifications are also referred to as edited nucleotides. For instance, most Adenosines in the tRNA *Wobble* nucleotide are edited (34th position, also corresponding to the N°1 nucleotide of the anticodon). *Wobble* adenosines are deaminated by Adenosine Deaminases Acting on RNA (ADAR), resulting in an Inosine (I). The main function of A to I editing is the diversification of base pairing capabilities of the *Wobble* position, as Inosine can pair to almost all nucleotides except Guanosine, thus significantly expanding tRNAs decoding capabilities (S. Srinivasan, Torres, and Ribas de Pouplana 2021).

All classes of RNAs involved in translation carry modified nucleotides. One of the most described RNA modifications is the mRNA cap structure in eukaryotes and viral

RNAs. mRNA cap is a sequentially modified structure that stabilizes mRNA residues. It consists of the addition of a guanosine through an inverted 5′-5′ triphosphate bridge on the 5’ terminus of the mRNA. This nucleotide is later methylated on the 7th nitrogen (m^7Gppp). A 2'-O-methyl group (Nm) is also found on the cap structure (also called cap0 methylation), and can be extended to the first and second transcribed nucleotides termed Cap1 and Cap2 (A. Ghosh and Lima 2010). Cap 2'-O-methylation is often used by viruses in order to escape innate immunity sensing of foreign RNAs, as well as allow their translation in the host cells either by hijacking the hosts modification machinery or evolving their own (Y. Chen and Guo 2016; Ringeard et al. 2019). In humans, Cap 1 is methylated by a SAM dependent Methyltransferase FTSJD1, while Cap1 Nm is deposited by FTSJD2 (Bélanger et al. 2010; Werner et al. 2011).

Ribosomal RNAs (rRNAs) are also rich in modified residues, especially Pseudouridine, and 2’-O-Methylation. rRNA modifications play an important role in stabilizing its secondary structures, but are also found in key translation sites and modulate interactions with mRNAs and tRNAs (Hoernes and Erlacher 2017).

Transfer RNAs stand out as the most heavily modified RNAs in the cell with an average of 13 modified nucleotides per molecule (~18% (T. Pan 2018)).

Transfer RNAs (tRNAs): adaptors in translation

tRNAs are the second most represented transcripts in eukaryotic cells, as they represent an average of 15% of total RNA. tRNAs are key components of the translation machinery, as they carry the amino acids corresponding to their anticodon sequence onto the ribosomal catalytic sites allowing the elongation of a nascent polypeptide. tRNA species are classified mainly by the decoded amino acid, for each aminoacid, there are several tRNAs that bind it, they are called isoacceptors. There are also isodecoders which are tRNAs that possess the same anticodon sequence

but a different core sequence. Surprisingly, the total of tRNA genes exceeds 500 in most eukaryotic genomes. This can be explained by the vital necessity for each tRNA species for protein synthesis and the high copy number allows to secure availability of all species in case of genetic alteration. Nonetheless, a study recently underlined the necessity of one isodecoder of $tRNA^{Arg}$ UCU over the four others, as its loss leads to neurodegeneration in mice, suggesting there might be tissue specificities of some isodecoders (Ishimura et al. 2014).

Mature tRNAs exhibit a conserved two dimensional structure known as the Cloverleaf, where the “leaves" represent the stem-loop secondary structures (Figure 6). tRNAs naturally fold into a tertiary structure resembling an inverted “L” shape (Figure 6). The secondary structures of a mature tRNA are the D-loop, the TΨC-loop (or T-arm), and the Anticodon loop (ACL). The D-loop is named after Dihydrouridine, one of the modified residues present twice on said loop. The D-loop is involved in tRNA tertiary structure stabilization, and recognition by aminoacyl tRNA synthases (Aars) (Robertus et al. 1974; Hardt et al. 1993). The TΨC-loop is present on the 3’ side of the tRNA, and named for the Thymidine, Pseudouridine, and Cytidine residues it carries. Also required for tRNA structure, the TΨC-Loop fold back over the D-loop in order to form and stabilize the L-structure. This structure is supported by hydrogen bonds between the D- and T-loop (Robertus et al. 1974; Chan, Chetnani, and Mondragón 2013). The ACL contains the tri-nucleotide 34-35-36 that directly base pairs to mRNA codon (Figure 6).

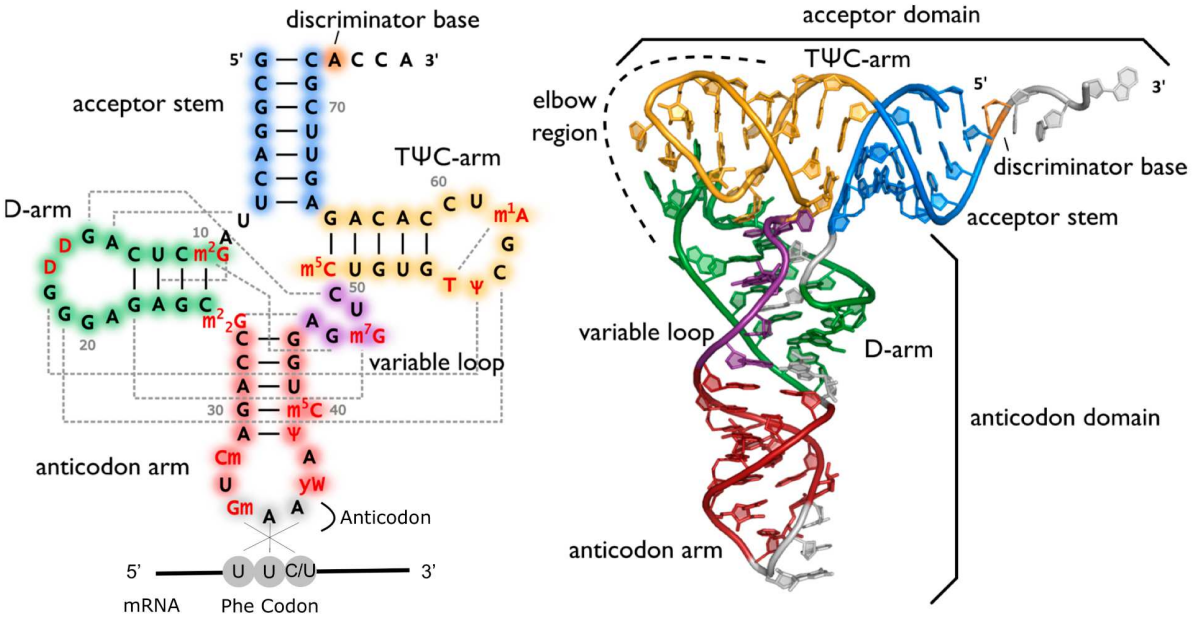

Saccharomyces cerevisiae tRNA Phe

Figure 6. tRNA two dimensional and three dimensional structure. On the left, the cloverleaf structure of cytosolic $tRNA^{Phe}$ from *S. cerevisiae* is represented. The acceptor stem in blue, the D-loop in green, the anticodon loop in red, the variable loop in purple, and TΨC loop in yellow. The anticodon is labelled in gray. Modified residues are highlighted in red. Gray dashed lines indicate the tertiary foldings resulting in tertiary structure as described in (H. Shi and Moore 2000). On the right, the same tRNA is represented after folding into the L-shaped tertiary structure. The acceptor stem and T-arm are stacked together to form the acceptor domain, while D- and anticodon loops form the anticodon domain. Both domains interact together by the elbow region. Adapted from (Lorenz, Lünse, and Mörl 2017).

tRNA genes are encoded in both nuclear genome (cytosolic tRNAs) and mitochondrial genomes (mitochondrial tRNAs), with a size between 70 and 90 nucleotides. Here, I focus on cytosolic tRNAs, their biogenesis and post transcriptional processing and modification.

A- tRNA biogenesis and processing

Cytosolic tRNAs are transcribed by RNA polymerase III in the nucleus, resulting in a pre-tRNA that later undergoes several processing steps (Figure 7A). The first nuclear maturation step is the trimming of the 5' and 3' extensions. The 5'-leader sequence is removed by RNase P, whereas the 3'-trailer sequence is later trimmed by tRNase Z

homologs in eukaryotes (Dubrovsky et al. 2004; Hopper, Pai, and Engelke 2010). Moreover, the maturation of the 3'-end required the addition of the trinucleotide CCA by tRNA nucleotidyltransferase, a crucial step for the function of tRNAs that allows quality control and tRNA aminoacylation (Figure 7A) (Hou 2010). The 3' CCA processing is a requirement in all domains of life, with the specificity of bacterial tRNAs that encode the 3' CCA tail, whilst Archaea and Eukarya require post transcriptional addition of CCA by a tRNA nucleotidyltransferase (Betat and Mörl 2015; Yue, Maizels, and Weiner 1996).

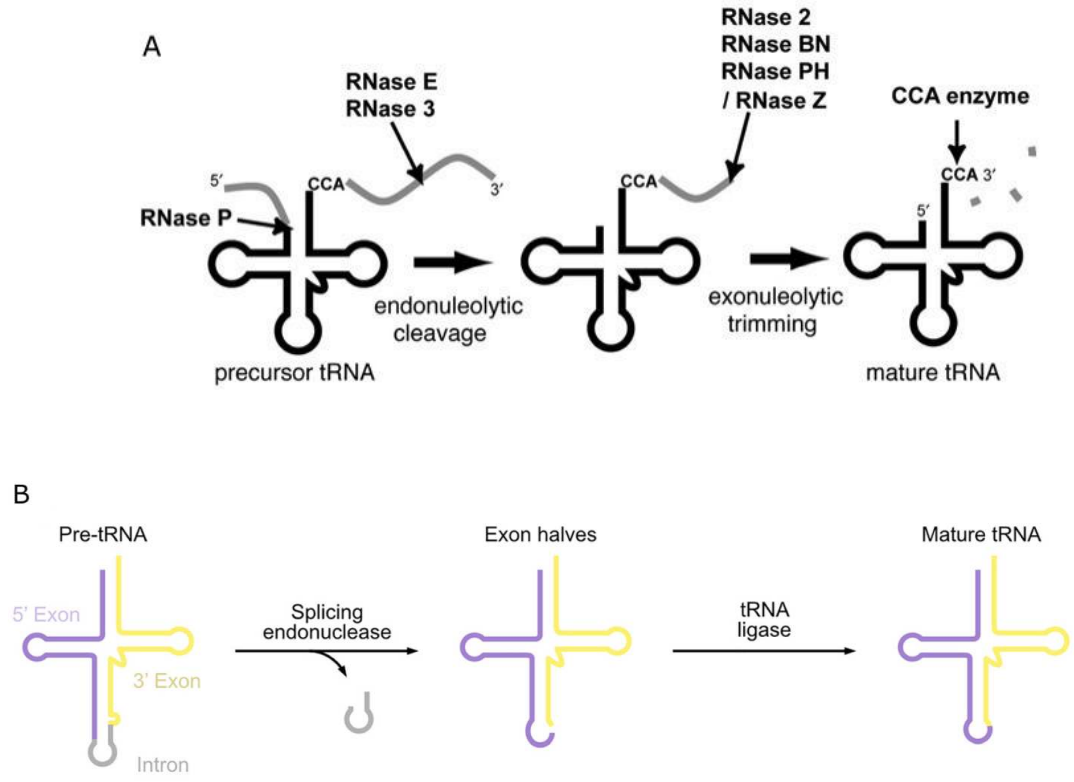

Figure 7. tRNA biogenesis (A) tRNA maturation by trimming of the 5′ leader sequence by RNase P homologs, then the 3′ trailer sequence by tRNase Z homologs. Residual 3' trailer sequence undergoes exonucleolytic trimming, and CCA addition by template-independent RNA polymerase Adapted from (Nakanishi and Nureki 2005). (B) Splicing of intron containing tRNAs. Overview of intron removal by splicing endonuclease, followed by ligation. The 5′ exon and 3' exon are represented in purple and yellow respectively, and the excised intron is gray. Adapted from (Gerber, Köhler, and Peschek 2022).

After cytoplasmic export, intron-containing tRNAs are spliced through two successive steps (Figure 7B). The subcellular localization, as well as the proteins involved in

tRNA splicing can vary, but show similar features as to the conservation of the tRNA splicing endonucleases (TSEN), and intron removal mechanisms. For instance, the yeast SEN complex localizes to the mitochondrial surface whereas the human TSEN complex is localized in the nucleus (Yoshihisa et al. 2003; Paushkin et al. 2004). In humans, a heterotetrameric complex of TSEN removes the intron, resulting in two tRNA halves (Sekulovski et al. 2021). Ligation of the two halves by the tRNA ligase complex results in a mature tRNA (Greer et al. 1983; Kroupova et al. 2021).

Interestingly, most defaults linked to tRNA processing, modification and turnover or fragmentation lead to neurological disorders at early developmental stages or neurodegenerative diseases (Reviewed in (Dimitrova, Teysset, and Carré 2019; Suzuki 2021; Angelova et al. 2018)).

B- tRNAs function in translation

For the sake of clarity of the preliminary data I will be presenting in the third results chapter, below is a short overview of the main steps of translation in eukaryotes. Generally, translation initiation in eukaryotes starts by the formation of a pre-initiation complex composed of the small ribosomal subunit, an initiator $tRNA^{Met}$, and various translation initiation factors as well as GTP. This complex recognizes and binds the cap structure (in the context of Cap-dependent translation initiation) and the small ribosomal subunit scans the 5'UTR for an open reading frame (Aitken and Lorsch 2012). When the AUG start codon is found, initiation factors are released, allowing accommodation of the large ribosomal subunit and the start of elongation (Hinnebusch 2011). During elongation the initiator tRNA translocates from the ribosomal A-site (Aminoacyl-site) to the P-site (Peptidyl-site), opening the way for the next charged tRNA into the A-site. A peptide bond forms between the two amino acids attached to the tRNAs in the P-site and the A-site. This step requires the action of translation elongation factors that bind the aminoacyl-tRNA (Xu, Liu, and Song 2021). After the peptide bond formation, the tRNA in the P-site is released through

the Exit site (E-site) and the tRNA in the A-site translocates into the P-site making way for the next one, and so on until a stop codon is reached (Dever, Dinman, and Green 2018). Upon arrival at a termination codon, no tRNAs usually bind the A-site, but rather are bound by release factors. The newly synthesized polypeptide is released from the tRNA in the P-site, and the ribosome dissociates and is further recycled (Hellen 2018). In some conditions, some tRNAs like $tRNA^{sec}$ and $tRNA^{Trp}$ are able to bind near-cognate stop codons and resume translation in the 3'UTR (Blanchet et al. 2018; Dabrowski, Bukowy-Bieryllo, and Zietkiewicz 2015). However this is a tightly regulated process, named stop codon readthrough that is programmed in many cases, and allows the proteome to expand (Eswarappa et al. 2014; Singh et al. 2019).

C- Anticodon loop (ACL) modifications: from translation fine-tuning to tRNA stability

An important part of tRNA processing is their chemical modification and editing. tRNA modification can occur at various steps of their biogenesis, in the nucleus and/or in the cytoplasm depending on the subcellular localization of the modification machineries, and the sequential order of modification. As stated above, the mere folding of tRNAs requires several modified residues including Dihydrouridine, crucial for the tRNA flexibility and structure (Dalluge et al. 1996).

tRNA anticodon loop modifications have been well documented for affecting their primary function in translation regarding efficiency, fidelity, aminoacylation and overall fine tuning. But also regarding the stability and turnover (Reviewed by (Tuorto and Lyko 2016; Valadon and Namy 2021)).

Certain non-essential modifications are crucial for tRNA stability, and altering the modification pathways can lead to tRNA decay (Alexandrov et al. 2006; Chernyakov et al. 2008; Tuorto et al. 2012). In contrast tRNA modification defects can lead to

tRNA fragmentation that sometimes results in accumulation of stable products, with many fates, including possible biological functions (Durdevic et al. 2013; Blanco et al. 2014; X. Wang et al. 2018; Angelova et al. 2020). As they show great diversity based on origin and structure, I will use the generic term tRNA fragments (tRFs) in this manuscript.

D- tRNA-derived fragments (tRFs)

tRNA fragments, also commonly referred to as tRNA derived small RNAs (tsRNAs) or tRNA-derived stress-induced small RNAs (tiRNAs) are small RNAs originating from cleavage of precursor or mature tRNAs (Y. S. Lee et al. 2009; Y. Xie et al. 2020). Since their discovery (Yudelevich 1971), few studies about tRFs were published, as they were likely viewed as simple byproducts of tRNA fragmentation/ decay, until the development of high throughput sequencing techniques which led to the discovery of high variety and stability of tRFs in many biological conditions (Figure 8). tRFs stability and accumulation thus raised questions about their possible biological functions as small non-coding RNAs (Y. S. Lee et al. 2009; Magee and Rigoutsos 2020). In many eukaryotes, the endonuclease Angiogenin is the main enzyme responsible for the production of tRNA halves (5' tRFs and 3' tRFs) by a single cut on the anticodon loop (Yamasaki et al. 2009; Fu et al. 2009; Saxena et al. 1992). Nonetheless, other enzymes have been shown to produce tRNA halves, like the human RNase 1 (Nechooshtan et al. 2020). Interestingly, the RNAse III Dicer, otherwise involved in mi- and si-RNA processing is also able to produce tRFs (Cole et al. 2009; Maute et al. 2013; Kazimierczyk et al. 2022).

Certain tRFs are produced under natural conditions and can vary by tissue distribution, or biological changes, like aging or stress (Yuan et al. 2021). tRFs can

be stabilized by the presence of modified nucleotides (Figure 8). Although some tRFs can be stabilized after endonucleolytic cleavage and maintain stem-loop structures (Costa et al. 2023). However, tRFs are often produced in higher amounts under stress conditions (hence the “tiRNA” designation above). These include viral infections, oxidative stress, starvation etc. (Yudelevich 1971; Ivanov 2015; Thompson et al. 2008; S. R. Lee and Collins 2005; Sharma et al. 2023).

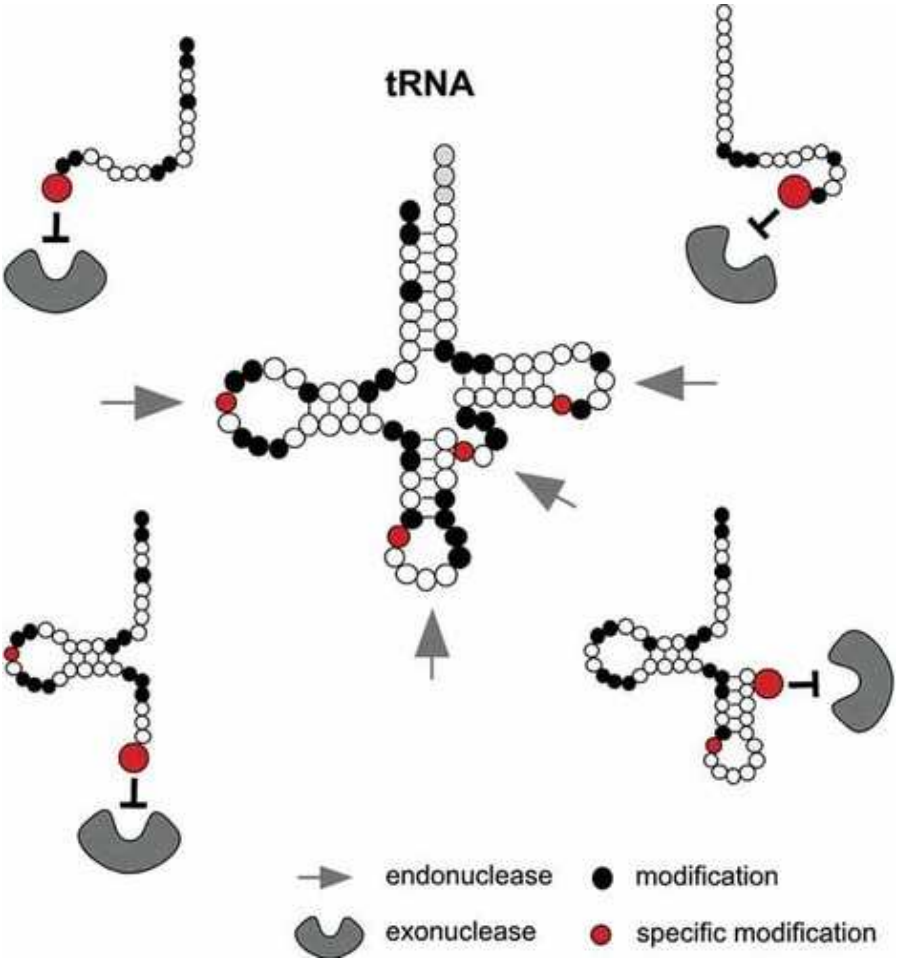

Figure 8. tRNA fragmentation and stabilization by RNA modifications. Different structures and sizes of tRFs originating from various regions of mature tRNAs. Modifications within various eukaryotic tRNAs are depicted in black, with those exhibiting protective effects exhibited in red. Loci with susceptibility to endo- or exonucleolytic cleavage are indicated with an arrow and a U shape respectively. Adapted from (Durdevic and Schaefer 2013).

Although stress conditions are the most inductive elements of tRNA fragmentation, defective tRNA modifications play an important role in tRNA stability and turnover. In

fact, mutants of tRNA modification enzymes can exhibit excessive tRNA fragmentation. Nonetheless, tRFs stability and persistence is highly dependent on their modification status (Figure 8). Whereas tRFs are produced by endonucleolytic activity, fragments are left vulnerable to exonucleases. In that regard, the presence of other modifications can play a protective role from endonucleases (Figure 8).

tRFs functions have been extensively studied over the last decades, spanning from gene regulatory functions to stress recovery and host pathogen interactions. Although tRFs have been linked to an overwhelming number of biological processes, I here focus on those related to gene regulation.

Interestingly, tRFs can act as canonical small regulatory RNAs in association with proteins of RNAi pathways. Like small regulatory RNAs, tRFs can bind Argonaute proteins and guide silencing of protein coding genes or transposable elements by sequence complementarity (Maute et al. 2013; Shigematsu and Kirino 2015; Schorn et al. 2017; Di Fazio et al. 2022; G. Li et al. 2022). By competing with canonical regulatory RNAs for Dicer or AGO binding, tRFs can deregulate RNAi pathways (Haussecker et al. 2010; Kuscu et al. 2018; Durdevic et al. 2013). In *Drosophila*, 5' tRNA halves bound to AGO2 mediate target specific silencing, and reduce global protein synthesis (S. Luo et al. 2018). These tRFs contain conserved seed regions, similar to those of miRNAs, complementary to ribosomal proteins' mRNAs, inducing reduction of protein synthesis, likely through RISC activity (S. Luo et al. 2018).

Besides their roles in AGO-mediated silencing, tRFs also interfere with gene expression by impeding translation. Through direct mRNA binding, interactions with ribosomes, or by displacing translation initiation factors, tRFs display a variety of

interactions with translation machineries (Deng et al. 2015; Keam et al. 2017; Lalande et al. 2020; Ivanov et al. 2011). Interestingly, tRNAs can serve as primers for reverse transcription of LTR (Long Terminal Repeat) retrotransposons (Marquet et al. 1995). Concomitantly, tRFs were also found to direct LTR-retrotransposon silencing by preventing tRNA priming of their retrotranscription (Schorn et al. 2017; Schorn and Martienssen 2018). Interestingly, mature tRNAs also mediate retrotransposon silencing through binding with the piRNA pathway protein Asterix in order to promote their silencing by piRNAs *Drosophila* and mammals (Ipsaro et al. 2021). tRFs are stable in extracellular fluids either by the presence of RNA modifications, maintained in stem-loop structure of nicked tRFs, and so on, tRFs are reportedly involved in intercellular communication through extracellular vesicles (Nechooshtan et al. 2020; Tosar and Cayota 2020; Baglio et al. 2015; Costa et al. 2023).

tRNA fragments and modifications in disease

Some tRNA fragments' overrepresentation are disease associated, especially cancers and neurological disorders (Anderson and Ivanov 2014; Pandey et al. 2021). For instance, mutations in the NSun2 (NOP2/Sun RNA Methyltransferase 2) an m^5C methyltransferase, leads to Dubowitz-like syndrome a neurodevelopmental disorder associated with intellectual disability and microcephaly (Abbasi-Moheb et al. 2012). Interestingly m^5C methyltransferases NSun2 and DnmT2 mutations are also linked to high tRNA fragmentation. Supporting these results, Lack of Nsun2 deposited m^5C in human cell lines and mice caused endonucleolytic cleavage of target tRNAs (Tuorto et al. 2012; Schaefer et al. 2010). Accumulation of a 5'tRF reduced translation globally, and reduced cell size and increased apoptosis of cortical, hippocampal and striatal neurons (Blanco et al. 2014). Many other modifications, including m^5C are associated with cancer. For example, altered NSun2 copy number is associated with oral and colorectal cancers (Okamoto et al. 2012; Elhardt et al. 2015). tRFs

dysregulation is observed in many cancers, some unrelated to tRNA modifications, but their differential expression is considered an asset in prognosis and diagnosis biomarker research. Because of the large spectrum of tRFs' activities, and various described functions, the importance of accurate quantification is crucial for biomarker research.

E- tRNA ACL modifications and translation fine-tuning

Some anticodon loop positions are found to be modified in most organisms, with a remarkable level of conservation. Below, I provide two examples of tRNA modified residues in position 37 located on the ACL, and their functions in translation and pathological implications.

N-threonylcarbamoyladenosine (t6A)

tRNA position 37 is a highly modified position in many organisms. A universally conserved ACL A37 modification is N-threonylcarbamoyladenosine (t6A) found in tRNAs decoding ANN codons (Where N stands for any of the four canonical nucleotides). $t6A_{37}$ requires the action of several proteins and two different complexes: the TsaC/TsaC2 family (El Yacoubi et al. 2009), and the KEOPS complex (M. Srinivasan et al. 2011). $t6A_{37}$ plays a structural role in the ACL interactions with the ribosome ensuring accurate decoding (Murphy et al. 2004). Loss of $t6A_{37}$ modification increases frameshifting frequency during translation, as well as inaccurate initiation codon selection. Predictably, defective t6A modification leads to severe translation defects, and leads to neurodegeneration, and renal disorders (Edvardson et al. 2017; D. A. Braun et al. 2017).

Wybutosine derivatives

Wybutosine derivatives (Yw) are also a category of heavy RNA modifications found specifically in position 37 of $tRNA^{Phe}$ isoacceptors in Archaea and Eukarya. Yw_{37}, like t6A, requires the action of several RNA modifying enzymes.

Interestingly, Yw_{37} is also involved in reading frame maintenance during translation (Carlson et al. 1999; Waas et al. 2007; Rosselló-Tortella et al. 2020). Reading frame maintenance is enforced through stabilization of codon-anticodon base pairing (Konevega et al. 2004). Defects of Yw_{37} hyper modifications are associated with increased drug resistance in human cancer cell lines, as well as poor survival of early stage colorectal cancer patients (Y. Pan et al. 2021; Rosselló-Tortella et al. 2020).

Interestingly, the full structure and modified residues of $tRNA^{Phe}$ modifications have been well described in the 1970s (Robertus et al. 1974; Altwegg and Kubli 1979). These studies paved the way for later discoveries regarding the sequential addition of these modifications as well as their subcellular localization (Kuchino et al. 1982). In fact, it was implied from many studies that G37 modification to wybutosine derivatives would require transport of the almost mature tRNA back into the nucleus for Trm5 to catalyze addition of an N-1 methyl group (m^1G) (Noma et al. 2006). m^1G37 is required for the further deposition of Cm32 and then Gm34. Both these residues are then required for the hyper modification of m^1G37 into wybutosine derivatives. (J. Li et al. 2020). In *S. cerevisiae* and *S. pombe, G37* hyper modification follows these same rules for Wybutosine 37 deposition (Guy et al. 2015). Remarkably, the same hierarchical order is conserved in humans and mice, where G37 is hyper modified into Peroxy-Wybutosine (O2Yw) (Guy et al. 2012, 2015; J. Li et al. 2020; Nagayoshi et al. 2021).

Ancient and glorious is 2’-O-Methylation (Nm)

2’-O-methylation (Nm - N corresponding to any of the four canonical ribonucleotides, also referred to as ribose methylation) is an RNA modification consisting of the addition of a single methyl group to the 2’ O position of the ribose. Nm is one of the most abundant and ubiquitous modifications along with pseudouridine and N-6-methyladenosine (Boccaletto et al. 2022). Found in all three domains of life, Nm is often viewed as one of the most ancient RNA modifications.

Nm is one of the few modifications that affect the ribose moiety, although several Nm nucleotide derivatives exist, carrying additional chemical residues. One example is m^6Am which corresponds to a 2’-O-methyladenosine carrying an additional methyl group on position 6 of the nitrogen base (Cesaro, Tarullo, and Fatica 2023).

Nm confers chemical properties that increase stacking, hydrophobicity, protection from endonucleolytic cleavage but also stabilizes the helical structures (Yildirim et al. 2014; Abou Assi et al. 2020).

A- Mapping and detection methods

Numerous mapping methods have been developed and/or adapted for Nm detection, some of whom have only been proven appropriate for site-specific detection, but not for systematic mapping. The difficulties often arise in the necessity for purification steps or the necessity for high starting material. Intrinsic differences between the classes of analyzed RNAs, can also pose an issue, like RNA abundance and modification status. One of the most ancient detection methods is Two Dimensional thin Layer Chromatography (Grosjean, Keith, and Droogmans 2004), an efficient method allowing separation of modified bases based on their chemical properties, but laborious, as well as requiring high starting material and readout knowledge. Other efficient chromatography based methods have been nicely adapted for Nm

detection, especially on low starting materials. High or Ultra- Performance Liquid Chromatography (UPLC/HPLC) coupled to tandem Mass Spectrometry (LC-MS/MS) successfully detected conserved Nm residues, notably on tRNAs (Glasser et al. 1992; Guy et al. 2012). Lack of sequence context due to the fragmentation steps, as well as the necessity of efficient purification steps of the RNA of interest are the main limitations of these techniques (Thüring et al. 2016).

The need for sequence-specific base resolution detection of Nm led to the use of different techniques relying on high throughput sequencing developed for efficient transcriptome wide mapping of Nm (Marchand et al. 2016; Zhu, Pirnie, and Carmichael 2017; Hsu et al. 2019). Ribomethseq is based on the premise that the presence of Nm prevents cleavage of the 3′-adjacent phosphodiester bond, notably in alkaline conditions. This way, random alkaline RNA fragmentation results in high protection of the N+1 to an Nm modified nucleotide, and after library preparation, the coverage profile displays a typical gap in the N+1 position due to low number of reads ending or starting at the Nm-protected position (Marchand et al. 2016). Although highly unbiased, the main limitation of RibomethSeq is its inability to be applicable for small RNAs. Nm-seq and RibOxi-seq are also next-generation sequencing based techniques for Nm mapping. These methods rely on periodate cleavage resistance of 2′-O-methylated 3'-termini (Zhu, Pirnie, and Carmichael 2017; Hsu et al. 2019; Dai et al. 2018). These methods are notably known to require substantial starting material.

2′-OMe-Seq is another high throughput sequencing method. It is based on the observation that the presence of Nm stops Reverse Transcriptase elongation at a low dNTP concentration. Followed by library preparation and sequencing, abortive cDNA products indicate the presence of an Nm-modified nucleotide (Incarnato et al. 2017). This method has been optimized for quantitative analysis by qPCR, rather than sequencing. Although, RT at low dNTP concentration is proven to be difficult to

achieve on tRNAs because of the presence of RT arresting modifications. Moreover, 3’ terminal ribose methylation is detected using RT-qPCR, based on the ability of 3′ end Nm of small RNAs to inhibit PolyA polymerase activity (N. Wang et al. 2018). Either by RT-based methods or next-generation sequencing, it appears there is no universal method for Nm mapping, as none of the current methods is bias-proof, rather, each can be more suitable for specific classes of RNA can based on size, modification status, and abundance. These techniques are often found to complement each other, and allow validation of modification sites through different approaches. A thorough comparative discussion of different techniques was recently published by (Motorin and Marchand 2018). New methods are now developed using direct RNAseq with Oxford Nanopore technologies (Lucas et al. 2023).

B- RNA 2’-O-methyltransferases

Nm is deposited by RNA methyltransferases using S-Adenosyl Methionine (SAM - also commonly called AdoMet) as a cofactor and donor of the methyl group.

Interestingly, the RNA and positions modified by RNA methyltransferases are strongly conserved especially within two main classes of RNA methyltransferases exist based on substrate recognition: Small Nucleolar RNA (snoRNA) guided methyltransferases and stand alone methyltransferases.

snoRNA guided 2’-O-methyltransferases

A subset of 2’-O-methyltransferases require specialized guide RNAs in order to define sequence specificity of ribose methylation using Box C/D Small Nucleolar RNA (snoRNA or SNORD).

snoRNAs are a distinct class of non-coding RNAs ranging from 60 to 120 nucleotides and serve essentially as guides for RNA modifications (Huang et al. 2022). There are

two types of snoRNAs based on different types of conserved consensus sequences: Box C/D snoRNAs (SNORDs) that mainly guide Nm, and Box H/ACA snoRNAs that mainly guide Pseudouridylation (Lafontaine et al. 1998; Balakin, Smith, and Fournier 1996; Cavaillé, Nicoloso, and Bachellerie 1996). There are also scaRNAs (Small Cajal-body specific RNAs) guiding Fibrillarin-mediated ribose methylation during the maturation of spliceosomal Small Nuclear RNAs in Cajal bodies (snRNAs). Additionally, scaRNAs can interact with pseudouridine synthases to modify snRNAs (Jády and Kiss 2001; Cao et al. 2018).

SNORDs carry a conserved C/D box (RUGAUAG/CUGA, where R represents a purine) and two additional degenerate C'/D' boxes (Ye et al. 2009). Additionally, two single stranded sequences located between the box C/D and box C'/D' serve as guide sequences and directly base pair with the target RNA sequence (Kiss-László et al. 1996). Through sequence complementarity, Fibrillarin is guided to complete ribose methylation exactly five nucleotides upstream of the box D or D' box (Kiss-László et al. 1996; Nicoloso et al. 1996; Cavaillé, Nicoloso, and Bachellerie 1996).

Additionally to rRNA 2'-O-methylation, $tRNA^{Met}$ Wobble Nm is mediated by SNORD97 and SCARNA97 guides associated with Fibrillarin (Vitali and Kiss 2019). Similarly, *Pxdn* mRNA was found to be Nm modified by Fibrillarin associated with two SNORDs in order to regulate its translation (Elliott et al. 2019).

Stand alone methyltransferases

This category of Nm Methyltransferase acts in a guide independent manner. Even though these enzymes do not require a guide RNA, they remain specific and the Nm sites can be very conserved throughout the evolution. Cap methyltransferases in eukaryotes are included in this category (Bélanger et al. 2010; Werner et al. 2011).

Highly diverse and numerous as opposed to guided methyltransferases, they often display high substrate specificity. While guided methyltransferases rely mainly on the diversity of box C/D snoRNAs to methylate several substrates, stand alone methyltransferases compensate by their diverse structures and protein partners allowing accommodation of several targets, but still preserving a high substrate specialization and specificity (Guy et al. 2012; Guy and Phizicky 2015). A nice example is the ability of eukaryotic tRNA Nm methyltransferases of the Trm7 family to modify the 32nd and 34th residues of the anticodon loop of specific tRNA species. In the latter case, sequence specificity is secured by interactions with conserved cofactors (Guy et al. 2012; Guy and Phizicky 2015) (See chapter on Trm7 family below).

C- The Trm7 family of ribose methyltransferases

First insights from *S. cerevisiae*

The Trm7 family of genes is a highly conserved family of ribose methyltransferases with homologs in prokaryotic organisms (Feder et al. 2003). In *Escherichia coli*, FtsJ/RrmJ is a ribose methyltransferase with 23S rRNA as a main substrate (Caldas et al. 2000). Homologs of *Ftsj/RrmJ* were extensively studied in the yeast model. MRM2 and SPB1, modifying mitochondrial and nuclear rRNAs respectively, display high phylogenetic conservation, including in humans, with a striking level of substrate overlap (Pintard, Bujnicki, et al. 2002). Trm7 represents a family of Rossmann-Fold SAM binding RNA methyltransferases with the conserved catalytic tetrad K-D-K-E (Figure 9) (Hirata et al. 2019; Graille 2022). It is one of the four phylogenetically conserved enzymes specializing in tRNA modifications in yeast species together with Trm3, Trm13 and Trm44 (Pintard, Lecointe, et al. 2002; Cavaillé, Chetouani, and Bachellerie 1999; Wilkinson et al. 2007; Kotelawala, Grayhack, and Phizicky 2008). As opposed to other yeast tRNA methyltransferases, Trm7 is specialized in anticodon

loop Nm modification on the 32nd and 34th nucleotides of tRNAs $^{Phe, Leu, Trp}$ ((Pintard, Lecointe, et al. 2002).

FTSJ1 is the Human ortholog of *Trm7*, sharing both high phylogenetic conservation, and a considerable level of substrate specificity, as they modify the same tRNA species at the same nucleotide positions (Guy et al. 2015; J. Li et al. 2020; Kawarada et al. 2017; Nagayoshi et al. 2021; Brazane et al. 2023).

In yeast, deposition of Nm by Trm7 requires separate binding of high molecular weight protein partners Trm732 and Trm734 in order to methylate the corresponding positions on tRNAs$^{Phe, Leu, Trp}$ (Pintard, Lecointe, et al. 2002; Guy et al. 2012). Both the Trm7 and the partners are required for Nm deposition on each position of the ACL, as lack of Trm732 or Trm734 results in Nm loss at the corresponding position (Guy et al. 2012; Funk et al. 2022). Likewise, FTSJ1 partners up with orthologs of Trm732 and Trm734 for methylation specificity namely THADA for Nm 32 deposition, and WDR6 for Nm34 deposition (Guy and Phizicky 2015; Guy et al. 2015; J. Li et al. 2020). A recent study resolved the structure of Trm7-Trm734 in complex with SAM revealing that Trm734 is likely required for the correct positioning of Trm7 catalytic pocket onto the ACL (Hirata et al. 2019). The structure depicted in Figure 9 below allows appreciation of the three WD-40 β-propeller domains of Trm734 (BPA, BPB, BPC), where BPA and BPC adopt a V-shape anchoring to the C-terminus of Trm7 (Figure 9A). Predicted docking of the D-arm of tRNA^{Phe} into the BPB domain allows positioning of the ACL close to the catalytic pocket of Trm7 (Figure 9B) (Hirata et al. 2019).

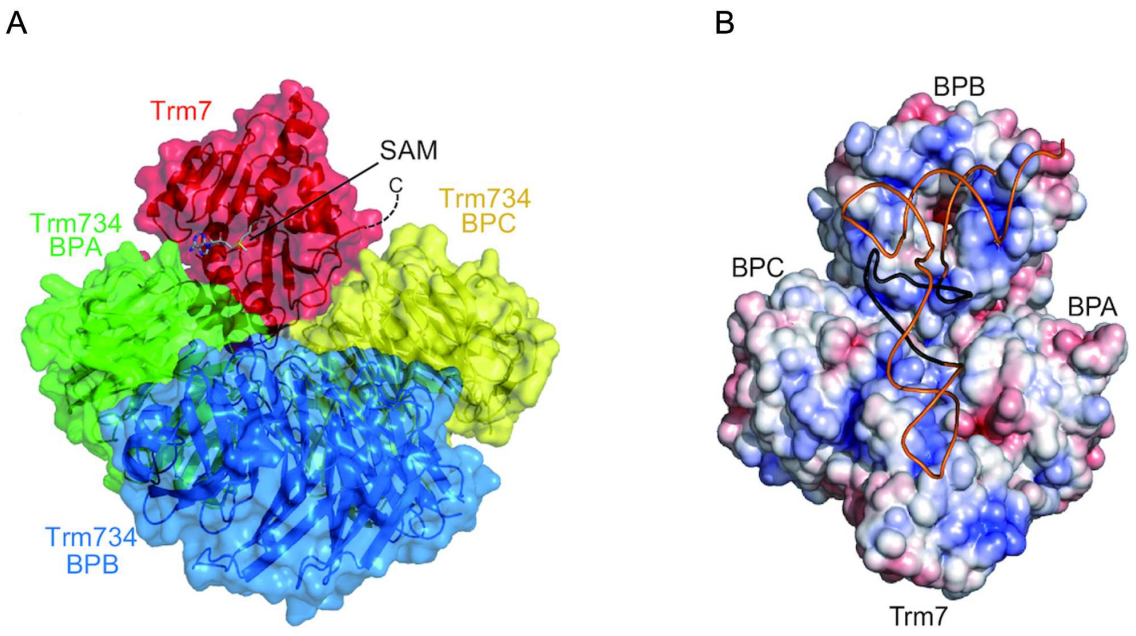

Figure 9. Structure of the wobble SAM binding methyl transfer complex Trm7-Trm734 (Hirata et al. 2019). **(A)** Structure of Trm7-Trm734 in complex with SAM. Trm734 is composed of three BP domains depicted in green (BPA), blue (BPB) and yellow (BPC). Trm7 is represented in red, and SAM in multicolor a stick model. **(B)** Surface model of Trm7-Trm734 with yeast $tRNA^{Phe}$ colors represent negative (red) and positive (blue) electrostatic potential. $tRNA^{Phe}$ depicted in orange (with the D-arm in black) fits the distribution of positive charges along the surface of the methyl transfer complex.

Consequently, mutations in either *Trm732* or *Trm734* both result in the loss of the Nm on the main substrate $tRNA^{Phe}$ (Guy et al. 2012; Guy and Phizicky 2015). The main phenotype associated with *Trm7* loss is severe growth defects including in the distant yeast *Schizosaccharomyces pombe* (Pintard, Lecointe, et al. 2002; Guy et al. 2012; Guy and Phizicky 2015). The conservation of the effectors of ACL ribose methylation is such that the Human FTSJ1 and THADA are able to rescue the growth defects associated with mutations of yeast Trm7 and partners. Moreover, yeast Trm7 methyltransferase is able to bind the human THADA to achieve modification of Cm32 (Guy and Phizicky 2015). Considerable knowledge of paramount importance about ACL Nm was obtained thanks to all the studies mentioned above on yeast Trm7. In fact, mutations in *FTSJ1* result in a rare neurodevelopmental disorder associated

with intellectual disability (ID) (Ramser et al. 2004; Froyen et al. 2007; Gong et al. 2008). The molecular mechanisms leading to FTSJ1 related ID remain unsolved, as for many other neurological disorders caused by RNA modifying pathways' alteration (Angelova et al. 2018; Dimitrova, Teysset, and Carré 2019; Suzuki 2021). In this regard, functional studies performed in yeast constitute therefore a crucial starting point for the understanding of Trm7 family functions, exploration of their potential roles in translation, and in disease etiology, all questions I tried to address to some extent during my PhD.

Anticodon loop Nm functions in translation: first clues

As tRNAs are central pieces in translation, it appears clear that alteration of their biology, especially on conserved ACL modifications, might cause deleterious effects on translation efficiency and/or fidelity. Pintard and colleagues have attributed the slow growth of *Trm7Δ* mutants to a general and mild (30%) translation drop (Pintard, Lecointe, et al. 2002). The growth defects are rescued by $tRNA^{Phe}$ overexpression in *S. cerevisiae* and *S. pombe*, while $tRNA^{Trp}$ and $tRNA^{Leu}$ failed to save the phenotype, suggesting a $tRNA^{Phe}$ dependent effect on growth, and likely on global translation rates (Guy et al. 2012; Guy and Phizicky 2015). However, a follow up article from the same lab argues that translation defects are spanning from activation of a robust general amino acid control response (GAAC) suggesting uncharged tRNAs. The authors attribute this response to uncharged $tRNA^{Phe}$. Although no detectable charging defect of the latter was observed in their experimental setup, the increase of available charged $tRNA^{Phe}$ rescued *Trm7Δ* growth defects in both yeast species (Han et al. 2018).

Besides the current understanding of Trm7 functions in yeast being largely attributed to $tRNA^{Phe}$, it remains unclear why the defective modification of a single $tRNA^{Phe}$ could lead to such dramatic and generalized effects on translation, and an impairment of brain function in humans. For one, we learned from a murine model of

Ftsj1 loss of function that growth defects seem to be a conserved feature, although the mutants primarily suffer from neurological defects, like reduced learning capacity, and insensitivity to pain, as well as anxiety-like phenotypes (Jensen et al. 2019; Nagayoshi et al. 2021). Besides the conservation of neurological phenotypes in the mouse model, it is noteworthy to mention that no other tissues examined seem to be affected by *Ftsj1* loss in mice, even if Ftsj1 is expressed ubiquitously, suggesting that it likely operates differently in complex organisms, and probably does not affect translation in such a generalized manner as it was observed in yeast.

Beyond the eukaryotic spectrum of the Trm7 enzymes, *E.coli Ftsj* (that modifies rRNA) is also involved in drastic translation alteration, displaying ribosome assembly defects, rather than reduced polysome levels observed in *Trm7Δ* yeast. This can be explained by the fact that 23S rRNA is the main substrate of prokaryotic Ftsj, and is important for 50S biogenesis and ribosome assembly (Bügl et al. 2000).

Altogether, global translation alteration upon Trm7 family loss appears to show some variations, likely depending on the species and organism complexity, and methylation specificity.

FTSJ1 and fine-tuning of translation

Translation defects associated with $tRNA^{Phe}$ were found to be conserved in human cells on a luciferase reporter carrying either of the two Phenylalanine codons. They found that TTT codons are less efficiently translated by $tRNA^{Phe(GAA)}$ when compared to TTC upon loss of FTSJ1's modification of $tRNA^{Phe}$ (J. Li et al. 2020). *In silico* analysis showed that around 40% of genes with high TTT bias are related to nervous system functions. This study once again associates translation defects due to FTSJ1 loss to $tRNA^{Phe}$ defective modification, but importantly provides a plausible molecular link to the nervous system (J. Li et al. 2020).

Interestingly, a comprehensive study on the *Ftsj1* mouse model was carried out by Nagayoshi and colleagues, who not only identified new substrates of mouse Ftsj1 and studied its function in translation, but also showed an implication in nervous system plasticity (Nagayoshi et al. 2021). Evidence of increased tRNA fragmentation, as well as impaired TTT codon translation were provided, consistently with previous observations in *Drosophila* and Human cells respectively (Angelova et al. 2020; J. Li et al. 2020).

Importantly, FTSJ1 has been linked to premature TGA stop codon recognition (Trzaska et al. 2020). While searching for drugs capable of inducing premature stop codon readthrough, the team was able to identify 2,6 Diaminopurine (DAP), a compound isolated from a fungus. Through FTSJ1 binding, DAP reduced its methyltransferase activity, thus mediating readthrough of TGA stop codons through Tryptophan incorporation by the unmodified $tRNA^{Trp}$ at position 34. This report and a recent one show for the first time implication of a different substrate of FTSJ1 (besides $tRNA^{Phe}$) in a mechanism related to translation (Trzaska et al. 2020; Carollo et al. 2023).

Interestingly, human AGO1 (hAGO1) was found among the few genes to undergo natural (terminal) stop codon readthrough and produced a stable isoform (Singh et al. 2019; S. Ghosh et al. 2020). This newly described isoform called AGO1x displays novel functions in preventing dsRNA accumulation thus reducing interferon response in breast cancer cells (S. Ghosh et al. 2020). The conservation of the proximal 3'UTR sequence of AGO1 suggests a conserved mechanism of terminal stop codon readthrough for AGO1x synthesis. The annotated TGA stop codon of AGO1, as well as the sequence downstream made it an excellent candidate for programmed stop codon readthrough (Eswarappa et al. 2014). Importantly, AGO1x readthrough is regulated by the *Let-7a* miRNA through a conserved complementary sequence motif 10 nucleotides downstream of the annotated stop codon (Singh et al. 2019).

Although the mechanism of programmed stop codon readthrough mediated by a miRNA remains unknown, AGO1x synthesis seems to be tightly regulated. Importantly AGO1x acts as a competitive inhibitor of the canonical miRNA pathway of gene regulation, as it can load miRNAs, like the canonical AGO1 protein, but is unable to achieve PTGS because of an inability to interact with other RISC partners, including GW182, thus making it an antagonist protein to the functions of its canonical and abundant counterpart (Singh et al. 2019).

FTSJ1-mediated readthrough occurs through incorporation of an unmodified $tRNA^{Trp(CCA)}$ on UGA premature termination codons, however, no studies link FTSJ1 to stop codon readthrough of terminal stop codons (Trzaska et al. 2020; Carollo et al. 2023). Furthermore, the amino acid incorporated instead of the stop codon in hAGO1x is yet to be identified. Therefore, one may speculate about a contribution of *FTSJ1* loss to the production of AGO1x through unmodified $tRNA^{Trp}$. This theory could explain the defects observed in AGO silencing pathways upon loss of FTSJ1 homologs in *Drosophila*.

Altogether, these studies suggest that FTSJ1's precise functions are yet to be explored, but also that other substrates of FTSJ1 besides $tRNA^{Phe}$ might be involved in translation fine-tuning, and probably in the etiology of FTSJ1 related intellectual disability. This represents an important basis for exploring the full spectrum of FTSJ1 functions, through stop codon readthrough or tRNA fragmentation, to codon specific regulation in the nervous system.

FTSJ1-related X-Linked Intellectual Disability

Often associated with an intellectual quotient below 70, intellectual disability (ID) is defined by the American psychiatric association as an alteration of general functioning and adaptive behavior starting during development. ID affects intellectual and reasoning abilities, memory and learning. ID also impairs social interactions and

behavior, as well as the practical abilities like self care, daily life organization (see https://www.psychiatry.org/dsm5). The prevalence of ID in the world population is estimated between 1 and 3% with higher incidence in males compared to females (Daily, Ardinger, and Holmes 2000; Maulik et al. 2011).

X-linked intellectual disability (XLID) is a generic term referring to a subset of neurodevelopmental disorders associated with ID and directly related to genetic alterations on the X chromosome (Raymond 2006). The classification of ID related disorders can be extremely challenging, as various neurological disorders are associated with ID and other behavior, social or learning impairments with no signature features to distinguish them from one another. NSXLID refers to a subset of ID cases with such varying degrees of physical, metabolic and neurological outcomes that only intellectual disability is the common trait (Kerr et al. 1991; Renieri et al. 2005). Therefore the difficulty of diagnosis has shifted the clinical characterization to genetic screening (Mostly by exome sequencing) as a first approach in recent years (Jansen, Vissers, and de Vries 2023).

Mutations of the locus of *FTSJ1* on the small arm of the X-chromosome (Xp11.23) are associated with various social and physical alterations in addition to ID (Freude et al. 2004; Froyen et al. 2007; R. Wang et al. 2019). Different loss of function mutations were functionally characterized (Refer to Table 1), and are associated with subsequent loss of Nm on tRNAs$^{Phe,\ Leu,\ Trp}$ (Guy et al. 2015; Nagayoshi et al. 2021; Brazane et al. 2023). In addition, to the loss of function mutations above, copy number alterations in the FTSJ1 locus appear to be associated with ID as well *(Bonnet et al. 2006; Honda et al. 2010; El-Hattab et al. 2011; R. Wang et al. 2019)*. This suggests the importance of balancing the expression of this RNA methyltransferase during development.

FTSJ1 Allele	Family	Mutation/Location	Effect	Reference
Ftsj1Δ	6 (AU)	Deletion of FTSJ1 and SLC38A5	Loss of FTSJ1	Froyen et al. 2007
FTSJ1-ss	A3	c.121 + 1delG, p.Gly41Valfs*10 (IVS2, G DEL, + 1)/ Exon 2	Significant reduction of FTSJ1 mRNA level (NMD)	Freude et al. 2004
196C > T	P48	c.196C>T, p.Gln66*/ Exon 4	Almost undetectable FTSJ1 transcripts (NMD)	Freude et al. 2004
655G > A	MRX44	c.655G > A, p.Glu191_Tyr218del/ Exon 9	Loss of exon 9, protein lacking 28 amino acids	Freude et al. 2004
A > G	MRX9	c.192-2A>G, p.Gly65Cysfs*18 (IVS3AS, A-G, -2)/ Intron 3	Truncated protein	Ramser et al. 2004
G > A	MRW06	c.571 + 1G > A, p.Glu191Glyfs*44/ Intron 8	Significant reduction of FTSJ1 mRNA level (NMD)	Takano et al. 2008
p.A26P	7	c.76G > C; p.Ala26Pro/ Exon 2	Altered FTSJ1 protein function	Guy et al. 2015
A > T	de novo variation	c.362-2A > T, r.362_414del/ p.Val121Glyfs*51	Skipping of exon 6, premature termination codon. Significant reduction of FTSJ1 mRNA (NMD)	Brazane et al. 2023 (Patient derived cells from Amélie Piton & Elise Schaefer) ClinVar VCV000981372.1
Y > N	de novo variation	c.34T > A; p.Tyr12Asn/ Exon 2	Deposited as pathogenic	Ambry Genetics Clinvar https://www.ncbi.nlm.nih.gov/clinvar/variation/208659/

Table 1. *FTSJ1* mutations associated with XLID (ss: splice site mutation, > substitution, del: deletion, c.N: nucleotide (xxx) mutated in coding DNA sequence (CDS), p. indicates amino position and its substitution on the final protein product. Adapted from (Dimitrova, Teysset, and Carré 2019).

Hemizygous mutations in FTSJ1 cause ID in males but the same mutations do not affect intellectual abilities of females, which is probably due to the inactivation of the altered X chromosome (Froyen et al. 2007; Takano et al. 2008).

Currently, insight into the molecular links between loss of tRNA methylation and XLID is still lacking, similarly to many other modification enzymes mutated in neurological disorders and cancers (Dimitrova, Teysset, and Carré 2019; Suzuki 2021). However, considerable contributions have been made with the development of detection methods and the use of model organisms with conserved molecular circuitry of modification. For example characterization of yeast ACL methylation complexes allowed discovery of their conservation in humans, as well as supported the requirement for tRNA modifications in a specific order. In fact, it was found that *FTSJ1* mutations in patient families 6 and A3 above (Table 1) showed abolished Cm32 and Gm34 on $tRNA^{Phe}$, consequently lack the Peroxywybutosine hypermodification of position 37 (o2yW37) (Guy et al. 2015). Moreover, a mutation affecting the catalytic pocket of FTSJ1 (family 7 above) lacks $tRNA^{Phe}$ Gm34, but carries Cm32 and o2yW37. The equivalent mutation on Trm7 in *S. cerevisiae* had the same outcome on the modification status of $tRNA^{Phe}$. This result supports once again the importance of correct $tRNA^{Phe}$ modification, especially on the wobble position when it comes to neurological function, and at the molecular level, for better codon-anticodon recognition (Guy et al. 2015; J. Li et al. 2020; Nagayoshi et al. 2021).

This knowledge acquired through model organisms as well as patient derived cells constitutes a solid basis for future research. Interestingly, studies on the Ftsj1 mouse model recapitulates neurological impairments including pain insensitivity, anxiety, impaired learning and memory (Jensen et al. 2019; Nagayoshi et al. 2021). In *Drosophila*, the discovery of *FTSJ1* orthologs provides an important contribution, as well as a starting point for studies regarding specific functions of each of the two modifications performed by FTSJ1 in an organism that evolved one enzyme for each position (Angelova et al. 2020; Brazane et al. 2023). Pending questions regarding the molecular function of FTSJ1 in RNAi pathways have become more intriguing, with the discovery of hAGO1 variants causing intellectual disability (Sakaguchi et al. 2019;

Niu et al. 2022; Schalk et al. 2022; Duan et al. 2023). Recent findings about AGO1 functions and pathogenesis also represented one of the areas of focus of my PhD.

4- PhD project and goals

During the four years of my PhD studies, I focused on the functions of the TRM7 family of RNA methyltransferases in Human cells, and the model organism *Drosophila melanogaster*. My work was organized toward three main axes of studies, the first one is related to the study of fly CG7009 (TRM7_34) function in small non-coding RNA pathways (Angelova et al. 2020). The second axis is related to the functional study of FTSJ1 functions in human cell lines (Brazane et al. 2023). The third and last one is a new project I initiated in order to understand whether FTSJ1 dependent wobble Nm affects protein synthesis, as observed in many wobble modification mutants, including the yeast counterpart.

Following the genome wide screen conducted in the lab a few years ago (Carré et al. 2013), a thorough study of the two fly orthologs *CG7009* (*TRM7_34*) and *CG5220* (*TRM7_32*) was reaching its final stages when I joined my team.

I- The first goal of my PhD was to perform revision experiments requested for this article (Angelova et al. 2020). These include studying the causality of small regulatory RNA pathways deregulation in *Drosophila FTSJ1* mutants by assessing the levels of AGO2, the main ubiquitous effector of the fly siRNA and AGO2-dependent miRNA pathways. Deregulation of the somatic piRNA pathway was also observed in *Drosophila FTSJ1* mutant background on ovarian follicular cells. In this regard I performed RT-qPCR experiments to assess relative derepression of target transposable elements in this tissue.

At the end of this project two questions remained unsolved, which led to the next chapters of my research.

- What is the mechanism linking tRNA 2'-O-Methylation loss to small non-coding RNA pathways deregulation?

- Is small non-coding RNA deregulation possibly linked to FTSJ1 related intellectual disability?

II- The second goal of my PhD was to contribute to the transcriptome and small RNA profiles of patient cells, as well as study the function of FTSJ1 in neurogenesis and neural morphology.

Previous studies on FTSJ1, including our own, suggest a function for *Wobble* Nm in translation efficiency and fidelity, notably in stop codon readthrough (Trzaska et al. 2020).

III- The third goal of my PhD was to investigate the potential functions of FTSJ1 in stop codon readthrough and codon specific regulation by FTSJ1 substrates in patient cells. To this end, I used polysome profiling and Ribosome footprint sequencing (RiboSeq) analysis with the help of Dr. Isabelle Hatin and Hugo Arbes from the lab of Dr. Olivier Namy at I2BC in Gif-sur-Yvette.

Results

Preamble

Following the genome wide screen conducted in the lab a few years ago (Carré et al. 2013), two *Drosophila* orthologs of the human *FTSJ1* were discovered and characterized. A thorough study of the two previously uncharacterized genes *CG7009* and *CG5220*, was conducted in the lab by two former PhD students Margarita T. Angelova and Dilyana G. Dimitrova. Characterization of their functions as tRNA 2'-O-Methyltransferases, of the full spectrum of tRNA substrates, as well as functional studies of their regulatory roles in the small non-coding RNA pathways were significantly advanced before I joined the lab.

Following my arrival to the lab of Dr. Carré as a Master student in 2019, and soon after as a PhD student, I started tackling the molecular mechanisms related to RNAi regulation by tRNA methylation enzymes that remained elusive. As it was observed that *CG7009* loss caused tRNA fragmentation and their accumulation, I performed small RNA quantifications from AGO2 precipitates in order to determine if the accumulated tRNA fragments create discrepancy in the natural loading of AGO2 in mutant condition for *CG7009*. These experiments have so far been inconclusive. I then focused on the requested revision experiments for an article (Angelova et al. 2020), namely RT-qPCR experiments to validate transposable elements deregulation in CG7009. Importantly, I also validated the downregulation of AGO2 mRNA, the main effector of RNAi silencing. This last observation re-open a whole field of investigation in my lab, mainly: how a tRNA methyltransferase affects small non-coding RNA pathways ? The article (Chapter I below and (Angelova et al. 2020)) was published in January 2020 in the *Nucleic Acids Research* journal, I signed this article as co-author.

The human *FTSJ1* is known for decades to be mutated in a genetic neurodevelopmental disorder associated with intellectual disability, but when I started my Master and PhD studies, little functional studies have been implemented on

FTSJ1, and no progress to elucidate the molecular mechanisms in place upon loss of *FTSJ1*. At the time, only three tRNA targets were found to be modified by FTSJ1 using Mass spec approaches on purified tRNAs known to be modified by the yeast counterpart Trm7. A project initiated by Dilyana arose with main questions revolving around the characterization of the full tRNA-ome of FTSJ1, as well as the investigation of potential of FTSJ1 to regulate small non-coding RNA pathways similarly to our original observations in *Drosophila*. This project was implemented by the virtue of patient derived Lymphoblastoid Cell Lines (LCL) that our lab acquired from collaborators in Australia and France (detailed in (Brazane et al. 2023)).

During my first year of PhD I focused mainly on studying the function of FTSJ1 in translation regulation with an emphasis on stop codon readthrough of *Drosophila* AGO2. First, I constructed and tested a construct containing AGO2 with a Flag tag downstream of the *in frame* UGA stop codon. The ribosome profiling experiments on patient cells, as well as the AGO2 readthrough project had been initially delayed by the COVID-19 pandemic, and ultimately gave no conclusive results for the latter one (See results chapter III). After my return to the lab, I managed to complete the transcriptome validation studies started by Dilyana, as well as initiated the studies of FTSJ1 in a new cellular model, the human Neural Progenitor cells (NPC). I managed to conclude this second article, and performed the revision experiments required by the reviewers. The article was published in April 2023 in the Life Science Alliance (LSA) journal (Brazane et al. 2023). For a short version in French, please refer to this highlight I wrote about this article that was published by the Sorbonne University press.

https://sciences.sorbonne-universite.fr/actualites/les-modifications-darn-modulent-la-morphologie-et-la-fonction-des-neurones

At the end of my PhD, I received new results from the ribosome profiling experiments that I performed on patient lymphocytes in collaboration with the lab of Dr. Olivier Namy, which brought insight into codon specific signatures associated with FTSJ1.

These results are part of the third results chapter dedicated to investigation of FTSJ1's role in translation.

Chapter I: *"tRNA 2'-O-methylation by a duo of TRM7/FTSJ1 proteins modulates small RNA silencing in Drosophila"*

A genome wide screen was conducted prior to this study revealing a novel regulator of the AGO2-dependant miRNA pathway in *Drosophila melanogaster* Schneider 2 (S2) cells. Deregulation in small non-coding RNA pathways in *Drosophila melanogaster* was observed upon knockdown of *CG7009*, an uncharacterized protein coding gene with high sequence homology to the Trm7 family of 2'-O-Methyltransferases. An additional paralog encoded by *Drosophila* species, also uncharacterized, called *CG5220* was discovered. Studies on genetic knock-down and loss of function (KO) mutations generated for each gene have demonstrated that *CG7009* and *CG5220* are functional orthologs of the yeast *Trm7* and human *FTSJ1* respectively, responsible for a rare genetic X-Linked intellectual disability.

Using MALDI-TOF mass spectrometry and the innovative RiboMethSeq method, we show that CG5220 and CG7009 catalyze tRNA 2'-O-methylation of the 32^{nd} and 34^{th} nucleotides respectively. This result highlights a fundamental difference between *Drosophila* and other species only encoding one enzyme for methylation of both positions like in mammals, yeast, and Archaea. Nonetheless, the tRNA substrates remain strongly conserved as Nm is deposited by Trm7 family enzymes in $tRNA^{Phe}$, $tRNA^{Trp}$ and $tRNA^{Leu}$. Additionally we identified for the first time Cm32 to be modified by TRM7 family members, namely CG5220, in $tRNA^{Gln}$ and $tRNA^{Glu}$. *CG7009* and *CG5220* mutants are viable and fertile although displaying deregulations in all of the three main small non-coding RNA pathways (mi-, si- and piRNA), as well as an increased tRNA fragmentation. Many phenotypes are associated with these mutations including a lifespan reduction, faulty antiviral response, and mobility issues. Our findings allowed for the first time the characterization of the gene products responsible for tRNA anticodon loop 2'-O-methylation in *Drosophila*. Consequently, the conservation of the modification profile of tRNAs Phe, Leu and Trp was found to be highly conserved, thus, we proposed re-naming these genes

TRM7_32 and *TRM7_34*, for their gene family, and corresponding substrate positions. This work also revealed, for the first time, an unexpected role for *Drosophila* 2'-O-Methylatransferases in all three canonical small non-coding RNA pathways through mechanisms that remain to be discovered. This last discovery opens a brand new investigation in my lab using human cells and tackles the conservation of these observations made in the fly model. This gave rise to the second part of the project (Chapter II results) of my PhD studies.

Supplemental material can be accessed online: https://academic.oup.com/nar/article/48/4/2050/5707191#supplementary-data

PRINT ISSN: 0305-1048
ONLINE ISSN: 1362-4962

Nucleic Acids Research

VOLUME 48 ISSUE 4 2020
https://academic.oup.com/nar

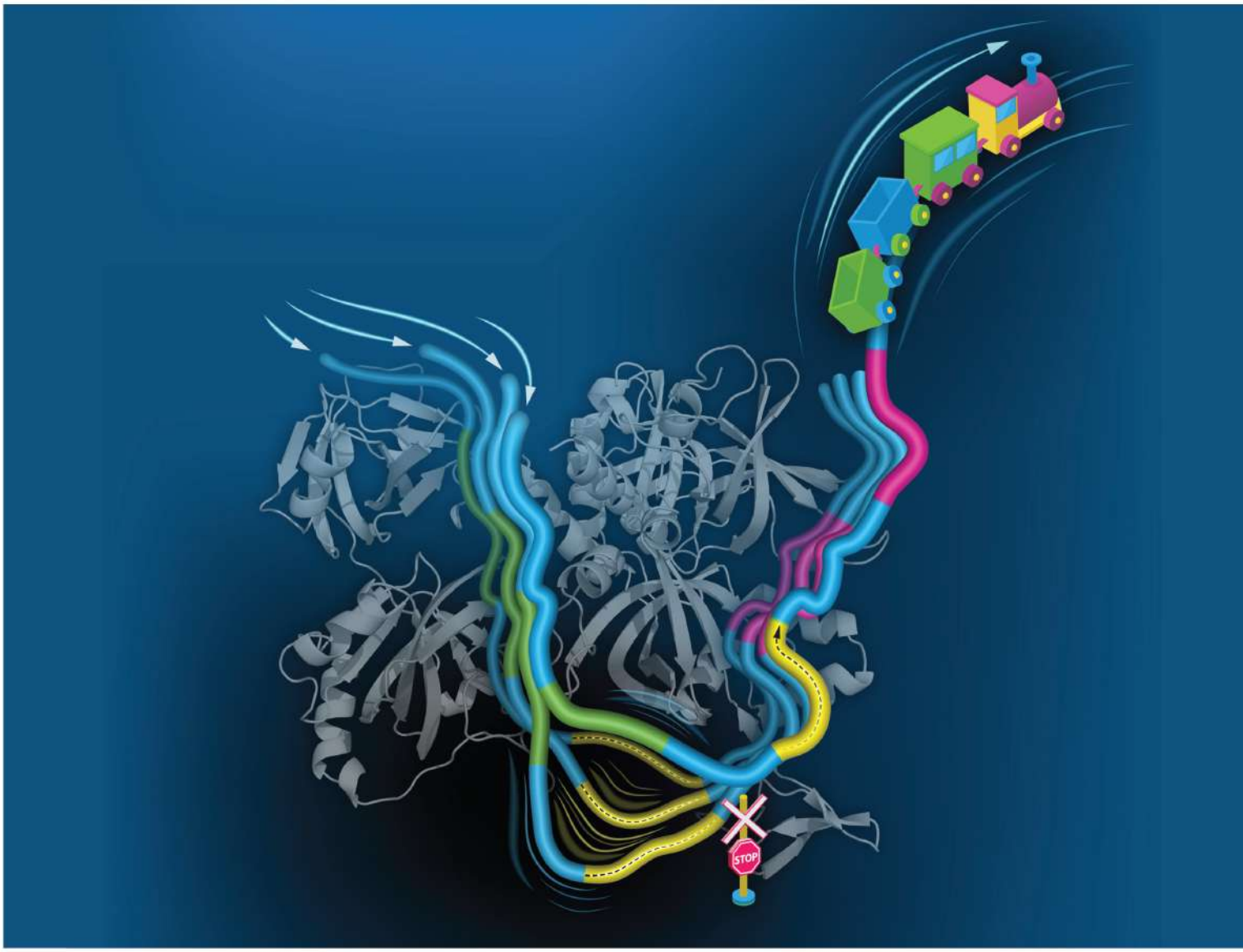

OXFORD
UNIVERSITY PRESS

Open Access

No barriers to access – all articles freely available online

2050–2072 *Nucleic Acids Research, 2020, Vol. 48, No. 4* *Published online 16 January 2020*
doi: 10.1093/nar/gkaa002

tRNA 2′-*O*-methylation by a duo of TRM7/FTSJ1 proteins modulates small RNA silencing in *Drosophila*

Margarita T. Angelova[1,†], Dilyana G. Dimitrova[1,†], Bruno Da Silva[1], Virginie Marchand[2], Caroline Jacquier[1], Cyrinne Achour[1], Mira Brazane[1], Catherine Goyenvalle[3], Valérie Bourguignon-Igel[2,4], Salman Shehzada[1], Souraya Khouider[1], Tina Lence[6], Vincent Guerineau[5], Jean-Yves Roignant[6,7], Christophe Antoniewski[8], Laure Teysset[1], Damien Bregeon[3], Yuri Motorin[4], Matthias R. Schaefer[9] and Clément Carré[1,*]

[1]Transgenerational Epigenetics & small RNA Biology, Sorbonne Université, Centre National de la Recherche Scientifique, Laboratoire de Biologie du Développement - Institut de Biologie Paris Seine, 9 Quai Saint Bernard, 75005 Paris, France, [2]Next-Generation Sequencing Core Facility, UMS2008 IBSLor CNRS-Université de Lorraine-INSERM, BioPôle, 9 avenue de la Forêt de Haye, 54505 Vandoeuvre-les-Nancy, France, [3]Eucaryiotic Translation, Sorbonne Université, CNRS, Institut de Biologie Paris Seine, Biological Adaptation and Ageing, Institut de Biologie Paris Seine, 9 Quai Saint bernard, 75005 Paris, France, [4]Ingénierie Moléculaire et Physiopathologie Articulaire, UMR7365, CNRS - Université de Lorraine, 9 avenue de la Forêt de Haye, 54505 Vandoeuvre-les-Nancy, France, [5]Institut de Chimie de Substances Naturelles, Centre de Recherche de Gif CNRS, 1 avenue de la Terrasse, 91198 Gif-sur-Yvette, France, [6]Institute of Molecular Biology, Ackermannweg 4, 55128, Mainz, Germany, [7]Center for Integrative Genomics, Génopode Building, Faculty of Biology and Medicine, University of Lausanne, CH-1015, Lausanne, Switzerland, [8]ARTbio Bioinformatics Analysis Facility, Sorbonne Université, CNRS, Institut de Biologie Paris Seine, 9 Quai Saint Bernard, 75005 Paris, France and [9]Division of Cell and Developmental Biology, Center for Anatomy and Cell Biology, Medical University of Vienna, Schwarzspanierstrasse 17, A-1090 Vienna, Austria

Received July 17, 2019; Revised December 30, 2019; Editorial Decision December 31, 2019; Accepted January 01, 2020

ABSTRACT

2′-*O*-Methylation (Nm) represents one of the most common RNA modifications. Nm affects RNA structure and function with crucial roles in various RNA-mediated processes ranging from RNA silencing, translation, self *versus* non-self recognition to viral defense mechanisms. Here, we identify two Nm methyltransferases (Nm-MTases) in *Drosophila melanogaster* (CG7009 and CG5220) as functional orthologs of yeast TRM7 and human FTSJ1. Genetic knockout studies together with MALDI-TOF mass spectrometry and RiboMethSeq mapping revealed that CG7009 is responsible for methylating the wobble position in tRNA^{Phe}, tRNA^{Trp} and tRNA^{Leu}, while CG5220 methylates position C32 in the same tRNAs and also targets additional tRNAs. *CG7009* or *CG5220* mutant animals were viable and fertile but exhibited various phenotypes such as lifespan reduction, small RNA pathways dysfunction and increased sensitivity to RNA virus infections. Our results provide the first detailed characterization of two TRM7 family members in *Drosophila* and uncover a molecular link between enzymes catalyzing Nm at specific tRNAs and small RNA-induced gene silencing pathways.

INTRODUCTION

The existence of RNA modifications has been known for over 50 years and many of the pioneering studies addressed the function of RNA modifications in abundantly expressed RNAs such as transfer RNAs (tRNAs) and ribosomal RNAs (rRNAs). tRNAs are the most heavily modified RNAs (up to 25% nucleotides/tRNA, (1)). tRNAs are modified post-transcriptionally and the biosynthesis of modified nucleosides requires different modification enzymes acting sometimes sequentially at distinct steps of tRNA maturation (2,3). The complex mechanisms underlying the stepwise modification of tRNAs were largely deciphered in the yeast *Saccharomyces cerevisiae*, as well as in studies conducted in prokaryotes and *Archaea*. More recently, some of the seminal findings in single-cell organisms were revisited using multi-cellular models, including studies that aim

*To whom correspondence should be addressed. Tel: +33 1 44 27 34 39; Fax: +33 1 44 27 34 16; Email: clement.carre@gmail.com
†The authors wish it to be known that, in their opinion, the first two authors should be regarded as Joint First Authors.

at understanding how mutations in tRNA modification enzymes affect organismal development and disease etiology.

2′-*O*-Methylation (Nm) is a common RNA modification. The addition of a methyl group to the 2′ hydroxyl of the ribose moiety of a nucleoside creates Nm (reviewed in (4,5)). Nm can occur at any nucleotide explaining the abundant nature of this modification. Nm residues are found at multiple and often highly conserved positions in tRNAs, rRNAs, and small nuclear RNAs (snRNAs) (6–8). In eukaryotes, RNA modification reactions resulting in Nm on rRNAs and snRNAs are frequently catalyzed by evolutionarily conserved C/D-box small RNAs (SNORDs) involving guide ribonucleoprotein particles (RNPs) which contain the Nm-methylase fibrillarin. Small nucleolar RNPs (snoRNPs) mediate the deposition of Nm at rRNAs (9–12) while small Cajal bodies RNPs (scaRNPs) direct Nm-modification to snRNAs (13–17). In contrast, most of the Nm deposition occurring in eukaryotic tRNAs is mediated by stand-alone proteins without the need for guidance by small RNAs. However, recently it was reported that one snoRNA and one scaRNA can guide Nm deposition to $tRNA^{Met}$ in mammalian cells (18). Importantly, Nm deposition occurs also at 3′-terminal nucleotides in small non-coding RNAs (sncRNAs) such as microRNAs (miRNAs) and small-interfering RNAs (siRNAs) in plants (19–21), in Argonaute-2 (Ago2)-loaded siRNAs and miRNAs in flies and in PIWI-interacting RNAs (piRNAs) in animals (22–24). More recently, Nm was also reported to be internally deposited in messenger RNA (mRNA) (25–27).

Nm can affect RNAs in multiple ways as it increases hydrophobicity, protects RNAs from nuclease degradation (18,24,28), stabilizes helical structures or modulates interactions with proteins or other RNAs (29–40).

An important variety of tRNA modifications are deposited at the wobble position N_{34} in the anticodon loop (ACL), and at the anticodon-adjacent position N_{37}. Among the different tRNA isoacceptors, these two positions contain highly conserved modifications, which is suggestive of their physiological importance. Accordingly, it was shown that ACL modifications prevented frameshifting during translation (41,42) and are thus necessary for the correct decoding of genetic information (43).

The methyltransferase complex catalysing Nm formation in the ACL of mammalian and yeast tRNAs comprises the Nm-methyltransferases (Nm-MTases) FTSJ1 or TRM7, respectively. These enzymes associate with specific proteins: THADA/TRM732 for Nm_{32} and WDR6/TRM734 for Nm_{34} formation (2,44,45). Cm_{32} and, more importantly Nm_{34}, are required for efficient formation of a third modification, wybutosine (yW) at m^1G_{37} in $tRNA^{Phe}$ (46–48). The same sequential circuitry is conserved in the phylogenetically distant yeast *Schizosaccharomyces pombe* (45), while the formation of peroxywybutosine (o2yW) at position 37 is also affected in humans lacking FTSJ1 (45,49).

Several studies have uncovered crucial roles for FTSJ1/TRM7 in normal and pathological conditions (reviewed in (4,5,50)). While in *S. cerevisiae* and *S. pombe*, lack of TRM7 affected translational regulation and growth (48,51,52), *FTSJ1* mutant mice showed impairment in their learning capacity, as well as significantly reduced pain sensing (hypoalgesia) and altered gene expression profiles (53). Similarly, in humans, several mutations in *FTSJ1* were shown to be causative of a neurodevelopmental disorder known as Non-Syndromic X-linked Intellectual Disability (NSXLID) (49,53–55). Importantly, expression of human FTSJ1 in yeast suppressed the severe growth defects observed in *trm7Δ* mutants, demonstrating that the TRM7 enzyme family and their RNA targets are highly conserved (45).

While the molecular function of yeast and human Nm-MTases acting on specific tRNAs has been established, the molecular mechanisms causing the complexity of observed mutant phenotypes have not been fully elucidated. Importantly, a tractable multicellular model system that would allow studying Nm-MTase function systematically and thereby bridge the growth phenotypes observed in *trm7* deficient yeast with the complex phenotypes observed in *FTSJ1*-mutant human has been lacking.

In this report, we show that, in contrast to yeast and humans, *Drosophila melanogaster* has evolved two Nm-MTase genes, *CG5220* and *CG7009*, whose products specialized their activity to respectively methylate positions 32 and 34 in the ACL of specific tRNAs. We demonstrate that the catalytic specificity of these Nm-MTases is dependent on the position rather than the identity of the ACL nucleotides. Importantly, lack of these proteins reduced *Drosophila* lifespan and impaired various cellular pathways, which employ small RNAs to achieve post-transcriptional silencing. Hence, *CG5220* and *CG7009* mutant animals were more sensitive to RNA virus infections and showed dysfunctional control of transposable elements, suggesting a molecular link between Nm RNA modifications and small RNA gene silencing pathways in *Drosophila*.

MATERIALS AND METHODS

Automig DRSC 2.0 genome-wide screening library

We screened 22.490 dsRNA of 400 bp length on average allowing the inactivation of 94.3% of all annotated *Drosophila* genes, including predicted genes (library version DRSC 2.0). About 13 900 genes are represented by the collection (∼66 assay plates), targeted on average by one to two dsRNAs per gene. More information about the DRSC Genome-wide RNAi Library (DRSC 2.0) can be found at the DRSC/TRiP Functional Genomics Resources. The recommended protocol was followed (56) on seven series of duplicated 384-well plates, which were screened over a period of three weeks. Briefly, 250 ng/well (5 μl at 50 ng/μl) of each dsRNAs were distributed into 384-well culture plates in 62 plates. One plate is organized in 16 rows (A-P) and 24 columns (1–24). Each well thus possesses a unique identification number consisting of the plate number followed by well coordinates. Each dsRNA has a unique identification number (DRSC#####). A *WellMate* dispenser (Matrix Technologies) was used to distribute the *automiG* S2R+ cell culture suspension into the 384-well plates (25.000 cells at a concentration of 2.5×10^6 cells/ml). After dsRNA internalization into the cells for one hour, 30 μl of 10% heat-inactivated fetal calf serum was added per well. The cells were incubated for 4 days with the dsRNA before the expression of *automiG* in order to allow the complete internalization of the dsRNAs, the degradation of the target mR-

NAs and the catabolism of the corresponding protein. At day 5, *automiG* expression was induced with 600 μM of $CuSO_4$/well. After 24 h of *automiG* induction, the cells were imaged on an *Opera* confocal microscope (Evotec Technologies, Perkin Elmer) using an automated acquisition system allowing fast imaging of the epifluorescence in each well of a large number of plates. In addition, Analyst®GT multimode reader (Molecular Devices) – a plate reader allowing the fast and sensible read-out of 40 plates per group was used.

A validation screen was performed in triplicate using the same conditions as those used in the primary screen described above. After a 48 hours incubation period, plates were centrifuged for one minute at 800 g and the culture medium was carefully removed. 25 μl of cracking buffer (125 mM Tris pH 6.8, 5% ß-mercapto-ethanol, 2% SDS, 4 M urea) was added in each well and 8 μl of protein extracts were analyzed by western blotting. Further information is available upon request and at the *DRSC/TRiP Functional Genomics Resources*, Harvard University.

Amino Acid conservation and phylogenetic analysis

Sequence alignments and visualization were performed in Kalign (www.ebi.ac.uk/Tools/msa/kalign/) and Unipro UGENE 1.32.0. Percentage of amino acid (aa) identities and coverages between CG7009, CG5220, TRM7 and FTSJ1 proteins were determined on the Ensembl project website (www.ensembl.org). For phylogenetic analysis, protein alignments were performed using mafft v7.407 with default parameters (57). Removal of positions with >50% of gaps was obtained by using trimal v1.4 (58). Phylogenetic analysis was performed using raxml v8.2.12 (59) under the PROTGAMMALG model by combining a rapid bootstrap analysis (100 replicates) and search for the best ML tree (-f a option).

Total RNA extraction for MALDI-TOF and RiboMethSeq analysis

3–5 days old females and males were homogenized on a Precellys 24® tissue homogenizer (Bertin Technology) in 1 ml TRI-reagent/50 flies (Sigma Aldrich). Total RNA from 20 ml of fly lysates (1000 flies), was extracted with 8 ml of chloroform and precipitated with two-thirds volumes of isopropanol. The pellets were air-dried and resuspended in RNase-free water.

Purification of $tRNA^{Phe(GAA)}$

Total RNA preparations (∼7 mg) were supplemented with LiCl to a final concentration of 0.8 M and incubated overnight at 4°C to precipitate high-molecular mass molecules. The precipitate was eliminated by centrifugation and the supernatant was supplemented with two volumes of 100% ethanol and incubated at –20°C for two hours to precipitate small RNAs. After centrifugation, pelleted small RNAs were washed twice in 70% ethanol and resuspended in one ml of RNase-free water. tRNAs were further purified using the NucleoBond RNA/DNA 400 kit (Macherey-Nagel) following manufacturer's instructions, except that the elution step was performed with 5 ml of 100 mM Tris–acetate (pH 6.3); 15% ethanol and 600 mM KCl. Eluted tRNA were ethanol precipitated and resuspended in one ml of RNase-free water. Purification of $tRNA^{Phe(GAA)}$ was performed using a 5′ biotinylated complementary oligonucleotide (5′-biotin-TGGTGCCGAAACCCGGGA TTGAACCGGGG-3′) coupled to Streptavidin Magnesphere Paramagnetic particles (Promega). Annealing of specific tRNA was performed in 1× TMA buffer (Tris–HCl pH 7.5 10 mM, ethylenediaminetetraacetic acid (EDTA) 0.1 mM, tetramethylammonium chloride 0.9 M) after heating the mixture at 95°C for 3 min followed by cooling to 60°C for 30 min. Paramagnetic particles were washed three times with 1× TMA buffer and specific $tRNA^{Phe(GAA)}$ was recovered by heating the final suspension at 95°C for 3 min. $tRNA^{Phe(GAA)}$ was desalted and concentrated four times to 50 μl using Vivacon 500 devices (Sartorius; 2000 MWCO) using 100 mM ammonium acetate (pH 5.3) as a final buffer. The average yield obtained from 7 mg of total RNA was ∼2–7 μg of purified $tRNA^{Phe(GAA)}$. *Note*: If used for RiboMethSeq, LiCl was washed away because of its interference with adaptor ligation during the cDNA library preparation.

MALDI-TOF analysis of digested $tRNA^{Phe(GAA)}$

For mass spectrometry analysis, ∼500 ng of $tRNA^{Phe(GAA)}$ were digested with 100 units of RNase T1 (Sigma) in a final volume of 10 μl at 37°C for 4 h. RNase T1 cleaves the phosphodiester bond between the 3′-guanylic residue and the 5′-OH residue of adjacent nucleotides and generates 3′-phosphate nucleosides. One microliter of digest was mixed with 9 μl HPA (40 mg/ml in water:acetonitrile 50:50) and 1 μl of the mixture was spotted on the MALDI plate and air-dried ('dried droplet' method). MALDI-TOF MS analyses were performed directly on the digestion products using an UltrafleXtreme spectrometer (Bruker Daltonique, France). Acquisitions were performed in positive ion mode.

RiboMethSeq

RiboMethSeq analysis of *D. melanogaster* tRNAs was performed as described in (60). Briefly, tRNAs extracted from whole flies were fragmented in 50 mM bicarbonate buffer pH 9.2 for 15 min at 95°C. The reaction was stopped by ethanol precipitation. The pellet was washed with 80% ethanol and sizes of generated RNA fragments were assessed by capillary electrophoresis using a small RNA chip on Bioanalyzer 2100 (Agilent, USA). RNA fragments were directly 3′-end dephosphorylated using 5 U of Antarctic Phosphatase (New England Biolabs, UK) for 30 min at 37°C. After inactivation of the phosphatase for 5 min at 70°C, RNA fragments were phosphorylated at the 5′-end using T4 PNK and 1 mM ATP for one hour at 37°C. End-repaired RNA fragments were then purified using RNeasy MinElute Cleanup kit (QIAGEN, Germany) according to the manufacturer's recommendations. RNA fragments were converted to library using NEBNext® Small RNA Library kit (ref#E7330S, New England Biolabs, UK or equivalent from Illumina, USA) following the manufacturer's instructions. DNA library quality was assessed using a High Sensitivity DNA chip on a Bioanalyzer 2100. Library sequencing

was performed on Illumina HiSeq 1000 in single-read mode for 50 nt. Primary analysis of sequencing quality was performed with RTA 2.12 software, to insure > Q30 quality score for >95% of obtained sequences.

Following SR50 sequencing run, demultiplexing was performed with BclToFastq v2.4, reads not passing quality filter were removed. Raw reads after demultiplexing were trimmed with Trimmomatic v0.32 (61). Alignment to the reference tDNA sequences was performed with bowtie 2 ver2.2.4 (62) in End-to-End mode. Uniquely mapped reads were extracted from *sam file by RNA ID and converted to *.bed format using bedtools v2.25.0 (63). Positional counting of 5′-and 3′-ends of each read was performed with awk Unix command. Further treatment steps were performed in R environment (v3.0.1). In brief, 5′-and 3′-end counts were merged together by RNA position and used for calculation of ScoreMEAN (derived from MAX Score described previously), as well as Scores A and B (64) and MethScore (65). Scores were calculated for two neighboring nucleotides. Profiles of RNA cleavage at selected (candidate and previously known) positions were extracted and visually inspected.

Northern blotting

For northern blotting analysis of tRNA, 10 μg of total RNA from adult flies were resolved on 15% urea-polyacrylamide gels, transferred to Hybond-NX membrane (GE Healthcare) and EDC-crosslinked (Sigma Aldrich). The membranes were probed with 5′-^{32}P end-labeled DNA oligonucleotides using T4 polynucleotide kinase (Fermentas). Hybridization was performed overnight at 38–40°C in PerfectHyb Plus (Sigma) hybridization buffer. Probe sequences are available in the Primers and Probes section. More details on NB procedure are available in (66,67).

RNA interference in S2R+ cells

Double-stranded RNAs (dsRNA) were synthesized by *in vitro* transcription (MEGAscript® T7 Kit, Ambion) of PCR products amplified from w^{1118} genomic DNA using primers flanked by T7 promoters. Sequences of amplicon templates for dsRNA production are available from the *Drosophila* RNAi Screening Center (http://www.flyrnai.org/cgi-bin/RNAi_gene_lookup_public.pl, e.g. Ago2: DRSC10847, CG7009: DRSC39198). PCR products for T7 transcription of *fushi tarazu* (Ftz) and Firefly luciferase dsRNAs were amplified using primers: T7_Ftz_FW and T7_Ftz_Rev and T7_F_Luc_FW and T7_F_Luc_Rev, respectively (Primers and Probes section and (66)).

S2R+ cell transfection

100 μl of cells at 10^6 cells/ml resuspended in Schneider's *Drosophila* medium (GIBCO, Invitrogen) were plated in 96-well plates. Cells were transfected with dsRNA or co-transfected with dsRNA and the corresponding sensor using Effectene (QIAGEN) following the manufacturer's instructions. Thirty minutes after transfection 50 μl Schneider's *Drosophila* medium (GIBCO, Invitrogen), completed with 10% heat-inactivated fetal calf serum, 100 U/ml penicillin and 100 mg/ml streptomycin were added. Cells were grown at 23°C without CO_2. After 24–48 h, $CuSO_4$ was added to a final concentration of 600 μM and GFP fluorescence was followed using an inverted epifluorescence basic microscope. For Ago2-mediated miRNA pathway involvement (*automiG*), cells were co-transfected with 0.1 μg of *automiG*-vector and 0.32 μg of dsRNA targeting either *Ago2, CG7009* or *Ftz, Dcr1, Dcr2, Drosha, Ago1*. Forty eight hours later, the *automiG* promoter was induced by adding $CuSO_4$ to a final concentration of 600 μM (more details in (66)).

For the luciferase assay experiment, S2R+ cells were treated for 4 days with dsRNA inactivating specifically the indicated genes. Cells were co-transfected with two plasmids expressing the Firefly and Renilla luciferases in addition to a dsRNA against Firefly. Luciferases activities were measured 48 h after transfection. The averages of the activity ratios from Firefly/Renilla luciferases from three independent biological replicates were plotted normalized to the average of a control dsRNA (GFP) which was set to 1 (+/– the standard deviations). * indicates $P < 0.05$ in a Student's *t*-test.

Western blotting

Expression of GFP was analyzed in *automiG* induced cells by western blotting using mouse anti-GFP (Roche®) and anti-Mbf1 antibodies (66) as loading and transfer control. Seventy two hours after the dsRNA transfection and *automiG* vector induction, the culture medium was removed and 80 μl of Sample Buffer Laemmli 2X (Sigma®) was added in each well. The samples were boiled (95°C) and 18 μl were loaded onto a 4–20% Mini-PROTEAN®TGX™ 12 well-gel (Bio-Rad). After transfer onto a PVDF (Amersham Hybond, GE Healthcare) or nitrocellulose membrane, membranes were blocked in 5% milk, dissolved in 1× TBS-T (20 mM Tris-Base, 150 mM NaCl, Tween-20 (Polyoxyethylene sorbitane monolaureate) to 0.05%) and incubated overnight with anti-GFP (1:2000) or anti-Mbf1 (1:10.000) antibodies diluted in the blocking solution. After three times 15 min washes, appropriate secondary antibody (1:10 000) coupled to alkaline phosphatase (Promega) was added and incubated for one hour at room temperature. Detection was performed using BCIP (5-bromo-4-chloro-3-indolyl-phosphate) and NBT (nitro-blue-tetrazolium, (ThermoFischer) reagents diluted in AP buffer (100 mM Tris–HCl pH 9.5, 100 mM NaCl, 5 mM $MgCl_2$).

automiW

Experiments with the *automiW* eyes sensor were performed as described in (68). Eye images of the same aged flies were acquired with an Axio-ApoTome (Zeiss) and ZEN2 software or with a WILD M3Z (Leica) binocular combined with a Q IMAGING Color 12 bit (Q27959) camera and QCapture Pro software.

DCV injection

Flies with the following genotypes were subjected to intra-thoracic injection with the

Drosophila C virus (DCV): $CG7009^{e02001}$/+ (controls). $CG7009^{e02001}$/$CG7009^{e02001}$(*CG7009* mutants). $CG5220^{K28A}$/$CG5220^{K28A}$(*CG5220* catalytically dead mutant). Two to four days old flies were divided in tubes of 10 (5 males + 5 females) and 20 flies from each genotype were injected with DCV while 20 other flies were injected with adult Injection Buffer (controls), containing 10 mM Tris pH 6.3 and 1 mM $MgCl_2$. Each fly was injected with 4.6 nl of *DCV* concentration of 2×10^6 PFU/ml (9.2 PFU/injection). Intra-thoracic injections were made using the Drummond Automatic Nanoliter Injector 'NANOJECT II'. After injection, flies were kept at 25°C. Three to four days after the injection and prior to death, three injected flies from each genotypes and conditions (+ or – DCV) were frozen at –20°C. Two to three flies from each condition were then crushed with a pestle in TRI-Reagent (Sigma Aldrich) and total RNA was extracted as described above. DNase digestion and RT-qPCR were carried out as described with DCV_FW and DCV_Rev-specific primers and primers for Rp49 for normalization (Primers and Probes section).

CRISPR/Cas9-mediated genome editing and genotyping

Mutant alleles for *CG5220* were generated using CRISPR/Cas9-mediated editing in *Drosophila* as previously described (69). The $CG5220^{K>A}$ allele was obtained using the gRNA (guide RNA) sequence: 5′-CTTCGAGCAACTTGAAGGCACTCC-3′ and a single-stranded DNA donor template ssDNA: 5′-TTCATATATT TATTTACAATGGGGAAAACATCAAAGGACAAA AGAGATATCTATTACCGACAAGCCAAAGACGA AGGCTGGAGGGCGAGGAGTGCCTTCGCGTTGC TCCACGTGGACGAAGCCTACGGAATTCTAA-3′ for homology-dependent repair to obtain the K to A mutation in CG5220:

A mix of 150 ng/μl vector expressing the gRNA and Cas9 protein as well as 150 ng/μl ssDNA were injected in pre-blastoderm w^{1118} embryos. Screening for flies containing the substitution was carried out by PCR on genomic DNA from single F1 males derived from crossing of injected individuals with a balancer stock. The screened sequences correspond to genomic fragments covering 438 bp of the *CG5220* gene. Fly stock denominations are $CG5220^{K>A}$. Visual sequence analysis was carried out using *4Peaks* and *ApE* software.

RT-qPCR

RNA was extracted from whole flies or from dissected ovaries using TRI-Reagent (Sigma Aldrich). After DNase digestion of total RNA using the TURBO DNA-free™ Kit (Ambion), 500 ng were used in a reverse transcription reaction with Random Primers (Promega) and SuperScript® II Reverse Transcriptase (Invitrogen). The cDNA was used to perform qPCR on a CFX96 Touch™ Real-Time PCR Detection System (Bio Rad) using target-specific primers. Rp49 was used for normalization (Primers and Probes section). The analysis was performed using ΔΔ Ct, on three biological replicates. Statistical analysis using a Student's t-test was performed and *P*-values were determined.

Production and affinity purification of recombinant fusion proteins

Glutathione *S*-transferase (GST) fusion constructs were generated by PCR amplification of full-length cDNAs of CG7009 available from BDGP (#SD16956) using standard PCR with VENT polymerase (New England BioLabs). Products were cloned between the EcoRI and NotI restriction sites of the pGEX-4T1 (GE Healthcare) vector using primers CG7009_EcoRI_ATG and CG7009_NotI_Stop. Amplification of full-length cDNAs of *CG33172* (clone MIP10235 in BDGP) was performed using standard PCR techniques using Q5 high fidelity DNA Polymerase (New England BioLabs). Amplification products were cloned between the HindIII and NotI restriction sites of the pET-28a (Novagen) vector (modified to contain FLAG peptide) using the primers CG33172_Hind_ATG and CG33172_NotI_Stop. Competent bacteria TOP10 (Invitrogen) were transformed by heat-shock with 100–200 ng of plasmid DNA according to each manufacturer's instructions. After expression on the corresponding antibiotic resistance genes by incubation for 0.5-1.5 h at 37°C under agitation of 250 rpm, 1/10 and 9/10 of the transformed bacteria were plated on LB agar plates, supplemented with the corresponding antibiotics. GST fusion proteins were expressed in *Escherichia coli* BL21 Star (DE3) (Invitrogen) or C41 (70) and purified over glutathione-coupled resin (Pharmacia) as previously described (71,72). The same protocol was used for purification of pET-28a Flag fusion proteins. Bound peptides were eluted with 400 μg/ml Flag peptide (Sigma) in BC100 buffer for 20 min on ice.

In vitro interaction of GST-CG7009 and FLAG-CG33172

Briefly, GST- alone (control) or fusion proteins GST::G7009 (pGEX4T1-CG7009) and FLAG::CG33172 (pET28a-FLAG-CG33172) were co-expressed in C41 (70) bacteria and purified over Flag-coupled resin (Sigma). Bound proteins were washed three times in 500 mM KCl and eluted on Bio-spin disposable chromatography columns (Bio-Rad) with flag peptide as described in (72). Western blot of the immunoprecipitated recombinant proteins was performed as described in the above section using anti-GST HRP (horseradish peroxidase) conjugate (1:10 000 Amersham GE Healthcare) for 60 min at room temperature under agitation. HRP was detected by enhanced chemiluminescent (ECL).

RNA-seq on S2R+ cells

Knock downs for *CG7009* and *LacZ* (control KD) in S2R+ were performed in a serum-free medium using 7.5 μg of dsRNA per 10^6 cells and stopped 2 h after cell starvation with the addition of the serum-supplemented medium. dsRNA treatment was repeated after 48 h. Cells were collected and total RNAs were extracted 96 h after the first treatment. Libraries were prepared using the Illumina TruSeq Sequencing Kit by following the manufacturer's protocol for paired-end read mode and directional sequencing on an Illumina NextSeq 500 with a read length of 42 bp.

Computational analysis of S2R+ RNA-seq experiments

Basecalling and demultiplexing were performed using bcl2fastq (v2.19). Individual samples were mapped using STAR ((73), v2.5.2b) against ensembl release 90 of the *D. melanogaster* genome (BDGP6). Gene counts were derived using featureCounts ((74), v. 1.5.1). RNA-Seq Analysis Differential expression analysis was performed using Bioconductor v2.38/ DESeq2 v1.18.1 (75,76). Genes were called sig. diff. expressed with an FDR below 5%. The sample Ctrl_3 was excluded as an outlier from the differential expression analysis. The gene list deduced from this analysis is available online at NAR as supplementary material (excel file) and the corresponding libraries publicly accessible for download (see Data availability for detail).

Small RNA sequencing and computational analysis

Library preparation was performed at Fasteris (http://www.fasteris.com). Total RNAs from ovaries were size selected (18 to 30 nt) on denaturing PAGE. The small RNA fraction was then depleted from the 2S rRNA (30 nt) using a highly specific probe developed by Fasteris. 2S rRNA-depleted small RNAs were used to generate multiplexed libraries with Illumina TruSeq Small RNA library preparation kits. Libraries were sequenced using Illumina HiSeq 4000 platforms. Fastq sequence reads were trimmed of the adapter sequences (5′-TGGAATTCTCGGGTGCCAAG-3′) and reads were mapped using Bowtie (77). Only 19–29 nt reads matching the reference sequences with zero or one mismatches were retained for subsequent analyses. For global annotation of the libraries, we used the release 6 of fasta reference files available in FlyBase, including transposon sequences (dmel-all-transposon_6.fasta) and the release 20 of miRBase (http://www.mirbase.org/). For library comparisons, read counts were normalized to the total number of small RNAs matching the *D. melanogaster* genome (release 6). Sequence length distributions and small RNA mappings were generated from bowtie alignments using Python and R (http://www.r-project.org/) scripts, which were wrapped and run in *Galaxy* instance from ARTbio platform (http://artbio.fr/). Tools and workflows used in this study are available for download at NAR as supplementary material (.ga files). The small RNA sequencing data discussed in this publication are accessible at European Nucleotide Archive (ENA) at EMBL-EBI under accession number PRJEB35301 (https://www.ebi.ac.uk/ena/data/view/PRJEB35301).

β-Gal staining of dissected ovaries

Stainings of ovaries were performed as follows: specific sensor lines were crossed with respective RNAi lines for knockdown in germ cells (*nanos*-GAL4) or follicle cells (*tj*-GAL4) of the G1 female ovaries followed by β-Gal staining performed on 3–7 days-old females. Ovaries were dissected in cold 1× PBS, kept on ice, fixed in glutaraldehyde (0.2%)/formaldehyde (2%)/1× PBS at room temperature for 5 min followed by three washes in 1× PBS. Tissues were then incubated in freshly prepared staining solution (1× PBS pH 7.5, 1 mM $MgCl_2$, 4 mM potassium ferricyanide, 4 mM potassium ferrocyanide, 1% Triton X-100, 2.7 mg/ml X-Gal) at 25°C overnight for *Gypsy::LacZ* detection and for 90 min for *burdock::LacZ* detection. The staining solution was prepared with 8% X-Gal (as dimethylformamide solution). After staining, tissues were transferred into 50% glycerol/50% EtOH and mounted for imaging.

Imaging

Ovary and eye images were acquired with a WILD M3Z (Leica) binocular combined with a Q IMAGING Color 12 bit (Q27959) camera and QCapture Pro software. Ovary sizes (area) were calculated in pixels using ImageJ. An unpaired Mann–Whitney (Wilcoxon) test was performed to evaluate the significance of the area differences (P-value $<$ 0.05) between mutant ovaries ($n = 11$) and genetic rescue ovaries ($n = 10$).

Weighing

Average weight for flies in milligrams (mg) was calculated for flies (3 days after hatching) measured on a precision balance (≥0.001 g) after heat dehydration at 95°C (15 min in an open 1.5 ml eppendorf tube) of frozen bodies ($n \geq 14$, where each n is a batch of 10 flies). P-value < 0.001 in a Student's t-test.

Lifespan assays

2–3-day-old male flies Da-GS; UAS-RNAi *CG5220*, *CG7009* were kept at 25 °C in vials with standard medium complemented (RU200) or not (RU0) with RU486. RNAi transgene induction using the Da-Gal4-GS (GeneSwitch) lines was described in (78). Briefly, the Gal4-GS protein is a GAL4 modified protein that recognizes and activates UAS-dependent transgenes only in the presence of RU486 added into *Drosophila* medium food. The number of flies tested was five times 30 flies. To monitor survival rates over time, flies were counted and transferred into new tubes every 2–3 days. Constitutive expression of *CG5220*, *CG7009* KD transgenes was induced by RU486 exposure (20 mg/ml) during adulthood. The exact same protocol was followed for the genetic mutants with the exception of the RU486 exposure. The number of flies tested was five times 30 flies per genotype.

Climbing assays

Sixteen day-old flies were gender-separated and placed into measuring cylinders to assess their locomotion using the climbing assay reported previously (79). Briefly, flies were tapped to the bottom and the number of flies that climb over the 10 cm threshold in 10 s intervals were recorded and counted. Ten female or male flies were used per experiment. Shown data are an average of six independent experiments. $*P < 0.01$; $***P < 0.0001$ in a Student's t-test.

Drosophila stocks

Lab stock ID#	Category	Genotype	Notes
w1118	Mutant allele	w1118	FlyBase ID FBal0018186
CG7009^{e02001}	Mutant allele	w1118; CG7009e02001 (mini-white)	Bloomington stock #18008 cleaned by backcrossing over 10 generations.
Def9487	Deficiency for *CG7009*	w1118; Df(3R)ED10845, P{3′.RS5+3.3′}ED10845 / TM6C, cu1 Sb1	Bloomington stock #9487
Def3340	Deficiency for *CG7009*	Df(3R)e-R1, Ki1/TM3, Sb1 Ser1	Bloomington stock #3340
BAC	Rescue allele for CG7009	w1118; CH322 177K12 (Pacman)	This work, FlyBase cloneFBlc0000784
CG5220$^{K>A}$	Mutant allele	w1118; CG5220 248.5.2 K28A/ TM3, Ser	This work
CG7009^{e02001}, CG5220 $^{K>A}$	Double mutant allele	w1118; CG7009e02001-G10 (mini w), CG5220 248.5.2 K28A/ TM6, Tb, Sb	This work
GMR-GAL4	GAL4 driver	P{GMR-GAL4.w-}	FBti0072862
tj-GAL4	GAL4 driver	P{tj-GAL4.U}	FBtp0089190
IR-white	RNAi white	y1 v1; P{TRiP.HMS00017}attP2	Bloomington stock: 33623
IR-Piwi	RNAi Piwi	w1118; UAS-IR(Piwi) CG 6122	VDRC N° stock: 22235 (GD)
IR-Ago2	RNAi Ago2	w1118; UAS-RNAi(Ago2)	VDRC N° stock: 49473 (GD)
IR-Ago2	RNAi Ago2	w1118;; UAS-RNAi(Ago2)	VDRC N° stock: 100356 (KK)
IR-CG7009	RNAi CG7009	w1118;; UAS-RNAi (CG7009)	VDRC N° stock: 27789 (GD)
IR-CG5220	RNAi CG5220	w1118;; UAS-RNAi (CG5220)	VDRC N° stock: 34972 (GD)
IR-CG5220	RNAi CG5220	w1118;; UAS-RNAi (CG5220)	VDRC N° stock: 108672 (KK)
IR-CG33172	RNAi CG33172	w1118; P{KK102903}VIE-260B	VDRC N° stock: 100006 (KK)
IR-CG15618	RNAi CG15618	w1118;; UAS-RNAi (CG15618)	VDRC N° stock: 40006 (KK)
shRNA-Moon	shRNA Moonshiner	w;; pW20>moon_sh2[attP2]/TM3, Sb	(Andersen *et al.*, 2017)
automiW	Genetic sensor	UAS-automiW (w+)	(Besnard-Guerin *et al.*, 2015)
Gypsy LacZ	Genetic sensor	R; tjgal4 / Cyo; Gypsy LacZ / Tb,Sb	(Sarot *et al.*, 2004)
Burdock LacZ	Genetic sensor	UAS>Dcr2; nosNGT-Gal4; nos-NLS::eGFP::LacZ::Burdock-3′UTR	(Handler *et al.*, 2013)
CC2	Double balanced line	w*; T(2;3)ap[Xa] / CyO, P{[w*] = Act-GFP}CC2; TM6C, Sb1 Tb1	Home-made
Da-GS	Inducible Gal4 under Daughterless promotor	w1118; DaGS-45	(Tricoire *et al.*, 2009)

Primers and probes

Primer	Sequence	Experiment
SD22 (RP49_FW)	GACGCTTCAAGGGACAGTATCTG	RT-qPCR
SD23 (RP49_Rev)	AAACGCGGTTCTGCATGAG	
CG7009_qPCR2_FW	GAGTTTTGTCTGCCCGATGG	
CG7009_qPCR2_Rev	ACTTGGCTCGTTTTCTGCAG	
CG5220_qPCR2_FW	GATTAACCCTGCTCGCGATG	
CG5220_qPCR2_Rev	TCCAGGGGATAAGATGCGTC	
DCV_FW	TCATCGGTATGCACATTGCT	
DCV_Rev	CGCATAACCATGCTCTTCTG	
(Gypsy (2772) _FW	CCAGGTCGGGCTGTTATAGG	
(Gypsy (2663) _Rev	GAACCGGTGTACTCAAGAGC	
LacZ_2_FW	ACTATCCCGACCGCCTTACT	
LacZ_2_Rev	GTGGGCCATAATTCAATTCG	
Roo_Fw	CGTCTGCAATGTACTGGCTCT	
Roo_Rev	CGGCACTCCACTAACTTCTCC	
Invader1_Fw	GTACCGTTTTTGAGCCCGTA	
Invader1_Rev	GCGAAGTAGCCTCCTTGATG	
R2_Fw	TAGCCCCGTAGAATGCCATT	
R2_Rev	AGTGGTTTCCTTTCCCTCGA	
Ago2_Fw	AGTGTAATAATCAGACGATTGG	
Ago2_Rev	AGGGATGGGTCACATCGGCTCC	
CG7009_EcoRI_ATG	AAGAATTCATGGGCAGGACTTCGAAGGATA	Cloning of recombinant proteins
CG7009_NotI_Stop	GCAGCGGCCGCTTACGTTACACAGGCACCTAACT	
CG33172_Hind_ATG	CAACTGGCAAAGCTTATGGTTTTGATTTCTGACGC	
CG33172_NotI_Stop	ACTGGCAGCGGCCGCTTAAAGTATATTACTTATGCTCATAGTCTGC	
T7_Ftz_FW	GAATTGTAATACGACTCACTATAGGGCTGGCAAAGTCGCCATTCT	dsRNA synthesis
T7_Ftz_Rev	GAATTGTAATACGACTC-ACTATAGGGCCAACATGTATCACCCCCA	
T7_F_Luc_Fw	TAATACGACTCACTATAGGGATGCACATATCGAGGTGGAC	
T7_F_Luc_Rev	TAATACGACTCACTATAGGGAGAATCTCACGCAGGCAGTTC	
CG7009 T7 F	ttaatacgactcactatagggagaTCCGATCGAAGGAGTCAAAC	
CG7009 T7 R	ttaatacgactcactatagggagaGCCATTTCTTCAACATTTCCTC	
LacZ T7 F	ttaatacgactcactatagggagaCAGGCTTTCTTTCACAGATG	
LacZ T7 R	ttaatacgactcactatagggagaCTGATGTTGAACTGGAAGTC	
CG7009-dTOPO FW	CACCATGGGCAGGACTTCGAAGGAT	Genotyping
CG7009-dTOPO Rev	TTACGTTACACAGGCACCTAACTTC	
CG7009-middle FW	TCCACTGGAATGCACGACTT	
CG7009-middle Rev	AAGTCGTGCATTCCAGTGGA	
pB-3SEQ	CGATAAAACACATGCGTCAATT	
pB-5SEQ	CGCGCTATTTAGAAAGAGAGA G	
VIE0197: 5220 mutant screening FW	GATATATCGATAGGCTGGCC	
VIE0198: 5220 mutant screening Rev	CAGGTATCGTAGAGTTTCCG	
tRNA Phe GAA 5′ probe (MA_075)	GCTCTCCCAACTGAGCTATTTCGGC	Northern blot
5S-rRNA probe (CA primer 5399)	CAACACGCGGTGTTCCCAAGCCG	
AS-miG1	AGAACGGCATCAAGGTGAACTTC	
2S-rRNA	TGCTTGGACTACATATGGTTGAGGGTTGTA	
Bantam	AATCAGCTTTCAAAATGATCTCA	
esi-2.1	GGAGCGAACTTGTTGGAGTCAA	

RESULTS

An RNAi screen identifies CG7009 as regulator of small RNA-mediated silencing pathways

We previously developed and characterized a self-silencing genetic sensor (*automiG*) that combines the expression of GFP with two miRNAs, miG-1 and miG-2, targeting GFP mRNA (Figure 1A and (66)). *AutomiG* self-silencing reports on the activity of canonical miRNA biogenesis factors such as Drosha and Dicer1 (Dcr1), and the function of siRNA-induced silencing complex (siRISC) factors such as Argonaute2 (Ago2) and Dicer2 (Dcr2) (66). Impairing the function of miRNA biogenesis or Ago2 silencing activity thus causes the de-repression of *automiG* self-silencing resulting in the expression of GFP. To identify additional regulators of these two RNA silencing pathways, a genome-wide RNA interference screen was performed in *Drosophila* S2 cells expressing the *automiG* sensor. Using a double-stranded RNA (dsRNA) collection library (the DRSC 2.0) allowed the down-regulation of 94.3% of all annotated *Drosophila* genes. The screen identified known regulators of miRNA biogenesis such as Drosha and Pasha, as well as siRNA pathway silencing key actors like Ago2 and Droj2 (80), demonstrating the validity of this approach. In addition, we identified 17 genes affecting a*utomiG* silencing, which had not yet been reported

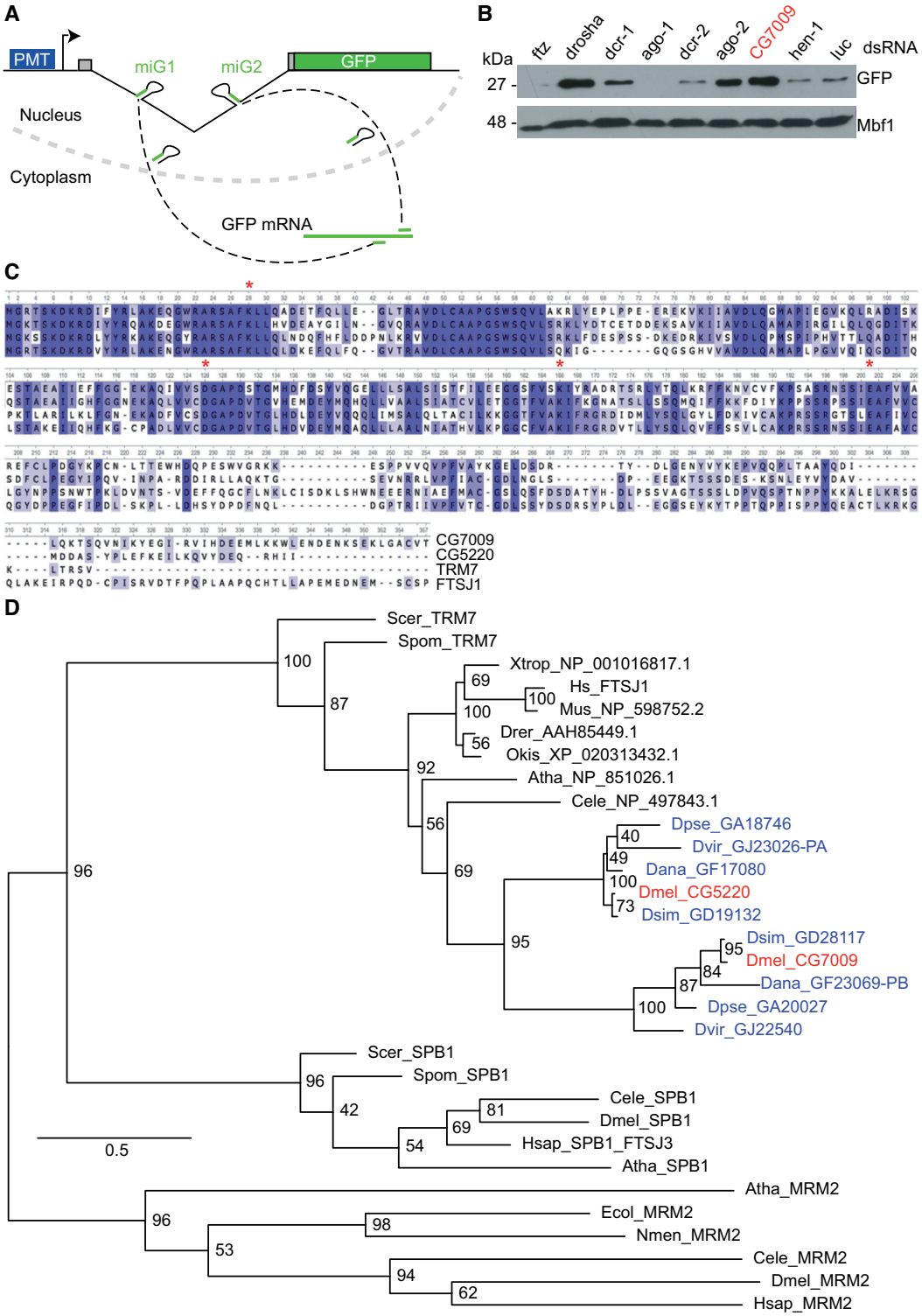

Figure 1. Identification of CG7009 and CG5220 as conserved TRM7 family proteins. (**A**) The *automiG* sensor. *automiG* carries a copper-inducible promoter (PMT) that drives the expression of two miRNAs (miG1 and miG2) and the GFP mRNA. Both miRNAs target the GFP mRNA with perfect complementarity. *AutomiG* repression is dependent on Ago2, Drosha, Pasha, Dicer-1 and Dicer-2 functions as reported previously (66). (**B**) CG7009 function affects *automiG* repression. Cells were soaked with the indicated double-stranded RNA (dsRNA), followed by *automiG* induction using copper sulfate. GFP expression was analyzed by western blotting. The Mbf1 protein was used as loading control. dsRNA against *Fushi tarazu* (*Ftz*) and luciferase (*luc*) served as negative KD controls. kDa: kilo Dalton. (**C**) Multiple amino acid sequence alignment of CG7009, CG5220, TRM7 (*S. cerevisiae*), and FTSJ1. The conserved predicted catalytic tetrad amino acids K–D–K–E are marked by red asterisks. Dark blue points to conserved amino acid in the three organisms. (**D**) *Drosophila* species evolved two TRM7 family proteins. Phylogenetic analysis of TRM7 and SBP1 MTases. The SBP1 family member RrmJ acting on rRNA was used as an outgroup. Color blue indicates TRM7 family proteins in *Drosophila* species other than *D. melanogaster*. Red indicates TRM7 family proteins in *D. melanogaster*.

to act in siRNA and/or miRNA pathways (Supplementary Figure S1A). Among those, *CG7009* stood out as an uncharacterized gene with sequence identity to annotated Nm-MTases. RNAi-mediated inactivation of CG7009 in S2 cells expressing *automiG* resulted in increased GFP expression when compared to control constructs (Figure 1B), as well as in a decrease of Ago2-loaded miG1, but not Ago1-loaded bantam miRNAs (Supplementary Figure S1B). In addition, a dual luciferase assay reporting specifically on siRNA pathway activity in S2 cells (81,82) confirmed that Dcr2/Ago2-dependent silencing was affected in cells with down-regulated CG7009 expression (Supplementary Figure S1C).

In order to obtain insights into the impact of CG7009 loss on gene expression control through Dcr2/Ago2-mediated post-transcriptional gene silencing, we performed a transcriptome analysis in *Drosophila* S2 cells upon knockdown (KD) of CG7009 expression. Surprisingly, KD of CG7009 led to the deregulation of only 110 genes (FDR < 0.01). Strikingly, the most statistically significant de-regulated gene (40% decrease, $\log_2$FC –0.7, FDR-adjusted *P*-value $7.73e^{-118}$) were *Ago2* transcripts (Supplementary Figure S1D), suggesting that CG7009 may act upstream of the siRNA pathway by regulating *Ago2* mRNA levels. The downregulation of *Ago2* transcripts in *Drosophila* S2 cells KD for CG7009 expression was confirmed by RT-qPCR on four independent biological replicates (Supplementary Figure S1E).

This genetic screen using *automiG* thus identified CG7009, a potential Nm-MTase, as a factor involved in miRNA biogenesis and/or Dcr2/Ago2-mediated post-transcriptional gene silencing.

CG7009 encodes a predicted Nm-MTase

Amino acid (aa) sequence analysis suggested that the protein encoded by CG7009 in *D. melanogaster* harbours a methyltransferase domain belonging to the conserved RlmE family and TRM7 subfamily of the class I-like SAM-binding methyltransferase superfamily (48). Sequence alignment of the putative CG7009 protein with the yeast Nm-MTase TRM7 showed 52% aa sequence identity, including the conserved KDKE motif in the active site, with 66% aa coverage (Figure 1C). FTSJ1 is the human ortholog of TRM7 (49). CG7009 shares 51% aa identity and 86% aa coverage with FTSJ1 (Figure 1C). Surprisingly, further alignment of CG7009 protein sequence with proteomes of different *Drosophila* species uncovered an additional gene, *CG5220*, whose annotated protein in *Drosophila melanogaster* displays 63% aa sequence identity with CG7009 (Figures 1C and D). Like CG7009, CG5220 was an uncharacterized protein with an amino acid composition that clearly showed an Nm-MTase signature (Figure 1C). Importantly, it was previously reported that overexpression of *Drosophila* CG5220 rescued the growth phenotype observed in *trm7Δ* mutant yeast (45). As CG7009, CG5220 displays high sequence similarity to TRM7 (48% aa identity and 83% aa coverage) as well as to FTSJ1 (58% aa identity and 82% aa coverage, Figure 1C). These findings pointed to CG7009 and CG5220 as potential paralogs and conserved members of the TRM7 Nm-MTases family in *Drosophila*.

Mutations in *CG7009* or *CG5220* are viable and fertile

To investigate the function of CG7009 and CG5220 during *Drosophila* development and to characterize the potential enzymatic activity of their gene products, we characterized existing mutations in *CG7009*, but also generated *CG5220* mutant flies. For *CG7009*, one *piggyBac* transposon insertion line ($CG7009^{e02001}$) and two genomic deletion lines (*Def3340* and *Def9487*) were obtained and precisely mapped at the molecular level (Supplementary Figure S2A–E). Both $CG7009^{e02001}$ homozygous mutants and trans-heteroallelic combinations with both deficiencies were incapable of transcribing *CG7009* properly. In addition, a transgenic rescue line containing the *CG7009* genomic locus was established through BAC transgenesis (83) resulting in an insertion of ∼20 kb genomic sequence in an ectopic genomic location (Supplementary Figure S2D, E). To address the function of CG5220, CRISPR/Cas9-mediated genome editing was used to create a *CG5220* mutant allele ($CG5220^{K>A}$), which substituted a conserved lysine at position 28 in the predicted catalytic domain with alanine (Figure 1C and Supplementary Figure S2F). The same substitution was reported to abolish the catalytic function of both yeast TRM7 and human FTSJ1 (49). Flies homozygous for either $CG7009^{e02001}$ or $CG5220^{K>A}$ or trans-heterozygous *CG7009* mutants, as well as $CG7009^{e02001}$, $CG5220^{K>A}$ double mutants survived until adulthood under standard conditions. We observed neither a major growth defect as reported for yeast (46,48) nor significant developmental delays in flies homozygous for either $CG7009^{e02001}$ or $CG5220^{K>A}$ or trans-heterozygous *CG7009* mutants. However, flies that were $CG7009^{e02001}$,$CG5220^{K>A}$ double mutant showed a measurable reduction of size and weight when compared to controls (Figure 2A).

CG7009 and CG5220 contribute to efficient miRNA Ago2-mediated RNA silencing *in vivo*

To address whether CG7009 affected small RNA silencing pathways *in vivo*, we expressed the *automiW* sensor, which is based on the knockdown of the *white* gene in the developing eye by means of *white*-targeting miRNAs loaded into Ago2 (68). Thereby, as *automiG* in cell culture, *automiW* is reporting on both miRNA biogenesis and Ago2-dependent silencing activities in flies. Combining this sensor construct with RNAi-mediated knockdown of CG7009 or CG5220, we observed increased eye coloration when compared to controls (Figure 2B). This result indicated that Ago2-dependent silencing or/and miRNAs biogenesis affecting this reporter was non-redundantly perturbed after knockdown of CG7009 or CG5220 expression, implicating thus both genes in general miRNA biogenesis and/or Ago2-dependent small interfering RNA-mediated gene silencing *in vivo* in *Drosophila*.

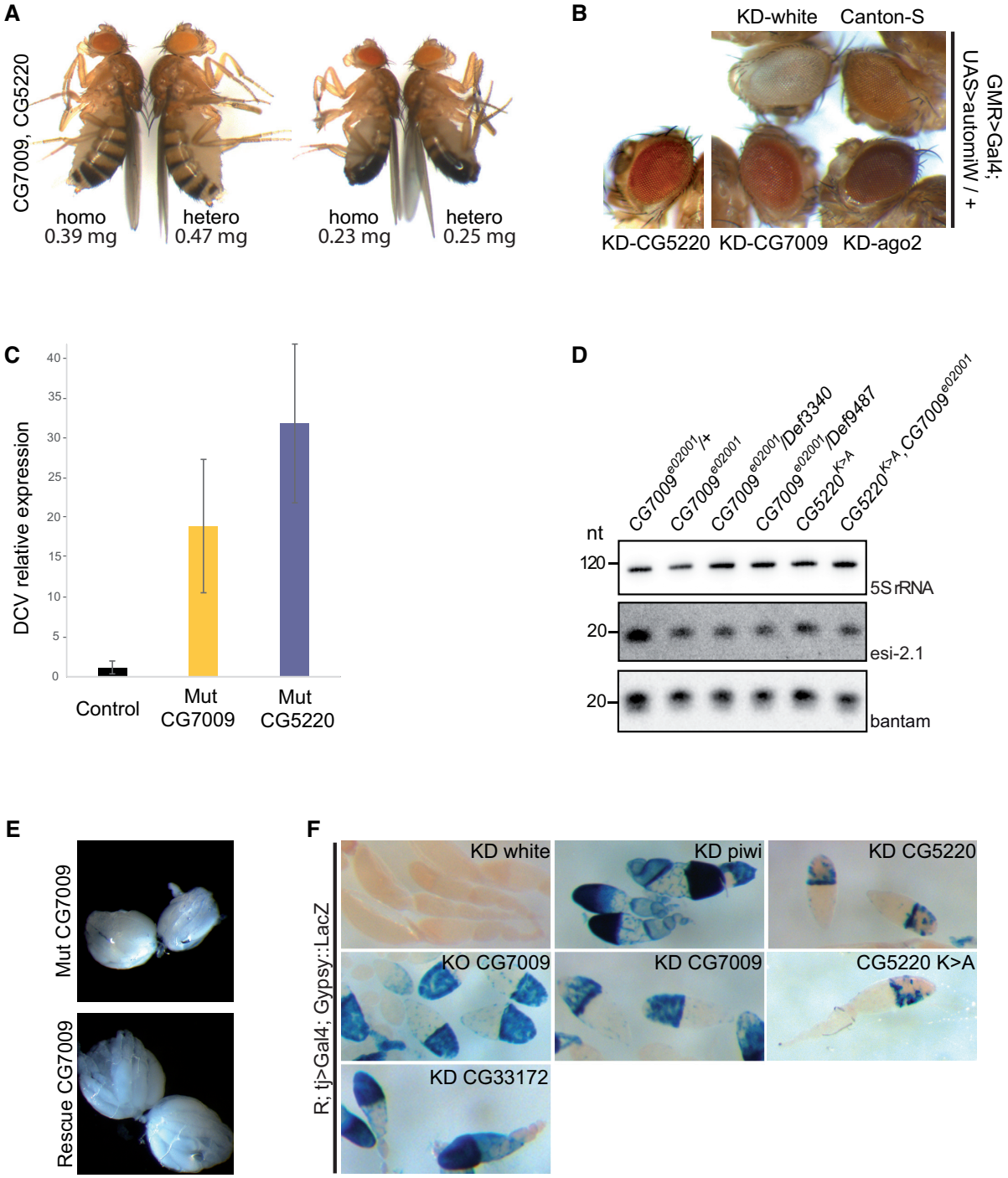

Figure 2. CG7009 and CG5220 affect small RNA silencing pathways. (**A**) Homozygous *CG7009, CG5220* double mutant flies display reduced adult weight and size. Images of adult females and males *CG7009, CG5220* homozygous double mutants (homo) compared to heterozygous double mutants (hetero). Below the images the average weight for flies in milligrams (mg) calculated for 3 days-old flies measured on a precision balance ($n > 100$ flies/ genotype; *P*-value < 0.001 in a Student's *t*-test) is indicated. The percentage change for female heterozygous *CG7009* and *CG5220* mutants *versus* homozygous *CG7009*, *CG5220* double mutant represents a decrease of 20.5%. The percentage change for male heterozygous *CG7009*, *CG5220* double mutant versus homozygous *CG7009*, *CG5220* double mutant represents a decrease of 8%. (**B**) CG7009 and CG5220 modulate Ago2-dependent gene silencing in somatic tissues. The UAS>*automiW* construct is a sensor derived from *automiG* by which two miRNAs target the *white* gene (68). KD indicates eye-specific GMR-Gal4/UAS-RNAi-mediated inactivation of the respective genes (*white*, *CG7009*, *CG5220* or *Ago2*). Canton-S *was* used as control for eye color determination. Darker eye coloration than Canton-S (top right) indicates that the *white* gene is not inactivated by Ago2-loaded miRNAs targeting *white*. Images were taken at the same age (5 days after hatching) for different genotypes. (**C**) The siRNA-dependent viral defence is compromised in *CG7009* and *CG5220* mutants. RT-qPCR using *Drosophila* C Virus (*DCV*)-specific primers three days after injection with *DCV* solution or solution free of DCV as control (not shown) in heterozygous $CG7009^{e02001}$ mutants (Control) or homozygous $CG7009^{e02001}$ (Mut CG7009) and $CG5220^{K>A}$ (Mut CG5220) mutants. Shown is *DCV* expression relative to *Rp49*. Error bars represent the standard deviation (s.d.) of the mean between two ($n = 2$) biological replicates (n is a mix of 2–3 flies). (**D**) Endogenous siRNA (esi-2.1) expression is reduced in *CG7009* and *CG5220* mutants. Northern blotting on total RNAs extracted from adult flies of

siRNA-mediated RNA silencing is impaired in *CG7009* and *CG5220* mutant flies

As small interfering RNA-mediated silencing is required for viral defence in *Drosophila* (84), we tested whether viral defence was impaired in *CG7009* or $CG5220^{K>A}$ adult mutant flies. To this end, purified *Drosophila* C virus (*DCV*) was injected into the thorax and the viral load was monitored by qRT-PCR 4 days after infection. The results of these experiments showed that flies lacking CG7009 or CG5220 function were significantly more sensitive to *DCV* infection when compared to control flies (Figure 2C). Furthermore, these results also suggested that *CG7009* and $CG5220^{K>A}$ mutants failed to initiate or maintain a proper response to viral infection which, together with the results of the *automiG*, *automiW* and siRNA-activity reporter assays (Figures 1B and 2B, Supplementary Figure S1C), strongly supported that both gene products were required for efficient Ago2-dependent small interfering RNA-mediated silencing activities in *Drosophila*.

To test whether Nm-MTase mutant conditions also affected other small RNAs, northern blotting was performed for interrogating the steady state levels of *esi-2.1*, an endogenous siRNA that depends on both Ago2 and Dcr2 activities (85). The results of these experiments showed that flies lacking CG7009 or CG5220 function displayed clearly reduced *esi-2.1* levels when compared to control flies (Figure 2D).

piRNA-mediated RNA silencing is affected in *CG7009* and *CG5220* mutant flies

During the characterization of *CG7009* mutants, we noticed that ovaries were significantly reduced in size when compared to BAC-rescued control flies (>10%; $P < 0.05$, Figure 2E). This ovarian size reduction was similar to previously described phenotype in several piRNA pathway gene mutants (86). Although the original *automiG*-based genetic screen was specifically designed to identify genes involved in miRNA biogenesis or Ago2-mediated silencing pathways, we tested whether CG7009 and CG5220 function also affected transposable element (TE) silencing through the piRNA pathway. To this end, the activity of a somatic piRNA-mediated silencing reporter (87) was monitored in adult ovaries. This reporter faithfully recapitulates the expression of the retro-transposon *gypsy* in ovarian follicle cells, in which abundant somatic piRNAs are produced in defence against mobile elements (87,88). Remarkably, piRNA-mediated silencing of this reporter was de-repressed in soma upon both, somatic follicle cell-specific knockdown of *CG5220* and *CG7009* expression, and also in *CG7009* or $CG5220^{K>A}$ mutants (Figure 2F). Furthermore, expression of both *LacZ* and endogenous *gypsy* mRNAs was elevated in *CG7009* mutants (Supplementary Figure S3A). In addition, the activity of a second piRNA-mediated silencing reporter in adult ovarian germ cells (89) was de-repressed upon germline-specific knockdown of CG5220 and CG7009 expression (Supplementary Figure S3B). Finally, in addition to *gypsy* and *burdock*, the expression of additional TEs (Roo, Invader1 and R2) was elevated in *CG7009* mutants (Supplementary Figure S3C). Taken together, these results suggested that both Nm-MTases contribute to piRNA pathway-mediated TE silencing in *Drosophila*.

Small non-coding RNA biogenesis is not globally affected in *CG7009* mutants

To gain more insights into the observed de-regulation of small non-coding RNAs in Nm-MTase mutants, we performed a small RNA sequencing analysis in ovaries from *CG7009* mutants and controls. The results showed that neither the sncRNA class distribution (Figure 3A) nor the TE-derived sncRNAs size profile distribution (Figure 3B) was globally affected in *CG7009* mutant ovaries when compared to controls.

However, when focusing the analysis on *gypsy*-derived piRNAs, we detected a decrease of both sense and antisense piRNAs targeting *gypsy* in *CG7009* mutants when compared to controls (Figure 3C), which confirmed the *gypsy* de-repression observed when using a *gypsy* sensor line and RT-qPCR assays (Figure 2F and Supplementary Figure S3A).

Notably, the entire miRNA population was significantly ($P < 0.05$) decreased in *CG7009* mutants when compared to controls (~ 20% versus ~30% respectively, Figure 3A) supporting the observed decrease of Ago2-loaded miRNAs (miG1) after knockdown of CG7009 expression in *automiG*-expressing S2 cells (Supplementary Figure S1B).

Taken together, these small non-coding RNA sequencing analyses suggested that the de-regulation of small RNA-mediated gene silencing observed in both *CG7009* and *CG5220* mutants (Figures 2D and F, Supplementary Figures S3A–C) was not caused by a global failure in small RNA biogenesis.

Mutations in *CG7009* and *CG5220* affect lifespan and mobility

Although a size and weight reduction of *CG7009*, *CG5220* double mutant adult flies could be observed (Figure 2A), no other severe mutant phenotypes affecting adult fly mor-

←

the indicated genotypes was performed using esi-2.1, bantam-specific probes and a 5S rRNA probe as loading and transfer control. nt: nucleotide. (**E**) The *CG7009* mutation is associated with ovarian size reduction. The images show representative examples of ovaries from 4 days-old fertilized females raised on fresh yeast from trans-heterozygous $CG7009^{e02001}/Def9487$ mutants (Mut CG7009) and Rescue $CG7009\ (BAC)/+;\ CG7009^{e02001}/Def9487$ mutants (Rescue CG7009); $n \geq 10$ for each genotype; Mut: mutant. An unpaired Mann–Whitney (Wilcoxon) test was used to calculate the significance of the ovary area differences between mutant and rescue genotypes. The percentage change from the mutant and the rescue genotypes represents a decrease of 10.5% with a P-value < 0.05 (W = 23, P-value = 0.02416). (**F**) CG7009 and CG5220 are involved in *gypsy* TE-repression in *Drosophila* ovaries. The *Gypsy::LacZ* sensor is silenced through *tj*>Gal4-mediated expression of an UAS-RNAi line (KD) against the *white* gene in follicle cells (R; *tj*>Gal4/ +; Gypsy::LacZ/UAS-*white*-RNAi). *Gypsy* silencing is disrupted using RNAi lines against *Piwi* (KD *piwi*), *CG7009* (KD CG7009), *CG5220* (KD CG5220) and *CG33172* (KD CG33172). The *Gypsy::LacZ* sensor was also de-repressed in *CG7009* null mutants (KO CG7009) and $CG5220^{K>A}$ homozygous mutants (CG5220 K>A). KD: knock down; KO: knock out; no blue coloration = no β-Gal staining.

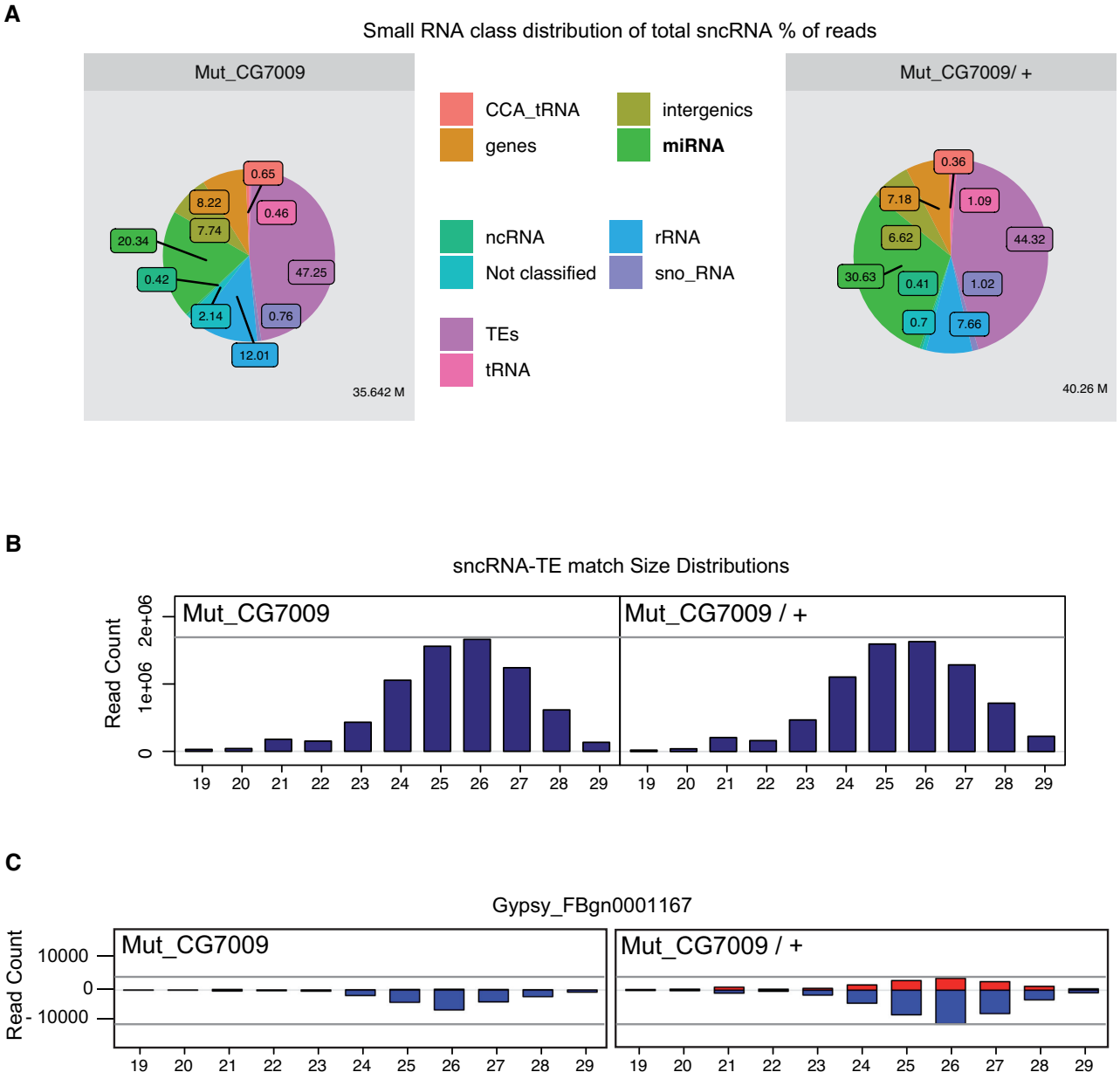

Figure 3. Small non-coding RNA biogenesis is not globally affected in *CG7009* mutants. (**A**) Class distribution of ovarian small RNAs (19–29 nt) matching the whole *Drosophila* genome reveals a significant decrease of miRNAs between control (Mut_CG7009/ +) and $CG7009^{e02001}$ homozygous mutants (Mut_CG7009). Circle circumference represents the depth of the library (indicated in million reads at the bottom right). $n = 2$ libraries for each genotype: Mut_CG7009: $CG7009^{e02001}$ homozygous mutant, while $CG7009^{e02001}$/ + represents the control heterozygous condition. Color code in the middle panel indicates each small RNA read matching to a category of *Drosophila* small RNA (miRNA: microRNA derived sequences, rRNA: rRNA derived sequences, snoRNA: small nucleolar RNA, gene indicated small RNA sequences derived from a coding genes, etc.). Sequencing of two $CG7009^{e02001}$ homozygous mutant libraries ($M = 201490$, SD = 21875.26) showed significantly decreased miRNA read numbers $t(2) = 5.89735$ when compared to the two $CG7009^{e02001}$/+ control libraries ($M = 307354$, SD = 14248.2). The P-value is 0.04867. The result was significant at $P < 0.05$. (**B**) Size distribution (19–29 nt) of small RNA read counts matching TE-derived sequences in *Drosophila* ovaries. One experiment is shown for each genotype, Mut_CG7009: $CG7009^{e02001}$ homozygous mutant, while $CG7009^{e02001}$/ + represents the control heterozygous condition. Horizontal grey line indicates the highest value and is depicted for better comparison between the two presented conditions. (**C**) Size distribution of small RNA read counts from ovaries matching *gypsy* retro-element sequences reveals that 23–29 nt piRNAs against *gypsy* are reduced in *CG7009* mutants compared to controls. Positive and negative values correspond to sense (red) and antisense (blue) reads, respectively. Horizontal grey lines indicate the highest values (sense and antisense) and are depicted for better comparison between the two presented conditions.

phology was noticeable. Importantly however, using a drug-inducible UAS/GAL4 system (78), *CG7009* and *CG5220* double knockdown flies displayed reduced lifespan when compared to controls of the same genetic background without induction of the KD transgenes. Indeed, double knockdown flies lived, on average, ∼25 days shorter than controls (Figure 4A). The $CG5220^{K>A}$, $CG7009^{e02001}$ double mutant flies also displayed reduced life span, confirming the effect of the KD experiments (Figure 4B). Lastly, homozygous $CG7009^{e02001}$ or $CG5220^{K>A}$mutant flies as well as $CG7009^{e02001}$,$CG5220^{K>A}$ double mutants appeared sluggish and less active in a climbing assay (79), supporting the notion of general locomotion defects in flies with impaired Nm-MTase function (Figure 4C).

CG7009 and CG5220 are Nm-MTases acting on tRNAs

To test whether CG7009 is an Nm-MTase, recombinant proteins were expressed and purified from *E. coli*. *In vitro* methylation assays using *in vitro*-synthesized *Drosophila* $tRNA^{Phe(GAA)}$ did not reveal activity of recombinant CG7009 protein. In order to ascertain the predicted catalytic activities of CG7009 and CG5220, we analyzed the Nm methylation status of *Drosophila* $tRNA^{Phe}$, which is a substrate of TRM7 in yeast and of FTSJ1 in human, using control, $CG7009^{e02001}$ and $CG5220^{K>A}$mutant flies. We performed sequence-specific purification of $tRNA^{Phe}$ using biotinylated DNA oligonucleotides coupled to streptavidin matrices followed by RNase digestion and MALDI-TOF mass spectrometry. RNase A has a preference for hydrolysis at pyrimidine residues, while RNase T1 is strictly guanosine-specific. Because Nm at a given nucleotide position (*n*) protects the adjacent 3′-phosphodiester bond to the neighboring nucleotide (position *n+1*) against nuclease attacks, various specific digestion products of *Drosophila* $tRNA^{Phe}$ can be expected as a result of RNase A or RNase T1 activities. In addition, according to the reported modification profile of *Drosophila* $tRNA^{Phe}$ (1,90) which includes Nm at C_{32} and G_{34}, specific RNA fragments could thus be predicted (Figure 5A and Supplementary Figures S4A and B).

First, we determined RNA fragments that were obtained after RNase A hydrolysis of $tRNA^{Phe}$, which should provide information on the Nm-modification status at C_{32}. MALDI-TOF analysis revealed almost no RNA fragment of 1327.2 Da ($AGAC_{32}p$ fragment) in control flies indicating that C_{32} was modified with Nm thereby blocking RNase A activity at this position in $tRNA^{Phe}$ from control and rescue flies (Figure 5A and Supplementary Figures S5A and B). This fragment increased significantly in $CG5220^{K>A}$ mutants suggesting loss of protection from RNase A activity in animals lacking CG5220. Interestingly, the increase in RNase A-mediated $tRNA^{Phe}$ fragmentation observed in $CG5220^{K>A}$ mutants could only be moderately observed when using $tRNA^{Phe}$ from $CG7009^{e02001}$,$CG5220^{K>A}$ double mutant flies (Figure 5A and Supplementary Figure S5A) indicating that C_{32} protection from RNase A was largely independent of CG7009. In support of this notion, the $CG7009^{e02001}$ mutation alone did not affect the RNAse A digestion profiles when compared to control (Figure 5A and Supplementary Figure S5A) or BAC rescue $CG7009^{e02001}$

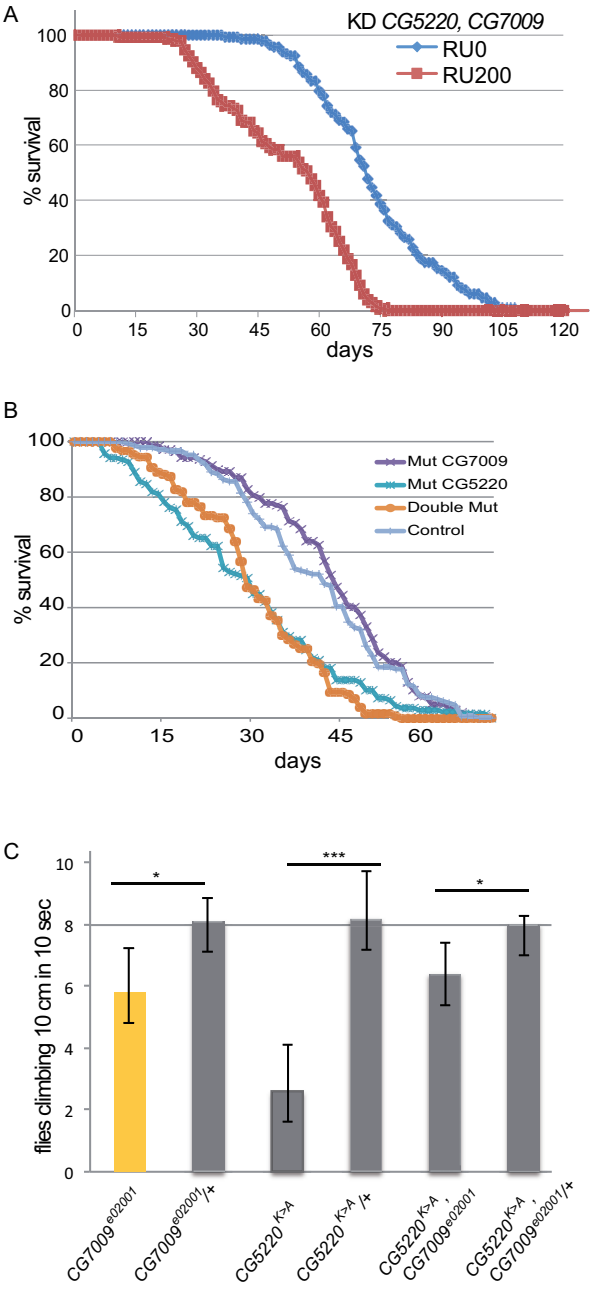

Figure 4. Mutations in *CG7009* and *CG5220* affect lifespan and mobility. (**A**) Simultaneous downregulation of *CG7009, CG5220* expression results in reduced lifespan. Survival curves of males expressing an RU486-inducible RNAi transgene against CG7009 and CG5220 with (RU200) or without (RU0) RU486-mediated RNAi transgene induction. Constitutive expression (RU200) of *CG5220*, *CG7009* KD transgenes was induced by RU486 exposure (20 mg/ml during adulthood). The curves represent the average values of five biological replicates of 30 flies per experiment. (**B**) Homozygous double mutant $CG5220^{K>A}$, $CG7009^{e02001}$ results in reduced lifespan. Survival curves of indicated males homozygous mutant for $CG5220^{K>A}$(Mut CG5220), homozygous mutant for $CG7009^{e02001}$ (Mut CG7009), homozygous double mutant $CG5220^{K>A}$, $CG7009^{e02001}$ (Double Mut) and heterozygous $CG7009^{e02001}$/+ used as control condition (Control). The curves represent the average values of five biological replicates of 30 flies per experiment. (**C**) CG7009 and CG5220 control fly behavior. Bar graphs represent data of 16 days-old male or female flies (10 flies/experiment) that climbed over 10 cm in 10 s (≥6 independent measurements for each genotype) and the standard deviation of the mean. *$P < 0.01$; ***$P < 0.0001$ in a Student's *t*-test.

A

	Digestion	Fragment of interest	Expected ion (m/z)	Control	*CG7009 e02001*	*CG7009* BAC Rescue	CG5220 *K>A*	*Double mutant*
$tRNA^{Phe(GAA)}$	RNase A	$AGAC_{32}p$	1327,202	absent	absent	absent	present	present
	RNase T1	$ACm_{32}UG_{34}p$	1318,191	absent	present	absent	absent	absent
		$AC_{32}UG_{34}p$	1304,175	absent	present	absent	absent	present

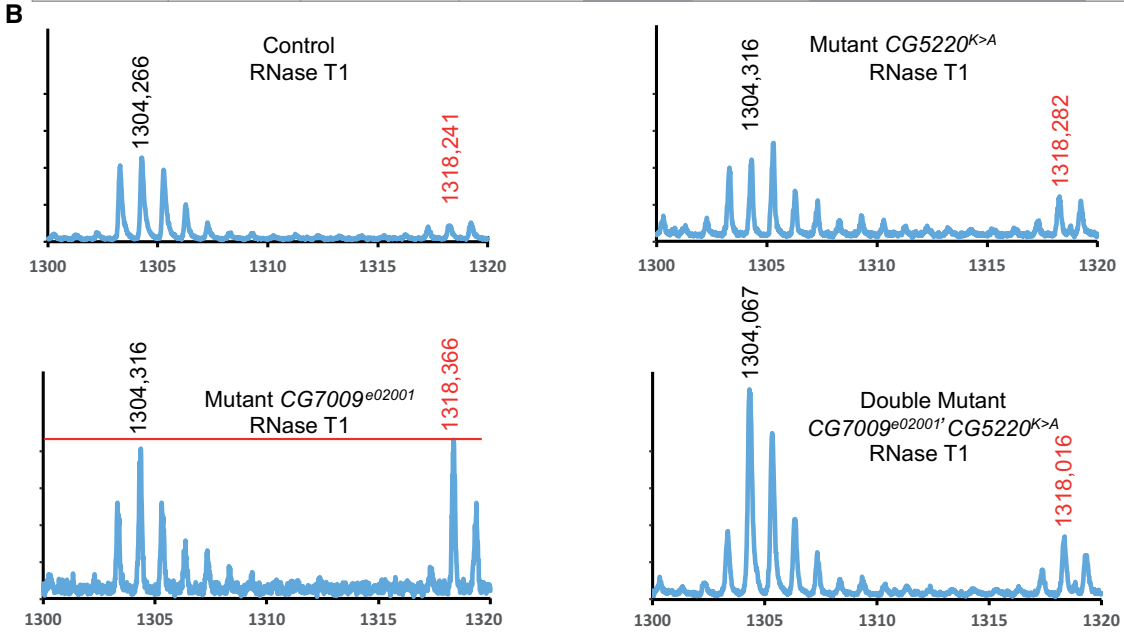

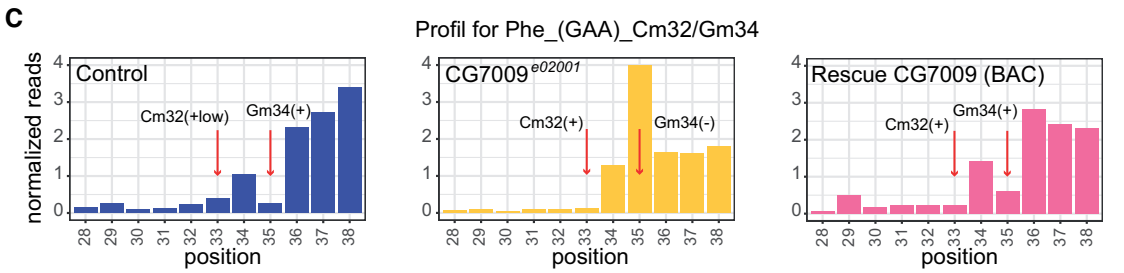

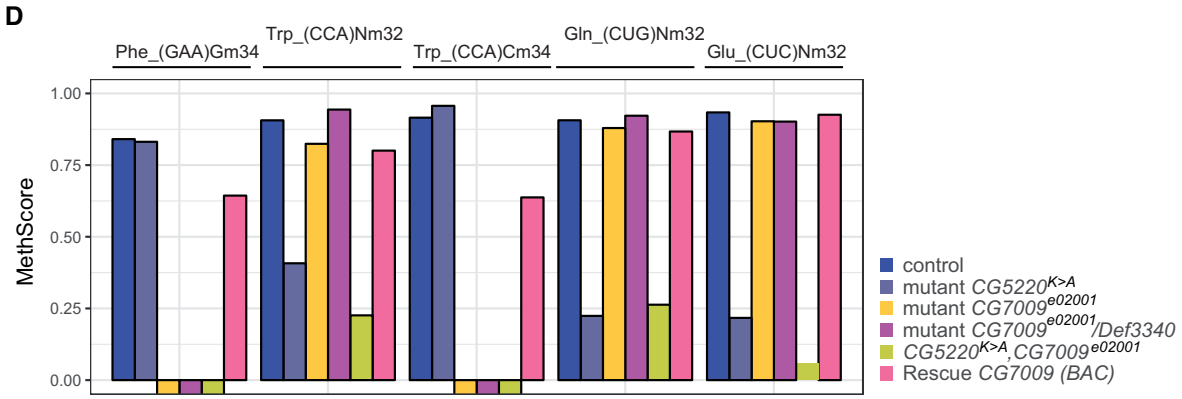

Figure 5. CG7009 & CG5220 are TRM7-like tRNA Nm MTases in *Drosophila*. (**A**) Presence (present) or absence (absent) of Nm-containing RNA fragments and their sizes (m/z in Daltons) upon RNase A or T1 digestion of $tRNA^{Phe(GAA)}$ extracted from *Drosophila* adult heterozygous $CG7009^{e02001}$ mutants (Control), homozygous $CG7009^{e02001}$ mutants (CG7009 e02001), homozygous *CG7009* mutants rescue (CG7009 BAC Rescue), homozygous

flies (Supplementary Figure S5B). These results indicated that CG5220, but not CG7009, harbors an activity that protects tRNA^{Phe} at C_{32} against RNase A digest, therefore making CG5220 the main candidate for an Nm-MTase at this position in *Drosophila*.

Next, we obtained RNase T1 digestion profiles to deduce the G_{34} modification status of tRNA^{Phe} in both control and Nm-MTase mutant flies. MALDI-TOF analysis showed a $ACm_{32}UG_{34}p$ fragment (1318,1 Da) that could not be detected in control flies indicating that G_{34} was modified with Nm thereby blocking RNase T1 activity at this position in wild type tRNA^{Phe} (Figures 5A and B). This fragment increased significantly in *CG7009^{e02001}* mutants suggesting loss of protection from RNase T1 activity in animals without CG7009. The RNase T1 digestion profiles from controls and *CG5220$^{K>A}$* mutant flies were comparable (Figures 5A and B and Supplementary Figure S5B) indicating that CG7009 but not CG5220 is implicated in protecting G_{34} from RNase T1 digestion in tRNA^{Phe}. Finally, digest of tRNA^{Phe} from *CG7009^{e02001},CG5220$^{K>A}$* double mutant flies with RNase T1 produced a fragment ($AC_{32}UG_{34}p$) that was completely unmodified (1304 Da) suggesting that CG5220 and CG7009 are the responsible Nm-MTase activities that modify C_{32} and G_{34} in tRNA^{Phe}, respectively (Figures 5A and B).

Collectively, these data demonstrated that genetic mutation of two candidate Nm-MTases in *Drosophila* resulted in the reciprocal loss of two conserved ACL modifications in tRNA^{Phe} strongly suggesting that CG5220 and CG7009 are indeed functional methyltransferases responsible for the deposition of Nm at C_{32} and G_{34} of tRNA^{Phe}, respectively. Interestingly, our results also suggest that *Drosophila melanogaster*, and likely other *Drosophila* species, evolved two distinct TRM7 family members to ribose-methylate the ACL on substrate tRNAs (Figure 1D).

Methylation specificity of both MTases depends on nucleotide position

To obtain a comprehensive picture of the Nm-MTase specificity for CG7009 and CG5220 *in vivo*, we performed RiboMethSeq analysis on *Drosophila* tRNAs. RiboMethSeq allows RNA-wide Nm detection based on random RNA fragmentation by alkaline hydrolysis followed by library preparation and sequencing (64,65). The presence or absence of Nm can be appreciated from characteristic coverage profiles of the 5′-/3′-ends of cDNAs. Since Nm residues protect the adjacent 3′-phosphodiester bond to the neighbouring nucleotide from hydrolysis, a gap in the coverage at the *n+1* position indicates the presence of a 2′-*O*-methylated nucleotide at position *n*. When analyzing the 2′-*O*-methylation status at position 34 for tRNA^{Phe} in control individuals, reads at position 35 (equals *n+1*) were under-represented in regard to their direct nucleotide neighbors (Figure 5C and Supplementary Figures S6A and B). This demonstrated that, Nm was present at G_{34} in *Drosophila* tRNA^{Phe} as previously reported (90) and as shown by MALDI-TOF MS analysis (Figure 5A). Similarly, RiboMethSeq profile analysis of *CG5220$^{K>A}$* mutants indicated G_{34} to be methylated (Supplementary Figures S6A and B). Importantly, the presence of Nm at G_{34} in *CG5220$^{K>A}$* mutant confirmed that CG5220 was not involved in the formation of ribose methylation at this position. On the contrary, in two different *CG7009* mutants, as well as in *CG7009^{e02001}, CG5220$^{K>A}$* double mutants, protection against hydrolysis at position 35 was totally abolished when compared to the control heterozygote profile (Figure 5C and Supplementary Figures S6A and B), confirming that CG7009 is the Nm-MTase for G_{34} of tRNA^{Phe} in *Drosophila* and that CG5220 alone is not able to methylate this position. Importantly, the expression of an additional gene copy of CG7009 in the *CG7009^{e02001}* mutant background (Rescue CG7009 (BAC)) rescued the lost protection against hydrolysis at G_{34} of tRNA^{Phe} (Figure 5C and Supplementary Figure S6B). In addition, RiboMethSeq analysis was performed for position 33 of tRNA^{Phe} (*n* + 1 to the expected Nm at C_{32} (Figure 5A and (90)), which confirmed that CG5520, but not CG7009, was responsible for ribose methylation at position 32 on tRNA^{Phe} (Figure 5C and Supplementary Figures S6A and B).

Furthermore, RiboMethSeq analysis also identified other tRNAs potentially methylated by CG7009 and CG5220, some of which were already known as substrates of TRM7 orthologs in other species. For instance, we found CG7009-dependent methylation at position C_{34} and CG5520-dependent Nm at position C_{32} of tRNA^{Trp} (Figure 5D and Supplementary Figure S7). Strikingly, the methylated nucleotide at position 34 in tRNA^{Trp} of *Drosophila* is a cytosine, like in humans and in yeast (1,45,48,49). Importantly, RiboMethSeq scores clearly showed that CG7009

CG5220$^{K>A}$ mutants (CG5220 *K>A*), and double homozygous mutants *CG7009^{e02001},CG5220$^{K>A}$* (Double mutant). (**B**) MALDI TOF-MS spectrum of fragments resulting from RNase T1 digestion of tRNA$^{Phe\text{-}(GAA)}$ originating from heterozygous adult *CG7009^{e02001}*/+ mutants (Control), homozygous *CG7009^{e02001}* mutants (Mutant *CG7009^{e02001}*), red line indicates the maximum value (1318 Da) and is depicted for better comparison between the 2 peaks values. Homozygous *CG5220$^{K>A}$* mutants (Mutant CG5220$^{K>A}$) and double homozygous mutants *CG7009^{e02001},CG5220$^{K>A}$* (Double Mutant *CG7009^{e02001},CG5220$^{K>A}$*) as indicated. Relevant peaks are identified by their m/z values in Daltons (X-axis). (**C**) RiboMethSeq analysis of Nm at positions C_{32} and G_{34} in tRNA$^{Phe(GAA)}$ from whole heterozygous adult *CG7009^{e02001}*/+ mutants (Control), homozygous *CG7009^{e02001}* mutants (CG7009^{e02001}) and rescued *CG7009^{e02001}* mutants (Rescue CG7009 (BAC)) as indicated. Normalized cleavage efficiencies, calculated from combined 5′- and 3′-end coverage of tRNAs are shown for the neighboring nucleotides (+/– 5) of the respective ribose methylation position. The positions of interest (C_{32} and G_{34}) in tRNA$^{Phe(GAA)}$ are indicated by red arrows. Protection against cleavage is indicated (+): protected and as (–): not protected. Protection at Cm_{32} in control flies was only moderate, indicating incomplete tRNA methylation (+low). (**D**) Methylation scores (MethScore) for five 2′-*O*-methylated positions in tRNAs showing altered methylation in *CG5220* and/or *CG7009* indicated mutants. MethScore (Score C), representing the level of ribose methylation was calculated from protection profiles. Data are shown for positions 32 and 34 in different *D. melanogaster* tRNAs as measured in heterozygous adult *CG7009^{e02001}*/+ mutants (control), homozygous *CG5220$^{K>A}$* mutant (mutant *CG5220$^{K>A}$*), two independent genetic background mutants for *CG7009* (homozygous *CG7009^{e02001}* or *trans*-heterozygous *CG7009^{e02001}/Def3340* mutant), double homozygous *CG7009^{e02001},CG5220$^{K>A}$* mutant and rescue BAC *CG7009^{e02001}/Def3340* flies (Rescue CG7009 (BAC)). Score at Cm_{32} for tRNA$^{Phe(GAA)}$ in control flies is only moderate (not shown and Figure 5C), indicating incomplete tRNA methylation.

(and not CG5220) methylated this position (Figure 5D and Supplementary Figure S7) indicating that CG7009 can deposit Nm on G and C nucleotides. The same observation was made for CG7009-mediated methylation of C_{34} in $tRNA^{Leu(CAA)}$, which was in agreement with previous data showing that FTSJ1 was responsible for depositing Nm at $f5C_{34}/hm5C_{34}$ in human $tRNA^{Leu(CAA)}$ ((44) and Supplementary Figures S6C and S7). In addition, we identified previously unknown Nm-MTase substrate tRNAs. For instance, RiboMethSeq uncovered CG5220-dependent methylation of $tRNA^{Gln}$ and $tRNA^{Glu}$ at position C_{32} (Figure 5D and Supplementary Figure S7). 2′-*O*-methylated C_{32} in $tRNA^{Glu(UUC)}$ had previously been reported in *Drosophila* (1,91). Interestingly, cytosine 32 was also reported to be 2′-*O*-methylated in human $tRNA^{Gln}$ by a yet unidentified enzyme (1). Our data thus suggest that the human ortholog of CG5220, FTSJ1, may be the Nm-MTase responsible for the modification at this position.

Altogether, detailed RiboMethSeq analysis confirmed the MALDI-TOF MS results (Figure 5A, B and Supplementary Figure S5), demonstrating that CG5220 is specialized for depositing Nm at C_{32} nucleotides while CG7009 is responsible for modifying the wobble position. Furthermore, the discovery of additional tRNA substrates (Figure 5D and Supplementary Figure S7) for both Nm-MTases suggested that their respective specificity is dependent on the position rather than on the nature of nucleotide (C, U or G).

CG33172 is part of the Nm–MTase complex

Yeast TRM7 associates with two distinct proteins that are required for its catalytic activity (45,46). Deposition of Nm at C_{32} by TRM7 is supported by binding to TRM732 while the interaction with TRM734 is necessary for addition of Nm at position 34. THADA and WDR6 are the orthologs of TRM732 and TRM734 in humans, respectively, and their interactions with FTSJ1 are conserved (49). In *Drosophila*, CG15618, also known as DmTHADA (92), is the potential ortholog of TRM732 and THADA, while CG33172 is the putative ortholog of TRM734 and WDR6 (Figure 6A). Importantly, CG33172, TRM734 and WDR6 are members of the WD40-repeat-containing domain superfamily that contains also the human protein WDR4, another tRNA-MTase cofactor that, like FTSJ1, when mutated is associated with neurodevelopmental disorders (93,94).

The use of the *automiW* sensor combined with dsRNA-mediated knockdown of CG15618 and CG33172 in the *Drosophila* eye recapitulated the Ago2-mediated small RNA silencing failure observed in *CG7009* and *CG5220* mutants (Figure 6B). Interestingly, dsRNA-mediated knockdown of CG33172 using the *Gypsy-LacZ* sensor also recapitulated the somatic piRNA-mediated silencing failure observed in both *CG7009* and *CG5220* mutants (Figure 2F), indicating genetic interactions between CG7009/CG5220-mediated functions and these gene products.

In order to test for physical interactions between CG7009, CG15618 and CG33172, we cloned FLAG-tagged CG15618 and CG33172 with the aim of co-expressing these proteins along with GST::CG7009 in bacteria. While co-expression of FLAG::CG15618 was technically challenging due to the size of this protein (197 kDa), FLAG::CG33172 could be expressed and immunoprecipitated using anti-FLAG antibodies. The precipitate was tested for the presence of GST::CG7009 by using western blotting and anti-GST antibodies. The results showed that FLAG::CG33172 co-precipitated with GST-CG7009 but not GST alone indicating a direct interaction between these two proteins (Figure 6C). Collectively, these observations suggested the existence of an Nm-MTase complex containing CG7009 and at least one accessory protein, CG33172, which might be required for depositing Nm at position 34 on selected tRNAs.

Nm limits endonucleolytic cleavage of $tRNA^{Phe}$ and stabilizes $tRNA^{Phe}$ fragments

We next addressed the mechanisms underlying the defects in the Ago2-mediated small RNA silencing activity observed in Nm-MTase mutant flies. It has been reported that loss of m^5C and Queuosine from specific tRNAs resulted in increased tRNA fragmentation in *Drosophila (95)* and mammals (96,97). Furthermore, it was proposed that tRNA fragments (tRFs) could affect small RNA silencing pathways through binding to Dicer and Argonaute proteins thereby reducing their activity (95,98–101). In addition, during the preparation of this manuscript, a study showed that Nm_{34} protected $tRNA^{Met(CAT)}$ from endonucleolytic cleavage by stress-induced angiogenin in human cells (18). We therefore tested if lack of Nm at positions 32 and 34 of $tRNA^{Phe}$ affected its endonucleolytic cleavage during heat stress conditions. A heterozygous $CG7009^{e02001}$ mutant (control), a CG7009 transheterozygous mutant ($CG7009^{e02001}/Def3340$) and the rescue line for CG7009 (Rescue *CG7009*) were analyzed by northern blotting with a specific probe complementary to the 5′- end of $tRNA^{Phe}$ before and after heat shock exposure. Two clear hybridization signals were observed, corresponding to mature tRNAs (∼70 nt) and tRFs (∼35 nt, Figure 7A). tRNA fragmentation increased significantly in $CG7009^{e02001}/Def3340$ mutants. Importantly, increased tRNA fragmentation was rescued in Rescue *CG7009* flies (Figure 7A), demonstrating that CG7009 function affected tRNA fragmentation of $tRNA^{Phe}$. Of note, global steady state levels of mature tRNAs were not affected in $CG7009^{e02001}/Def3340$ mutants (Figure 7A), suggesting limited pan-translational defects in flies without functional CG7009, while not excluding defective translation of specific proteins. Interestingly, we did not observe heat stress-dependent effects on tRNA fragmentation in $CG7009^{e02001}/Def3340$ nor in other *CG7009* mutant combinations (Figures 7A and B), indicating that increased tRNA fragmentation in *CG7009* mutants might be the result of increased $tRNA^{Phe}$ turnover. Furthermore, when compared to *CG7009* single mutants, we did not observe increased $tRNA^{Phe}$ fragmentation in $CG5220^{K>A}$ single nor in $CG7009/CG5220^{K>A}$ double mutants (Figure 7B), suggesting that Nm at position G_{34}, and not C_{32}, limits fragmentation of $tRNA^{Phe}$, while 3′ terminal Cm_{32} might exert a stabilizing effect on tRFs ($tRF^{Phe}Cm_{32}$) that were produced in *CG7009* mutants.

A

Drosophila *aa* sequences	Human or **yeast** sequences	% aa identity (Ensembl)
CG15618 1746 aa	THADA 1953 aa	29.23%
CG33172 998 aa	WDR6 1121 aa	23.21%
CG15618 1746 aa	**TRM732** 1420 aa	23.18%
CG33172 998 aa	**TRM734** 1013 aa	22.77%

B

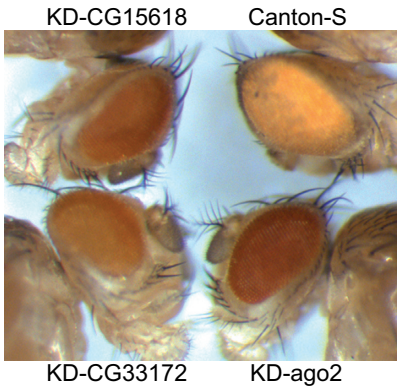

C

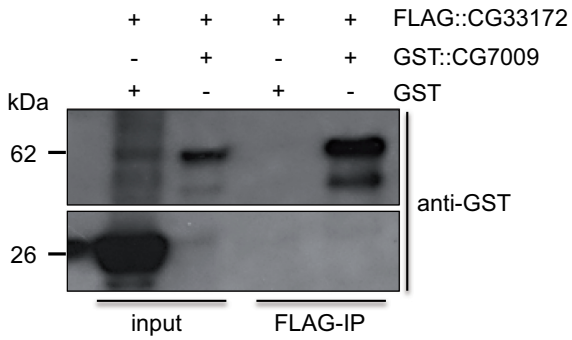

Figure 6. CG33172 is a partner of the Nm-MTase complex in *Drosophila*. (**A**) Percentage of amino acid (aa) identity between CG15618, human THADA and yeast TRM732, and between CG33172, human WDR6 and yeast TRM734 (RTT10). Alignment was performed using BLAST/ BLAT tool at www.ensembl.org. (**B**) CG33172 and CG15618 modulate Ago2-dependent silencing in adults flies. *CG33172* and *CG15618* expression was knocked down by using UAS-RNAi lines and eye- specific *GMR*-Gal4, [w-] driver (indicated as KD), as in Figure 2B. Canton-S (wild type, [w+]) and *Ago2* KD were used as controls. A darker eye coloration than Canton-expressing *automiW* lines (top right) indicates that the miRNAs of the sensor are failing to inactivate the *white* gene through impaired miRNA biogenesis or/and Ago2-dependent silencing. (**C**) CG33172 interacts with CG7009 *in vitro*. Co-immunoprecipitation of recombinant and epitope-tagged CG7009 and CG33172 after co-expression in bacteria. Western blotting using anti-GST antibody on protein extracts from input fractions co-expressing GST::CG7009 and FLAG::CG33172 and after FLAG-IP; Lower panel, Anti-GST WB reveals a GST 'alone' signal in the co-expressed GST and FLAG::CG33172. Inputs correspond to 10% of 10 μg of protein eluates. The expected protein sizes are 26 kDa (GST) and 62 kDa (GST::CG7009). WB, western blot; kDa, kilodaltons.

DISCUSSION

While performing an RNAi genome-wide screen for modulators of miRNA biogenesis or Ago2-dependent small RNA silencing in *Drosophila*, we identified a previously uncharacterized gene (*CG7009*) with sequence homology to Nm-MTases of the TRM7/FTSJ1 subfamily of MTase proteins. Surprisingly, through subsequent sequence analysis, we also identified CG5220 in *Drosophila,* which although sharing considerable sequence homology with CG7009 was not uncovered by the genetic screen in S2 cells. Furthermore, when re-testing (both visually and by western blotting) the *automiG* read-out (GFP expression) upon efficient CG5220 knockdown in S2 cells, we obtained variable and inconclusive results, which supported the fact that CG5220 was not uncovered as modulator of miRNA biogenesis or Ago2-dependent small RNA silencing by the original screen in S2 cells. However, since RNAi-mediated knockdown of CG5220 expression and a genetic mutation of the predicted catalytic motif in CG5220 ($CG5220^{K>A}$ mutant) affected both the *automiW* sensor in adult *Drosophila* eyes and also sensors reporting on piRNA-mediated TE silencing in the germline, we believe that CG5220 function might be required only in certain tissues but not in embryo-derived S2 cells.

By characterizing the molecular function of these predicted Nm-MTases, we demonstrated that both genes encode RNA methyltransferases depositing Nm on tRNAs while displaying specialized activity at two distinct positions in the ACL. These findings reveal that, in contrast to yeast and humans, which encode only one Nm-MTase gene capable of methylating the ACL, *D. melanogaster* has evolved two distinct enzymes, each specialized in the methylation of only one position in the ACL of conserved tRNA targets. Interestingly, it appears also that other *Drosophila* species evolved and maintained these closely related TRM7/FTSJ1

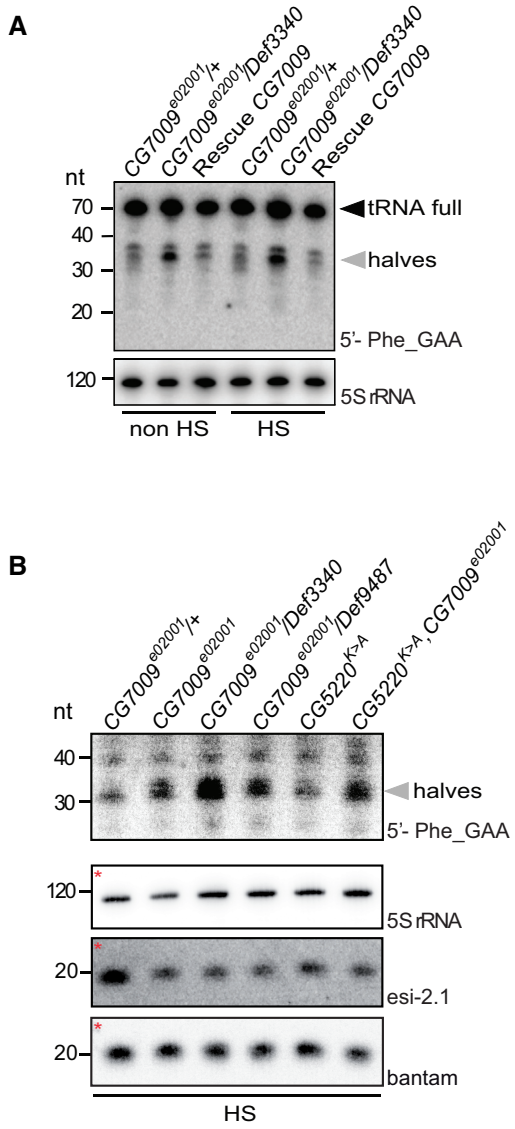

Figure 7. Nm limits endonucleolytic cleavage of $tRNA^{Phe}$. (**A**) Northern blot characterization of 5′- $tRNA^{Phe(GAA)}$-derived tRFs. Northern blot on total RNAs extracted from whole heterozygous $CG7009^{e02001}$ control flies ($CG7009^{e02001}$/+), *trans*-heterozygous for $CG7009^{e02001}$/*Def3340* or rescued mutants for *CG7009* (rescue *CG7009*) as indicated using a 5′-$tRNA^{Phe(GAA)}$ -specific probe and a 5S rRNA probe as loading and transfer control. Mature $tRNA^{Phe}$ size is 73 nt (full length). 5′-$tRNA^{Phe}$-derived tRNA fragments (5′-tRF^{Phe}) were detected at ∼35 nt (halves). The same experiment was performed on heat-shocked flies (one hour at 37°C in a water bath), RNAs were extracted after 5 h at 25°C (indicated as HS, heat shock). nt: nucleotide. (**B**) The same experiment as in Figure 7A above was performed on heat-shocked flies (one hour at 37°C in a water bath). The same membrane as shown in Figure 2D was stripped and reprobed with a $tRNA^{Phe(GAA)}$ -specific probe. Figures 7B and 2D thus contain identical images (marked with *) for bantam, 5S and esi-2.1 for a better comparison. RNAs were extracted after 5 hours of recovery at 25°C (indicated as HS, heat shock) with indicated genotypes. Double homozygous mutant is indicated as $CG7009^{e02001}$,$CG5220^{K>A}$. Homozygous mutant for *CG7009* is indicated as $CG7009^{e02001}$. Homozygous mutant for *CG5220* is indicated as $CG5220^{K>A}$. *Trans*-heterozygous mutants for *CG7009* alleles are indicated as $CG7009^{e02001}$/*Def3340* and $CG7009^{e02001}$/*Def9487* nt: nucleotide.

paralogs. Mass spectrometry analysis and RiboMethSeq confirmed this peculiarity, raising the possibility that independent Nm deposition in the ACL of specific tRNAs by two enzymes, rather than one, might be functionally significant, in particular since expression and activity of both enzymes can be independently regulated. Importantly, our analysis also reports novel substrates of the TRM7 subfamily of Nm MTases.

Interestingly, and in agreement with studies on various RNA modification enzymes in other organisms, Nm-MTases in *Drosophila* are not required for organismal viability or fertility. However, Nm-MTases mutants displayed reduced lifespan and behavioral phenotypes manifested as general mobility defects (Figure 4). Although the use of the genetic double mutants $CG5220^{K>A}$, $CG7009^{e02001}$ confirmed the outcome of the double KD experiments, it remains to be seen whether the effects on lifespan can be solely attributed to the loss of the catalytic function of CG5220 and not CG7009, because the genetic background of the presented experiments (Figure 4B) differed slightly in terms of generations times after isogenization.

Abolishing the catalytic function of both genes in the same animal did not reveal additional morphological mutant phenotypes with the notable exception of a reduction in size and weight, highlighting a potential role of these Nm-MTases in specific, but not general, translational control as previously reported for *trm7* mutant yeast (46,48,51,52) and as recently highlighted for internally deposited Nm on specific mRNA in humans (27).

Nm modifications in the ACL of specific tRNAs can affect translational efficiency and fidelity (51,52,102). Consistently, Nm deposition in mRNA also affects translation through interference with tRNA decoding efficiency and thus can potentially rewire the genetic code (27,103,104). Interestingly, it was recently proposed that TRM7 can also methylate substrates that are not tRNAs including mRNAs in yeast (25) suggesting that TRM7 family members can act as multi-substrate Nm-MTases, thereby modulating translation through modification of codons (mRNA) and anticodons (tRNA). Importantly, loss of Nm at tRNA positions 32 and 34 in *trm7* mutant yeast activated the general amino acid control pathway (GAAC, (52)), affected translation rates and, consequently, cell growth (46,48). Thus, the observed reduction of size and mass (Figure 2A) in flies without TRM7 family members supports the hypothesis that *CG5220* and *CG7009* mutations affect translational efficiency in *Drosophila*.

Importantly, a lack of Nm at the wobble position in *CG7009* mutants affected tRNA fragmentation patterns. tRNA fragmentation is a conserved response to various stress conditions affecting protein synthesis, apoptosis signalling and the modulation of small non-coding RNA pathways (105–108). An influence of internal Nm modifications on tRNA stability has only been described very recently (18). In support of the notion that Nm in tRNAs might modulate their stability, we found that Nm_{34} is protective against tRNA fragmentation in the ACL. However, in contrast to the increase in detectable tRFs in *CG7009* mutants, the lower level of tRFs in *CG7009*, *CG5220* double mutants suggests that CG5220 function affects tRNA fragment abundance positively once produced. Furthermore,

since *CG5220* mutants did not display tRFs, we propose that tRFs produced by ACL cleavage in *CG7009* mutants may be stabilized through the existence of a 3′ terminal Nm at position 32 (likely deposited by CG5220). Since Hen1-mediated deposition of Nm at RNA 3′- termini (22,109) stabilizes small RNAs in various organisms, such a mechanism could explain the abundance and apparent stability of tRFs in *CG7009* single mutants, in contrast to the low abundance of tRFs in *CG5220* single and *CG7009*, *CG5220* double mutants.

Importantly, loss of function of either CG7009 or both Nm-MTases impaired Ago2- as well as Piwi-dependent small RNA silencing pathways *in vivo*. Furthermore, *DCV* infection assays and lower esi-2.1 production in adult Nm-MTase mutant flies confirmed a function for CG7009 and CG5220 as regulators of siRNA pathway-mediated mobile element control. In addition, the observation that the total miRNA population was reduced by 10% in *CG7009* mutants when compared to control (Figure 3A), indicated that Nm-MTases function affected small RNA silencing pathways in a pleiotropic fashion and suggested that these Nm-MTases genes could even act upstream of small RNA biogenesis and function. Indeed, both RNA and small RNA sequencing analysis suggested that the manifestation of these phenotypes could partially be due to the transcriptional downregulation of *Ago2* mRNA in *CG7009* mutant flies or after knockdown of CG7009 in S2 cells. On the other hand, tRFs can associate with Dicer, Argonaute and Piwi proteins (98–101,110). One potential consequence of such interactions could be a reduction in the capacity of small RNA pathway components to process or bind to canonical RNA substrates. Indeed, tRF-mediated titration of proteins away from canonical substrates has been reported (95,111–113).

Finally, our study identifies CG33172 as a binding partner of CG7009. Interestingly, the yeast ortholog of CG33172, TRM734, was reported to control the steady state levels of TE as does TRM7 (114). Here, we have shown that the *Drosophila* orthologs of TRM734 and TRM7 (CG331772 and CG7009, CG5220, respectively) also affected TEs through siRNA and piRNA-mediated silencing pathways. Furthermore, sncRNA pathways and TE expression (R2 and especially *gyspy)* in *Drosophila* glial and neuronal cells have already been associated with decreased lifespan as well as with the manifestation of neurodegenerative disease (115–117).

Importantly, mutations in human WDR4 impaired tRNA m^7G_{46} methylation and caused microcephalic primordial dwarfism (94). CG33172 belongs to the WD-Repeat (WDR) family of proteins and is the ortholog of human WDR6. Interestingly, both WDR6 and FTSJ1 were identified as principal human host restriction factors against *vaccinia* virus indicating that this Nm-MTase complex functions at the interface of host-virus interactions (118). In support of the notion that Nm modifications modulate mobile and repeat element control, human Nm-MTase FTSJ3 can be hijacked by HIV-1 to methylate viral mRNAs resulting in avoidance of being sensed by the host innate immune system (26).

Our study thus strongly supports the emerging notion that an important biological impact of Nm-MTase activity is mobile element control affecting TEs and viruses. Importantly, our results in *Drosophila* also indicate that the molecular machinery necessary for depositing Nm in tRNAs and the associated physiological importance are conserved throughout evolution.

In summary, this study provides a comprehensive *in vivo* characterization of two Nm-MTases and associated functions in *D. melanogaster,* demonstrating the importance of enzymes of the TRM7/FTSJ1 family in contributing to small non-coding RNA silencing pathways. The peculiarity of *Drosophila* species having evolved two TRM7/FTSJ1 gene products with specialized activity towards specific positions in tRNAs for *D. melanogaster* strongly suggests that Nm in other *Drosophila* species is deposited at ACLs by two TRM7/FTSJ1 enzymes. Importantly, our results also support the notion that the stability of particular tRFs could depend on their RNA modification status. Regarding the respective specificity of ACL methylation in the *Drosophila* clade, we propose to rename the identified *Drosophila* genes as *dTrm7_34* (for *CG7009*) and *dTrm7_32* (for *CG5220*).

DATA AVAILABILITY

The RNA sequencing data discussed in this publication have been deposited in NCBI's Gene Expression Omnibus (119) and are accessible through GEO Series accession number GSE134354 (https://www.ncbi.nlm.nih.gov/geo/query/acc.cgi?acc=GSE134354). The small RNA sequencing data discussed in this publication have been deposited in the European Nucleotide Archive (ENA) at EMBL-EBI under accession number PRJEB35301 (https://www.ebi.ac.uk/ena/data/view/PRJEB35301).

SUPPLEMENTARY DATA

Supplementary Data are available at NAR Online.

ACKNOWLEDGEMENTS

We would like to thank the DRSC/TRiP Functional Genomics Resources for the DRSC 2.0 genome-wide screening library. Bloomington *Drosophila* Stock Center for fly reagents; the *Drosophila* Genomics Resource Center at Indiana University and BDGP for plasmids; Jean-Luc Imler for sharing DCV preparations; Romain Derelle for the phylogenetics analysis; Valérie Biou and Bruno Miroux for the C41 bacteria; members of the *TErBio* laboratory and ARTbio bioinformatic platform as well as Stephan Eberhard for helpful discussions and reading of the manuscript; Josette Pidoux, Elma Shalatzi, Marius van den Beek, Elie Makardijian, Michael Rera and Ludivine Roumbo for experimental help. C.C. would like to thank Lucien Carré for having been there. Support by the IMB Genomics Core Facility and the use of its NextSeq500 (INST 247/870-1 FUGG) is gratefully acknowledged. We also thank Nastasja Kreim from the Core facility Bioinformatics for her great support. J-Y.R., Y.M., M.S. and C.C. are members of the European EPITRAN COST Action (CA16120).

Author contributions: M.T.A., D.G.D., B.d.S., S.S., M.B., S.K. and C.C. performed all experiments in regard to fly

genetics, lifespan measurements, *CG7009* allele characterizations and RNAs preparation. M.S designed the strategy and created the *CG5220*$^{K>A}$ allele. C.A. generated and screened the *CG7009, CG5220* double mutants. C.J., C.A. and C.C. designed and performed the genetic and secondary sensor screens. C.G. and D.B. purified tRNAs. V.G. performed Mass Spectrometry and analysed the data with D.B. and C.G., V.M. and V.B.I. performed RiboMethSeq. RiboMethSeq computational analyses were performed by Y.M., J.Y.R. and T.L. performed transcriptome sequencing libraries preparation and computational analysis was performed at the IMB Genomics Core Facility and ARTbio. ARTbio performed the small non-coding RNA computational analysis. M.S. performed northern blot experiments. C.A., M.T.A. and C.C. performed GST pull down experiments. M.T.A., D.G.D., Y.M. and C.C. prepared Figures and Tables. C.C. conceived the project. M.T.A., D.G.D., L.T., J.Y.R., Y.M., M.S. and C.C. wrote the manuscript.

FUNDING

C.C. received financial support from CNRS and Sorbonne Université, Fondation Maladies Rares (FMR), IBPS 'Action Incitative 2018', the COST action EPITRAN CA16120; M.T.A. and D.G.D. had PhD fellowships from the Ministère de la Recherche et de l'Enseignement Supérieur at the doctoral school Complexité du Vivant (ED515); M.S. was supported by the Austrian Science Foundation [FWF-P29094]; Research in the laboratory of J.-Y.R. was supported by the Deutsch-Israelische Projektkooperation (DIP) RO 4681/6-1 and DFG RO4681/9-1 in the framework of the SPP1784 "Chemical biology of native nucleic acid modifications"; Fondation ARC pour la Recherche sur le Cancer for funding support (to M.T.A. and D.G.D., 4th year PhD); 'Réseau André Picard', the 'Société Française de Génétique' for traveling fellowship grants (to M.T.A. and D.G.D.); COST action 'EPITRAN' CA16120 for traveling fellowship grants (to D.G.D., M.B. and C.C.). Funding for open access charge: Sorbonne Université.
Conflict of interest statement. None declared.

REFERENCES

1. Boccaletto,P., Machnicka,M.A., Purta,E., Piatkowski,P., Baginski,B., Wirecki,T.K., de Crécy-Lagard,V., Ross,R., Limbach,P.A., Kotter,A. *et al.* (2018) MODOMICS: a database of RNA modification pathways. 2017 update. *Nucleic Acids Res.*, **46**, D303–D307.
2. Guy,M.P. and Phizicky,E.M. (2014) Two-subunit enzymes involved in eukaryotic post-transcriptional tRNA modification. *RNA Biol.*, **11**, 1608–1618.
3. Barraud,P., Gato,A., Heiss,M., Catala,M., Kellner,S. and Tisné,C. (2019) Time-resolved NMR monitoring of tRNA maturation. *Nat. Commun.*, **10**, 3373.
4. Dimitrova,D.G., Teysset,L. and Carré,C. (2019) RNA 2′-O-methylation (Nm) modification in human diseases. *Genes*, **10**, 117.
5. Ayadi,L., Galvanin,A., Pichot,F., Marchand,V. and Motorin,Y. (2019) RNA ribose methylation (2′-O-methylation): occurrence, biosynthesis and biological functions. *Biochim. Biophys. Acta Gene Regul. Mech.*, **1862**, 253–269.
6. Somme,J., Van Laer,B., Roovers,M., Steyaert,J., Versées,W. and Droogmans,L. (2014) Characterization of two homologous 2′-O-methyltransferases showing different specificities for their tRNA substrates. *RNA*, **20**, 1257–1271.
7. Rebane,A., Roomere,H. and Metspalu,A. (2002) Locations of several novel 2′-O-methylated nucleotides in human 28S rRNA. *BMC Mol. Biol.*, **3**, 1.
8. Darzacq,X., Jády,B.E., Verheggen,C., Kiss,A.M., Bertrand,E. and Kiss,T. (2002) Cajal body-specific small nuclear RNAs: a novel class of 2′-O-methylation and pseudouridylation guide RNAs. *EMBO J.*, **21**, 2746–2756.
9. Cavaillé,J., Nicoloso,M. and Bachellerie,J.P. (1996) Targeted ribose methylation of RNA in vivo directed by tailored antisense RNA guides. *Nature*, **383**, 732–735.
10. Bachellerie,J.P., Cavaillé,J. and Hüttenhofer,A. (2002) The expanding snoRNA world. *Biochimie*, **84**, 775–790.
11. Reichow,S.L., Hamma,T., Ferre-D'Amare,A.R. and Varani,G. (2007) The structure and function of small nucleolar ribonucleoproteins. *Nucleic Acids Res.*, **35**, 1452–1464.
12. Henras,A.K., Soudet,J., Gérus,M., Lebaron,S., Caizergues-Ferrer,M., Mougin,A. and Henry,Y. (2008) The post-transcriptional steps of eukaryotic ribosome biogenesis. *Cell. Mol. Life Sci.*, **65**, 2334–2359.
13. Mao,Y.S., Zhang,B. and Spector,D.L. (2011) Biogenesis and function of nuclear bodies. *Trends Genet.*, **27**, 295–306.
14. Massenet,S., Bertrand,E. and Verheggen,C. (2017) Assembly and trafficking of box C/D and H/ACA snoRNPs. *RNA Biol.*, **14**, 680–692.
15. Meier,U.T. (2017) RNA modification in Cajal bodies. *RNA Biol.*, **14**, 693–700.
16. Jády,B.E. and Kiss,T. (2001) A small nucleolar guide RNA functions both in 2′-O-ribose methylation and pseudouridylation of the U5 spliceosomal RNA. *EMBO J.*, **20**, 541–551.
17. Kishore,S., Gruber,A.R., Jedlinski,D.J., Syed,A.P., Jorjani,H. and Zavolan,M. (2013) Insights into snoRNA biogenesis and processing from PAR-CLIP of snoRNA core proteins and small RNA sequencing. *Genome Biol.*, **14**, R45.
18. Vitali,P. and Kiss,T. (2019) Cooperative 2′-O-methylation of the wobble cytidine of human elongator tRNAMet(CAT) by a nucleolar and a Cajal body-specific box C/D RNP. *Genes Dev.*, **33**, 741–746.
19. Li,J., Yang,Z., Yu,B., Liu,J. and Chen,X. (2005) Methylation protects miRNAs and siRNAs from a 3′-end uridylation activity in Arabidopsis. *Curr. Biol.*, **15**, 1501–1507.
20. Yu,B., Yang,Z., Li,J., Minakhina,S., Yang,M., Padgett,R.W., Steward,R. and Chen,X. (2005) Methylation as a crucial step in plant microRNA biogenesis. *Science*, **307**, 932–935.
21. Zhao,Y., Mo,B. and Chen,X. (2012) Mechanisms that impact microRNA stability in plants. *RNA Biol.*, **9**, 1218–1223.
22. Horwich,M.D., Li,C., Matranga,C., Vagin,V., Farley,G., Wang,P. and Zamore,P.D. (2007) The Drosophila RNA methyltransferase, DmHen1, modifies germline piRNAs and single-stranded siRNAs in RISC. *Curr. Biol.*, **17**, 1265–1272.
23. Saito,K., Sakaguchi,Y., Suzuki,T., Suzuki,T., Siomi,H. and Siomi,M.C. (2007) Pimet, the drosophila homolog of hen1, mediates 2′-o-methylation of piwi- interacting rnas at their 3′ ends. *Genes Dev.*, **21**, 1603–1608.
24. Kurth,H.M. and Mochizuki,K. (2009) 2′-O-methylation stabilizes Piwi-associated small RNAs and ensures DNA elimination in Tetrahymena. *RNA*, **15**, 675–685.
25. Bartoli,K.M., Schaening,C., Carlile,T. and Gilbert,W.V. (2018) Conserved methyltransferase spb1 targets mrnas for regulated modification with 2′-O-methyl ribose. bioRxiv doi: https://doi.org/10.1101/271916, 08 March 2018, preprint: not peer reviewed.
26. Ringeard,M., Marchand,V., Decroly,E., Motorin,Y. and Bennasser,Y. (2019) FTSJ3 is an RNA 2′-O-methyltransferase recruited by HIV to avoid innate immune sensing. *Nature*, **565**, 500–504.
27. Elliott,B.A., Ho,H.-T., Ranganathan,S.V., Vangaveti,S., Ilkayeva,O., Assi,H.A., Choi,A.K., Agris,P.F. and Holley,C.L. (2019) Modification of messenger RNA by 2′-O-methylation regulates gene expression in vivo. *Nat. Commun.*, **10**, 3401.
28. Sproat,B.S., Lamond,A.I., Beijer,B., Neuner,P. and Ryder,U. (1989) Highly efficient chemical synthesis of 2′-O-methyloligoribonucleotides and tetrabiotinylated derivatives; novel probes that are resistant to degradation by RNA or DNA specific nucleases. *Nucleic Acids Res.*, **17**, 3373–3386.

29. Byszewska,M., Śmietański,M., Purta,E. and Bujnicki,J.M. (2014) RNA methyltransferases involved in 5′ cap biosynthesis. *RNA Biol.*, **11**, 1597–1607.
30. Kumar,S., Mapa,K. and Maiti,S. (2014) Understanding the effect of locked nucleic acid and 2′-O-methyl modification on the hybridization thermodynamics of a miRNA-mRNA pair in the presence and absence of AfPiwi protein. *Biochemistry*, **53**, 1607–1615.
31. Yildirim,I., Kierzek,E., Kierzek,R. and Schatz,G.C. (2014) Interplay of LNA and 2′-O-methyl RNA in the structure and thermodynamics of RNA hybrid systems: a molecular dynamics study using the revised AMBER force field and comparison with experimental results. *J. Phys. Chem. B*, **118**, 14177–14187.
32. Inoue,H., Hayase,Y., Imura,A., Iwai,S., Miura,K. and Ohtsuka,E. (1987) Synthesis and hybridization studies on two complementary nona (2′-O-methyl) ribonucleotides. *Nucleic Acids Res.*, **15**, 6131–6148.
33. Kawai,G., Yamamoto,Y., Kamimura,T., Masegi,T., Sekine,M., Hata,T., Iimori,T., Watanabe,T., Miyazawa,T. and Yokoyama,S. (1992) Conformational rigidity of specific pyrimidine residues in tRNA arises from posttranscriptional modifications that enhance steric interaction between the base and the 2′-hydroxyl group. *Biochemistry*, **31**, 1040–1046.
34. Majlessi,M., Nelson,N.C. and Becker,M.M. (1998) Advantages of 2′-O-methyl oligoribonucleotide probes for detecting RNA targets. *Nucleic Acids Res.*, **26**, 2224–2229.
35. Tsourkas,A., Behlke,M.A. and Bao,G. (2002) Hybridization of 2′-O-methyl and 2′-deoxy molecular beacons to RNA and DNA targets. *Nucleic Acids Res.*, **30**, 5168–5174.
36. Lebars,I., Legrand,P., Aimé,A., Pinaud,N., Fribourg,S. and Di Primo,C. (2008) Exploring TAR–RNA aptamer loop–loop interaction by X-ray crystallography, UV spectroscopy and surface plasmon resonance. *Nucleic Acids Res.*, **36**, 7146–7156.
37. Hou,Y.-M., Zhang,X., Holland,J.A. and Davis,D.R. (2001) An important 2′-OH group for an RNA–protein interaction. *Nucleic Acids Res.*, **29**, 976–985.
38. Lacoux,C., Di Marino,D., Pilo Boyl,P., Zalfa,F., Yan,B., Ciotti,M.T., Falconi,M., Urlaub,H., Achsel,T., Mougin,A. *et al.* (2012) BC1-FMRP interaction is modulated by 2′-O-methylation: RNA-binding activity of the tudor domain and translational regulation at synapses. *Nucleic Acids Res.*, **40**, 4086–4096.
39. Jones,S., Daley,D.T.A., Luscombe,N.M., Berman,H.M. and Thornton,J.M. (2001) Protein–RNA interactions: a structural analysis. *Nucleic Acids Res.*, **29**, 943–954.
40. Treger,M. and Westhof,E. (2001) Statistical analysis of atomic contacts at RNA–protein interfaces. *J. Mol. Recognit.*, **14**, 199–214.
41. Björk,G.R., Durand,J.M., Hagervall,T.G., Leipuviene,R., Lundgren,H.K., Nilsson,K., Chen,P., Qian,Q. and Urbonavicius,J. (1999) Transfer RNA modification: influence on translational frameshifting and metabolism. *FEBS Lett.*, **452**, 47–51.
42. Bregeon,D. (2001) Translational misreading: a tRNA modification counteracts a 2 ribosomal frameshift. *Genes Dev.*, **15**, 2295–2306.
43. Agris,P.F. (2004) Decoding the genome: a modified view. *Nucleic Acids Res.*, **32**, 223–238.
44. Kawarada,L., Suzuki,T., Ohira,T., Hirata,S., Miyauchi,K. and Suzuki,T. (2017) ALKBH1 is an RNA dioxygenase responsible for cytoplasmic and mitochondrial tRNA modifications. *Nucleic Acids Res.*, **45**, 7401–7415.
45. Guy,M.P. and Phizicky,E.M. (2015) Conservation of an intricate circuit for crucial modifications of the tRNAPhe anticodon loop in eukaryotes. *RNA*, **21**, 61–74.
46. Guy,M.P., Podyma,B.M., Preston,M.A., Shaheen,H.H., Krivos,K.L., Limbach,P.A., Hopper,A.K. and Phizicky,E.M. (2012) Yeast Trm7 interacts with distinct proteins for critical modifications of the tRNAPhe anticodon loop. *RNA*, **18**, 1921–1933.
47. Noma,A., Kirino,Y., Ikeuchi,Y. and Suzuki,T. (2006) Biosynthesis of wybutosine, a hyper-modified nucleoside in eukaryotic phenylalanine tRNA. *EMBO J.*, **25**, 2142–2154.
48. Pintard,L., Lecointe,F., Bujnicki,J.M., Bonnerot,C., Grosjean,H. and Lapeyre,B. (2002) Trm7p catalyses the formation of two 2′-O-methylriboses in yeast tRNA anticodon loop. *EMBO J.*, **21**, 1811–1820.
49. Guy,M.P., Shaw,M., Weiner,C.L., Hobson,L., Stark,Z., Rose,K., Kalscheuer,V.M., Gecz,J. and Phizicky,E.M. (2015) Defects in tRNA anticodon loop 2′-o-methylation are implicated in nonsyndromic x-linked intellectual disability due to mutations in FTSJ1. *Hum. Mutat.*, **36**, 1176–1187.
50. Angelova,M.T., Dimitrova,D.G., Dinges,N., Lence,T., Worpenberg,L., Carré,C. and Roignant,J.-Y. (2018) The emerging field of epitranscriptomics in neurodevelopmental and neuronal disorders. *Front. Bioeng. Biotechnol.*, **6**, 46.
51. Chou,H.-J., Donnard,E., Gustafsson,H.T., Garber,M. and Rando,O.J. (2017) Transcriptome-wide analysis of roles for tRNA modifications in translational regulation. *Mol. Cell*, **68**, 978–992.
52. Han,L., Guy,M.P., Kon,Y. and Phizicky,E.M. (2018) Lack of 2′-O-methylation in the tRNA anticodon loop of two phylogenetically distant yeast species activates the general amino acid control pathway. *PLoS Genet.*, **14**, e1007288.
53. Jensen,L.R., Garrett,L., Hölter,S.M., Rathkolb,B., Rácz,I., Adler,T., Prehn,C., Hans,W., Rozman,J., Becker,L. *et al.* (2018) A mouse model for intellectual disability caused by mutations in the X-linked 2′-O-methyltransferase Ftsj1 gene. *Biochim. Biophys. Acta Mol. Basis Dis.*, **1865**, 2083–2093.
54. Freude,K., Hoffmann,K., Jensen,L.-R., Delatycki,M.B., des Portes,V., Moser,B., Hamel,B., van Bokhoven,H., Moraine,C., Fryns,J.-P. *et al.* (2004) Mutations in the FTSJ1 gene coding for a novel S-adenosylmethionine-binding protein cause nonsyndromic X-linked mental retardation. *Am. J. Hum. Genet.*, **75**, 305–309.
55. Ramser,J., Winnepenninckx,B., Lenski,C., Errijgers,V., Platzer,M., Schwartz,C.E., Meindl,A. and Kooy,R.F. (2004) A splice site mutation in the methyltransferase gene FTSJ1 in Xp11.23 is associated with non-syndromic mental retardation in a large Belgian family (MRX9). *J. Med. Genet.*, **41**, 679–683.
56. Flockhart,I., Booker,M., Kiger,A., Boutros,M., Armknecht,S., Ramadan,N., Richardson,K., Xu,A., Perrimon,N. and Mathey-Prevot,B. (2006) FlyRNAi: the Drosophila RNAi screening center database. *Nucleic Acids Res.*, **34**, D489–D494.
57. Katoh,K. and Standley,D.M. (2013) MAFFT multiple sequence alignment software version 7: improvements in performance and usability. *Mol. Biol. Evol.*, **30**, 772–780.
58. Capella-Gutiérrez,S., Silla-Martínez,J.M. and Gabaldón,T. (2009) trimAl: a tool for automated alignment trimming in large-scale phylogenetic analyses. *Bioinformatics*, **25**, 1972–1973.
59. Stamatakis,A. (2014) RAxML version 8: a tool for phylogenetic analysis and post-analysis of large phylogenies. *Bioinformatics*, **30**, 1312–1313.
60. Marchand,V., Pichot,F., Thüring,K., Ayadi,L., Freund,I., Dalpke,A., Helm,M. and Motorin,Y. (2017) Next-generation sequencing-based ribomethseq protocol for analysis of trna 2′-o-methylation. *Biomolecules*, **7**, E13.
61. Bolger,A.M., Lohse,M. and Usadel,B. (2014) Trimmomatic: a flexible trimmer for Illumina sequence data. *Bioinformatics*, **30**, 2114–2120.
62. Langmead,B., Trapnell,C., Pop,M. and Salzberg,S.L. (2009) Ultrafast and memory-efficient alignment of short DNA sequences to the human genome. *Genome Biol.*, **10**, R25.
63. Quinlan,A.R. (2014) BEDTools: the swiss-army tool for genome feature analysis. *Curr. Protoc. Bioinformatics*, **47**, 11.12.1–11.12.34.
64. Birkedal,U., Christensen-Dalsgaard,M., Krogh,N., Sabarinathan,R., Gorodkin,J. and Nielsen,H. (2015) Profiling of ribose methylations in RNA by high-throughput sequencing. *Angew. Chem. Int. Ed Engl.*, **54**, 451–455.
65. Marchand,V., Blanloeil-Oillo,F., Helm,M. and Motorin,Y. (2016) Illumina-based RiboMethSeq approach for mapping of 2′-O-Me residues in RNA. *Nucleic Acids Res.*, **44**, e135.
66. Carré,C., Jacquier,C., Bougé,A.-L., de Chaumont,F., Besnard-Guerin,C., Thomassin,H., Pidoux,J., Da Silva,B., Chalatsi,E., Zahra,S. *et al.* (2013) AutomiG, a biosensor to detect alterations in miRNA biogenesis and in small RNA silencing guided by perfect target complementarity. *PLoS One*, **8**, e74296.
67. Genenncher,B., Durdevic,Z., Hanna,K., Zinkl,D., Mobin,M.B., Senturk,N., Da Silva,B., Legrand,C., Carré,C., Lyko,F. *et al.* (2018) Mutations in Cytosine-5 tRNA Methyltransferases Impact Mobile Element Expression and Genome Stability at Specific DNA Repeats. *Cell Rep.*, **22**, 1861–1874.
68. Besnard-Guérin,C., Jacquier,C., Pidoux,J., Deddouche,S. and Antoniewski,C. (2015) The cricket paralysis virus suppressor

inhibits microRNA silencing mediated by the Drosophila Argonaute-2 protein. *PLoS One*, **10**, e0120205.
69. Gokcezade,J., Sienski,G. and Duchek,P. (2014) Efficient CRISPR/Cas9 plasmids for rapid and versatile genome editing in Drosophila. *G3*, **4**, 2279–2282.
70. Miroux,B. and Walker,J.E. (1996) Over-production of proteins in Escherichia coli: mutant hosts that allow synthesis of some membrane proteins and globular proteins at high levels. *J. Mol. Biol.*, **260**, 289–298.
71. Näär,A.M., Taatjes,D.J., Zhai,W., Nogales,E. and Tjian,R. (2002) Human CRSP interacts with RNA polymerase II CTD and adopts a specific CTD-bound conformation. *Genes Dev.*, **16**, 1339–1344.
72. Carré,C. and Shiekhattar,R. (2011) Human GTPases associate with RNA polymerase II to mediate its nuclear import. *Mol. Cell. Biol.*, **31**, 3953–3962.
73. Dobin,A., Davis,C.A., Schlesinger,F., Drenkow,J., Zaleski,C., Jha,S., Batut,P., Chaisson,M. and Gingeras,T.R. (2013) STAR: ultrafast universal RNA-seq aligner. *Bioinformatics*, **29**, 15–21.
74. Liao,Y., Smyth,G.K. and Shi,W. (2014) featureCounts: an efficient general purpose program for assigning sequence reads to genomic features. *Bioinformatics*, **30**, 923–930.
75. Huber,W., Carey,V.J., Gentleman,R., Anders,S., Carlson,M., Carvalho,B.S., Bravo,H.C., Davis,S., Gatto,L., Girke,T. *et al.* (2015) Orchestrating high-throughput genomic analysis with Bioconductor. *Nat. Methods*, **12**, 115–121.
76. Love,M.I., Huber,W. and Anders,S. (2014) Moderated estimation of fold change and dispersion for RNA-seq data with DESeq2. *Genome Biol.*, **15**, 550.
77. Langmead,B. (2010) Aligning short sequencing reads with bowtie. *Curr. Protoc. Bioinformatics*, doi:10.1002/0471250953.bi1107s32.
78. Tricoire,H., Battisti,V., Trannoy,S., Lasbleiz,C., Pret,A.-M. and Monnier,V. (2009) The steroid hormone receptor EcR finely modulates Drosophila lifespan during adulthood in a sex-specific manner. *Mech. Ageing Dev.*, **130**, 547–552.
79. Bahadorani,S. and Hilliker,A.J. (2008) Cocoa confers life span extension in Drosophila melanogaster. *Nutr. Res.*, **28**, 377–382.
80. Iwasaki,S., Kobayashi,M., Yoda,M., Sakaguchi,Y., Katsuma,S., Suzuki,T. and Tomari,Y. (2010) Hsc70/Hsp90 chaperone machinery mediates ATP-dependent RISC loading of small RNA duplexes. *Mol. Cell*, **39**, 292–299.
81. Rehwinkel,J., Natalin,P., Stark,A., Brennecke,J., Cohen,S.M. and Izaurralde,E. (2006) Genome-wide analysis of mrnas regulated by drosha and argonaute proteins in drosophila melanogaster. *Mol. Cell. Biol.*, **26**, 2965–2975.
82. Rehwinkel,J. (2005) A crucial role for GW182 and the DCP1:DCP2 decapping complex in miRNA-mediated gene silencing. *RNA*, **11**, 1640–1647.
83. Venken,K.J.T., He,Y., Hoskins,R.A. and Bellen,H.J. (2006) P [acman]: a BAC transgenic platform for targeted insertion of large DNA fragments in D. melanogaster. *Science*, **314**, 1747–1751.
84. Galiana-Arnoux,D., Dostert,C., Schneemann,A., Hoffmann,J.A. and Imler,J.-L. (2006) Essential function in vivo for Dicer-2 in host defense against RNA viruses in drosophila. *Nat. Immunol.*, **7**, 590–597.
85. Okamura,K., Balla,S., Martin,R., Liu,N. and Lai,E.C. (2008) Two distinct mechanisms generate endogenous siRNAs from bidirectional transcription in Drosophila melanogaster. *Nat. Struct. Mol. Biol.*, **15**, 581–590.
86. Karam,J.A., Parikh,R.Y., Nayak,D., Rosenkranz,D. and Gangaraju,V.K. (2017) Co-chaperone Hsp70/Hsp90-organizing protein (Hop) is required for transposon silencing and Piwi-interacting RNA (piRNA) biogenesis. *J. Biol. Chem.*, **292**, 6039–6046.
87. Sarot,E., Payen-Groschêne,G., Bucheton,A. and Pélisson,A. (2004) Evidence for a piwi-dependent RNA silencing of the gypsy endogenous retrovirus by the Drosophila melanogaster flamenco gene. *Genetics*, **166**, 1313–1321.
88. Olivieri,D., Sykora,M.M., Sachidanandam,R., Mechtler,K. and Brennecke,J. (2010) An in vivo RNAi assay identifies major genetic and cellular requirements for primary piRNA biogenesis in Drosophila. *EMBO J.*, **29**, 3301–3317.
89. Handler,D., Meixner,K., Pizka,M., Lauss,K., Schmied,C., Gruber,F.S. and Brennecke,J. (2013) The genetic makeup of the Drosophila piRNA pathway. *Mol. Cell*, **50**, 762–777.
90. Altwegg,M. and Kubli,E. (1979) The nucleotide sequence of phenylalanine tRNA2 of Drosophila melanogaster: four isoacceptors with one basic sequence. *Nucleic Acids Res.*, **7**, 93–105.
91. Altwegg,M. and Kubli,E. (1980) The nucleotide sequence of glutamate tRNA4 of Drosophila melanogaster. *Nucleic Acids Res.*, **8**, 215–223.
92. Moraru,A., Cakan-Akdogan,G., Strassburger,K., Males,M., Mueller,S., Jabs,M., Muelleder,M., Frejno,M., Braeckman,B.P., Ralser,M. *et al.* (2017) THADA regulates the organismal balance between energy storage and heat production. *Dev. Cell*, **41**, 72–81.
93. Li,D., Burch,P., Gonzalez,O., Kashork,C.D., Shaffer,L.G., Bachinski,L.L. and Roberts,R. (2000) Molecular cloning, expression analysis, and chromosome mapping of WDR6, a novel human WD-repeat gene. *Biochem. Biophys. Res. Commun.*, **274**, 117–123.
94. Shaheen,R., Abdel-Salam,G.M.H., Guy,M.P., Alomar,R., Abdel-Hamid,M.S., Afifi,H.H., Ismail,S.I., Emam,B.A., Phizicky,E.M. and Alkuraya,F.S. (2015) Mutation in WDR4 impairs tRNA m(7)G46 methylation and causes a distinct form of microcephalic primordial dwarfism. *Genome Biol.*, **16**, 210.
95. Durdevic,Z., Mobin,M.B., Hanna,K., Lyko,F. and Schaefer,M. (2013) The RNA methyltransferase Dnmt2 is required for efficient Dicer-2-dependent siRNA pathway activity in Drosophila. *Cell Rep.*, **4**, 931–937.
96. Blanco,S., Dietmann,S., Flores,J.V., Hussain,S., Kutter,C., Humphreys,P., Lukk,M., Lombard,P., Treps,L., Popis,M. *et al.* (2014) Aberrant methylation of tRNAs links cellular stress to neuro-developmental disorders. *EMBO J.*, **33**, 2020–2039.
97. Wang,X., Matuszek,Z., Huang,Y., Parisien,M., Dai,Q., Clark,W., Schwartz,M.H. and Pan,T. (2018) Queuosine modification protects cognate tRNAs against ribonuclease cleavage. *RNA*, **24**, 1305–1313.
98. Couvillion,M.T., Bounova,G., Purdom,E., Speed,T.P. and Collins,K. (2012) A Tetrahymena Piwi bound to mature tRNA 3′ fragments activates the exonuclease Xrn2 for RNA processing in the nucleus. *Mol. Cell*, **48**, 509–520.
99. Shigematsu,M. and Kirino,Y. (2015) tRNA-derived short Non-coding RNA as interacting partners of argonaute proteins. *Gene Regul. Syst. Bio.*, **9**, 27–33.
100. Martinez,G., Choudury,S.G. and Slotkin,R.K. (2017) tRNA-derived small RNAs target transposable element transcripts. *Nucleic Acids Res.*, **45**, 5142–5152.
101. Schorn,A.J., Gutbrod,M.J., LeBlanc,C. and Martienssen,R. (2017) LTR-Retrotransposon Control by tRNA-Derived Small RNAs. *Cell*, **170**, 61–71.
102. Ashraf,S.S., Guenther,R.H., Ansari,G., Malkiewicz,A., Sochacka,E. and Agris,P.F. (2000) Role of modified nucleosides of yeast tRNA(Phe) in ribosomal binding. *Cell Biochem. Biophys.*, **33**, 241–252.
103. Hoernes,T.P., Clementi,N., Faserl,K., Glasner,H., Breuker,K., Lindner,H., Hüttenhofer,A. and Erlacher,M.D. (2016) Nucleotide modifications within bacterial messenger RNAs regulate their translation and are able to rewire the genetic code. *Nucleic Acids Res.*, **44**, 852–862.
104. Choi,J., Indrisiunaite,G., DeMirci,H., Ieong,K.-W., Wang,J., Petrov,A., Prabhakar,A., Rechavi,G., Dominissini,D., He,C. *et al.* (2018) 2′-O-methylation in mRNA disrupts tRNA decoding during translation elongation. *Nat. Struct. Mol. Biol.*, **25**, 208–216.
105. Lyons,S.M., Fay,M.M. and Ivanov,P. (2018) The role of RNA modifications in the regulation of tRNA cleavage. *FEBS Lett.*, **592**, 2828–2844.
106. Saikia,M., Krokowski,D., Guan,B.-J., Ivanov,P., Parisien,M., Hu,G.-F., Anderson,P., Pan,T. and Hatzoglou,M. (2012) Genome-wide identification and quantitative analysis of cleaved tRNA fragments induced by cellular stress. *J. Biol. Chem.*, **287**, 42708–42725.
107. Anderson,P. and Ivanov,P. (2014) tRNA fragments in human health and disease. *FEBS Lett.*, **588**, 4297–4304.
108. Durdevic,Z. and Schaefer,M. (2013) tRNA modifications: Necessary for correct tRNA-derived fragments during the recovery from stress? *BioEssays*, **35**, 323–327.
109. Saito,K., Sakaguchi,Y., Suzuki,T., Suzuki,T., Siomi,H. and Siomi,M.C. (2007) Pimet, the Drosophila homolog of HEN1, mediates 2′-O-methylation of Piwi- interacting RNAs at their 3′ ends. *Genes Dev.*, **21**, 1603–1608.

110. Brennecke,J., Aravin,A.A., Stark,A., Dus,M., Kellis,M., Sachidanandam,R. and Hannon,G.J. (2007) Discrete small RNA-generating loci as master regulators of transposon activity in Drosophila. *Cell*, **128**, 1089–1103.
111. Ivanov,P., Emara,M.M., Villen,J., Gygi,S.P. and Anderson,P. (2011) Angiogenin-induced tRNA fragments inhibit translation initiation. *Mol. Cell*, **43**, 613–623.
112. Ivanov,P., O'Day,E., Emara,M.M., Wagner,G., Lieberman,J. and Anderson,P. (2014) G-quadruplex structures contribute to the neuroprotective effects of angiogenin-induced tRNA fragments. *Proc. Natl. Acad. Sci. U.S.A.*, **111**, 18201–18206.
113. Goodarzi,H., Liu,X., Nguyen,H.C.B., Zhang,S., Fish,L. and Tavazoie,S.F. (2015) Endogenous tRNA-Derived fragments suppress breast cancer progression via YBX1 displacement. *Cell*, **161**, 790–802.
114. Nyswaner,K.M., Checkley,M.A., Yi,M., Stephens,R.M. and Garfinkel,D.J. (2008) Chromatin-associated genes protect the yeast genome from Ty1 insertional mutagenesis. *Genetics*, **178**, 197–214.
115. Li,W., Prazak,L., Chatterjee,N., Grüninger,S., Krug,L., Theodorou,D. and Dubnau,J. (2013) Activation of transposable elements during aging and neuronal decline in Drosophila. *Nat. Neurosci.*, **16**, 529–531.
116. Krug,L., Chatterjee,N., Borges-Monroy,R., Hearn,S., Liao,W.-W., Morrill,K., Prazak,L., Rozhkov,N., Theodorou,D., Hammell,M. *et al.* (2017) Retrotransposon activation contributes to neurodegeneration in a Drosophila TDP-43 model of ALS. *PLoS Genet.*, **13**, e1006635.
117. Chang,Y.-H. and Dubnau,J. (2019) The gypsy endogenous retrovirus drives non-cell-autonomous propagation in a drosophila tdp-43 model of neurodegeneration. *Curr. Biol.*, **29**, 3135–3152.
118. Sivan,G., Glushakow-Smith,S.G., Katsafanas,G.C., Americo,J.L. and Moss,B. (2018) Human host range restriction of the vaccinia virus c7/k1 double deletion mutant is mediated by an atypical mode of translation inhibition. *J. Virol.*, **92**, e01329-18.
119. Edgar,R., Domrachev,M. and Lash,A.E. (2002) Gene Expression Omnibus: NCBI gene expression and hybridization array data repository. *Nucleic Acids Res.*, **30**, 207–210.

A

#	Function (known or predicted)	Gene name	CG number
1	protein histidine phosphatase activity	*janA*	CG7933
2	Unknown		CG12688
3	Hsp90 protein binding; chaperone binding; prostaglandin-E synthase activity.	*p23*	CG16817
4	rRNA processing; translation.		CG1789
5	Unknown		CG18537
6	Unknown		CG42240
7	Unknown		CG5866
8	mRNA splicing/ binding		CG3542
9	protein transporter	*AP-50*	CG7057
10	phospholipase A1		CG6283
11	Electron transport	*wal*	CG8996
12	alpha-amylase activity	*Amy-p/Amy-d*	CG18730
13	Antibacterial peptide metabolism	*Anp*	CG1361
14	tRNA/ rRNA methyltransferase		CG7009
15	Sensorial perception odorant binding	*Obp19c*	CG15457
16	response to virus; post-mating behavior	*EPebIII*	CG11390
17	Calcium ion binding		CG5890
18	RNA silencing	*Drosha*	CG8730
19	RNA silencing	*pasha*	CG1800
20	RNA silencing	*Ago2*	CG7439
21	RNA silencing	*Droj2*	CG8863

B

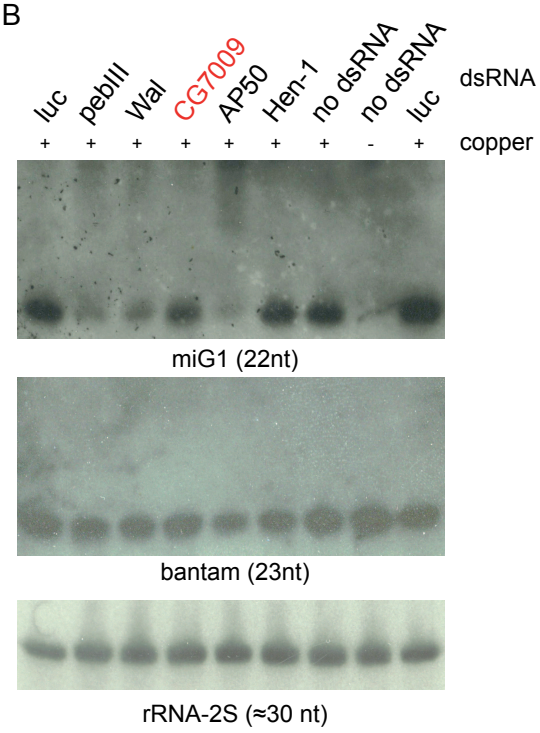

C

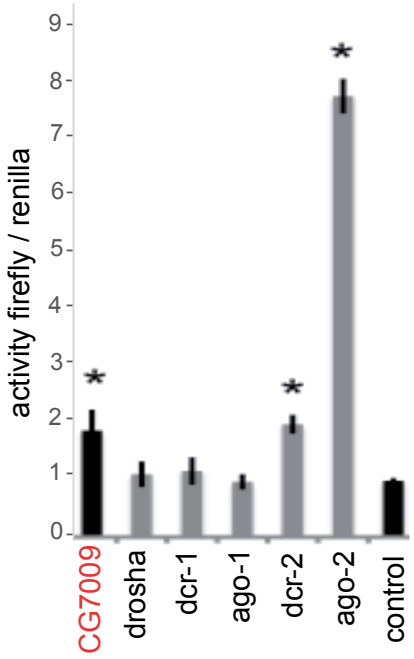

D

	Log2 fold changes
ND4	-1
Cyt-b	-0,91
ND1	-0,83
Col	-0,82
ColII	-0,76
Ago2	-0,7
ND5	-0,66
ATPase6	-0,62
lrRNA	-0,52
exd	-0,34

E

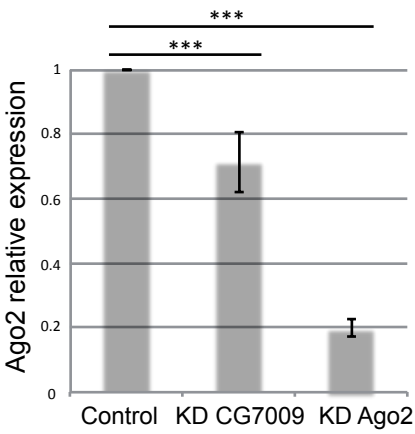

Sup_Figure.1

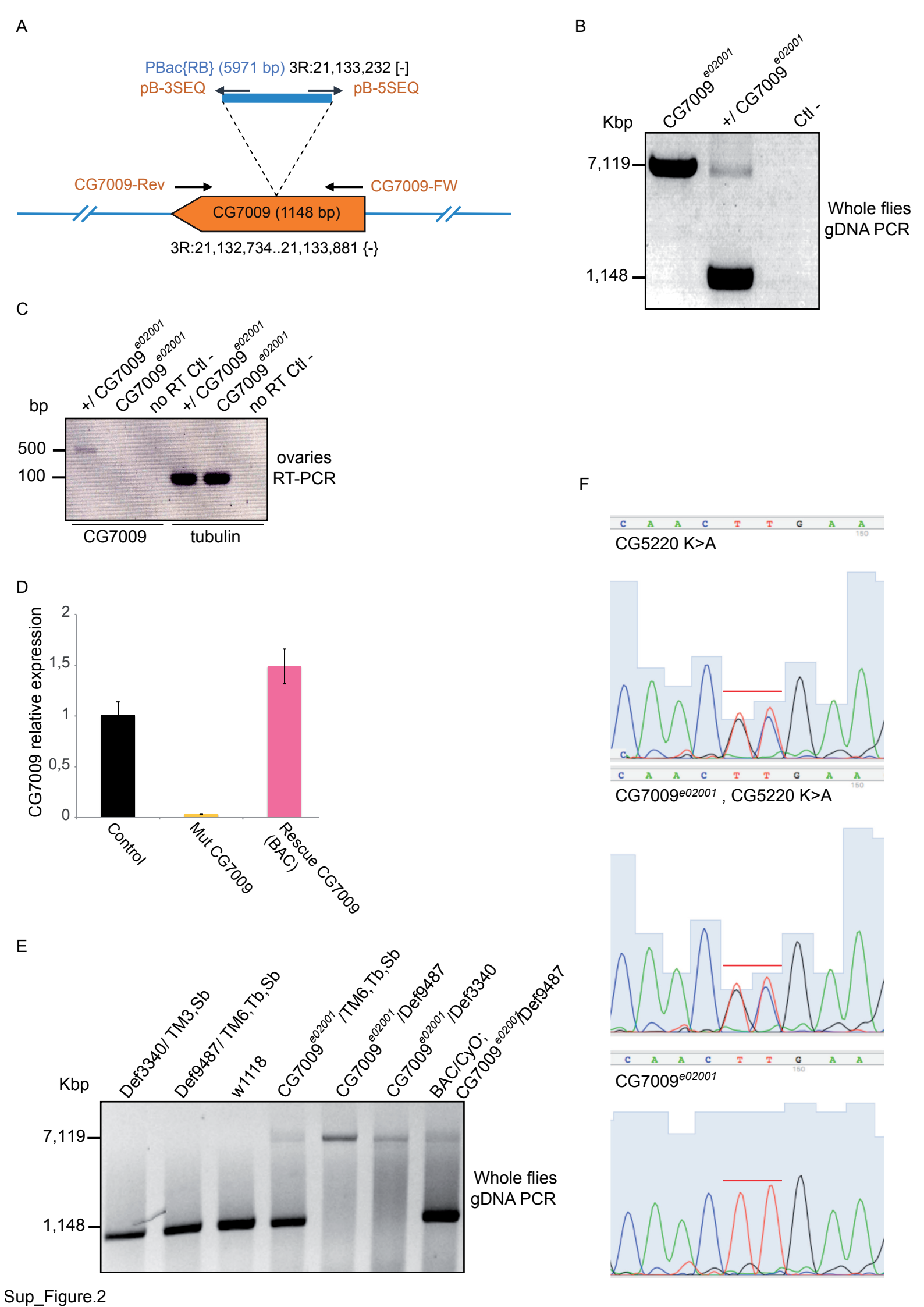
A
PBac{RB} (5971 bp) 3R:21,133,232 [-]
pB-3SEQ
pB-5SEQ
CG7009-Rev
CG7009-FW
CG7009 (1148 bp)
3R:21,132,734..21,133,881 {-}
B
Kbp
CG7009 e02001
+/ CG7009 e02001
Ctl -
7,119
1,148
Whole flies
gDNA PCR
C
bp
+/ CG7009 e02001
CG7009 e02001
no RT Ctl -
+/ CG7009 e02001
CG7009 e02001
no RT Ctl -
500
100
ovaries
RT-PCR
CG7009
tubulin
D
CG7009 relative expression
2
1,5
1
0,5
0
Control
Mut CG7009
Rescue CG7009 (BAC)
E
Kbp
Def3340/ TM3,Sb
Def9487/ TM6,Tb,Sb
w1118
CG7009 e02001 /TM6,Tb,Sb
CG7009 e02001 /Def9487
CG7009 e02001 /Def3340
BAC/CyO; CG7009 e02001/Def9487
7,119
1,148
Whole flies
gDNA PCR
F
C A A C T T G A A
CG5220 K>A
CG7009 e02001 , CG5220 K>A
CG7009 e02001

Sup_Figure.2

A

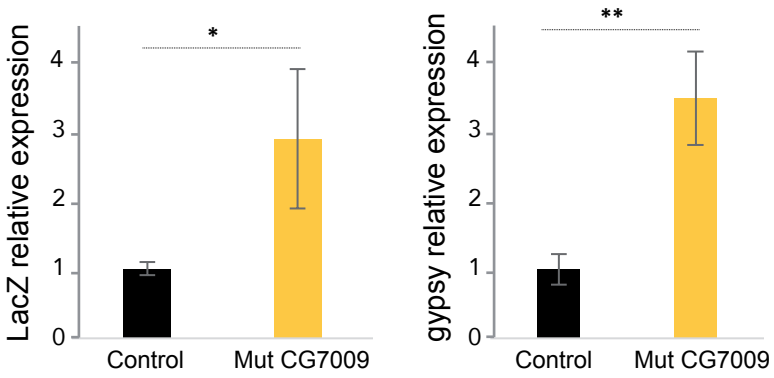

B

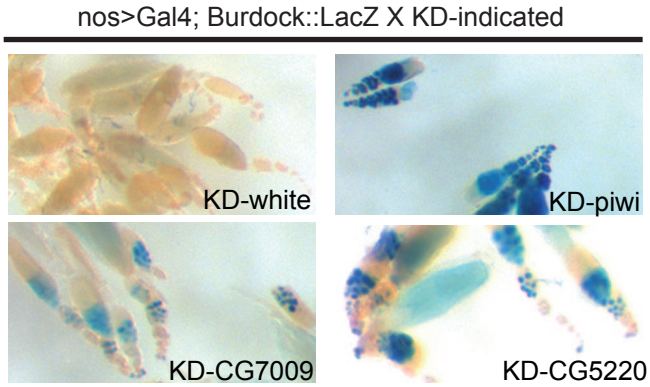

C

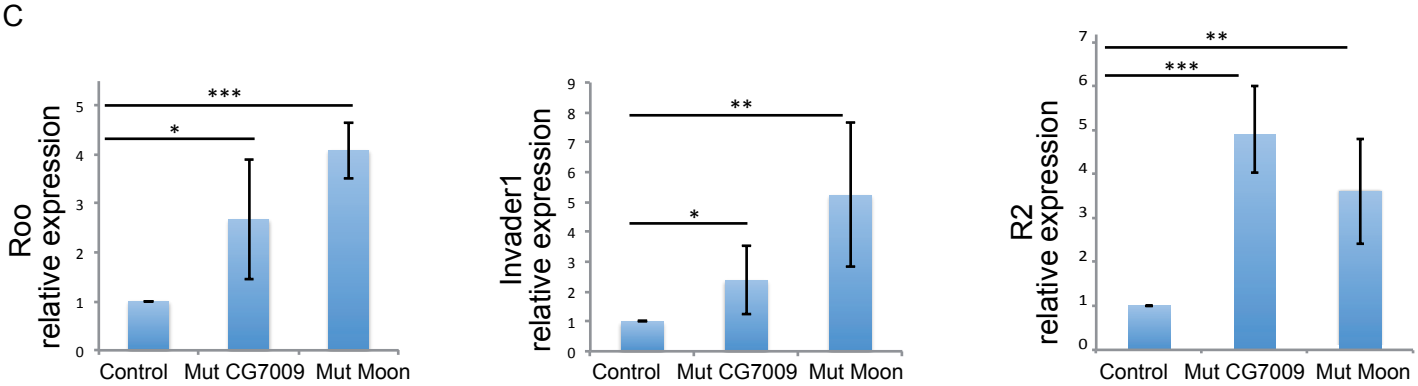

Sup_Figure.3

A

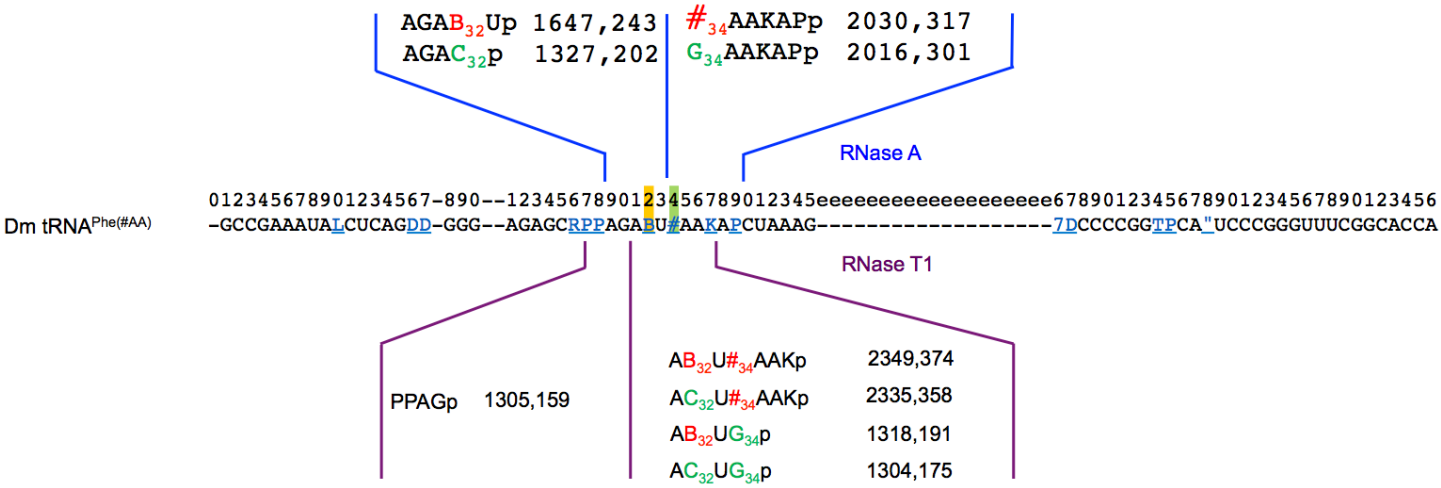

B

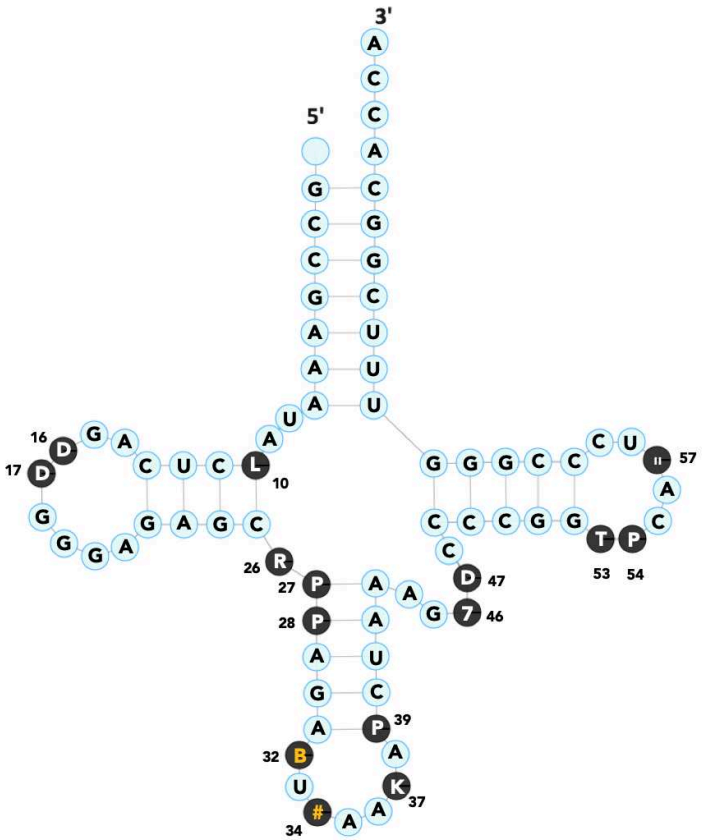

L N2-methylguanosine

D dihydrouridine

R N2,N2-dimethylguanosine

P pseudouridine

B 2′-O-methylcytidine

2′-O-methylguanosine

K 1-methylguanosine

7 7-methylguanosine

" 1-methyladenosine

T 5-methyluridine

Sup_Figure 4

A

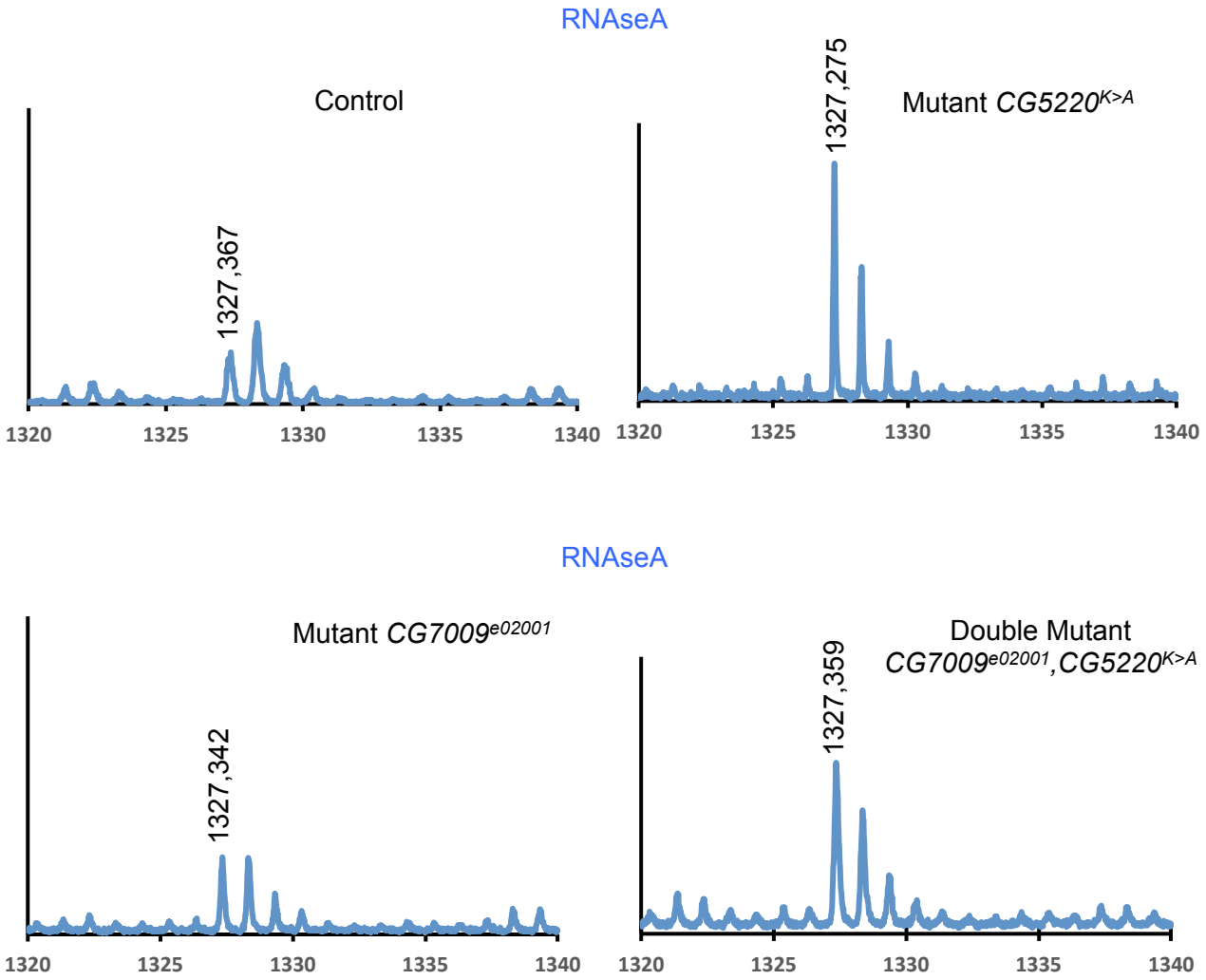

B

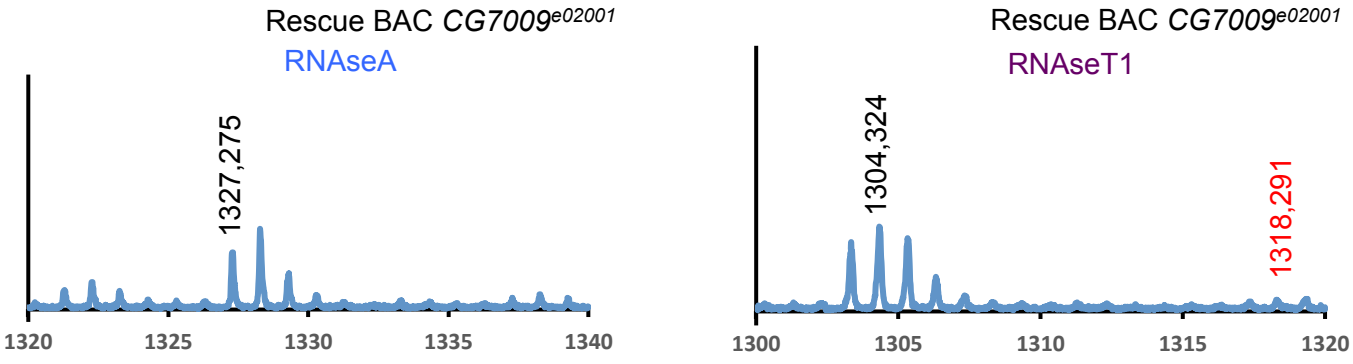

Sup_Figure 5

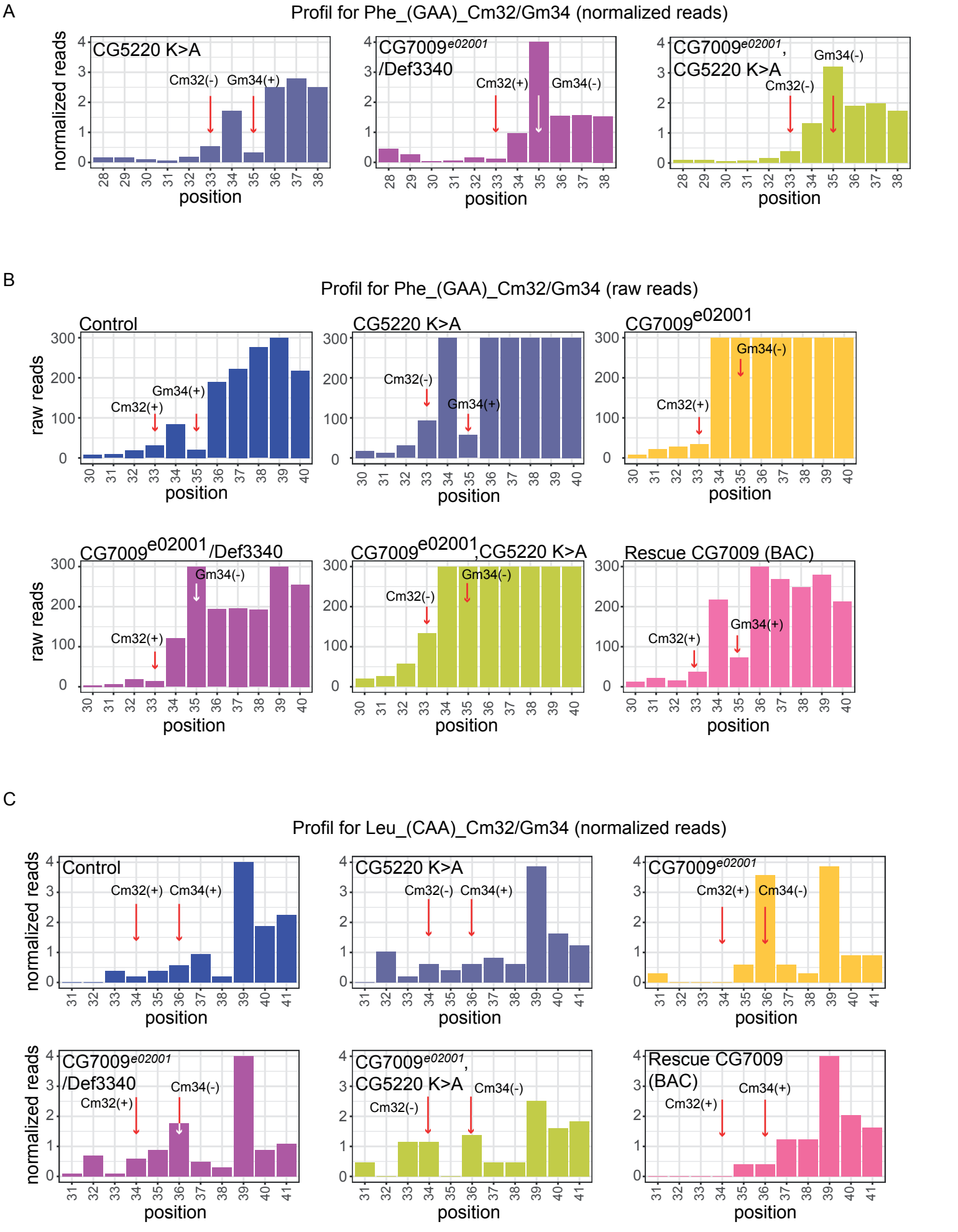
A
Profil for Phe_(GAA)_Cm32/Gm34 (normalized reads)
normalized reads
CG5220 K>A
Cm32(-) Gm34(+)
CG7009e02001 /Def3340
Cm32(+) Gm34(-)
CG7009e02001, CG5220 K>A
Cm32(-) Gm34(-)
position
B
Profil for Phe_(GAA)_Cm32/Gm34 (raw reads)
raw reads
Control
Cm32(+) Gm34(+)
CG5220 K>A
Cm32(-) Gm34(+)
CG7009e02001
Cm32(+) Gm34(-)
CG7009e02001 /Def3340
Cm32(+) Gm34(-)
CG7009e02001,CG5220 K>A
Cm32(-) Gm34(-)
Rescue CG7009 (BAC)
Cm32(+) Gm34(+)
position
C
Profil for Leu_(CAA)_Cm32/Gm34 (normalized reads)
normalized reads
Control
Cm32(+) Cm34(+)
CG5220 K>A
Cm32(-) Cm34(+)
CG7009e02001
Cm32(+) Cm34(-)
CG7009e02001 /Def3340
Cm32(+) Cm34(-)
CG7009e02001, CG5220 K>A
Cm32(-) Cm34(-)
Rescue CG7009 (BAC)
Cm32(+) Cm34(+)
position

Sup_Figure.6

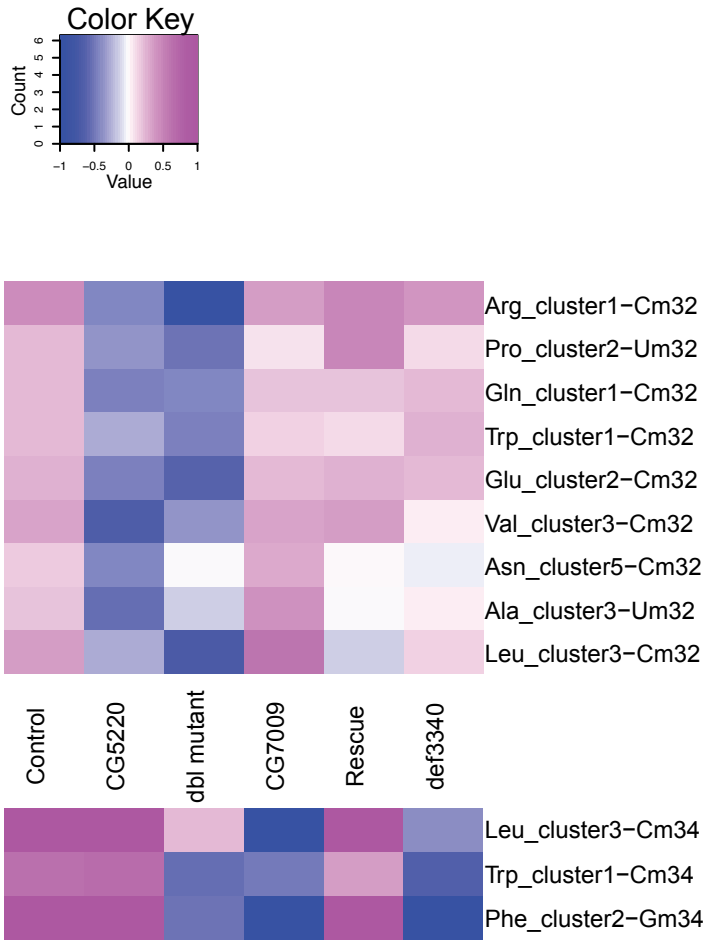
Color Key
Count
0 1 2 3 4 5 6
−1 −0.5 0 0.5 1
Value
Arg_cluster1−Cm32
Pro_cluster2−Um32
Gln_cluster1−Cm32
Trp_cluster1−Cm32
Glu_cluster2−Cm32
Val_cluster3−Cm32
Asn_cluster5−Cm32
Ala_cluster3−Um32
Leu_cluster3−Cm32
Control
CG5220
dbl mutant
CG7009
Rescue
def3340
Leu_cluster3−Cm34
Trp_cluster1−Cm34
Phe_cluster2−Gm34

Sup_Figure.7

Supplementary Figure Legend

Figure S1.

A, List of the validated genes in the RNAi genome-wide screen. Indicated are the genes that scored positively in the *automiG* screen, their described or predicted function in FlyBase, the gene name (when available), and the CG number, according to FlyBase. Blue colored names indicate genes already known in RNA silencing pathways. Red point to CG7009.

B, Northern blot characterization of miG1 Ago2-loaded miRNA in KD *CG7009 automiG* S2 cells. Northern blot on total RNAs extracted from *automiG* transfected S2 cells induced (+) or not (-) with copper sulfate for *automiG* expression and KD using dsRNA transfection on indicated genes were performed using miG1 (Ago2 loaded) or bantam (Ago1 loaded) miRNAs specific probes and a 2S rRNA probe as loading and transfer control. nt: nucleotide.

C, siRNA sensor (80, 81) reveal failure in Dcr2/ Ago2-dependent siRNA pathway. After 4 days of treatment with a dsRNA specifically inactivating the indicated gene, S2 cells were co-transfected with 2 vectors expressing firefly and Renilla (control) luciferases in addition to dsRNA targeting firefly luciferase (dsRNA Fluc). Firefly and renilla activities were measured 48 hours after transfection. The averages of the ratios of firefly/renilla activity for three independent experiments with standard deviations of the means.d are represented, the average for the dsRNA GFP (control) being set at 1. * indicates $p < 0.05$ *versus* control in a Student's t-test.

D, Ago2 mRNA is downregulated upon *CG7009* KD. The heat map shows the top 10 differentially expressed genes in S2 cells upon *CG7009* KD versus control (*LacZ* KD) in a RNA sequencing experiment. log2 Fold Change is indicated (padj = FDR-adjusted *p*-value for Ago2 is $7.73e^{-118}$). Red to yellow heat map colored table (Red: most down-regulated; yellow, less down-regulated). KD of *CG7009* led to the deregulation of 173 genes including 45 up and 128 down. 110 genes were deregulated with a corrected *p*-value (Benjamini and Hochberg, FDR) < 0.01.

E, Ago2 mRNA is downregulated upon *CG7009* KD. RT-qPCR using *Ago2*-specific primers on *automiG*-expressing S2 cells KD for *CG7009* (KD CG7009), *Ago2* (KD Ago2) and mock (Control). Error bars represent the standard deviation (s.d.) between four independent biological replicates. ****p-value* < 0.001 in a Student's t-test.

Figure S2.

A, schematic representation of the $CG7009^{e02001}$ allele showing the genomic location of the insertion and the size of the PBac{RB} transgenic transposon. The four hybridizing

oligonucleotides used in the genomic PCR analysis are represented with arrows representing their annealing locations and orientation (sequences in *Primers and Probes section*).

B, Agarose gel electrophoretic separation of the PCR reaction made on gDNA (genomic DNA) of adult flies *CG7009* homozygous or heterozygous for the mutant allele *CG7009*^{e02001} or Ctl - (no DNA) using CG7009-FW and CG7009-Rev primers. Expected sizes in base paired (Kbp) are indicated on the left.

C, Reverse Transcription PCR (RT-PCR) on total RNA extracts from ovaries. Electrophoretic separation of the RT-PCR reaction made on total RNA of flies *CG7009* homozygous or *CG7009* heterozygous for the mutant allele *CG7009*^{e02001} or no RT control (no reverse transcriptase in the RT reaction). The used primers for the PCR reaction are CG7009-middle Rev and CG7009-FW (expected product size 500nt) and tubulin primers (expected product size 150nt).

D, Reverse Transcription qPCR (RT-qPCR) on total RNA extracts from adult females of the indicated genotypes. *CG7009*^{e02001} heterozygous (Control), *CG7009*^{e02001} homozygous mutant (Mut CG7009) and rescue CG7009 (BAC).

E, Genotyping by PCR on genomic DNA of heterozygous *Def9487* and *Def3340* and *CG7009*^{e02001}. BAC (rescue) / CyO ; *CG7009*^{e02001} / *Def9487* lines, w1118 and *CG7009*^{e02001} homozygous lines. PCR on gDNA extracted from adult single flies with the indicated genotypes using primers CG7009-FW and CG7009-Rev. The band at 1148 bp corresponds to the WT *CG7009* locus, the band at 7119 bp corresponds to the mutant allele *CG7009*^{e02001}, containing the inserted *PiggyBac* transposon (Supplementary Figure S2A, B). BAC: Bacterial Artificial Chromosome containing the wild type *CG7009* genomic region; CyO; TM3,Sb; TM6,Tb,Sb: balancer chromosomes; Kbp: Kilo base pairs; gDNA genomic DNA.

F, Validation by sanger sequencing of the CRISPR/Cas9 mutants *CG5220*$^{K>A}$ and double mutant *CG5220*$^{K>A}$*, CG7009*^{e02001} recombination. Briefly, *CG5220* PCR fragments were amplified by PCR from flies gDNA bearing the *CG7009*^{e02001} allele (giving the [w+] phenotype) and the mutations *CG5220*$^{K>A}$. The corresponding simple mutant *CG5220*$^{K>A}$ (heterozygous for *CG5220*$^{K>A}$) was used as positive controls and flies characterized with no *CG5220* mutation were used as negative controls (*CG7009*^{e02001}). All sequencing experiments were performed on heteroallelic combinations over balanced chromosomes, explaining the double peaks at the edited region. The results were obtained using 4Peaks. They correspond to a PCR products obtained using VIE0197/VIE0198 primers and sequenced with the primer VIE0198. The targeted nucleotides are indicated under the red lines.

Figure S3.

A, RT-qPCR on ovaries heterozygous (control) or homozygous (Mut CG7009) for *CG7009*^{e02001} expressing the *Gypsy::LacZ* sensor (tj>Gal4/ +; Gypsy::LacZ) using *gyspy*- or *LacZ*- specific primers as described in Figure 2F. Error bars represent the standard deviation (s.d.) between three independent biological replicates. **p*-value < 0.05; ***p*-value < 0.01; ***p-value < 0.001 in a Student's t-test.

B, CG7009 and CG5220 are involved in *burdock* germinal TE-repression in *Drosophila* ovaries. *burdock::LacZ* sensor is silenced in germinal cells using nos>Gal4-mediated expression of an UAS-RNAi line (KD) targeting the *white* gene (KD control, nos>Gal4/ +; burdock::LacZ/UAS-*white*-RNAi). *Burdock* silencing is disrupted using *piwi* KD (positive control: blue coloration = β-Gal staining) and after KD of *CG7009* and *CG5220* expression.

C, RT-qPCR on ovaries from *w1118* (Control), homozygous for *CG7009*^{e02001} (Mut CG7009) or knockdown (Mut Moon), using *Roo, Invader1* or *R2* specific primers. Error bars represent the standard deviation (s.d.) between three to four independent biological replicates. **p*-value < 0.05; ***p*-value < 0.01; ***p-value < 0.001 in a Student's t-test.

Figure S4.

A, Sequence of *Drosophila melanogaster* tRNA$^{Phe(GAA)}$ with m/z values of fragments containing 2'-O-methyl-guanylate (#) and/or 2'-O-methyl-cytidylate (B) in daltons. The expected fragments resulting from RNase A (top) and RNase T1 (bottom) digestion of tRNA$^{Phe(GAA)}$ with the indicated Nm modification are zoomed in.

B, Schematic representation of 2D-structure of tRNA$^{Phe(GAA)}$ of *Drosophila*. Cm_{32} (B) and Gm_{34} (#) are indicated in yellow. **Bottom right**: Names of the different modifications present on *Drosophila* tRNA$^{Phe(GAA)}$ based on the Modomics and tRNAdb nomenclature**.**

Figure S5.

A, Related to Figures 5A and 5B. MALDI TOF-MS spectrum of fragments resulting from RNase A digestion of tRNA$^{Phe(GAA)}$ originating from indicated genotypes.

B, Related to Figures 5A and 5B. **Left panel,** MALDI TOF-MS spectrum of fragments resulting from RNase A digestion of tRNA$^{Phe(GAA)}$ originating from indicated genotypes (homozygous adult *CG7009*^{e02001} mutants rescued with one CG7009 WT copy (BAC)). **Right panel**: MALDI TOF-MS spectrum of fragments resulting from RNase T1 digestion of tRNA$^{Phe(GAA)}$ originating

from the indicated genotypes (homozygous adult *CG7009*^{e02001} mutants rescued with one CG7009 WT copy (BAC)). Relevant peaks are identified by their m/z values.

Figure S6.

A, Related to Figure 5C. RiboMethSeq analysis of tRNA$^{Phe(GAA)}$ modification at positions Cm_{32} and Gm_{34}. Alkaline fragmentation-based RiboMethSeq was performed on total RNAs extracted from whole flies homozygous mutant for *CG5220*$^{K>A}$, homozygous for *CG7009*^{e02001}/ *Def3340* and homozygous *CG5220*$^{K>A}$, *CG7009*^{e02001} double mutant as indicated. Normalized cleavage efficiencies, calculated from combined 5'-end and 3'-end coverages, are shown for the ± 5 neighboring nucleotides. The positions of interest (Cm_{32} and Gm_{34}) in tRNA$^{Phe(GAA)}$ are indicated by red arrows. Protection against cleavage is indicated as (+): protected, and as (-): not protected. Normalized cleavage efficiencies at Cm_{32} in *CG7009* mutant flies is moderate, indicating incomplete ribose methylation. A different visualisation for tRNA$^{Phe(GAA)}$ at position C32 and C34 is depicted in Figure S6B.

B, Related to Figure 5C and Supplementary Figure S6A. RiboMethSeq was performed as described in Supplementary Figure S6A for tRNA$^{Phe(GAA)}$ on 6 indicated genotypes. For a better visualization, raw read counts are presented in an non-normalized fashion (raw reads). The positions of interest (Cm_{32} and Gm_{34}) in tRNA$^{Phe(GAA)}$ are indicated by red arrows. Protection against cleavage is indicated as (+): protected and as (-): not protected. *CG7009*^{e02001}/+ mutants (Control), homozygous *CG5220*$^{K>A}$ mutant (*CG5220 K>A*), two independent genetic background mutants for *CG7009*: homozygous *CG7009*^{e02001} (*CG7009*^{e02001}) or trans-heterozygous *CG7009*^{e02001}/*Def3340* mutant (*CG7009*^{e02001}/*Def3340)*, double homozygous *CG7009*^{e02001},*CG5220*$^{K>A}$ mutant (*CG7009*^{e02001},*CG5220* K>A) and rescue BAC; *CG7009*^{e02001}/*Def3340* (Rescue CG7009 (BAC)).

C, RiboMethSeq was performed as described in Figure 5C and Supplementary Figure S6A for tRNA$^{Leu(CAA)}$ on 6 indicated genotypes. Normalized cleavage efficiencies, calculated from combined 5'-end and 3'-end coverages, are shown for the ± 5 neighboring nucleotides. The positions of interest (Cm_{32} and Gm_{34}) in tRNA$^{Leu(CAA)}$ are indicated by red arrows. Protection against cleavage is indicated as (+): protected and as (-): not protected. *CG7009*^{e02001}/+ mutants (Control), homozygous *CG5220*$^{K>A}$ mutant (*CG5220 K>A*), two independent genetic background mutants for *CG7009*: homozygous *CG7009*^{e02001} (*CG7009*^{e02001}) or trans-heterozygous *CG7009*^{e02001}/*Def3340* mutant (*CG7009*^{e02001}/*Def3340)*, double homozygous

CG7009^{e02001},*CG5220*$^{K>A}$ mutant (*CG7009*^{e02001},*CG5220* K>A) and rescue BAC; *CG7009*^{e02001}/*Def3340* (Rescue CG7009 (BAC)).

Figure S7.

Heatmap of normalized MethScores (ScoreC) for tRNA positions Cm/Um$_{32}$ and Cm/Gm$_{34}$ in different mutant backgrounds. Pink color corresponds to a high methylation compared to the average MethScores, blue or white color to lower methylation. Simplified genotypes are indicated in the middle (detailed genotypes in Figures S6B and S6C legends above), affected tRNA isoacceptors are given on the right. Scale of the color key (-1 to +1) is indicated at the top.

Chapter II: "The ribose methylation enzyme FTSJ1 has a conserved role in neuron morphology and learning performance"

The article above focused on the functional characterization of *FTSJ1* orthologs in *Drosophila*, the model organism that was most used in our lab, as well as their functions in small non-coding RNA pathways. The initiation of a project on the human counterpart FTSJ1 necessitated the use of new cellular models including patient derived lymphocytes, neural progenitors, as well as CRISPR HeLa cells.

In this study, we characterized a new FTSJ1 pathogenic variant from a new Lymphoblastoid cell line. In order to study the molecular functions of FTSJ1, we started by analyzing the full spectrum of tRNA substrates using patient lymphocytes carrying four different *FTSJ1* loss of function variants as well as control lymphocytes from healthy individuals. Using the RibomethSeq approach, we validated the previously characterized targets, as well as described new ones, namely Nm32 on specific isoacceptor $tRNA^{Gln}$,$tRNA^{Gly}$ $tRNA^{Arg}$ $tRNA^{Cys}$ $tRNA^{Val}$.

In order to understand the role of FTSJ1 in gene expression regulation we performed transcriptome analysis on these same cells, which revealed deregulation of several hundred genes, including many associated with brain morphogenesis.

As we previously observed deregulation of the small non-coding RNA pathways in mutants of the fly orthologs (Angelova et al. 2020), we analyzed the small RNA populations using small RNAseq, which identified deregulation of certain miRNAs, suggesting a potential miRNAs dependant regulation of key mRNA targets. Furthermore, we demonstrate that FTSJ1-depleted human immature neurons display an overgrowth of dendritic spines, as well as a thin long morphology when compared to control cells. Similar observations were done in neuromuscular junctions of *Drosophila* third instar larvae, consistently with the locomotory defects observed in these mutants. Expectedly, all fly mutant combinations are associated with cognitive defects, particularly, in long-term memory. Overall, our study integrates new

knowledge regarding the human FTSJ1 targets, and its function in brain morphogenesis gene regulation. Importantly our work highlights the conservation of substrates of the *FTSJ1* family of genes and the learning impairments associated with their loss.

Life Science Alliance

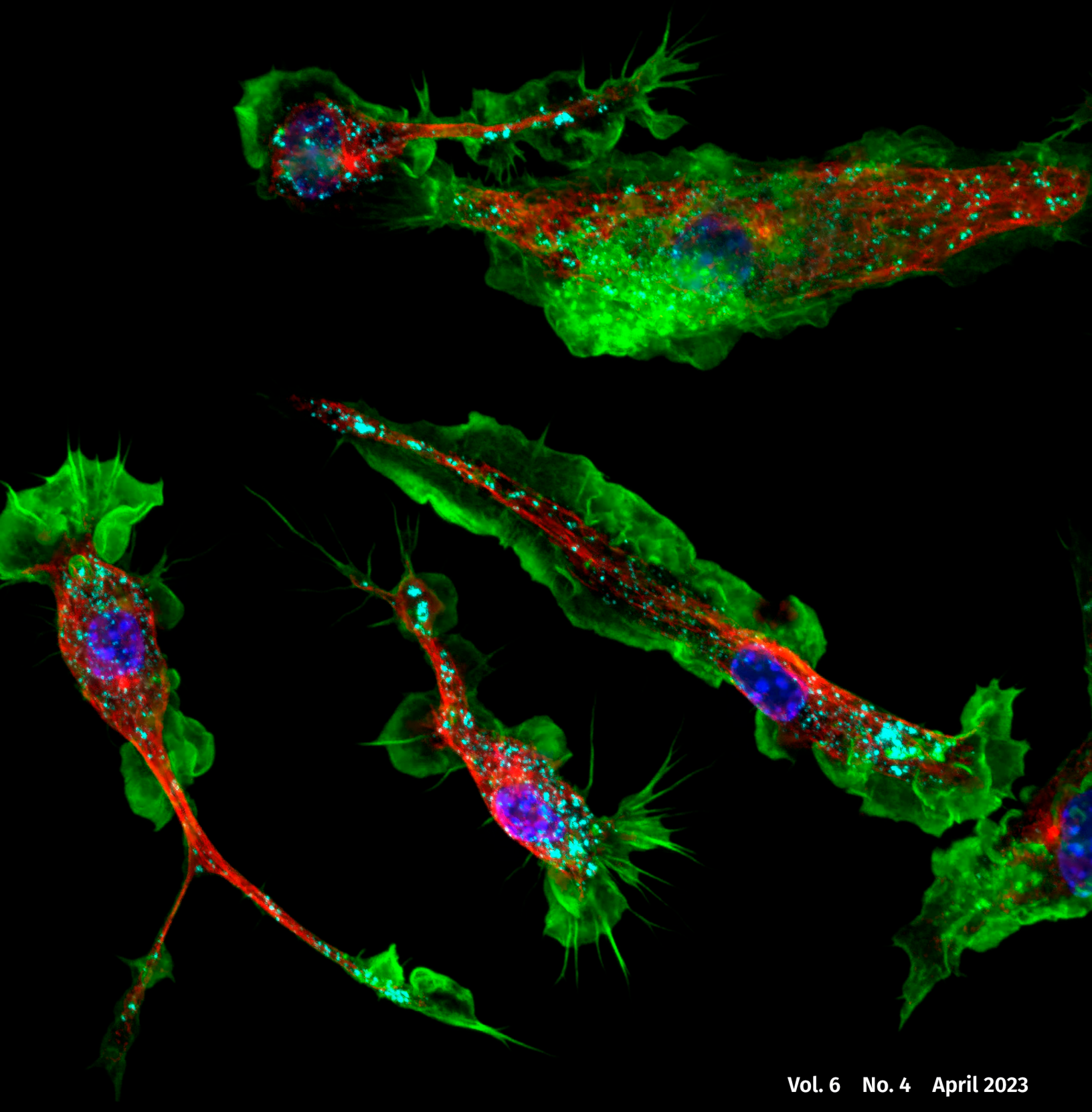

Vol. 6 No. 4 April 2023

Research Article

TRANSPARENT PROCESS OPEN ACCESS Life Science Alliance

The ribose methylation enzyme FTSJ1 has a conserved role in neuron morphology and learning performance

Mira Brazane[1,*], Dilyana G Dimitrova[1,*], Julien Pigeon[2], Chiara Paolantoni[3], Tao Ye[4], Virginie Marchand[5], Bruno Da Silva[1], Elise Schaefer[6], Margarita T Angelova[1], Zornitza Stark[7], Martin Delatycki[7], Tracy Dudding-Byth[8], Jozef Gecz[9], Pierre-Yves Plaçais[10], Laure Teysset[1], Thomas Préat[10], Amélie Piton[4], Bassem A Hassan[2], Jean-Yves Roignant[3,11], Yuri Motorin[12], Clément Carré[1]

FTSJ1 is a conserved human 2′-O-methyltransferase (Nm-MTase) that modifies several tRNAs at position 32 and the wobble position 34 in the anticodon loop. Its loss of function has been linked to X-linked intellectual disability (XLID), and more recently to cancers. However, the molecular mechanisms underlying these pathologies are currently unclear. Here, we report a novel *FTSJ1* pathogenic variant from an X-linked intellectual disability patient. Using blood cells derived from this patient and other affected individuals carrying *FTSJ1* mutations, we performed an unbiased and comprehensive RiboMethSeq analysis to map the ribose methylation on all human tRNAs and identify novel targets. In addition, we performed a transcriptome analysis in these cells and found that several genes previously associated with intellectual disability and cancers were deregulated. We also found changes in the miRNA population that suggest potential cross-regulation of some miRNAs with these key mRNA targets. Finally, we show that differentiation of FTSJ1-depleted human neural progenitor cells into neurons displays long and thin spine neurites compared with control cells. These defects are also observed in *Drosophila* and are associated with long-term memory deficits. Altogether, our study adds insight into FTSJ1 pathologies in humans and flies by the identification of novel FTSJ1 targets and the defect in neuron morphology.

DOI 10.26508/lsa.202201877 | Received 15 December 2022 | Revised 8 January 2023 | Accepted 10 January 2023 | Published online 31 January 2023

Introduction

RNA modifications represent a novel layer of post-transcriptional gene regulation (Saletore et al, 2012; Angelova et al, 2018; Zhao et al, 2020). Because of their variety and dynamic nature, they rapidly adapt gene expression programs in response to developmental changes or environmental variations. One of the most abundant RNA modifications is 2′-O-methylation (ribose methylation, Nm). Nm can affect the properties of RNA molecules in multiple ways, for example, stability, interactions, and functions (Kawai et al, 1992; Kurth & Mochizuki, 2009; Lacoux et al, 2012). Nm residues are abundant in ribosomal RNAs and tRNAs (Erales et al, 2017; Marchand et al, 2017), but are also found in other RNA types such as small nuclear RNAs (Darzacq, 2002; Dai et al, 2017), small non-coding RNAs (Li et al, 2005; Yu et al, 2005; Horwich et al, 2007; Saito et al, 2007; Kurth & Mochizuki, 2009), and mRNAs (Darzacq, 2002; Dai et al, 2017; Bartoli et al, 2018 *Preprint*). Many Nm positions are conserved through evolution, and their presence is essential for maintaining healthy physiological functions. Eukaryotic mRNAs are 5′-end–capped with a 7-methylguanosine (m^7G), which is important for processing and translation of mRNAs. In addition, Cap methyltransferases catalyse Nm of the first and second transcribed nucleotides and were shown to be important for innate immune surveillance, and neuronal development and activity (Lee et al, 2020; Haussmann et al, 2022). The loss of certain Nm modifications and/or Nm-modifying enzymes has been associated with various pathological conditions (reviewed in Dimitrova et al [2019]),

[1]Transgenerational Epigenetics & Small RNA Biology, Sorbonne Université, Centre National de la Recherche Scientifique, Laboratoire de Biologie du Développement - Institut de Biologie Paris Seine, Paris, France [2]Paris Brain Institute-Institut du Cerveau (ICM), Sorbonne Université, Inserm, CNRS, Hôpital Pitié-Salpêtrière, Paris, France [3]Center for Integrative Genomics, Génopode Building, Faculty of Biology and Medicine, University of Lausanne, Lausanne, Switzerland [4]Institute of Genetics and Molecular and Cellular Biology, Strasbourg University, CNRS UMR7104, INSERM U1258, Illkirch, France [5]Université de Lorraine, CNRS, INSERM, EpiRNASeq Core Facility, UMS2008/US40 IBSLor,Nancy, France [6]Service de Génétique Médicale, Hôpitaux Universitaires de Strasbourg, Institut de Génétique Médicale d'Alsace, Strasbourg, France [7]Victorian Clinical Genetics Services, Murdoch Children's Research Institute, Melbourne, Australia; Department of Paediatrics, The University of Melbourne, Melbourne, Australia [8]University of Newcastle, Newcastle, Australia [9]Adelaide Medical School and Robinson Research Institute, The University of Adelaide; South Australian Health and Medical Research Institute, Adelaide, Australia [10]Energy & Memory, Brain Plasticity Unit, CNRS, ESPCI Paris, PSL Research University, Paris, France [11]Institute of Pharmaceutical and Biomedical Sciences, Johannes Gutenberg-University Mainz, Mainz, Germany [12]Université de Lorraine, CNRS, UMR7365 IMoPA, Nancy, France

Correspondence: clement.carre@gmail.com; clement.carre@sorbonne-universite.fr
*Mira Brazane and Dilyana G Dimitrova contributed equally to this work

including cancers (Liu et al, 2017; El Hassouni et al, 2019; He et al, 2020; Marcel et al, 2020) and brain diseases (Jia et al, 2012; Abe et al, 2014; Guy et al, 2015; Cavaillé, 2017).

FTSJ1 is a human tRNA 2′-O-methyltransferase (Nm-MTase), which belongs to the large phylogenetically conserved superfamily of RrmJ/fibrillarin RNA methyltransferases (Bügl et al, 2000; Feder et al, 2003). Human male individuals bearing a hemizygous loss of function variant in the *FTSJ1* gene suffer from significant limitations both in intellectual functioning and in adaptive behaviour (Freude et al, 2004; Froyen et al, 2007; Guy et al, 2015). Similar phenotypes, including impaired learning and memory capacity, were recently observed in *Ftsj1* KO mice that also present a reduced body weight and bone mass, and altered energy metabolism (Jensen et al, 2019; Nagayoshi et al, 2021). In flies, we recently showed that the loss of the two *FTSJ1* homologs (i.e., *Trm7_32* and *Trm7_34*) provokes reduced lifespan and body weight and affects RNAi antiviral defences and locomotion (Angelova et al, 2020). Finally, *Ftsj1* mutants in yeast (Δ*trm7*) grow poorly because of a constitutive general amino acid control activation and the possible reduced availability of aminoacylated $tRNA^{Phe}$ (Pintard et al, 2002; Guy et al, 2012; Han et al, 2018). Interestingly, this growth phenotype can be rescued by human FTSJ1, indicating a conserved evolutionary function.

Most of the knowledge on FTSJ1's molecular functions is derived from yeast studies. Trm7 in *Saccharomyces cerevisiae* methylates positions 32 and 34 in the anticodon loop (ACL) of specific tRNA targets: $tRNA^{Phe(GAA)}$, $tRNA^{Trp(CCA)}$, and $tRNA^{Leu(UAA)}$ (Pintard et al, 2002; Guy et al, 2012). To achieve 2′-O-methylation, Trm7 teams up with two other proteins: Trm732 for the methylation of cytosine at position 32, and Trm734 for the methylation of cytosine or guanine at position 34 (Guy et al, 2012; Li et al, 2020). The presence of both Cm_{32} and Gm_{34} in $tRNA^{Phe(GAA)}$ is required for efficient conversion of m^1G_{37} to wybutosine (yW_{37}) by other proteins. This molecular circuitry is conserved in the phylogenetically distinct *Schizosaccharomyces pombe* and humans (Noma et al, 2006; Guy et al, 2015; Guy & Phizicky, 2015; Li et al, 2020). In *Drosophila*, we found that Trm7_32 and Trm7_34 modify, respectively, positions 32 and 34 in the ACL on $tRNA^{Phe(GAA)}$, $tRNA^{Trp(CCA)}$, and $tRNA^{Leu(CAA)}$ (Angelova et al, 2020). In this organism, we also identified novel tRNA targets for these two enzymes ($tRNA^{Gln(CUG)}$ and $tRNA^{Glu(CUC)}$), which raised the question about their conservation in humans. A recent publication reported that human FTSJ1 modifies position 32 of another $tRNA^{Gln}$ isoacceptor, $tRNA^{Gln(UUG)}$ (Li et al, 2020). This study performed in HEK293T cells tested a selected subset of tRNAs using tRNA purification followed by MS analysis. It was shown that position 32 of $tRNA^{Arg(UCG)}$, $tRNA^{Arg(CCG)}$, and $tRNA^{Arg(ACG)}$, and position 34 of $tRNA^{Arg(CCG)}$ and $tRNA^{Leu(CAG)}$ are also 2′-O-methylated by human FTSJ1. $tRNA^{Arg(ACG)}$ was originally identified as a target of fly Trm7_32 (Angelova et al, 2020), whereas human $tRNA^{Leu(CAA)}$ (Kawarada et al, 2017) and yeast $tRNA^{Leu(UAA)}$ (Guy et al, 2012) were predicted targets of FTSJ1 and Trm7, respectively. However, a comprehensive and unbiased (not selected) analysis of all possible FTSJ1 tRNA targets was not performed, particularly in human patient samples, leaving the full spectrum of FTSJ1 tRNA substrates yet to be identified.

Previously, the enzymatic activity of mammalian FTSJ1 on selected tRNAs has been revealed through HPLC (Guy et al, 2015) and more recently through ultra-performance liquid chromatography–mass spectrometry/mass spectrometry (Li et al, 2020; Nagayoshi et al, 2021). Both approaches analyse mononucleotides derived from selected tRNAs and are based on already reported sequences. The exact position of the modified nucleotide was thus inferred from available information on tRNA sequences and modification profiles database (Jühling et al, 2009; Chan & Lowe, 2016; Boccaletto et al, 2018). Recently, a new method called RiboMethSeq was established and allows the identification of Nm sites in a complete unbiased manner, based on the protection conferred by the ribose methylation to alkaline digestion (Marchand et al, 2016, 2017). This offers the possibility to identify every Nm site regulated by a particular enzyme, especially when investigating abundant RNAs, such as tRNAs.

In this study, we took advantage of this novel approach to identify the full set of FTSJ1's tRNA targets in humans. We report a novel *FTSJ1* pathogenic variant from an X-linked intellectual disability (XLID) patient. Using blood cells derived from this affected individual and other individuals carrying distinct *FTSJ1* mutations, we performed an unbiased and comprehensive RiboMethSeq analysis to map the ribose methylation on all tRNAs and revealed new targets. In addition, we performed a transcriptome analysis in these FTSJ1-depleted cells and found that several genes previously associated with intellectual disability (ID) and cancers were deregulated. We also found changes in the miRNA population that suggest potential cross-regulation of some miRNAs with these key mRNA targets. Finally, in accordance with the known importance of FTSJ1 during brain development in mice and its involvement in ID in humans, we showed that human neural progenitor cells (NPCs) with inactivated FTSJ1 present abnormal neurite morphology. We also observed this phenotype in *Drosophila* and a specific deficit in long-term memory. Altogether, our study reveals new targets potentially involved in FTSJ1 pathologies in humans and demonstrates a conserved function in neuron morphology and function.

Results

Comprehensive identification of human FTSJ1 tRNA targets

To identify new tRNA targets of human FTSJ1, we compared the Nm modification profiles of positions 32 and 34 for all detectable tRNA species in human lymphoblastoid cell lines (LCLs) obtained from control individuals (n = 4) versus LCLs obtained from individuals with XLID harbouring loss of function and pathogenic variants in *FTSJ1* (n = 5, from four unrelated families) (Table 1). Four of these affected individuals were already described and harbour distinct molecular defects: a splice variant leading to a premature stop codon (Freude et al, 2004) (LCL65AW and LCL65JW), a deletion encompassing *FTSJ1* and its flanking gene *SLC38A5* (Froyen et al, 2007) (LCL11), and a missense variant (p.Ala26Pro) affecting an amino acid located close to FTSJ1 catalytic pocket, resulting in the loss of Gm_{34}, but not of Cm_{32}, in human $tRNA^{Phe}$ (Guy et al, 2015) (LCL22). The last individual was not reported nor characterized before. This patient presents mild ID and behavioural manifestations and harbours a de novo pathogenic variant affecting the consensus acceptor splice site of exon 6 (NM_012280.3: c.362-2A > T) (LCL-MM). This mutation leads to the skipping of exon 6 in the mRNA

Table 1. FTSJ1 targets tRNA^{Phe} at positions 32 and 34 in humans.

Individual	Cm_{32}	Gm_{34}	LCL code name
Control individuals	Present	Present	LCL16, LCL18, LCL24, LCL54
Affected individuals with *FTSJ1* variant	Absent	Absent	LCL65AW, LCL65JW, LCL11, LCLMM
Affected individual with *FTSJ1* variant	Present	Absent	LCL22

Control and affected *FTSJ1* individuals' Nm status at positions 32 and 34 of human tRNA^{Phe}.

(r.362_414del) leading to a frameshift and a premature stop codon (p.Val121Glyfs*51) (Fig S1A). *FTSJ1* mRNA steady-state level in LCL-MM was significantly reduced when compared to LCL from control individuals (Fig S1B). In addition, treating the LCL-MM cells with cycloheximide to block translation, and thus the nonsense-mediated mRNA decay (NMD) pathway (Tarpey et al, 2007), led to an increase in *FTSJ1* mRNA abundance (Fig S1C). This result suggests that *FTSJ1* mRNA from LCL-MM cells is likely degraded via the NMD pathway.

To obtain a comprehensive picture of the Nm-MTase specificity for FTSJ1 in vivo, we performed RiboMethSeq analysis on LCLs isolated from affected individuals described above and compared with LCLs from healthy individuals. RiboMethSeq allows tRNA-wide Nm detection based on random RNA fragmentation by alkaline hydrolysis followed by library preparation and sequencing ([Marchand et al, 2017] and see the Materials and Methods section). Using this approach, we could confirm the known FTSJ1 targets (e.g., tRNA$^{Phe(GAA)}$ and tRNA$^{Trp(CCA)}$) and assign the FTSJ1-deposited Nm modifications to their predicted positions in the ACL (C_{32} and N_{34}; Fig 1). However, using only the MethScore calculation we could not detect a variation for Cm_{32} in tRNA$^{Phe(GAA)}$. This scoring strategy shows its limits in some particular situations as MethScore is calculated for two neighbouring nucleotides; thus, the simultaneous loss of two closely located Nm residues (e.g., Cm_{32} and Gm_{34} in tRNA^{Phe}) makes the analysis of MethScore misleading (Angelova et al, 2020). Moreover, the presence of multiple RT-arresting hypermodifications (e.g., m^{1}G37/o2yW37 [Anreiter et al, 2021]) in the same

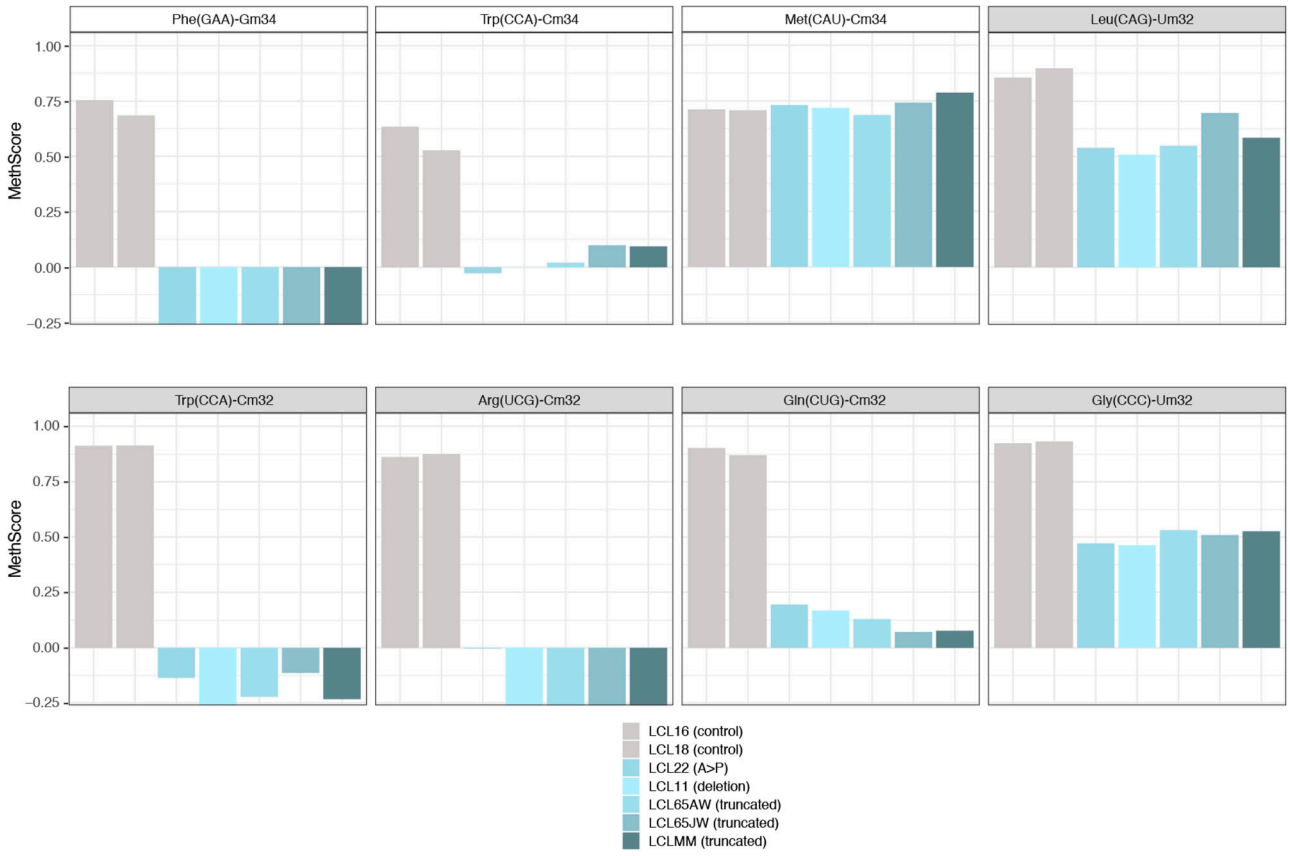

Figure 1. FTSJ1 targets multiple tRNAs at positions 32 and 34 in humans.
Methylation scores (MethScore) for 2′-O-methylated positions in tRNAs showing altered methylation in *FTSJ1* loss of function mutant LCLs. MethScore (Score C), representing the level of ribose methylation, was calculated from protection profiles. Data are shown for positions 32 and 34 in different *H. sapiens* tRNAs as measured in different LCL lines that are indicated with a different colour code. Grey: control LCL; blue: *FTSJ1* mutant LCLs. Met(CAU)-Cm34 is not deposited by FTSJ1 and shown here as a control (unaltered methylation in *FTSJ1* mutants).

Table 2. FTSJ1 targets multiple human tRNAs at positions 32 and 34.

tRNA target	*Humans*				*Drosophila*		*S. cerevisiae*		*Mouse*	
	Current RiboMethSeq		Previous HPLC/MS		Previous RiboMethSeq		Previous HPLC and/or MS		Previous HPLC/MS	
	N32	*N34*	*N32*	*N34*	*N32*	*N34*	*N32*	*N34*	*N32*	*N34*
Arg (UCG1)[a]	**Cm**	no	**Cm** (Li et al, 2020)	**no**	no	no	n.d.	n.d.	n.d.	n.d.
Arg (CCG)	**Um**	no	**Um, Cm** (Li et al, 2020)	**Cm**[#] (Li et al, 2020)	no	no	n.d.	n.d.	n.d.	n.d.
Arg (ACG)	**Cm***	**I**	**Cm** (Li et al, 2020)	no	**Cm** (Angelova et al, 2020)	no	n.d.	n.d.	**Cm** (Nagayoshi et al, 2021)	n.d.
Arg (UCG2)[a]	**Cm**	no	n.d.	n.d.	n.d.	n.d.	n.d.	n.d.	n.d.	n.d.
Leu (CAG_CAA) 91%_9%	**Um**	**no**	no	**Cm**[@] (Kawarada et al, 2017; Li et al, 2020)	**Cm** (Angelova et al, 2020)	**Cm** (Angelova et al, 2020)	n.d.	n.d.	n.d.	**Um_** hm^5**Cm** (Nagayoshi et al, 2021)
Leu (UAA)	no	**U^{2}m***	n.d.	no	no	no	**Cm** (Guy et al, 2012)	ncm^5**Um** (Glasser et al, 1992; Guy et al, 2012)	**Cm** (Nagayoshi et al, 2021)	ncm^5**Um** (Nagayoshi et al, 2021)
Leu (A/IAG) 76%	**U/ψm**	**I**	n.d.	no	no	no	n.d.	n.d.	**Ψm** (Nagayoshi et al, 2021)	n.d.
Leu (UAG) 24%	**U/ψm**	**no**	n.d.	no	no	no	n.d.	n.d.	**Um** (Nagayoshi et al, 2021)	n.d.
Phe (GAA)	**Cm***	**Gm**	**Cm** (Guy et al, 2015; Li et al, 2020; Nagayoshi et al, 2021)	**Gm** (Guy et al, 2015; Li et al, 2020; Nagayoshi et al, 2021)	**Cm*** (Angelova et al, 2020)	**Gm** (Angelova et al, 2020)	**Cm** (Guy et al, 2012)	**Gm** (Guy et al, 2012)	**Cm** (Nagayoshi et al, 2021)	**Gm** (Nagayoshi et al, 2021)
Trp (CCA)	**Cm**	**Cm**	**Cm** (Guy et al, 2015; Li et al, 2020; Nagayoshi et al, 2021)	**Cm** (Guy et al, 2015; Li et al, 2020; Nagayoshi et al, 2021)	**Cm** (Angelova et al, 2020)	**Cm** (Angelova et al, 2020)	**Cm** (Guy et al, 2012)	**Cm** (Guy et al, 2012)	**Cm** (Nagayoshi et al, 2021)	**Cm** (Nagayoshi et al, 2021)
Gln (CUG_UUG) 92%_8%	**Cm**	no	**Cm** (Li et al, 2020)	n.d.	**Cm** (Angelova et al, 2020)	no	n.d.	n.d.	**Cm** (Nagayoshi et al, 2021)	
Gly (CCC)	**Um**	no	n.d.	no	no	no	n.d.	n.d.	n.d.	n.d.
Val (AAC_CAC_TAC) 73%_26%_1%	no	**I (AAC)**	**Cm** (Nagayoshi et al, 2021)	n.d.	**Cm** (Angelova et al, 2020)	no	n.d.	n.d.	**Cm** (Nagayoshi et al, 2021)	
Pro (AGG_CGG_UGG) 34%_23%_42%	**Um***	**I (AGC)**	no	n.d.	n.d.	n.d.	n.d.	n.d.	n.d.	n.d.

(Continued on following page)

Table 2. Continued

tRNA target	*Humans*				*Drosophila*		*S. cerevisiae*		*Mouse*	
	Current RiboMethSeq		Previous HPLC/MS		Previous RiboMethSeq		Previous HPLC and/or MS		Previous HPLC/MS	
	N32	*N34*	*N32*	*N34*	*N32*	*N34*	*N32*	*N34*	*N32*	*N34*
Cys (GCA_ACA) 97%_3%	**Cm***	no	n.d.	n.d.	n.d.	n.d.	n.d.	n.d.	n.d.	n.d.
Met (CAU) *non-*FTSJ1 *Target*	no	**Cm**	no	**Cm** (Vitali & Kiss, 2019; Li et al, 2020)	no	no	no	no	n.d.	n.d.

A summary of tRNA nucleotides revealed to date, including by the current study, as targets of human FTSJ1, and those targeted by *Drosophila* Trm7_32 and Trm7_34, and yeast Trm7 in the respective organisms. For the tRNA targets are given the isotype (determined by the bound amino acid) and the isoacceptor (determined by the ACL sequence). In blue are highlighted the studies done with the site-specific RiboMethSeq, and in grey, the ones done by mass spectrometry single-nucleotide analysis. n.d. stands for non-determined and indicates that the tRNA was not tested or if tested the data were not analysable. no stands for non-detected Nm. Cm, Gm, and Um stand for 2′-O-methylated, respectively, C, G, and U nucleotides. * indicates Nm RiboMethSeq detection by visual inspection of the raw read profile, not MethScore; see Fig S1D for an example. When several anticodon sequences are present for tRNA isoacceptors, proportion of every sequence in the healthy subject is indicated at the bottom. Cm$^{\#}$ indicates Cm detection in Li et al (2020) that could be because of a high sequence similarity with another tRNAArg, tRNAArg(CCG)-2-1 containing a C32. The observed Cm decrease in *FTSJ1* KO cells in this study may come from C32 of tRNAArg(CCG)-2-1 that was modified by FTSJ1 and not from the C34 level of tRNAArg(CCG). Cm$^{@}$ indicates hm5Cm34 or f5Cm34 in tRNALeu(CAA) shown in Kawarada et al (2017). I stands for inosine (FTSJ1-independent). U$^{?}$m* indicates clear FTSJ1 dependence; however, the exact nature of this modified U remains unknown. tRNAArg (UCG) and (CCG) have identical sequences but differ only at positions 32 and 34.
[a]stands for UCG isodecoders (sequences in the Materials and Methods section). tRNALeu (A/IAG) and (UAG) are isoacceptors, they differ only by the N34 nucleotide, and both have Um32 (or ψm32).

tRNA regions impairs RT, thereby reducing the number of cDNAs spanning the ACL. Nevertheless, considering all these potential limitations when using only MethScore calculation, a visual inspection of raw cleavage profiles was performed (Fig S1D and Table 2) and revealed to be the most appropriate. When visualizing raw read count profile, reads' end number at position 33 (Cm_{32}) of $tRNA^{Phe(GAA)}$ was increased in *FTSJ1*-mutated cells (Fig S1D), indicating a loss of Cm_{32} of $tRNA^{Phe(GAA)}$ in *FTSJ1*-mutated LCLs. Thus, using both MethScore (Fig 1) and visual inspection on all RiboMethSeq human tRNA sequences (Fig S1D) we were able to confirm known FTSJ1 tRNA targets and, importantly, discover new FTSJ1-dependent Cm_{32}/Um_{32} modifications in $tRNA^{Gly}$, $tRNA^{Leu}$, $tRNA^{Pro}$, and $tRNA^{Cys}$ (see Table 2 for isoacceptor details). Unexpectedly, Um_{34} in $tRNA^{Leu(UAA)}$ also demonstrated clear FTSJ1 dependence; however, the exact nature of this modified nucleotide remains unknown (Table 2). In contrast, the protection signal observed at position 32 in human $tRNA^{Ala(A/IGC)}$ is not FTSJ1-dependent and most likely results from ψm_{32} (visible in HydraPsiSeq [Marchand et al, 2022] profiling) and not Um_{32}.

FTSJ1 loss of function deregulates mRNA steady-state level

To obtain insights into the impact of *FTSJ1* loss on gene expression, we performed a transcriptome analysis in patient and control LCLs. Transcript differential expression analysis shows that FTSJ1 dysfunction led to a deregulation of 686 genes (Table 3 and Fig S2A and B). This relatively low number is in agreement with a previous report showing 775 genes deregulated in human HeLa cells knock down for *FTSJ1* (Trzaska et al, 2020), and with the 110 mRNAs deregulated in KD of one *FTSJ1 Drosophila* ortholog (Angelova et al, 2020).

Even though LCLs do not have a neural origin, analysis of the genes deregulated in affected individuals revealed a clear enrichment (FE = 7.9 with *P*-value = 7.44×10^{-6} and FDR = 4.40×10^{-3}) in biological process gene ontology (GO) term corresponding to brain morphogenesis (Fig 2A). In addition, and similar to what we reported in a previous mRNA-seq analysis of *Drosophila* S2 cells knocked down for *Trm7_34* (Angelova et al, 2020), five of the top 10 most enriched terms were related to mitochondrial biological processes. Also, in agreement with a recently described role of human FTSJ1 in translational control (Trzaska et al, 2020; Nagayoshi et al, 2021) and of yeast Trm7 in the general amino acid control pathway (Han et al, 2018), four biological processes related to translation were affected in *FTSJ1*-mutated LCLs (FE > 3.5, Fig 2A).

To strengthen the transcriptome analysis, we selected three representative and disease-relevant deregulated mRNAs based on their fold change level of expression and related involvement in brain or cancer diseases. Mutations in the human *ZNF711* gene were previously reported to be involved in the development of ID (van der Werf et al, 2017). The mRNA-seq and qRT–PCR analyses showed a significant down-regulation of *ZNF711* mRNA in *FTSJ1* mutant LCLs when compared to control LCLs (Table 3 and Fig 2B). BTBD3 activity is known to direct the dendritic field orientation during development of the sensory neuron in the mouse cortex (Matsui et al, 2013) and to regulate mouse behaviours (Thompson et al, 2019). We found that *BTBD3* mRNA was significantly up-regulated in both mRNA-seq and qRT–PCR analyses (Fig 2B). Lastly, SPARC (Tai & Tang, 2008) and more recently FTSJ1 (Holzer et al, 2019; He et al, 2020) gene product activities were proposed to be involved in both metastasis and tumour suppression. In the absence of FTSJ1, we could confirm that *SPARC* mRNA was significantly reduced (Table 3 and Fig 2B). Taken together, these results show deregulation of some mRNAs linked to cancer and brain functioning in *FTSJ1* affected individuals' blood-derived LCLs.

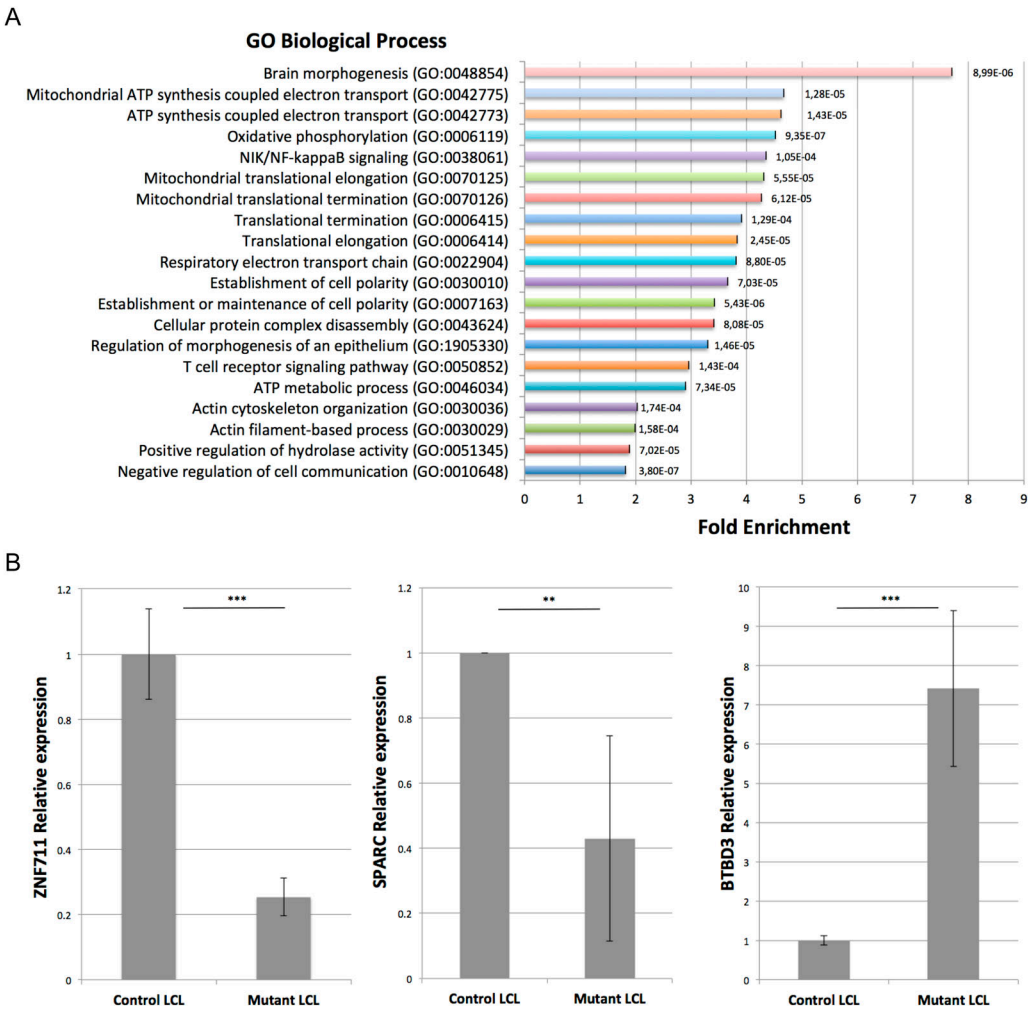

Figure 2. *FTSJ1* loss of function leads to mRNA deregulation in XLID affected individuals' LCLs.
(A) *FTSJ1* loss of function mRNA GO term. GO analysis of the 686 deregulated genes in *FTSJ1* function–deficient LCLs derived from XLID affected individuals (five mutants versus two control LCLs); *P*-values are indicated with error bars on the right of each box. The most enriched GO term is brain morphogenesis. GO analysis was performed using http://geneontology.org/. **(B)** qRT–PCR analysis confirms deregulation in *ZNF711*, *BTBD3*, and *SPARC* mRNA expression levels. Normalized to *GAPDH* steady-state levels. n > 3. *P*-values were calculated with a paired *t* test: $^{**}P < 0.01$ and $^{***}P < 0.001$. WT values: mean of two control *FTSJ1* LCLs. Mutant values: mean of all (×5) *FTSJ1* mutant LCLs of this study, or two (LCL MM and LCL 65JW) for *ZNF711* qRT-PCR.

FTSJ1 loss of function affects the miRNA population

Our previous work on the *Drosophila* homologs of *FTSJ1*, *Trm7_32* and *Trm7_34*, showed that their loss of functions led to perturbations in the small non-coding RNA gene silencing pathways, including the miRNA population (Angelova et al, 2020). To address whether such small RNA perturbations are conserved in XLID affected individuals, we performed small RNA sequencing on the five LCLs carrying *FTSJ1* loss of function variants compared with the four LCLs from control individuals. The principal component analysis of the different *FTSJ1* loss of function cell lines shows a high similarity and thus clusters on the principal component analysis plot, whereas the WT lines were more dispersed, possibly explained by their geographic origins (Fig S3A). The DESeq2 differential expression analysis showed statistically significant deregulation of 36 miRNAs when comparing *FTSJ1* mutants to control LCLs. 17 miRNAs were up- and 19 down-regulated (Figs 3A and S3B and $\log_2$ FC and adjusted *P*-values in Table S1). Importantly, as already reported in *Drosophila* (Angelova et al, 2020), the global miRNA distribution was not drastically affected, thus ruling out general involvement of FTSJ1 in miRNA biogenesis.

Next, we sought for possible links between the 36 significantly deregulated miRNAs in *FTSJ1* mutant cells and neuronal functions or neurodevelopmental disorders. Interestingly, 21 of these miRNAs were already identified in other small RNA-seq studies performed in the context of brain diseases such as epilepsy, and Parkinson's and Alzheimer's diseases (Lau et al, 2013; Kretschmann et al, 2015; Ding et al, 2016; Roser et al, 2018). In addition, 29 of the deregulated miRNAs were linked to different types of cancers (Lund, 2010; Watahiki et al, 2011; Li et al, 2015; Khuu et al, 2016; Yang et al, 2017; Jiang et al, 2018), including 21 involved specifically in brain-related cancers, mostly in glioblastoma (Gillies & Lorimer, 2007; Shi et al, 2008; Lund, 2010; Conti et al, 2016) (Fig 3B and Table 4).

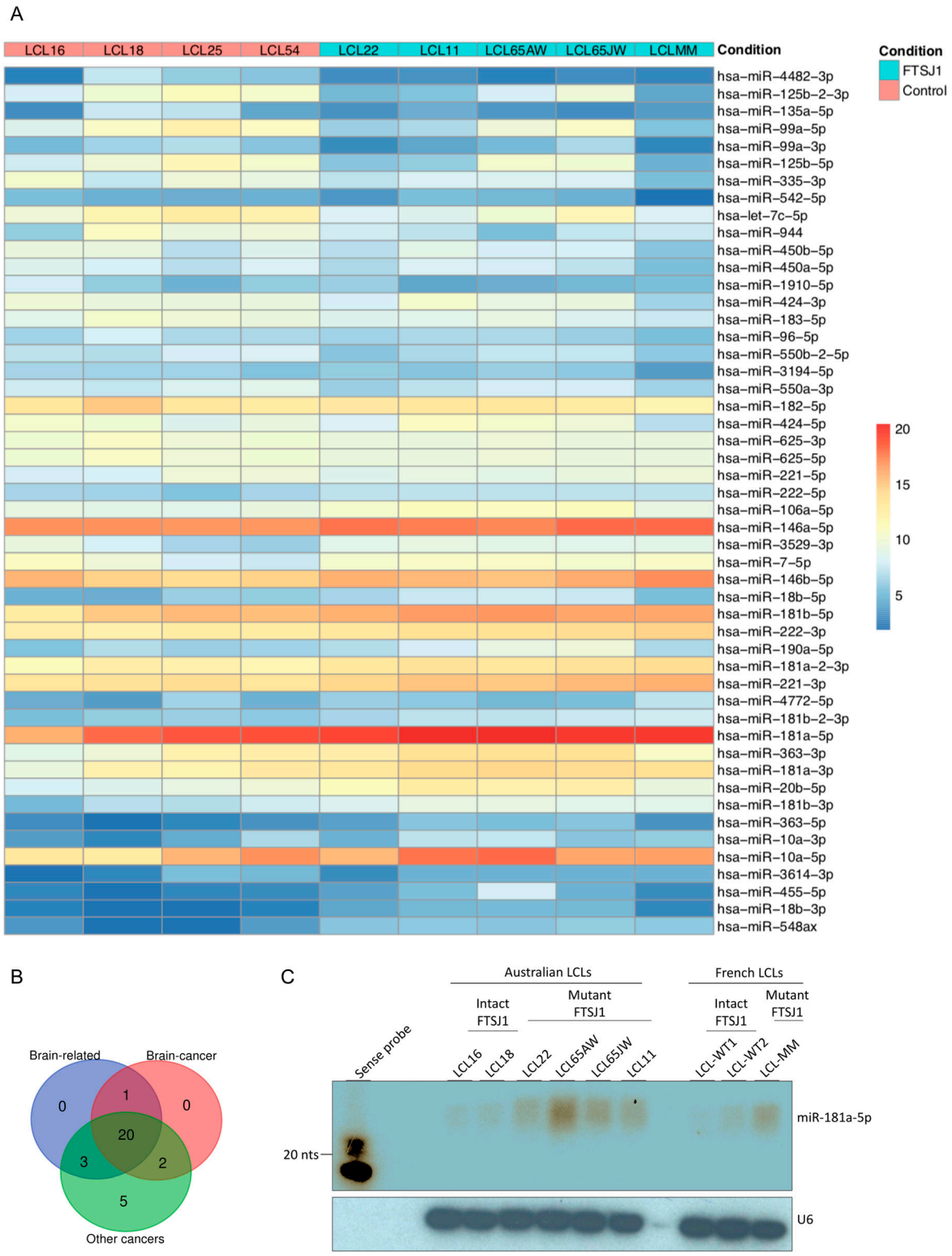

Figure 3. *FTSJ1* loss of function leads to miRNA deregulation in XLID affected individuals' LCLs.
(A) Heat map generated using the pheatmap package in R showing the 50 best deregulated miRNAs in *P*-values, and sorted fold change from most down-regulated (blue) to most up-regulated (red) is represented in two experimental conditions: *FTSJ1* loss of function LCLs (blue turquoise) compared with controls LCLs (pink). Condition points to the FTSJ1 LCL status, WT (control) or mutated for the *FTSJ1* gene (FTSJ1). The data come from normalized and variance-stabilizing transformed read counts using the DESeq2 package in R. **(B)** Bibliographic search (Table 4) of the miRNAs deregulated in *FTSJ1* loss of function LCLs reveals evidence for many of them as being implicated in cancers or brain development and brain diseases. The number of miRNAs related to brain, cancer, and brain–cancer specifically is indicated

To strengthen the small RNA-seq data, four hemizygous *FTSJ1* LCLs (control) and five LCL mutants for *FTSJ1* were analysed by Northern blotting with a specific probe complementary to *miRNA-181a-5p*. We selected this miRNA as it was highly up-regulated in our small RNA-seq analysis and it was previously reported to be involved in vascular inflammation and atherosclerosis (Su et al, 2019), and expressed in neuronal cells in mammals (Dostie et al, 2003). One clear hybridization signal was observed in all *FTSJ1* mutant LCLs corresponding to mature *miRNA-181a-5p* (Fig 3C). In contrast, the four control LCLs show no or weak signal even after image over-exposure (Fig 3C). Together, these results demonstrate that *FTSJ1* loss of function affects specifically the steady-state levels of some miRNA and suggest that the deregulation of miRNA-mediated gene silencing observed in *FTSJ1* mutant LCLs was not caused by a global failure in miRNA biogenesis (Figs 3A and S3B and Table S1).

FTSJ1 mutation perturbates the silencing activity of *miR-181a-5p* miRNA

As some of the *FTSJ1*-deregulated miRNAs and mRNAs were implicated in similar biological processes such as cancer and brain function, we wondered whether there were some miRNA::mRNA pairs that could be involved in these commonly deregulated processes. Using miRNet 2.0 (Chang et al, 2020), we performed a bioinformatics cross-analysis of the small RNA-seq and mRNA-seq datasets. We found a subset of *FTSJ1*-deregulated miRNAs that were previously shown to modulate some of the *FTSJ1*-deregulated mRNAs. For instance, the *SPARC* mRNA is an experimentally confirmed target of *miR-10a-5p* (Bryant et al, 2012; Wang et al, 2020). This result thus suggests that *SPARC* mRNA down-regulation observed in *FTSJ1* mutants may be due to its increased silencing by the up-regulated *miR-10a-5p*. This cross-analysis also revealed that the *BTBD3* gene is potentially targeted by *miR-181a*-5p (He et al, 2015), the two of which were up-regulated in XLID affected individuals' blood-derived LCLs (Fig 3A and C and Table 4), implicating a possible connection between them that differs from the canonical miRNA silencing pathway. LCLs are known to be hardly transfectable (Nagayoshi et al, 2021); however, *miR-181a-5p* and *BTBD3* are expressed similarly in HeLa cells (Fig S4A). Thus, by mimicking *miR-181a-5p* expression or repression, we show that *miR-181a-5p* silences *BTBD3* in HeLa cells (Fig S4B), strongly suggesting that *BTBD3* mRNA is a bona fide target of *miR-181a-5p*. Strikingly, in *FTSJ1* mutant cells, the silencing activity of *miR-181a-5p* on *BTBD3* is compromised in both HeLa and LCL. Interestingly, despite the fact that 39 *ZNF* mRNAs were found potentially regulated by *miR-181a-5p* (Table 4 and [He et al, 2015]) and the over-representation of this miRNA in *FTSJ1* mutant (Fig 3A and C and Table S1), no evidence of miRNA regulation was yet found for *ZNF711*, a gene previously reported to be involved in the development of ID (van der Werf et al, 2017).

FTSJ1 is involved in human neuronal morphology during development

The loss of *FTSJ1* in humans gives rise to XLID, yet the underlying mechanism is still unclear. Defects in both neuronal morphology (Chen et al, 2021) and behaviour (Jensen et al, 2019) have been reported in patients affected by a wide range of ID disorders, with a variety of genetic aetiologies and their corresponding mouse models. To address whether the loss of human *FTSJ1* also affects neuronal morphology, we altered FTSJ1 activity using 2,6-diaminopurine (DAP) (Trzaska et al, 2020; Palma & Lejeune, 2021) in human NPCs. DAP is a recently discovered drug that binds to FTSJ1 and inhibits its methyltransferase activity (Trzaska et al, 2020; Palma & Lejeune, 2021). Immunostainings were performed for Sox2, a transcription factor expressed in NPCs, and doublecortin (DCX), a microtubule-associated protein expressed in differentiating NPCs or immature neurons, reflecting neurogenesis. Importantly, the DAP treatment did not significantly affect the differentiation of the NPCs (DCX−) to immature neurons (DCX+) (Fig 4A). This is in agreement with previous reports showing the absence of severe brain morphological defects in mice mutated for *Ftsj1* (Jensen et al, 2019; Nagayoshi et al, 2021). However, DCX-positive cells treated with 100 μM DAP showed a 25% increase in the number of interstitial protrusions, likely filopodia, on their neurites compared with the smoother appearance of the neurites of untreated control cells (Fig 4B and C). These spines' morphological defects on DAP-treated DCX+ cells are reminiscent of those observed on mature neurons from mutant mice of the fragile X mental retardation protein (*Fmr1*) (Braun & Segal, 2000) and from human patients' brains that suffer from the fragile X syndrome (Irwin et al, 2000). Furthermore, similar findings were recently reported in mouse brains mutated for *Ftsj1* (Nagayoshi et al, 2021), suggesting that this is a conserved phenotypic consequence of the loss of *FTSJ1*.

Drosophila FTSJ1 ortholog is involved in neuronal morphology during development

To further address whether the control of neuron morphology by FTSJ1 is a conserved feature across evolution, we dissected the neuromuscular junctions (NMJs) of *Drosophila* larvae carrying mutations in the orthologs of the *FTSJ1* gene, and larvae fed with DAP (Trzaska et al, 2020; Palma & Lejeune, 2021). Examination of the NMJs in *Trm7_32* and *Trm7_34* double homozygous mutant larvae or larvae fed with DAP revealed a significant synaptic overgrowth when compared to control larvae (Fig 5). Furthermore, as observed for the human NPC treated with DAP (Fig 4B and C), the neurite branching was strongly increased in both double mutant and DAP-fed larvae (Fig 5). However, the overall length of the axons was not significantly altered. These results indicate that *Drosophila* FTSJ1s, like human FTSJ1, control neuronal morphology.

respectively in the blue, green, and red circles. The Venn diagram was generated by http://bioinformatics.psb.ugent.be/webtools/Venn/. **(C)** Northern blot analysis with ^{32}P-labelled probe specific for *hsa-miR-181a-5p* confirms the up-regulation of this miRNA in *FTSJ1* loss of function condition already detected by small RNA-seq analysis. A ^{32}P-labelled probe specific for human U6 RNA was used to assess equal loading on the blot.

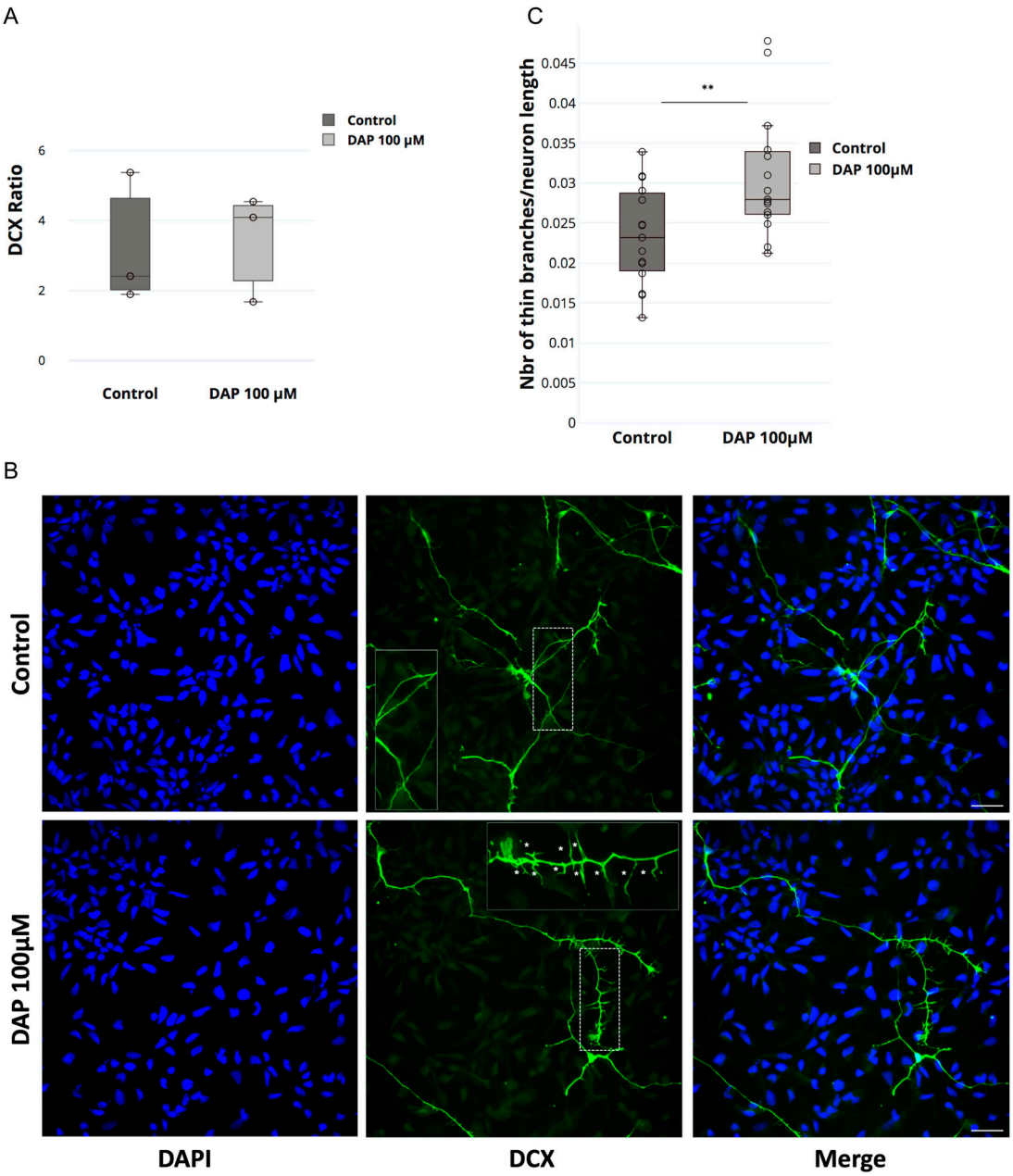

Figure 4. FTSJ1 depletion affects human neurons' spine morphology.
(A) DAP-induced FTSJ1 inhibition does not affect human NPC to immature neuron differentiation. Immunostainings for DCX and SOX2 were performed on human iPSC-derived NPCs treated with either 100 μM DAP or equal volume of H_2O for 24 h. Cells were numbered on microscopy acquisitions, and the ratio of DCX-expressing cells over total cell number was calculated and expressed in fold change. Error bars represent SD of three independent experiments; n.s., not significant (over 1,400 cells numbered for a single experiment). **(B)** Lower panel: human NPCs inhibited for FTSJ1 with 100 μM DAP for 24 h (DAP 100 μM) present an increased number of neurite spines during NPC to immature neuron differentiation. DCX protein expressed in immature neurons is marked in green (DCX). Dashed white line represents the *zoom-in* zone depicted in the top right corner with a continuous white line. White stars (*) in the magnified inset point to the fine spine neurites. Upper panel: untreated NPCs (control). Nuclear staining was performed using DAPI depicted in blue (DAPI). **(C)** Quantification of thin spines of DCX-positive cells ((B) above). Thin projections were numbered and normalized over the total length of the immature neurons as traced and measured by Simple Neurite Tracer (Fiji plugin). Quantifications were carried out on five acquisitions for each experiment (control and DAP 100 μM) (>40 branches/acquisition on average). White scale bar: 30 μm. Aggregate of three independent experiments. Wilcoxon–Mann–Whitney's test, $^{**}P$ = 0.0098.

Reward learning requires FTSJ1 activity in *Drosophila*

FTSJ1 loss of function affected individuals suffer from significant limitations both in intellectual functioning and in adaptive behaviour. Similar phenotypes including impaired learning and memory capacity were recently observed in *Ftsj1* KO mice that also present a reduced body weight and bone mass, and altered energy metabolism (Jensen et al, 2019; Nagayoshi et al, 2021). In flies, we

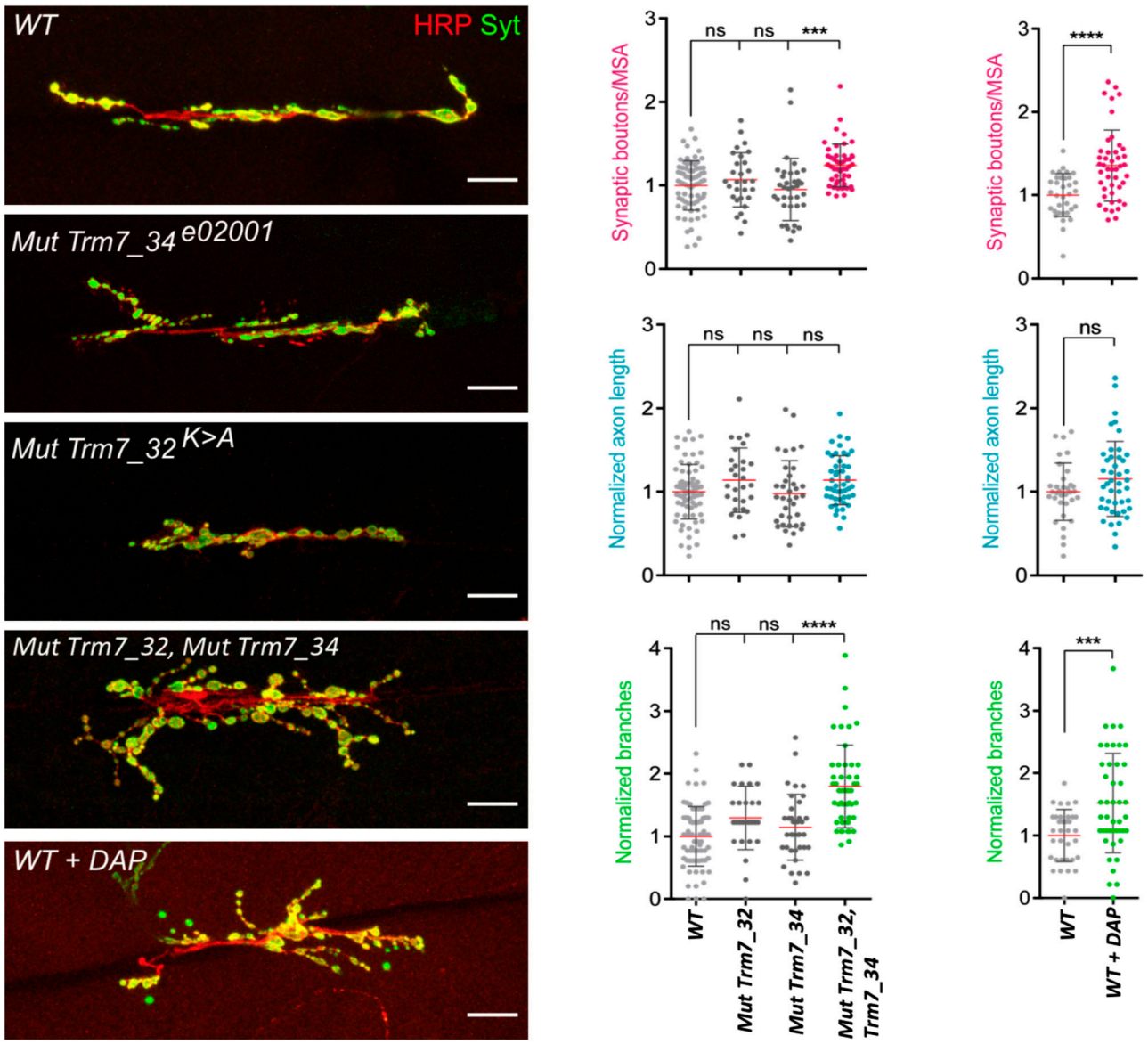

Figure 5. FTSJ1-dependent Nm regulates axonal morphology in the *Drosophila* nervous system.
Left panel: representative confocal images of muscle-6/7 NMJ synapses of larval abdominal hemisegments A2–A3 for the indicated genotypes labelled with anti-synaptotagmin (green) and HRP (red) to reveal the synaptic vesicles and the neuronal membrane. White scale bar: 20 μm. Right panel: quantification of normalized bouton number (total number of boutons/muscle surface area [μm^2 × 1,000]) (top), normalized axon length (middle), and normalized branching (bottom) of NMJ 6/7 in A2–A3 of the indicated genotypes. Bars show the mean ± SEM. Multiple comparisons were performed using one-way ANOVA with a post hoc Sidak–Bonferroni correction (n.s., not significant; *P < 0.05; ***P < 0.001; and ****P < 0.0001). Numbers of replicated neurons (n) are as follows: 74 for WT; 36 for *Trm7_32*; 29 for *Trm7_34*; 48 for *Trm7_32*; *Trm7_34*; and 34 for WT untreated and 45 for WT treated with DAP. *Canton-S* larvae were used as WT control.

recently showed that the loss of *FTSJ1* orthologs causes reduced lifespan and body weight, and locomotion defects (Angelova et al, 2020).

To address whether fly memory was also altered in these mutants, we applied an appetitive conditioning assay. We found that short-term memory of single *Trm7_34* or *Trm7_32* and double *Trm7_34*;*Trm7_32* heterozygous mutant flies was indistinguishable from that of wild-type controls (Fig 6A). However, long-term memory (LTM) was significantly impaired in all of these three mutant combinations (Fig 6B). Importantly, naive heterozygous mutant flies detected sugar properly and behave normally when exposed to repellent odours used in the olfactory memory assay (Fig 6C and D), suggesting that the LTM defect was not due to a confounding alteration of sensory abilities. Thus, these results indicate that the *Drosophila FTSJ1* orthologs *Trm7_34* and *Trm7_32* have a specific function in LTM, and importantly demonstrate clearly that both tRNA Nm32 and Nm34 modifications have function in long-term memory.

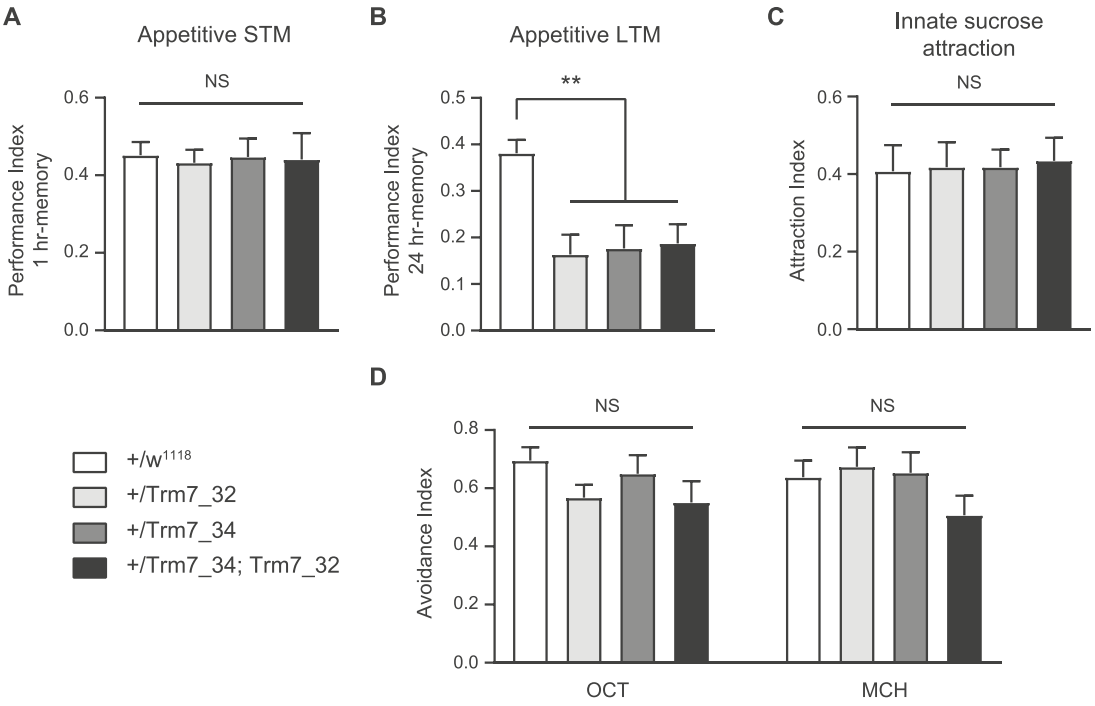

Figure 6. *Drosophila FTSJ1* ortholog *Trm7_34* mutants are defective for appetitive long-term memory.
Behavioural performances are reported as the mean±SEM. Statistical significance was tested with a one-way ANOVA followed by Tukey's post hoc pairwise comparisons. Asterisks on the barplots indicate the level of significance of the pairwise comparison with control. The *P*-value indicated in the legend corresponds to the output of the ANOVA. **(A)** Flies were starved on mineral water for 21 h and then trained with an appetitive associative olfactory learning protocol (odour paired with sucrose ingestion). Short-term memory performance was measured 1 h after learning. The short-term memory score of single *Trm7_32* (+/Trm7_32) and *Trm7_34* (+/Trm7_34), and double *Trm7_32*; *Trm7_34* (Trm7_32; Trm7_34) heterozygous mutant flies was not different from their genotypic controls (+/w^{1118}) (n = 12 per condition; *P* = 0.99). **(B)** Flies were starved on mineral water for 21 h and then trained with an appetitive associative olfactory learning protocol (odour paired with sucrose ingestion). Long-term memory performance was measured 24 h after learning. The long-term memory score of single *Trm7_32* (+/Trm7_32) and *Trm7_34* (+/Trm7_34), and double *Trm7_32*; *Trm7_34* (Trm7_32; Trm7_34) heterozygous mutant flies was severely impaired as compared to their genotypic controls (+/w^{1118}) (n = 16–19 per condition; *P* = 0.0007). **(C)** Flies were starved on mineral water for 21 h, and their attraction to sucrose was then measured. The innate sucrose preference of single *Trm7_32* (+/Trm7_32) and *Trm7_34* (+/Trm7_34), and double *Trm7_32*; *Trm7_34* (Trm7_32; Trm7_34) heterozygous mutant flies was not different from their genotypic controls (+/w^{1118}) (n = 14 per condition; *P* = 0.99). **(D)** Flies were starved on mineral water for 21 h, and their avoidance to the odorants used in the olfactory memory assays, 3-octanol (OCT) and 4-methylcyclohexanol (MCH), was then measured. The innate odour avoidance of single *Trm7_32* (+/Trm7_32) and *Trm7_34* (+/Trm7_34), and double *Trm7_32*; *Trm7_34* (Trm7_32; Trm7_34) heterozygous mutant flies was not different from their genotypic controls (+/w^{1118}) (n = 10 per condition; OCT: *P* = 0.26; MCH: *P* = 0.28).

Discussion

In this study, we characterized at the molecular and cellular levels the effect of *FTSJ1* loss of function in human cells. We used the innovative RiboMethSeq method to analyse the Nm status from five patients carrying a distinct loss of *FTSJ1* functions, which led us to the identification of new human FTSJ1 tRNA targets. Furthermore, we identify specific transcripts and miRNA that are misregulated in the absence of FTSJ1, which may contribute to the FTSJ1 pathologies, and suggest potential cross-regulation among them. Lastly, we show for the first time that the lack of FTSJ1 alters the morphology of human neurons, a phenotype that is conserved in *Drosophila* and is associated with long-term memory deficits.

The power of the RiboMethSeq approach is that it allows to analyse the Nm status of the totality of transcribed tRNA species and not only selected tRNAs based on the prior but incomplete knowledge of FTSJ1 targets. Furthermore, this approach covers the whole tRNA-ome and thus can identify variations in Nm at the single nucleotide resolution, which is very useful to distinguish tRNA isoacceptors for instance that differ by only a few nucleotides. Our results from the RiboMethSeq performed on patient and control LCLs confirmed the already known human tRNA targets of FTSJ1. For instance, Cm_{32} and Cm_{34} of $tRNA^{Trp(CCA)}$, and position 34 in $tRNA^{Phe(GAA)}$ and $tRNA^{Leu(CAG)}$ were validated by our approach. Only Cm_{32} of $tRNA^{Phe(GAA)}$, which is a well-known target of FTSJ1, could not be validated at the first glance. The analysis of this position is challenging because of low read numbers necessary for its quantification. This is the result of two confounding factors. On the one hand, the calculation of MethScores (Fig 1A) is based on the two neighbouring nucleotides (Marchand et al, 2016). Because FTSJ1 deposits Nm at both 32 and 34 positions in $tRNA^{Phe}$, the calculated MethScore at position 32 is affected when position 34 of the same tRNA is also Nm-modified. On the other hand, we previously reported that $tRNA^{Phe(GAA)}$ ACL positions are challenging to detect because of the specific hyper-modification on position 37 of $tRNA^{Phe}$ (Angelova et al, 2020). Indeed, $o2yW_{37}/m^1G_{37}$ impairs RT, thereby reducing the number of cDNAs spanning the ACL. Nevertheless, deeper visual inspection of the raw read profile shows that

Nm at position 32 was indeed lost in *FTSJ1*-mutated cells when compared to control LCL (Fig S1D), confirming the previous reports.

Importantly, we confirmed recent ($tRNA^{Arg(UCG)}$ and $tRNA^{Gln(CUG)}$) and identified novel ($tRNA^{Gly(CCC)}$, $tRNA^{Leu(UAA)}$, $tRNA^{Pro}$, and $tRNA^{Cys(GCA)}$; Table 2) tRNA targets for human FTSJ1. In the case of $tRNA^{Arg(UCG)}$, we confirmed not only a new target for FTSJ1, but also a modification, which was not previously reported in MODOMICS but only recently in the HEK293 *FTSJ1* CRISPR mutant (Li et al, 2020). Indeed, C_{32} is known to be m^3C and not Nm-modified for the two other isoacceptors ($tRNA^{Arg(CCU)}$ and $tRNA^{Arg(UCU)}$) (Boccaletto et al, 2018). Similarly, there was no evidence for a human Cm_{32} $tRNA^{Gln(CUG)}$ and only the other isoacceptor $tRNA^{Gln(UUG)}$ was reported in MODOMICS as 2′-O-methylated at C_{32}. Still, Cm_{32} on $tRNA^{Gln(CUG)}$ was recently discovered as a target of *Drosophila* Trm7_32 (Angelova et al, 2020). Among the newly uncovered FTSJ1 targets in this study, Um_{32} $tRNA^{Gly(CCC)}$ was the only one that has been reported in MODOMICS; however, the enzyme responsible for this modification was yet unknown. Our results demonstrate that FTSJ1 is the dedicated human Nm-MTase that installs Um_{32}/Cm_{32} and $Cm_{34}/Um_{34}/Gm_{34}$ residues on human tRNAs.

Our transcriptomic analysis also highlighted novel transcripts and miRNA targets that may play important roles in the development of the diseases. For instance, we found 36 differentially expressed miRNAs, most of which were already associated with brain diseases and functioning and/or cancer development. Strikingly, the most prevalent associated cancer types were the ones related to the brain tissues. Consistently with the post-transcriptional regulatory role of miRNAs, we also found through mRNA-seq an enrichment of brain morphogenesis–related mRNAs differentially expressed in *FTSJ1* loss of function when compared to control LCLs. Interestingly, a cross-analysis of these two RNA-sequencing experiments revealed potential miRNA::target mRNA couples among the deregulated RNA populations. This is indicative of possible miRNA silencing changes in the absence of FTSJ1, similar to what we report earlier in *Drosophila FTSJ1* mutant orthologs. The predicted miRNA::mRNA couples need to be further validated individually in neuronal tissues, although their report from *miRnet* database (Chang et al, 2020) already includes experimental evidence on the miRNA::mRNA regulation, particularly for *BTBD3* and *SPARC* mRNAs (Bryant et al, 2012; He et al, 2015; Wang et al, 2020). In addition to the reported prediction (He et al, 2015), we show that *BTBD3* is a bona fide *miR-181a-5p* target. Surprisingly, both *BTBD3* and *miR-181a-5p* were up-regulated in *FTSJ1*-depleted patient cells. Although the precise mechanism is not known yet, our results suggest that Nm-MTase genes could act upstream of small RNA biogenesis and function through transcriptional down-regulation of Argonaute mRNA in *Drosophila FTSJ1* mutants (Angelova et al, 2020) and in human cells (not shown). On the contrary, tRNA fragment (tRF) abundance seen in *FTSJ1* mutant fly (Angelova et al, 2020) and mice (Nagayoshi et al, 2021) can associate with Dicer, Argonaute, and Piwi proteins, thus affecting their silencing function. Such tRF-mediated titration of proteins away from canonical substrates has been previously reported in *Drosophila* and human cell lines (Durdevic et al, 2013; Goodarzi et al, 2015).

Affected individuals carrying mutations in *FTSJ1* suffer from XLID (Freude et al, 2004; Ramser et al, 2004; Guy et al, 2015), but the mechanism underlying this pathology has remained elusive. A recent report from Nagayoshi et al added some insight by showing that *Ftsj1* loss of function in mice provokes dendritic spine overgrowth at hippocampus and cortex neurons (Nagayoshi et al, 2021), suggesting that a similar alteration of neuron morphology may exist in human patients, which might impair their functioning. Indeed, we observed long, thin protrusion in human neurons affected for FTSJ1 activity. These protrusions are very similar in size and shape to the dendritic spines observed in hippocampus and cortex neurons of *Ftsj1* loss of function mice (Nagayoshi et al, 2021). A similar observation was also described earlier for *Fmr1* mutant mice (Braun & Segal, 2000) and *FMRP* human affected individuals' brains suffering from ID (Irwin et al, 2000). More examples of improper neuron morphology and in particular spine immaturity were found in additional gene loss of functions causative of ID (Levenga & Willemsen, 2012). This suggests that the lack of proper neuronal morphology may be a common feature of ID. More work will be required to address how these changes in spine arborization occur in the absence of FTSJ1 and how this translates into the disease. Interestingly in this study, we found that *BTBD3* mRNA is significantly up-regulated in *FTSJ1*-mutated LCLs. Because BTBD3 controls dendrite orientation in mammalian cortical neurons (Matsui et al, 2013), it will be an interesting target to further characterize in the context of FTSJ1 ID pathology.

A synaptic overgrowth was also observed in *Drosophila*, indicating that this function of FTSJ1 is conserved across evolution. In addition, we found that the long-term memory but not the short-term was significantly altered in the absence of FTSJ1 in flies. This is consistent with the learning deficits observed in mice and humans. In contrast to human FTSJ1 and the yeast ortholog TRM7, *Drosophila* uses two distinct paralogs to methylate positions 32 and 34, respectively, on the tRNA ACL. Interestingly, we found that the lack of both Trm7_34 and Trm7_32 had an effect on long-term memory, suggesting that the methylations at wobble positions 34 and 32 are critical for this function. However, the lack of both modifications (as in mammalian *Ftsj1* mutant) is not cumulative regarding the memory deficit (Fig 6). This last observation is strongly supported by the affected human individual who harbours a missense variant (p.Ala26Pro, LCL22 in this study), resulting in loss of Gm_{34}, but not of Cm_{32}, in human $tRNA^{Phe}$ (Guy et al, 2015). Further studies should aim to understand how the loss of methylation at these ACL positions affects the learning and memory functions.

The heterogeneity of ID makes it extremely challenging for genetic and clinical diagnoses (Ilyas et al, 2020). Our RiboMethSeq and transcriptomic approaches performed on XLID affected individuals have with high confidence extended the panel of FTSJ1's targets. Because our investigation was carried out on LCLs derived from the blood of affected individuals, our resource provides potential new biomarkers for diagnosis of FTSJ1-related ID in future. For instance, *miR-181a-5p*, which is detected only in patient-derived blood cells, constitutes already a good candidate for such purpose. Therefore, our study highlights the usefulness of companion diagnostics in clinical settings, in addition to exome sequencing, for potential discovery of prognostic markers of complex diseases.

Table 3. *FTSJ1* loss of function leads to mRNA deregulation in XLID affected individuals' LCLs.

#	Symbol	baseMean_ mutant	baseMean_ wt	log_2 FoldChange_ Mutant_ versus_WT	padj	#	Symbol	baseMean_ mutant	baseMean_ wt	log_2 FoldChange_ Mutant_ versus_WT	padj
1	SASH1	1002.73	7.65	7.33	2.69×10^{-41}	36	RNASE6	639.96	1645.30	−1.72	1.43×10^{-7}
2	FCRL4	515.44	7.09	6.05	2.08×10^{-26}	37	CD38	3629.12	297.01	2.52	1.60×10^{-7}
3	GSTT1	381.66	1.49	8.82	1.81×10^{-18}	38	LOC728640	2914.46	2322.11	0.80	2.04×10^{-7}
4	PPP1R21	5078.43	6380.13	−1.06	1.92×10^{-17}	39	APBB2	1332.24	3371.16	−2.21	2.18×10^{-7}
5	TINAG	522.56	2.62	7.59	5.23×10^{-17}	40	USMG5	7566.88	6750.46	0.76	2.45×10^{-7}
6	ADCY6	544.04	17.61	3.38	1.20×10^{-16}	41	FBN2	638.23	76.83	3.67	2.64×10^{-7}
7	DSC2	990.21	134.24	3.01	9.55×10^{-15}	42	HTR7	2.11	273.06	−21.67	3.12×10^{-7}
8	IL17RB	3188.28	616.47	3.45	1.22×10^{-14}	43	ALOX5	1890.29	5091.55	−2.91	3.96×10^{-7}
9	ABCA12	1267.89	3695.42	−3.75	1.49×10^{-14}	44	DDX60L	962.23	110.32	2.42	5.75×10^{-7}
10	JAZF1	333.25	17.53	5.14	1.99×10^{-14}	45	B3GALNT1	617.28	26.67	4.51	8.73×10^{-7}
11	TNRC6C	1612.67	274.90	2.90	3.30×10^{-14}	46	COX7B	12243.87	9892.47	0.64	1.05×10^{-6}
12	SYNE1	4579.60	5860.78	−0.97	2.35×10^{-13}	47	CBLB	3203.88	5817.18	−1.72	1.33×10^{-6}
13	CPXM1	2071.71	6.69	8.34	2.34×10^{-12}	48	PAPLN	1212.67	3785.94	−1.77	1.35×10^{-6}
14	FNIP2	787.53	60.32	2.80	8.93×10^{-12}	49	ANKRD26P3	561.85	2.58	8.71	1.79×10^{-6}
15	CDH2	1169.70	45.93	5.50	1.06×10^{-10}	50	ACVR2B	355.06	771.16	−1.78	1.88×10^{-6}
16	TBX15	2674.86	22.11	5.58	1.52×10^{-10}	51	RBPMS	341.58	0.52	8.65	2.01×10^{-6}
17	C14orf105	2783.34	168.09	3.35	4.51×10^{-10}	52	PSMD7	34420.17	28659.74	0.64	2.07×10^{-6}
18	AMPD3	1793.58	4186.29	−2.29	5.50×10^{-10}	53	MPHOSPH8	33819.66	28333.28	0.63	2.38×10^{-6}
19	GAS2	2013.39	25.82	5.45	7.09×10^{-10}	54	CTSW	110.71	8.47	5.36	2.71×10^{-6}
20	EVC	293.08	3187.02	−6.61	7.09×10^{-10}	55	MYO9B	10534.78	14242.52	−0.53	2.84×10^{-6}
21	TNFAIP2	1331.48	3608.85	−1.82	1.15×10^{-9}	56	IQGAP2	6537.41	9197.51	−1.20	3.22×10^{-6}
22	TSPYL5	829.00	72.33	3.10	1.19×10^{-9}	57	AMOTL1	2535.84	68.85	3.67	3.94×10^{-6}
23	HERC5	11068.07	2191.72	1.45	1.98×10^{-9}	58	MANEAL	354.94	982.06	−1.69	4.72×10^{-6}
24	UBE2QL1	205.44	53.77	3.16	2.23×10^{-9}	59	SPATS2L	7329.68	2990.72	0.97	4.97×10^{-6}
25	ARHGAP6	3915.43	352.19	3.53	2.73×10^{-9}	60	VEGFB	6472.65	5415.88	0.90	5.21×10^{-6}
26	SLAIN1	6757.48	3157.85	1.24	2.73×10^{-9}	61	ATP1B1	7552.46	859.00	2.47	5.25×10^{-6}
27	CERS6	5027.25	5425.85	−1.13	3.74×10^{-9}	62	SIX3	800.36	1203.65	−6.36	5.25×10^{-6}
28	ATP8B1	296.62	13.02	3.73	5.99×10^{-9}	63	LOC285972	1639.86	2658.04	−1.16	7.04×10^{-6}
29	GRIA3	43.74	504.25	−3.95	7.66×10^{-9}	64	MYO18A	8284.31	9316.46	−0.69	8.77×10^{-6}
30	MARCH8	1078.97	1225.73	−1.64	7.68×10^{-9}	65	L1TD1	67.03	1.01	8.23	8.90×10^{-6}
31	DUSP4	17734.90	5898.88	1.94	1.58×10^{-8}	66	RRP7B	3521.07	2614.81	0.94	9.80×10^{-6}
32	EPB41L5	1929.07	494.79	1.93	1.70×10^{-8}	67	SPARC	4705.62	16484.18	−1.60	1.51×10^{-5}
33	ZNF711	1265.24	3592.15	−3.34	1.05×10^{-7}	68	ESF1	32558.55	26226.19	0.69	1.60×10^{-5}
34	RGS2	1264.73	83.46	3.85	1.26×10^{-7}	69	FUT8	10906.46	16945.75	−0.94	1.64×10^{-5}
35	TP53BP2	2231.99	622.32	2.13	1.41×10^{-7}	70	MIR363	109.28	0.00	8.71	1.71×10^{-5}

A list of the 70 most significantly deregulated mRNAs in *FTSJ1* LCL mutants versus controls.

Table 4. Bibliographic search on miRNAs deregulated in *FTSJ1* loss of function LCL mutant cell lines.

miRNA	Brain-related	Brain cancer–related	Cancer-related
hsa-miR-20b-5p	—	—	Khuu et al (2016)
hsa-miR-222-3p	Lau et al (2013), Kretschmann et al (2015), Kan et al (2012), Risbud & Porter (2013)	Gillies & Lorimer (2007), Zhang et al (2010)	—
hsa-miR-548ax	—	Neuroblastoma for other miR-548 family members	Watahiki et al (2011) (also others cancers for other miR-548 family members)
hsa-miR-125b-2-3p	yes	yes	yes
hsa-miR-221-3p	Kretschmann et al (2015), Kan et al (2012), Risbud & Porter (2013), Ding et al (2016), Ma et al (2016), Roser et al (2018)	(see miR-222-3p)	Fornari et al (2008)
hsa-miR-335-3p	yes	yes	yes
hsa-miR-181b-2-3p	(see miR(181a-5p))	(see miR(181a-5p))	(see miR(181a-5p))
hsa-miR-99a-5p	yes	yes	yes
hsa-miR-10a-5p	Gui et al (2015), Roser et al (2018)	Tehler et al (2011), Lund (2010)	Tehler et al (2011), Lund (2010)
hsa-miR-181b-3p	(see miR(181a-5p))	(see miR(181a-5p))	(see miR(181a-5p))
hsa-miR-106a-5p	yes	yes	yes
hsa-miR-181a-2-3p	(see miR(181a-5p))	(see miR(181a-5p))	(see miR(181a-5p))
hsa-miR-146a-5p	yes	yes	yes
hsa-miR-4482-3p	—	—	—
hsa-miR-125b-5p	yes	yes	yes
hsa-miR-450b-5p	—	—	yes
hsa-miR-424-3p	yes	—	yes
hsa-miR-363-3p	Lau et al (2013), Kiyosawa et al (2019)	Conti et al (2016), Qiao et al (2013)	Jiang et al (2018), Ye et al (2017), Hu et al (2016), Wang et al (2016), Karatas et al (2016), Chapman et al (2015), Zhang et al (2016), Khuu et al (2016)
hsa-let-7c-5p	—	—	—
hsa-miR-450a-5p	yes	—	yes
hsa-miR-18b-5p	—	—	—
hsa-miR-550a-3p	—	—	yes
hsa-miR-181a-5p	Zhang et al (2017), Ding et al (2016), Roser et al (2018)	Shi et al (2008)	Yang et al (2017), Li et al (2015)
hsa-miR-550b-2-5p	—	—	yes
hsa-miR-181a-3p	(see miR(181a-5p))	(see miR(181a-5p))	(see miR(181a-5p))
hsa-miR-181b-5p	(see miR(181a-5p))	(see miR(181a-5p))	(see miR(181a-5p))
hsa-miR-183-5p	yes	yes	yes
hsa-miR-99a-3p	yes	yes	yes
hsa-miR-135a-5p	yes	yes	yes
hsa-miR-146b-5p	yes	yes	yes
hsa-miR-542-5p	—	yes	yes
hsa-miR-944	yes	—	yes
hsa-miR-625-5p	—	—	—
hsa-miR-625-3p	—	—	—
hsa-miR-4772-5p	—	—	yes
hsa-miR-182-5p	yes	yes	yes
Total #	24	23	30

The list shows for each miRNA whether any link was found to brain development or brain-related diseases, also to cancer and specifically to brain cancers. The references are given for most of the miRNAs. The colour code of the miRNA names indicates whether they were found to be up- (red) or down-regulated (blue) in *FTSJ1* mutant LCLs derived from XLID affected individuals compared with control LCLs derived from healthy individuals.

Materials and Methods

FTSJ1 variants and LCLs

The various LCLs were generated using established methods from blood samples of XLID affected or healthy male individuals. The cells were cultured in RPMI 1640 medium with L-glutamine and sodium bicarbonate (ref. R8758-500ML; Sigma-Aldrich) supplemented with 10% FBS (Gibco) and 1% penicillin–streptomycin (ref. P0781; Sigma-Aldrich) at 37°C with 5% CO_2. Cells were split at ½ dilution ~24 h before being collected for RNA extraction with TRI Reagent (Sigma-Aldrich) following the manufacturer's instructions.

6514AW and 6514JW (LCL65AW and LCL65JW in this study): Family A3—LCLs from two brothers with mild or severe ID associated with psychiatric manifestations (anger, aggression, anxiety, depression, schizophrenia requiring medication) bearing a splice variant in *FTSJ1:* c.121 + 1delG (Freude et al, 2004). This variant leads to a retention of intron 2, creating a premature stop codon (p.Gly41Valfs*10). Part of the transcripts undergo nonsense-mediated mRNA decay.

11716IJ (LCL11 in this study): Family A18—LCL from one male with moderate to severe ID without dysmorphic features carrying an interstitial microdeletion at Xp11.23. The extent of the deletion was subsequently delineated to about 50 kb by regular PCR and included only the *SLC38A5* and *FTSJ1* genes. qPCR with the *FTSJ1*-ex3 primers is negative, thus demonstrating the complete deletion of the *FTSJ1* locus (Froyen et al, 2007).

22341SR (LCL22 in this study): Family 7 (A26P)—LCL from one male with moderate ID and psychiatric features (mild anxiety and compulsive behaviour) carrying a missense mutation c.76G > C; p.Ala26Pro in *FTSJ1*. This family has been reported previously (Guy et al, 2015).

LCL-MM: This is a newly reported family. The LCL has been generated from one male with mild ID, facial dysmorphia (hypertelorism, pointed chin, ears turned back), speech delay, attention disorders, and behavioural problems carrying a hemizygous de novo variant c.362-2A > T in *FTSJ1*. The mutation is predicted to disrupt the acceptor splice site of exon 6 (NM_012280.3: c.362-2A > T). This variant causes a skipping of the entire exon 6 in the mRNA (r.362_414del) leading to a frameshift and a premature stop codon (p.Val121Glyfs*51) (Fig S1A). Part of the transcripts undergo nonsense-mediated mRNA decay (Fig S1C). Consequently, a strong decrease of the corresponding mRNA steady-state level is observed (Fig S1B). This variant was deposited in the *ClinVar* database (VCV000981372.1). The research on LCL-MM was performed according to a research protocol approved by a local ethics committee (Comité Consultatif de Protection des Personnes dans la Recherche Biomédicale—CCPPRB). Written informed consent was obtained from the patient and his legal representatives.

18451PK (LCL18 in this study), 16806JD (LCL16 in this study), 3-2591 (LCL25 in this study), and 3-5456 (LCL54 in this study): LCL established from control males. Four LCLs not mutated in the *FTSJ1* gene from unaffected males of a similar age were used as controls. Written informed consent was obtained from those individuals, and previously described LCLs were obtained from patients and their legal representatives in the original publications described above.

LCL MM variant characterization at the mRNA level

As the *FTSJ1* mRNA was highly down-regulated in LCL MM, characterization of the *FTSJ1* transcript for this experiment was performed on total RNAs from cells treated with cycloheximide (see the NMD inhibition test section protocol below). This allowed a threefold increase in *FTSJ1* mRNA in LCL MM (Fig S1B). 1 μg of total RNAs from wild-type LCL 25 and LCL MM was treated with DNase I (M0303S; New England Biolabs), and RT was carried out with random hexamer primers (S0142; Thermo Fisher Scientific) using SuperScript III Reverse Transcriptase (18080-044; Invitrogen), following the supplier's protocol. *FTSJ1* cDNAs were amplified from 2 μl of RT reaction using the following PCR primers: Forward: 5′-GGCAGTTGACCTGTGTGCAGC-3′; Reverse: 5′-CCCTCTAGGTCCAGTGGGTAAC-3′. PCR products were sequenced using the Sanger method with a forward primer hybridizing in exon 5: 5′-CCACTGCCAAGGAGATCA-3′ (Fig S1A). Sequences are available upon request. Briefly, this variant causes a skipping of the entire exon 6 in the mRNA leading to a frameshift and a premature stop codon, thus undergoing nonsense-mediated mRNA decay as shown in Fig S1C. Consequently, a strong decrease of the corresponding mRNA steady-state level is observed (Fig S1B). This MM variant was deposited in the *ClinVar* database (VCV000981372.1).

RiboMethSeq

RiboMethSeq analysis of human LCL tRNAs was performed as described in Marchand et al (2017). Briefly, tRNAs extracted from LCLs were fragmented in 50 mM bicarbonate buffer, pH 9.2, for 15 min at 95°C. The reaction was stopped by ethanol precipitation. The pellet was washed with 80% ethanol, and sizes of generated RNA fragments were assessed by capillary electrophoresis using a small RNA chip on Bioanalyzer 2100 (Agilent Technologies). RNA fragments were directly 3′-end–dephosphorylated using 5 U of Antarctic phosphatase (New England Biolabs) for 30 min at 37°C. After inactivation of the phosphatase for 5 min at 70°C, RNA fragments were phosphorylated at the 5′-end using T4 PNK and 1 mM ATP for 1 h at 37°C. End-repaired RNA fragments were then purified using RNeasy MinElute Cleanup Kit (QIAGEN) according to the manufacturer's recommendations. RNA fragments were converted to library using NEBNext Small RNA Library Kit (ref. E7330S; New England Biolabs) following the manufacturer's instructions. DNA library quality was assessed using a High Sensitivity DNA chip on Bioanalyzer 2100. Library sequencing was performed on Illumina HiSeq 1000 in a single-read mode for 50 nt. Primary analysis of sequencing quality was performed with RTA 2.12 software, to ensure > Q30 quality score for >95% of obtained sequences.

After SR50 sequencing run, demultiplexing was performed with BclToFastq v2.4, and reads not passing quality filter were removed. Raw reads after demultiplexing were trimmed with Trimmomatic v0.32 (Bolger et al, 2014). Alignment to the reference tDNA sequences was performed with bowtie 2 ver2.2.4 (Langmead et al, 2009) in end-to-end mode. Uniquely mapped reads were extracted from *.sam file by RNA ID and converted to *.bed format using bedtools v2.25.0 (Quinlan, 2014). Positional counting of 5′- and 3′-ends of each read was performed with awk Unix command. Further treatment steps were performed in R environment (v3.0.1). In brief, 5′- and 3′-end counts were merged together by RNA position and used for the calculation of ScoreMEAN (derived from MAX Score)

(Pichot et al, 2020), and Scores A and B (Birkedal et al, 2015) and MethScore (Score C) (Marchand et al, 2016). Scores were calculated in the window of −2 to +2 neighbouring nucleotides. Profiles of RNA cleavage at selected (candidate and previously known) positions were extracted and visually inspected.

Analysis of human tRNA 2′-O-methylation by RiboMethSeq was performed using the optimized non-redundant collection of reference tRNA sequences. This reduced collection contains 43 tRNA species and was validated by analysis of several experimentally obtained RiboMethSeq datasets (Pichot et al, 2021). Alignment of RiboMethSeq reads obtained in this study also confirmed low content in ambiguously mapped reads. In order to establish a reliable map of Nm positions in the human tRNA anticodon loop, RiboMethSeq cleavage profiles were used to calculate detection scores (Mean and ScoreA2) (Pichot et al, 2020). However, this scoring strategy shows its limits in the case of short and highly structured RNAs (like tRNAs), because the cleavage profile is highly irregular. In addition, because these scores are calculated for two neighbouring nucleotides, the simultaneous loss of two closely located Nm residues (e.g., Cm_{32} and Gm_{34} in $tRNA^{Phe}$) makes analysis of raw score misleading (Angelova et al, 2020). Moreover, the presence of multiple RT-arresting modifications (Anreiter et al, 2021) in the same tRNAs (m^1A, m^1G, m^22 G, m^3C, etc.) reduces coverage in the upstream regions. Considering all these limitations, visual inspection of raw cleavage profiles revealed to be the most appropriate, because changes in protection of a given nucleotide represent modulation of its Nm methylation status. Analysis of alignment statistics demonstrated that most of the human tRNAs are well represented in the analysed datasets and proportion of uniquely mapped reads were >90% for all tRNA sequences, except the tRNA Leu_CCA family, composed of three highly similar species. Only limited coverage of totally mapped reads <7,500 reads/tRNA (~100 reads/position) was obtained for five tRNAs (Arg_TCG, Leu_CAA2, Ser_CGA_TGA1, Thr_CGT, and Tyr_ATA).

To identify potential Nm32/Nm34 residues, raw cleavage profiles of the 11-nt region around pos 33 were visually inspected and profiles for WT samples were compared with *FTSJ1* mutants. Because of the limited number of mapped raw reads, coverage in the anticodon loop for Leu_CAA, Ser_CGA_TGA1, Thr_CGT, and Tyr_ATA was insufficient; thus, these species were excluded from further analysis. The results of this analysis are given in Table 2. This analysis allowed to identify 10 Nm32 and four Nm34 modifications on the tRNA ACL. Inosine residues formed by deamination of A34 at the wobble tRNA position (FTSJ1-independent) are visible in the sequencing data and are also shown in Table 2. 10 Nm32 and three Nm34 modifications were found to be FTSJ1-dependent. The only exception is Cm34 in tRNAMet_CAT known to be formed by snoRNA-guided fibrillarin (Vitali & Kiss, 2019). Comparison of these data with previously reported Nm modifications in the human tRNA anticodon loop demonstrated that 2/3 of the observed sites have been described, either in tRNAdb2009 ([Jühling et al, 2009], http://trnadb.bioinf.uni-leipzig.de/) or in two recent studies that used LC–MS/MS analysis (Li et al, 2020; Nagayoshi et al, 2021). Table 2 also shows those modifications in other organisms including yeast, mice, and *Drosophila*. We were not able to confirm Nm residues previously reported in tRNASec_TCA (Nm34) and tRNAVal_AAC(Cm32); however, because of sequence similarity, tRNAVal_AAC clusters together with two other tRNAVal (CAC and TAC1). tRNALeu_AAG and Leu_TAG have similar sequences and thus were not distinguished by sequencing; however, Nm32 was detected.

mRNA sequencing and data analysis

mRNA sequencing was performed as in Khalil et al (2018). 5 μg of total RNA was treated with 1 MBU of DNase (BaseLine-Zero DNase; Epicentre) for 20 min at 37°C to remove residual genomic DNA contamination. RNA quality was verified by a PicoRNA chip on Bioanalyzer 2100 (Agilent Technologies) to ensure RIN (RNA integrity number) > 8.0. PolyA + fraction was isolated from 4.5 μg of DNase-treated total RNA using NEBNext Oligo d(T)25 Magnetic Beads Kit (New England Biolabs), according to the manufacturer's recommendations. PolyA + enrichment and the absence of residual ribosomal RNA contamination were verified using PicoRNA chips on Bioanalyzer 2100 (Agilent Technologies). PolyA + fraction (1 ng for each sample) was used for whole-transcriptome library preparation using ScriptSeq v2 RNA-seq Kit (Illumina). Libraries amplified in 14 PCR cycles were purified using Agencourt AMPure XP Beads (Beckman Coulter), at a ratio 0.9× to remove adapter dimer contamination. Quality of the libraries was verified by HS DNA Chip on Bioanalyzer 2100 (Agilent Technologies) and quantification done by Qubit 2.0 with an appropriate RNA quantification kit. Sequencing was performed on HiSeq 1000 (Illumina) in single-read SR50 mode. About 50 million of raw sequencing reads was obtained for each sample. Adapters were trimmed by Trimmomatic v0.32 (Bolger et al, 2014) and the resulting sequencing reads aligned in sensitive-local mode by Bowtie 2 v2.2.4 (Langmead & Salzberg, 2012) to hg19 build of human genome. Differential expression was analysed using *.bam files in the DESeq2 package (Love et al, 2014) under R environment. Analysis of KEGG and gene ontology pathways for differentially expressed genes was done under R environment.

Small RNA sequencing and data analysis

Small RNA-seq libraries were generated from 1,000 ng of total RNA using TruSeq Small RNA Library Prep Kit (Illumina), according to the manufacturer's instructions. Briefly, in the first step, RNA adapters were sequentially ligated to each end of the RNA, first the 3′ RNA adapter that is specifically modified to target microRNAs and other small RNAs, then the 5′ RNA adapter. Small RNA ligated with 3′ and 5′ adapters was reverse-transcribed and PCR-amplified (30 s at 98°C; [10 s at 98°C, 30 s at 60°C, 15 s at 72°C] × 13 cycles; 10 min at 72°C) to create cDNA constructs. Amplified cDNA constructs of 20–40 nt were selectively isolated by acrylamide gel purification followed by ethanol precipitation. The final cDNA libraries were checked for quality and quantified using capillary electrophoresis and sequenced on the Illumina HiSeq 4000 at the Institut de Génétique et de Biologie Moléculaire et Cellulaire (IGBMC) GenomEast sequencing platform.

For small RNA data analysis, adapters were trimmed from total reads using FASTX_Toolkit (http://hannonlab.cshl.edu/fastx_toolkit/). Only trimmed reads with a length between 15 and 40 nucleotides were kept for further analysis. Data analysis was performed according to the published pipeline ncPRO-seq (Chen et al, 2012). Briefly, reads were mapped onto the human genome assembly hg19 with Bowtie v1.0.0. The annotations for miRNAs were done

with miRBase v21. The normalization and comparisons of interest were performed using the test for differential expression, proposed by Love et al (2014) and implemented in the Bioconductor package DESeq2 v1.22.2 (http://bioconductor.org/). MicroRNA target prediction was performed using miRNet 2.0 (Chang et al, 2020).

Northern blotting

For Northern blotting analysis of tRNAs, 5 μg of total RNA from human LCLs was resolved on 15% urea–polyacrylamide gels for ~2 h in 0.5× TBE buffer at 150 V, then transferred to Hybond-NX membrane (GE Healthcare) in 0.5× TBE buffer for 1 h at 350 mA of current and EDC–cross-linked for 45 min at 60°C with a solution containing 33 mg/ml of 1-ethyl-3-(3-dimethylaminopropyl) carbodiimide (EDC) (Sigma-Aldrich), 11 ng/μl of 1-methylimidazole, and 0.46% of HCl. The membranes were first prehybridized for 1 h at 42°C in a hybridization buffer containing 5×SSC, 7% SDS, 5.6 mM NaH_2PO_4, 14.4 mM Na_2HPO_4, and 1× Denhardt's solution. DNA oligonucleotide probes were labelled with ^{32}P at the 5′-end by T4 polynucleotide kinase following the manufacturer's instructions (Fermentas). The membranes were hybridized with the labelled probes overnight at 42°C in the hybridization buffer, then washed twice for 15 min in wash buffer A (3× SSC and 5% SDS) and twice in wash buffer B (1× SSC and 1% SDS) before film exposure at −80°C for variable time durations. Probe sequences are available in the Primers, probes, and sequences section.

qRT–PCR

RNA was extracted from human LCLs using TRI Reagent (Sigma-Aldrich). After DNase digestion of total RNA using the TURBO DNA-free Kit (Ambion), 1 μg was used in a RT reaction with random primers (Promega) and RevertAid Reverse Transcriptase (ref. EP0442; Thermo Fisher Scientific). The cDNA was used to perform qPCR on a CFX96 Touch Real-Time PCR Detection System (Bio-Rad) using target-specific primers. *hGAPDH* was used for normalization (Primers, probes, and sequences section). The analysis was performed using ΔΔ Ct, on at least three biological replicates. Statistical analysis using a bilateral *t* test was performed, and *P*-values were calculated.

NMD inhibition test

LCLs were seeded in 25-cm cell culture flasks at a density of 3×10^6 cells and treated with 100 μg/ml of cycloheximide or equal volume of water as a control for 6 h. Cells were harvested by centrifugation (75003607 Rotor; Thermo Fisher Scientific) at 1,000 rpm for 5 min and flash-frozen in liquid nitrogen. RNA extraction was carried out using TRI Reagent (Sigma-Aldrich) following the supplier's protocol. DNase I digestion was carried out using RNase-free DNase I (M0303S; New England Biolabs), and RT on 1 μg of DNase-treated total RNA was performed using RevertAid Reverse Transcriptase. Quantitative PCR was performed as specified above using specific primers for *FTSJ1* and *GAPDH*.

miRNA complementation experiments

mirVana miRNA mimics and inhibitors were used for *hsa-miR-181a-5p* overexpression/inhibition (4464066 and 4464084; Ambion). HeLa cells were transfected with corresponding mirVana miRNA in 24-well plates at a density of 20,000 cells per well, using Lipofectamine RNAiMAX (Cat #13778100; Invitrogen). We set up the transfection ratios to 15 pmol of miRNA mimic/μl of Lipofectamine, and 30 pmol of miRNA inhibitor/μl of Lipofectamine. Cells were harvested 48 h post-transfection and assayed for target gene expression. miRNA quantification was performed by qRT–PCR on *miR-181a-5p* using QIAGEN's miRCURY LNA miRNA PCR System. RT is performed using miRCURY LNA RT Kit (339340) and qPCR using miRCURY LNA SYBR Green PCR Kit (339346). LNA-enhanced primers were used for miRNA SYBR Green qPCR (refer to the list of primers and probes).

Primers, probes, and sequences

Northern blot analysis was performed using *hsa-miR-181a-5p*–specific probes with the following sequences: 5′-AACATTCAACGCTGTCGGTGAGT-3′ (sense probe) and 5′-ACTCACCGACAGCGTTGAATGTT-3′ (antisense probe). Human U6–specific probe was used for detecting U6 as a loading control: 5′-GCAAGGATGACACGCAAATTCGTGA-3′ (sense probe) and 5′-TCACGAATTTGCGTGTCATCCTTGC-3′ (antisense probe). qPCR analysis (after an RT reaction performed with random primers) was performed with the use of primers with the following sequences:

Target gene	Primer	Sequence
BTBD3	Forward	5′-TGGCAGATGTACATTTTGTGG-3′
	Reverse	5′-AACACAGAGCTCCCAACAGC-3′
SPARC	Forward	5′-GAGAAGGTGTGCAGCAATGA-3′
	Reverse	5′-AAGTGGCAGGAAGAGTCGAA-3′
GAPDH	Forward	5′-CAACGGATTTGGTCGTATTGG-3′
	Reverse	5′-GCAACAATATCCACTTTACCAGAGTTAA-3′
FTSJ1	Forward	5′-CCATTCTTACGACCCAGATTTCA-3′
	Reverse	5′-CCCTCTAGGTCCAGTGGGTAAC-3′
ZNF711	Forward	5′-CACACGCCAGACTCTAGAATGG-3′
	Reverse	5′-CCATTCCAGCCACAAAATCTTG-3′
hsa-miR-181a-5p	Cat #339306; QIAGEN	GeneGlobe ID—YP00206081
UniSp6 (miRNA Spike in)	Cat #339306; QIAGEN	GeneGlobe ID—YP00203954

UCG isodecoder sequences (refer to Table 2) >hs_tRNA Arg_CCG_TCG_(UCG1)_gaccgcgtggcctaatggataaggcgtctgacttcggatcagaagattgagggttcgagtcccttcgtggtcgcca > hs_tRNAArg_TCG_(UCG2)_ggccgngtggcctaatggataaggcgtctgacttcggatcanaagattgcaggttngagtnctgccncggtcgcca.

iPSC culture and maintenance

iPSC cell line WTSIi002 purchased from EBISC (European bank for induced pluripotent cells) was maintained on feeder-free conditions on Geltrex LDEV-Free hESC-qualified Reduced Growth Factor Basement Membrane Matrix (A1413302; Thermo Fisher Scientific) in Essential 8 Flex Media Kit (A2858501; Thermo Fisher Scientific) with 0,1% penicillin–streptomycin (15140122; Thermo Fisher Scientific).

iPSC differentiation in dorsal NPCs

To obtain neural progenitor cells (NPCs) from the dorsal telencephalon, embryoid bodies (EBs) were formed by incubating iPSC clusters with Accutase (A1110501; Thermo Fisher Scientific) for 7 min at 37°C and dissociated into single cells. To obtain EB of the same size, 3×10^6 cells were added per well in the AggreWell 800 plate (34815; STEMCELL Technologies) with Essential 8 Flex Media supplemented with Stemgent hES Cell Cloning & Recovery Supplement (1×, STE01-0014-500; Ozyme) and incubated at 37°C with 5% CO_2 (day 1). After 24 h in culture (day 0), EBs from each microwell were collected by pipetting up and down the medium several times and transferred into Corning non-treated culture dishes (CLS430591-500EA; Merck) in EB medium containing DMEM/F12 GlutaMAX (35050061; Thermo Fisher Scientific), 20% KnockOut Serum Replacement (10828028; Thermo Fisher Scientific), 1% non-essential amino acid (11140035; Thermo Fisher Scientific), 0,1% penicillin–streptomycin (15140122; Thermo Fisher Scientific), and 100 μM 2-mercaptoethanol (31350010; Thermo Fisher Scientific), supplemented with two inhibitors of the SMAD signalling pathway, 2.5 μM dorsomorphin (P5499; Sigma-Aldrich) and 10 μM SB-431542 (ab120163; Abcam). EB medium supplemented as described previously was changed every day for 5 d. On day 6, floating EBs are plated on 0.01% poly-L-ornithine (P4957; Sigma-Aldrich)– and 5 μg/ml laminin (L2020; Sigma-Aldrich)-coated dishes for rosette expansion in Neurobasal minus vitamin A (10888; Thermo Fisher Scientific), B-27 supplement without vitamin A (12587; Thermo Fisher Scientific), 1% GlutaMAX (35050061; Thermo Fisher Scientific), 0,1% penicillin–streptomycin (15140122; Thermo Fisher Scientific), and 100 μM 2-mercaptoethanol (31350010; Thermo Fisher Scientific). The neural medium was supplemented with 10 ng/ml epidermal growth factor (AF-100-15; PeproTech) and 10 ng/ml basic fibroblast growth factor (234-FSE-025; R&D Systems). From days 6 to 10, the medium was changed every day until the appearance of rosettes. On day 10, rosettes are manually picked up using a syringe and dissociated with Accutase, then seeded on poly-L-ornithine/laminin-coated dishes for expansion of dorsal NPCs. They were maintained with passage for two additional weeks to achieve a large pool of neural precursor cells (NPCs).

NPC drug treatment

NPCs are seeded in poly-L-ornithine– and laminin-coated coverslips in 24-well plates at a density of 2×10^5 cells per well. After 48 h, the medium is changed and combined with 100 μM of 2,6-diaminopurine (DAP) (247847; Sigma-Aldrich) or equal volume of sterile H_2O.

NPC immunostainings

24 h after DAP treatment, NPCs were fixed in 4% paraformaldehyde for 10 min, permeabilized, and blocked for 45 min with blocking buffer (PBS supplemented with 0.3% Triton X-100, 2% horse serum). Primary antibodies, Sox2 (1/500, AB5603; Millipore) and DCX (1/2,000, AB2253; Millipore), were incubated overnight at 4°C using the same solution. Cells were rinsed three times with PBS and incubated for 1 h at RT with secondary antibodies and DAPI (1/10,000, D9564; Sigma-Aldrich) diluted in the same solution and rinsed three times with PBS before mounting on slides with VectaShield Vibrance mounting medium.

Neuronal cell image acquisitions

Images were acquired in z-stacks using a confocal microscope Nikon A1R HD25 with a 60× objective. Images were flattened with a max-intensity Z-projection.

Neurogenesis quantification

All cells (DAPI) from each acquisition were numbered using Fiji's point tool. Cells expressing DCX (immature neurons) and SOX2 (NPCs and intermediates, which also started expressing DCX) were also numbered on five to six microscopy images. Over 1,400 cells were numbered for each condition in triplicate. A ratio of DCX-expressing cells is calculated over the total cell number and expressed in fold change and compared between DAP-treated and untreated cells.

Branching quantifications

All DCX-expressing neurons were traced using Simple Neurite Tracer from the Neuroanatomy plugin by Fiji. Length measurements of traces were performed using the Simple Neurite Tracer Measure Menu, and thin projections were counted manually using Fiji's point tool. Quantifications were performed on five acquisitions, and each IF experiment was done in triplicate. Ratios for the number of thin projections/neuron length (mm) were calculated and compared between DAP-treated and control cells.

Drosophila NMJ analysis

For NMJ staining, third instar larvae were dissected in cold PBS and fixed with 4% paraformaldehyde in PBS for 45 min. Larvae were then washed in PBST (PBS + 0.5% Triton X-100) six times for 30 min and incubated overnight at 4°C with mouse anti-synaptotagmin, 1:200 (3H2 2D7, Developmental Studies Hybridoma Bank, DSHB). After six 30-min washes with PBST, secondary antibody anti-mouse conjugated to Alexa Fluor 488 and TRITC-conjugated anti-HRP (Jackson

ImmunoResearch) were used at a concentration of 1:1,000 and incubated at room temperature for 2 h. Larvae were washed again six times with PBST and finally mounted in Vectashield (Vector Laboratories).

For DAP treatment, freshly hatched *Canton-S* flies were collected and placed on a normal food medium containing 600 μM of 2,6-diaminopurine (DAP) (247847; Sigma-Aldrich). After 5 d, third instar larvae were dissected and subjected to NMJ staining.

Images from muscles 6–7 (segments A2–A3) were acquired with a Zeiss LSM 710 confocal microscope. Serial optical sections at 1,024 × 1,024 pixels with 0.4 μm thickness were obtained with the ×40 objective. Bouton number was quantified using Imaris 9 software. ImageJ software was used to measure the muscle area and the NMJ axon length and branching. Statistical tests were performed in GraphPad (Prism 8).

Drosophila behavioural assays

Flies were raised at 25°C for associative memory assays and the corresponding controls. All behavioural experiments were performed on young adults (1–3 d-old). All behavioural experiments were performed on starved flies, which is a prerequisite for appetitive conditioning with a sucrose reinforcement. 0–2 d after hatching, flies were put on starvation for 21 h at 25°C on mineral water (Evian).

Appetitive memory assay

Appetitive associative conditioning was performed in custom-designed barrel-type apparatus as previously described (Colomb et al, 2009), which allows the parallel conditioning of three groups of flies. The odorants 3-octanol and 4-methylcyclohexanol, diluted in paraffin oil at a final concentration of 0.29 $g{\cdot}l^{-1}$, were used for conditioning and for the test of memory retrieval. Groups of 20–50 flies were subjected to one cycle of appetitive olfactory conditioning as follows: throughout the conditioning protocol, flies were submitted to a constant airflow at 0.6 $litres{\cdot}min^{-1}$. After 90 s of habituation, flies were first exposed to an odorant (the CS^+) for 1 min, whereas given access to dried sucrose, flies were then exposed 45 s later to a second odorant without shocks (the CS^-) for 1 min. 3-Octanol and 4-methylcyclohexanol were alternately used as CS^+ and CS^-. The memory test was performed in a T-maze apparatus. Each of the two arms of the T-maze was connected to a bottle containing one odorant (either 3-octanol or 4-methylcyclohexanol) diluted in paraffin oil. The global airflow from both arms of the T-maze was set to 0.8 $litres{\cdot}min^{-1}$. Flies were given 1 min in complete darkness to freely move within the T-maze. Then, flies from each arm were collected and counted. The repartition of flies was used to calculate a memory score as $(N_{CS+} - N_{CS-})/(N_{CS+} + N_{CS-})$. A single performance index value is the average of two scores obtained from two groups of genotypically identical flies conditioned in two reciprocal experiments, using either odorant as the CS^+. Thus, values of performance index range between −1 and +1, with the value of 0 (equal repartition) corresponding to "no memory." The indicated "n" is the number of independent performance index values for each genotype. LTM performance was assessed 24 h (±2 h) after conditioning, and short-term memory, 1 h (±30 min) after conditioning.

Innate odour avoidance and sucrose attraction assay

Innate sucrose preference was measured in a T-maze. Flies were given the choice for 1 min between one arm of the T-maze coated with dried sucrose, and one empty arm. There was no airflow in the T-maze for this assay. Flies were then collected from each arm and counted; an attraction index was calculated as $(N_{sucrose} - N_{empty})/(N_{sucrose} + N_{empty})$. The side of the T-maze with sucrose was alternated between experimental replicates. Innate odour avoidance was measured in a T-maze. One arm of the T-maze was connected to a bottle containing the tested odorant (3-octanol or 4-methylcyclohexanol) diluted in paraffin oil, and the other arm was connected to a bottle containing paraffin oil only. The global airflow from both arms of the T-maze was set to 0.8 $litres{\cdot}min^{-1}$. Flies were given 1 min in complete darkness to freely move within the T-maze. Flies were then collected from each arm and counted; an avoidance index was calculated as $(N_{air} - N_{odour})/(N_{air} + N_{odour})$. The side of the T-maze with odorant-interlaced air was alternated between experimental replicates.

Quantification and statistical analysis

All data are presented as the mean ± SEM. Performances from different groups (mutant and control) were statistically compared using one-way ANOVA followed by Tukey's post hoc pairwise comparison between the mutant genotypes and the control group.

Data Availability

The RNA-sequencing and small RNA-sequencing data discussed in this publication are deposited and fully accessible, either in NCBI's Gene Expression Omnibus accessible through GEO Series accession number GSE179384 for small RNA-seq or at the European Nucleotide Archive at EMBL-EBI under accession number PRJEB46400 for the RiboMethSeq and PRJEB46399 for RNA-seq.

Supplementary Information

Supplementary Information is available at https://doi.org/10.26508/lsa.202201877

Acknowledgements

We thank the patients and their families for their participation in the study. We also thank Christelle Thibaut-Charpentier from the GenomEast sequencing platform in Strasbourg, a member of the "France Génomique" consortium (ANR-10-INBS-0009), the Institut de Génétique Médicale d'Alsace, for their technical support, and Myriam Bronner from Nancy University Hospital for the establishment of the LCL-MM line. We thank Johann Schor and Laura Guédon for their help with behavioural experiments. Human NPC work was carried out at ICM's CELIS core facility and NPC imaging at the ICM Quant facility. We thank Dr. Bernard Moss (NIAID/NIH) for providing *FTSJ1* KO HeLa cells. We thank the members of the TErBio laboratory for helpful discussions and reading of the article. C Carré received financial support from the CNRS, Sorbonne Université (Emergence 2021_RNA-Mod-Diag), the Fondation Maladies Rares (Genomics-2018 #11809 and Genomics-2020 #12824), the IBPS-2020 Action Incitative, the Ligue National contre le cancer Île de France (RS21/76-29), and ANR (ANR-21-CE12-0022-01 #BiopiC). Work in the BA Hassan laboratory was supported by the Investissements d'Avenir programme

(ANR-10-IAIHU-06), Paris Brain Institute-ICM core funding, the Roger De Spoelberch Foundation Prize, and a grant from the Neuro-Glia Foundation. Research in the laboratory of J-Y Roignant is supported by University of Lausanne and the Deutsche Forschungsgemeinschaft RO 4681/9-1, RO4681/12-1, and RO4681/13-1. DG Dimitrova and M Brazane have PhD fellowships from the Ministère de la Recherche et de l'Enseignement Supérieur at the doctoral school Complexité du Vivant (ED515). We also thank the Fondation ARC pour la Recherche sur le Cancer and the FRM (Fondation pour la Recherche Médicale) for funding support to DG Dimitrova, MT Angelova, and M Brazane (FDT202204014985), fourth-year PhD; "Réseau André Picard," the "Société Française de Génétique" (to M Brazane, MT Angelova, and DG Dimitrova); and COST action "EPITRAN" CA16120 (to Y Motorin, J-Y Roignant, V Marchand, DG Dimitrova, M Brazane, MT Angelova, and C Carré) for travelling and training fellowships.

Author Contributions

M Brazane: data curation, formal analysis, validation, investigation, visualization, methodology, and writing—original draft, review, and editing.
DG Dimitrova: data curation, formal analysis, validation, investigation, visualization, methodology, and writing—original draft, review, and editing.
J Pigeon: resources, formal analysis, validation, methodology, and writing—review and editing.
C Paolantoni: data curation, formal analysis, validation, investigation, and visualization.
T Ye: data curation, software, formal analysis, validation, visualization, methodology, and writing—review and editing.
V Marchand: data curation, software, validation, and methodology.
B Da Silva: data curation, validation, investigation, visualization, and methodology.
E Schaefer: resources and writing—review and editing.
MT Angelova: formal analysis, validation, investigation, methodology, and writing—review and editing.
Z Stark: resources and writing—review and editing.
M Delatycki: resources and writing—review and editing.
T Dudding-Byth: resources and writing—review and editing.
J Gecz: resources, formal analysis, validation, methodology, and writing—review and editing.
P-Y Plaçais: resources, formal analysis, validation, investigation, visualization, methodology, and writing—review and editing.
L Teysset: validation, investigation, methodology, and writing—review and editing.
T Préat: formal analysis, validation, investigation, visualization, methodology, and writing—review and editing.
A Piton: resources, data curation, formal analysis, methodology, and writing—review and editing.
BA Hassan: resources, methodology, and writing—review and editing.
J-Y Roignant: formal analysis, validation, investigation, visualization, methodology, and writing—original draft, review, and editing.
Y Motorin: data curation, software, formal analysis, validation, investigation, visualization, methodology, and writing—original draft, review, and editing.
C Carré: conceptualization, resources, data curation, software, formal analysis, supervision, funding acquisition, validation, investigation, visualization, methodology, project administration, and writing—original draft, review, and editing.

Conflict of Interest Statement

The authors declare that they have no conflict of interest.

References

Abe M, Naqvi A, Hendriks G-J, Feltzin V, Zhu Y, Grigoriev A, Bonini NM (2014) Impact of age-associated increase in 2′-O-methylation of miRNAs on aging and neurodegeneration in Drosophila. *Genes Dev* 28: 44–57. doi:10.1101/gad.226654.113

Angelova MT, Dimitrova DG, Dinges N, Lence T, Worpenberg L, Carré C, Roignant J-Y (2018) The emerging field of epitranscriptomics in neurodevelopmental and neuronal disorders. *Front Bioeng Biotechnol* 6: 46. doi:10.3389/fbioe.2018.00046

Angelova MT, Dimitrova DG, Da Silva B, Marchand V, Jacquier C, Achour C, Brazane M, Goyenvalle C, Bourguignon-Igel V, Shehzada S, et al (2020) tRNA 2′-O-methylation by a duo of TRM7/FTSJ1 proteins modulates small RNA silencing in Drosophila. *Nucleic Acids Res* 48: 2050–2072. doi:10.1093/nar/gkaa002

Anreiter I, Mir Q, Simpson JT, Janga SC, Soller M (2021) New twists in detecting mRNA modification dynamics. *Trends Biotechnol* 39: 72–89. doi:10.1016/j.tibtech.2020.06.002

Bartoli KM, Schaening C, Carlile TM, Gilbert WV (2018) Conserved methyltransferase Spb1 targets mRNAs for regulated modification with 2′-O-methyl ribose. *BioRxiv*. doi:10.1101/271916 (Preprint posted March 8, 2018).

Birkedal U, Christensen-Dalsgaard M, Krogh N, Sabarinathan R, Gorodkin J, Nielsen H (2015) Profiling of ribose methylations in RNA by high-throughput sequencing. *Angew Chem Int Ed Engl* 54: 451–455. doi:10.1002/anie.201408362

Boccaletto P, Machnicka MA, Purta E, Piatkowski P, Baginski B, Wirecki TK, de Crécy-Lagard V, Ross R, Limbach PA, Kotter A, et al (2018) MODOMICS: A database of RNA modification pathways. 2017 update. *Nucleic Acids Res* 46: D303–D307. doi:10.1093/nar/gkx1030

Bolger AM, Lohse M, Usadel B (2014) Trimmomatic: A flexible trimmer for Illumina sequence data. *Bioinformatics* 30: 2114–2120. doi:10.1093/bioinformatics/btu170

Braun K, Segal M (2000) FMRP involvement in formation of synapses among cultured hippocampal neurons. *Cereb Cortex* 10: 1045–1052. doi:10.1093/cercor/10.10.1045

Bryant A, Palma CA, Jayaswal V, Yang YW, Lutherborrow M, Ma DD (2012) miR-10a is aberrantly overexpressed in Nucleophosmin1 mutated acute myeloid leukaemia and its suppression induces cell death. *Mol Cancer* 11: 8. doi:10.1186/1476-4598-11-8

Bügl H, Fauman EB, Staker BL, Zheng F, Kushner SR, Saper MA, Bardwell JC, Jakob U (2000) RNA methylation under heat shock control. *Mol Cell* 6: 349–360. doi:10.1016/s1097-2765(00)00035-6

Cavaillé J (2017) Box C/D small nucleolar RNA genes and the Prader-Willi syndrome: A complex interplay. *Wiley Interdiscip Rev RNA* 8. doi:10.1002/wrna.1417

Chan PP, Lowe TM (2016) GtRNAdb 2.0: An expanded database of transfer RNA genes identified in complete and draft genomes. *Nucleic Acids Res* 44: D184–D189. doi:10.1093/nar/gkv1309

Chang L, Zhou G, Soufan O, Xia J (2020) miRNet 2.0: Network-based visual analytics for miRNA functional analysis and systems biology. *Nucleic Acids Res* 48: W244–W251. doi:10.1093/nar/gkaa467

Chapman BV, Wald AI, Akhtar P, Munko AC, Xu J, Gibson SP, Grandis JR, Ferris RL, Khan SA (2015) MicroRNA-363 targets myosin 1B to reduce cellular migration in head and neck cancer. *BMC Cancer* 15: 861. doi:10.1186/s12885-015-1888-3

Chen C-J, Servant N, Toedling J, Sarazin A, Marchais A, Duvernois-Berthet E, Cognat V, Colot V, Voinnet O, Heard E, et al (2012) ncPRO-seq: A tool for annotation and profiling of ncRNAs in sRNA-seq data. *Bioinformatics* 28: 3147–3149. doi:10.1093/bioinformatics/bts587

Chen J, Lambo ME, Ge X, Dearborn JT, Liu Y, McCullough KB, Swift RG, Tabachnick DR, Tian L, Noguchi K, et al (2021) A MYT1L syndrome mouse model recapitulates patient phenotypes and reveals altered brain development due to disrupted neuronal maturation. Neuron 109: 3775–3792.e14. doi:10.1016/j.neuron.2021.09.009

Colomb J, Kaiser L, Chabaud M-A, Preat T (2009) Parametric and genetic analysis of Drosophila appetitive long-term memory and sugar motivation. *Genes Brain Behav* 8: 407–415. doi:10.1111/j.1601-183x.2009.00482.x

Conti A, Romeo SG, Cama A, La Torre D, Barresi V, Pezzino G, Tomasello C, Cardali S, Angileri FF, Polito F, et al (2016) MiRNA expression profiling in human gliomas: Upregulated miR-363 increases cell survival and proliferation. *Tumor Biol* 37: 14035–14048. doi:10.1007/s13277-016-5273-x

Dai Q, Moshitch-Moshkovitz S, Han D, Kol N, Amariglio N, Rechavi G, Dominissini D, He C (2017) Nm-seq maps 2′-O-methylation sites in human mRNA with base precision. *Nat Methods* 14: 695–698. doi:10.1038/nmeth.4294

Darzacq X (2002) Cajal body-specific small nuclear RNAs: A novel class of 2′-O-methylation and pseudouridylation guide RNAs. *EMBO J* 21: 2746–2756. doi:10.1093/emboj/21.11.2746

Dimitrova DG, Teysset L, Carré C (2019) RNA 2′-O-methylation (Nm) modification in human diseases. *Genes* 10: 117. doi:10.3390/genes10020117

Ding H, Huang Z, Chen M, Wang C, Chen X, Chen J, Zhang J (2016) Identification of a panel of five serum miRNAs as a biomarker for Parkinson's disease. *Parkinsonism Relat Disord* 22: 68–73. doi:10.1016/j.parkreldis.2015.11.014

Dostie J, Mourelatos Z, Yang M, Sharma A, Dreyfuss G (2003) Numerous microRNPs in neuronal cells containing novel microRNAs. *RNA* 9: 180–186. doi:10.1261/rna.2141503

Durdevic Z, Mobin MB, Hanna K, Lyko F, Schaefer M (2013) The RNA methyltransferase Dnmt2 is required for efficient Dicer-2-dependent siRNA pathway activity in Drosophila. *Cell Rep* 4: 931–937. doi:10.1016/j.celrep.2013.07.046

El Hassouni B, Sarkisjan D, Vos JC, Giovannetti E, Peters GJ (2019) Targeting the ribosome biogenesis key molecule fibrillarin to avoid chemoresistance. *Curr Med Chem* 26: 6020–6032. doi:10.2174/0929867326666181203133332

Erales J, Marchand V, Panthu B, Gillot S, Belin S, Ghayad SE, Garcia M, Laforêts F, Marcel V, Baudin-Baillieu A, et al (2017) Evidence for rRNA 2′-O-methylation plasticity: Control of intrinsic translational capabilities of human ribosomes. *Proc Natl Acad Sci U S A* 114: 12934–12939. doi:10.1073/pnas.1707674114

Feder M, Pas J, Wyrwicz LS, Bujnicki JM (2003) Molecular phylogenetics of the RrmJ/fibrillarin superfamily of ribose 2′-O-methyltransferases. *Gene* 302: 129–138. doi:10.1016/s0378-1119(02)01097-1

Fornari F, Gramantieri L, Ferracin M, Veronese A, Sabbioni S, Calin GA, Grazi GL, Giovannini C, Croce CM, Bolondi L, et al (2008) MiR-221 controls CDKN1C/p57 and CDKN1B/p27 expression in human hepatocellular carcinoma. *Oncogene* 27: 5651–5661. doi:10.1038/onc.2008.178

Freude K, Hoffmann K, Jensen L-R, Delatycki MB, des Portes V, Moser B, Hamel B, van Bokhoven H, Moraine C, Fryns J-P, et al (2004) Mutations in the FTSJ1 gene coding for a novel S-Adenosylmethionine–binding protein cause nonsyndromic X-linked mental retardation. *Am J Hum Genet* 75: 305–309. doi:10.1086/422507

Froyen G, Bauters M, Boyle J, Van Esch H, Govaerts K, van Bokhoven H, Ropers H-H, Moraine C, Chelly J, Fryns J-P, et al (2007) Loss of SLC38A5 and FTSJ1 at Xp11.23 in three brothers with non-syndromic mental retardation due to a microdeletion in an unstable genomic region. *Hum Genet* 121: 539–547. doi:10.1007/s00439-007-0343-1

Gillies JK, Lorimer IAJ (2007) Regulation of p27Kip1 by miRNA 221/222 in glioblastoma. *Cell Cycle* 6: 2005–2009. doi:10.4161/cc.6.16.4526

Glasser AL, el Adlouni C, Keith G, Sochacka E, Malkiewicz A, Santos M, Tuite MF, Desgrès J (1992) Presence and coding properties of 2′-O-methyl-5-carbamoylmethyluridine (ncm5Um) in the wobble position of the anticodon of tRNA(Leu) (U*AA) from brewer's yeast. *FEBS Lett* 314: 381–385. doi:10.1016/0014-5793(92)81510-s

Goodarzi H, Liu X, Nguyen HCB, Zhang S, Fish L, Tavazoie SF (2015) Endogenous tRNA-derived fragments suppress breast cancer progression via YBX1 displacement. *Cell* 161: 790–802. doi:10.1016/j.cell.2015.02.053

Gui Y, Liu H, Zhang L, Lv W, Hu X (2015) Altered microRNA profiles in cerebrospinal fluid exosome in Parkinson disease and Alzheimer disease. *Oncotarget* 6: 37043–37053. doi:10.18632/oncotarget.6158

Guy MP, Phizicky EM (2015) Conservation of an intricate circuit for crucial modifications of the tRNAPhe anticodon loop in eukaryotes. *RNA* 21: 61–74. doi:10.1261/rna.047639.114

Guy MP, Podyma BM, Preston MA, Shaheen HH, Krivos KL, Limbach PA, Hopper AK, Phizicky EM (2012) Yeast Trm7 interacts with distinct proteins for critical modifications of the tRNAPhe anticodon loop. *RNA* 18: 1921–1933. doi:10.1261/rna.035287.112

Guy MP, Shaw M, Weiner CL, Hobson L, Stark Z, Rose K, Kalscheuer VM, Gecz J, Phizicky EM (2015) Defects in tRNA anticodon loop 2′-O-methylation are implicated in nonsyndromic X-linked intellectual disability due to mutations in FTSJ1. *Hum Mutat* 36: 1176–1187. doi:10.1002/humu.22897

Han L, Guy MP, Kon Y, Phizicky EM (2018) Lack of 2′-O-methylation in the tRNA anticodon loop of two phylogenetically distant yeast species activates the general amino acid control pathway. *PLoS Genet* 14: e1007288. doi:10.1371/journal.pgen.1007288

Haussmann IU, Wu Y, Nallasivan MP, Archer N, Bodi Z, Hebenstreit D, Waddell S, Fray R, Soller M (2022) CMTr cap-adjacent 2′-O-ribose mRNA methyltransferases are required for reward learning and mRNA localization to synapses. *Nat Commun* 13: 1209. doi:10.1038/s41467-022-28549-5

He S, He ZX, Zeng S, Zhou ZW, Zhou SF (2015) Hsa-microRNA-181a is a regulator of a number of cancer genes and a biomarker for endometrial carcinoma in patients: A bioinformatic and clinical study and the therapeutic implication. *Drug Des Dev Ther* 9: 1103–1175. doi:10.2147/dddt.s73551

He Q, Yang L, Gao K, Ding P, Chen Q, Xiong J, Yang W, Song Y, Wang L, Wang Y, et al (2020) FTSJ1 regulates tRNA 2′-O-methyladenosine modification and suppresses the malignancy of NSCLC via inhibiting DRAM1 expression. *Cell Death Dis* 11: 348. doi:10.1038/s41419-020-2525-x

Holzer K, Ori A, Cooke A, Dauch D, Drucker E, Riemenschneider P, Andres-Pons A, DiGuilio AL, Mackmull M-T, Baßler J, et al (2019) Nucleoporin Nup155 is part of the p53 network in liver cancer. *Nat Commun* 10: 2147. doi:10.1038/s41467-019-10133-z

Horwich MD, Li C, Matranga C, Vagin V, Farley G, Wang P, Zamore PD (2007) The Drosophila RNA methyltransferase, DmHen1, modifies germline piRNAs and single-stranded siRNAs in RISC. *Curr Biol* 17: 1265–1272. doi:10.1016/j.cub.2007.06.030

Hu F, Min J, Cao X, Liu L, Ge Z, Hu J, Li X (2016) MiR-363-3p inhibits the epithelial-to-mesenchymal transition and suppresses metastasis in colorectal cancer by targeting Sox4. *Biochem Biophys Res Commun* 474: 35–42. doi:10.1016/j.bbrc.2016.04.055

Ilyas M, Mir A, Efthymiou S, Houlden H (2020) The genetics of intellectual disability: Advancing technology and gene editing. *F1000Research* 9: 22. doi:10.12688/f1000research.16315.1

Irwin SA, Galvez R, Greenough WT (2000) Dendritic spine structural anomalies in fragile-X mental retardation syndrome. *Cereb Cortex* 10: 1038–1044. doi:10.1093/cercor/10.10.1038

Jensen LR, Garrett L, Hölter SM, Rathkolb B, Rácz I, Adler T, Prehn C, Hans W, Rozman J, Becker L, et al (2019) A mouse model for intellectual disability caused by mutations in the X-linked 2′-O-methyltransferase Ftsj1 gene. *Biochim Biophys Acta* 1865: 2083–2093. doi:10.1016/j.bbadis.2018.12.011

Jia Y, Mu JC, Ackerman SL (2012) Mutation of a U2 snRNA gene causes global disruption of alternative splicing and neurodegeneration. *Cell* 148: 296–308. doi:10.1016/j.cell.2011.11.057

Jiang C, Cao Y, Lei T, Wang Y, Fu J, Wang Z, Lv Z (2018) microRNA-363-3p inhibits cell growth and invasion of non-small cell lung cancer by targeting HMGA2. *Mol Med Rep* 17: 2712–2718. doi:10.3892/mmr.2017.8131

Jühling F, Mörl M, Hartmann RK, Sprinzl M, Stadler PF, Pütz J (2009) tRNAdb 2009: Compilation of tRNA sequences and tRNA genes. *Nucleic Acids Res* 37: D159–D162. doi:10.1093/nar/gkn772

Kan AA, van Erp S, Derijck AAHA, de Wit M, Hessel EVS, O'Duibhir E, de Jager W, Van Rijen PC, Gosselaar PH, de Graan PNE, et al (2012) Genome-wide microRNA profiling of human temporal lobe epilepsy identifies modulators of the immune response. *Cell Mol Life Sci* 69: 3127–3145. doi:10.1007/s00018-012-0992-7

Karatas OF, Suer I, Yuceturk B, Yilmaz M, Oz B, Guven G, Cansiz H, Creighton CJ, Ittmann M, Ozen M (2016) Identification of microRNA profile specific to cancer stem-like cells directly isolated from human larynx cancer specimens. *BMC Cancer* 16: 853. doi:10.1186/s12885-016-2863-3

Kawai G, Yamamoto Y, Kamimura T, Masegi T, Sekine M, Hata T, Iimori T, Watanabe T, Miyazawa T, Yokoyama S (1992) Conformational rigidity of specific pyrimidine residues in tRNA arises from posttranscriptional modifications that enhance steric interaction between the base and the 2′-hydroxyl group. *Biochemistry* 31: 1040–1046. doi:10.1021/bi00119a012

Kawarada L, Suzuki T, Ohira T, Hirata S, Miyauchi K, Suzuki T (2017) ALKBH1 is an RNA dioxygenase responsible for cytoplasmic and mitochondrial tRNA modifications. *Nucleic Acids Res* 45: 7401–7415. doi:10.1093/nar/gkx354

Khalil A, Medfai H, Poelvoorde P, Kazan MF, Delporte C, Van Antwerpen P, EL-Makhour Y, Biston P, Delrée P, Badran B, et al (2018) Myeloperoxidase promotes tube formation, triggers ERK1/2 and Akt pathways and is expressed endogenously in endothelial cells. *Arch Biochem Biophys* 654: 55–69. doi:10.1016/j.abb.2018.07.011

Khuu C, Sehic A, Eide L, Osmundsen H (2016) Anti-proliferative properties of miR-20b and miR-363 from the miR-106a-363 cluster on human carcinoma cells. *Microrna* 5: 19–35. doi:10.2174/2211536605666160322151813

Kiyosawa N, Watanabe K, Toyama K, Ishizuka H (2019) Circulating miRNA signature as a potential biomarker for the prediction of analgesic efficacy of hydromorphone. *Int J Mol Sci* 20: 1665. doi:10.3390/ijms20071665

Kretschmann A, Danis B, Andonovic L, Abnaof K, van Rikxoort M, Siegel F, Mazzuferi M, Godard P, Hanon E, Fröhlich H, et al (2015) Different microRNA profiles in chronic epilepsy versus acute seizure mouse models. *J Mol Neurosci* 55: 466–479. doi:10.1007/s12031-014-0368-6

Kurth HM, Mochizuki K (2009) 2′-O-methylation stabilizes Piwi-associated small RNAs and ensures DNA elimination in Tetrahymena. *RNA* 15: 675–685. doi:10.1261/rna.1455509

Lacoux C, Di Marino D, Pilo Boyl P, Zalfa F, Yan B, Ciotti MT, Falconi M, Urlaub H, Achsel T, Mougin A, et al (2012) BC1-FMRP interaction is modulated by 2′-O-methylation: RNA-binding activity of the tudor domain and translational regulation at synapses. *Nucleic Acids Res* 40: 4086–4096. doi:10.1093/nar/gkr1254

Langmead B, Salzberg SL (2012) Fast gapped-read alignment with Bowtie 2. *Nat Methods* 9: 357–359. doi:10.1038/nmeth.1923

Langmead B, Trapnell C, Pop M, Salzberg SL (2009) Ultrafast and memory-efficient alignment of short DNA sequences to the human genome. *Genome Biol* 10: R25. doi:10.1186/gb-2009-10-3-r25

Lau P, Bossers K, Janky R, Salta E, Frigerio CS, Barbash S, Rothman R, Sierksma ASR, Thathiah A, Greenberg D, et al (2013) Alteration of the microRNA network during the progression of Alzheimer's disease. *EMBO Mol Med* 5: 1613–1634. doi:10.1002/emmm.201201974

Lee Y-L, Kung F-C, Lin C-H, Huang Y-S (2020) CMTR1-Catalyzed 2′-O-ribose methylation controls neuronal development by regulating Camk2α expression independent of RIG-I signaling. *Cell Rep* 33: 108269. doi:10.1016/j.celrep.2020.108269

Levenga J, Willemsen R (2012) Perturbation of dendritic protrusions in intellectual disability. *Prog Brain Res* 197: 153–168. doi:10.1016/B978-0-444-54299-1.00008-X

Li J, Yang Z, Yu B, Liu J, Chen X (2005) Methylation protects miRNAs and siRNAs from a 3′-end uridylation activity in arabidopsis. *Curr Biol* 15: 1501–1507. doi:10.1016/j.cub.2005.07.029

Li Y, Kuscu C, Banach A, Zhang Q, Pulkoski-Gross A, Kim D, Liu J, Roth E, Li E, Shroyer KR, et al (2015) miR-181a-5p inhibits cancer cell migration and angiogenesis via downregulation of Matrix metalloproteinase-14. *Cancer Res* 75: 2674–2685. doi:10.1158/0008-5472.can-14-2875

Li J, Wang Y-N, Xu B-S, Liu Y-P, Zhou M, Long T, Li H, Dong H, Nie Y, Chen PR, et al (2020) Intellectual disability-associated gene ftsj1 is responsible for 2′-O-methylation of specific tRNAs. *EMBO Rep* 21: e50095. doi:10.15252/embr.202050095

Liu B, Li J, Zheng M, Ge J, Li J, Yu P (2017) MiR-542-3p exerts tumor suppressive functions in non-small cell lung cancer cells by upregulating FTSJ2. *Life Sci* 188: 87–95. doi:10.1016/j.lfs.2017.08.018

Love MI, Huber W, Anders S (2014) Moderated estimation of fold change and dispersion for RNA-seq data with DESeq. *Genome Biol* 15: 550. doi:10.1186/s13059-014-0550-8

Lund AH (2010) miR-10 in development and cancer. *Cell Death Differ* 17: 209–214. doi:10.1038/cdd.2009.58

Ma W, Li Y, Wang C, Xu F, Wang M, Liu Y (2016) Serum miR-221 serves as a biomarker for Parkinson's disease. *Cell Biochem Funct* 34: 511–515. doi:10.1002/cbf.3224

Marcel V, Kielbassa J, Marchand V, Natchiar KS, Paraqindes H, Nguyen Van Long F, Ayadi L, Bourguignon-Igel V, Lo Monaco P, Monchiet D, et al (2020) Ribosomal RNA 2-O-methylation as a novel layer of inter-tumour heterogeneity in breast cancer. *NAR Cancer* 2: zcaa036. doi:10.1093/narcan/zcaa036

Marchand V, Blanloeil-Oillo F, Helm M, Motorin Y (2016) Illumina-based RiboMethSeq approach for mapping of 2′-O-Me residues in RNA. *Nucleic Acids Res* 44: e135. doi:10.1093/nar/gkw547

Marchand V, Pichot F, Thüring K, Ayadi L, Freund I, Dalpke A, Helm M, Motorin Y (2017) Next-generation sequencing-based RiboMethSeq protocol for analysis of tRNA 2′-O-methylation. *Biomolecules* 7: 13. doi:10.3390/biom7010013

Marchand V, Bourguignon-Igel V, Helm M, Motorin Y (2022) Analysis of pseudouridines and other RNA modifications using HydraPsiSeq protocol. *Methods* 203: 383–391. doi:10.1016/j.ymeth.2021.08.008

Matsui A, Tran M, Yoshida AC, Kikuchi SS, U M, Ogawa M, Shimogori T (2013) BTBD3 controls dendrite orientation toward active axons in mammalian neocortex. *Science* 342: 1114–1118. doi:10.1126/science.1244505

Nagayoshi Y, Chujo T, Hirata S, Nakatsuka H, Chen C-W, Takakura M, Miyauchi K, Ikeuchi Y, Carlyle BC, Kitchen RR, et al (2021) Loss of Ftsj1 perturbs codon-specific translation efficiency in the brain and is associated with X-linked intellectual disability. *Sci Adv* 7: eabf3072. doi:10.1126/sciadv.abf3072

Noma A, Kirino Y, Ikeuchi Y, Suzuki T (2006) Biosynthesis of wybutosine, a hyper-modified nucleoside in eukaryotic phenylalanine tRNA. *EMBO J* 25: 2142–2154. doi:10.1038/sj.emboj.7601105

Palma M, Lejeune F (2021) Deciphering the molecular mechanism of stop codon readthrough. *Biol Rev* 96: 310–329. doi:10.1111/brv.12657

Pichot F, Marchand V, Ayadi L, Bourguignon-Igel V, Helm M, Motorin Y (2020) Holistic optimization of bioinformatic analysis pipeline for detection and quantification of 2′-O-methylations in RNA by RiboMethSeq. *Front Genet* 11: 38. doi:10.3389/fgene.2020.00038

Pichot F, Marchand V, Helm M, Motorin Y (2021) Non-redundant tRNA reference sequences for deep sequencing analysis of tRNA abundance and epitranscriptomic RNA modifications. *Genes* 12: 81. doi:10.3390/genes12010081

Pintard L, Lecointe F, Bujnicki JM, Bonnerot C, Grosjean H, Lapeyre B (2002) Trm7p catalyses the formation of two 2′-O-methylriboses in yeast tRNA anticodon loop. *EMBO J* 21: 1811–1820. doi:10.1093/emboj/21.7.1811

Qiao J, Lee S, Paul P, Theiss L, Tiao J, Qiao L, Kong A, Chung DH (2013) miR-335 and miR-363 regulation of neuroblastoma tumorigenesis and metastasis. *Surgery* 154: 226–233. doi:10.1016/j.surg.2013.04.005

Quinlan AR (2014) BEDTools: The Swiss-army tool for genome feature analysis. *Curr Protoc Bioinformatics* 47: 11.12.1–11.12.34. doi:10.1002/0471250953.bi1112s47

Ramser J, Winnepenninckx B, Lenski C, Errijgers V, Platzer M, Schwartz CE, Meindl A, Kooy RF (2004) A splice site mutation in the methyltransferase gene FTSJ1 in Xp11.23 is associated with non-syndromic mental retardation in a large Belgian family (MRX9). *J Med Genet* 41: 679–683. doi:10.1136/jmg.2004.019000

Risbud RM, Porter BE (2013) Changes in microRNA expression in the whole hippocampus and hippocampal synaptoneurosome fraction following pilocarpine induced status epilepticus. *PLoS One* 8: e53464. doi:10.1371/journal.pone.0053464

Roser AE, Caldi Gomes L, Schünemann J, Maass F, Lingor P (2018) Circulating miRNAs as diagnostic biomarkers for Parkinson's disease. *Front Neurosci* 12: 625. doi:10.3389/fnins.2018.00625

Saito K, Sakaguchi Y, Suzuki T, Suzuki T, Siomi H, Siomi MC (2007) Pimet, the Drosophila homolog of HEN1, mediates 2′-O-methylation of Piwi-interacting RNAs at their 3′ ends. *Genes Dev* 21: 1603–1608. doi:10.1101/gad.1563607

Saletore Y, Meyer K, Korlach J, Vilfan ID, Jaffrey S, Mason CE (2012) The birth of the epitranscriptome: Deciphering the function of RNA modifications. *Genome Biol* 13: 175. doi:10.1186/gb-2012-13-10-175

Shi L, Cheng Z, Zhang J, Li R, Zhao P, Fu Z, You Y (2008) hsa-mir-181a and hsa-mir-181b function as tumor suppressors in human glioma cells. *Brain Res* 1236: 185–193. doi:10.1016/j.brainres.2008.07.085

Su Y, Yuan J, Zhang F, Lei Q, Zhang T, Li K, Guo J, Hong Y, Bu G, Lv X, et al (2019) MicroRNA-181a-5p and microRNA-181a-3p cooperatively restrict vascular inflammation and atherosclerosis. *Cell Death Dis* 10: 365. doi:10.1038/s41419-019-1599-9

Tai IT, Tang MJ (2008) SPARC in cancer biology: Its role in cancer progression and potential for therapy. *Drug Resist Updates* 11: 231–246. doi:10.1016/j.drup.2008.08.005

Tarpey PS, Lucy Raymond F, Nguyen LS, Rodriguez J, Hackett A, Vandeleur L, Smith R, Shoubridge C, Edkins S, Stevens C, et al (2007) Mutations in UPF3B, a member of the nonsense-mediated mRNA decay complex, cause syndromic and nonsyndromic mental retardation. *Nat Genet* 39: 1127–1133. doi:10.1038/ng2100

Tehler D, Høyland-Kroghsbo NM, Lund AH (2011) The miR-10 microRNA precursor family. *RNA Biol* 8: 728–734. doi:10.4161/rna.8.5.16324

Thompson SL, Welch AC, Ho EV, Bessa JM, Portugal-Nunes C, Morais M, Young JW, Knowles JA, Dulawa SC (2019) Btbd3 expression regulates compulsive-like and exploratory behaviors in mice. *Transl Psychiatry* 9: 222. doi:10.1038/s41398-019-0558-7

Trzaska C, Amand S, Bailly C, Leroy C, Marchand V, Duvernois-Berthet E, Saliou J-M, Benhabiles H, Werkmeister E, Chassat T, et al (2020) 2,6-Diaminopurine as a highly potent corrector of UGA nonsense mutations. *Nat Commun* 11: 1509. doi:10.1038/s41467-020-15140-z

van der Werf IM, Van Dijck A, Reyniers E, Helsmoortel C, Kumar AA, Kalscheuer VM, de Brouwer AP, Kleefstra T, van Bokhoven H, Mortier G, et al (2017) Mutations in two large pedigrees highlight the role of ZNF711 in X-linked intellectual disability. *Gene* 605: 92–98. doi:10.1016/j.gene.2016.12.013

Vitali P, Kiss T (2019) Cooperative 2′-O-methylation of the wobble cytidine of human elongator tRNAMet(CAT) by a nucleolar and a Cajal body-specific box C/D RNP. *Genes Dev* 33: 741–746. doi:10.1101/gad.326363.119

Wang S-H, Zhang W-J, Wu X-C, Weng M-Z, Zhang M-D, Cai Q, Zhou D, Wang J-D, Quan Z-W (2016) The lncRNA MALAT1 functions as a competing endogenous RNA to regulate MCL-1 expression by sponging miR-363-3p in gallbladder cancer. *J Cell Mol Med* 20: 2299–2308. doi:10.1111/jcmm.12920

Wang H, Lin S-Y, Hu F-F, Guo A-Y, Hu H (2020) The expression and regulation of HOX genes and membrane proteins among different cytogenetic groups of acute myeloid leukemia. *Mol Genet Genomic Med* 8: e1365. doi:10.1002/mgg3.1365

Watahiki A, Wang Y, Morris J, Dennis K, O'Dwyer HM, Gleave M, Gout PW, Wang Y (2011) MicroRNAs associated with metastatic prostate cancer. *PLoS One* 6: e24950. doi:10.1371/journal.pone.0024950

Yang C, Tabatabaei SN, Ruan X, Hardy P (2017) The dual regulatory role of MiR-181a in breast cancer. *Cell Physiol Biochem* 44: 843–856. doi:10.1159/000485351

Ye J, Zhang W, Liu S, Liu Y, Liu K (2017) miR-363 inhibits the growth, migration and invasion of hepatocellular carcinoma cells by regulating E2F3. *Oncol Rep* 38: 3677–3684. doi:10.3892/or.2017.6018

Yu B, Yang Z, Li J, Minakhina S, Yang M, Padgett RW, Steward R, Chen X (2005) Methylation as a crucial step in plant microRNA biogenesis. *Science* 307: 932–935. doi:10.1126/science.1107130

Zhang C-Z, Zhang J-X, Zhang A-L, Shi Z-D, Han L, Jia Z-F, Yang W-D, Wang G-X, Jiang T, You Y-P, et al (2010) MiR-221 and miR-222 target PUMA to induce cell survival in glioblastoma. *Mol Cancer* 9: 229. doi:10.1186/1476-4598-9-229

Zhang P-F, Sheng L-L, Wang G, Tian M, Zhu L-Y, Zhang R, Zhang J, Zhu J-S (2016) miR-363 promotes proliferation and chemo-resistance of human gastric cancer via targeting of FBW7 ubiquitin ligase expression. *Oncotarget* 7: 35284–35292. doi:10.18632/oncotarget.9169

Zhang S-F, Chen J-C, Zhang J, Xu J-G (2017) miR-181a involves in the hippocampus-dependent memory formation via targeting PRKAA1. *Sci Rep* 7: 8480. doi:10.1038/s41598-017-09095-3

Zhao L-Y, Song J, Liu Y, Song C-X, Yi C (2020) Mapping the epigenetic modifications of DNA and RNA. *Protein Cell* 11: 792–808. doi:10.1007/s13238-020-00733-7

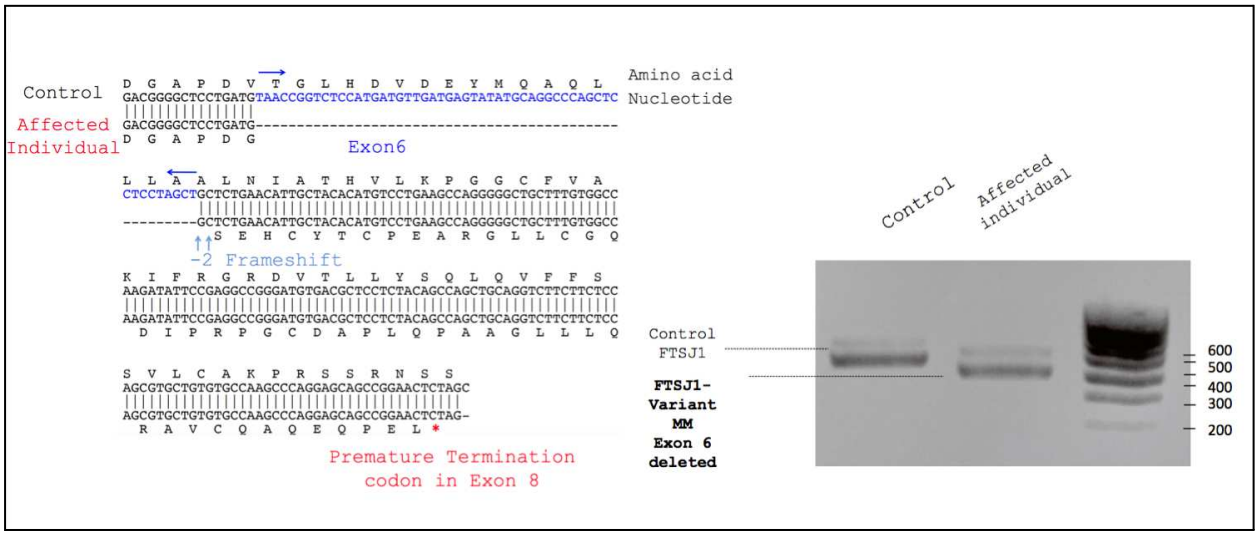

Figure S1A: Characterization of the FTSJ1 transcript variant MM.

FTSJ1 transcripts were amplified from total RNA by RT–PCR of a control (LCL25) and the affected individual LCL MM harbouring a splice site mutation predicted to cause the skipping of exon 6 (see the Materials and Methods section). PCR products were run in 1% agarose gel + 0.5X TAE buffer. Predictably, a size shift is observed between the amplified products in the control as compared to the MM variant (right panel). Sanger sequencing confirmed skipping of the entire exon 6, thus disrupting the reading frame and appearance of a premature termination codon in exon 8 (left panel, see detail in the Materials and Methods section).

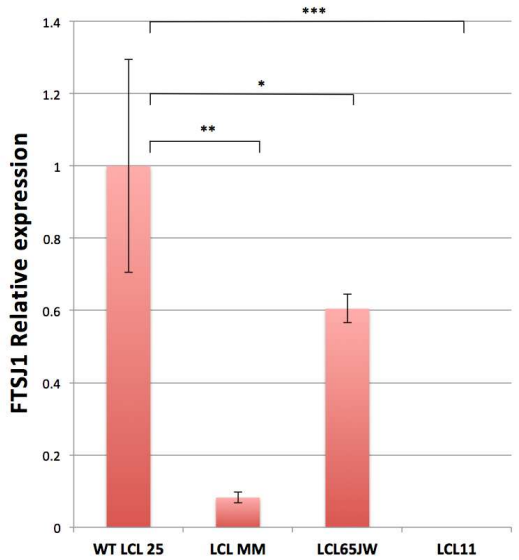

Figure S1B. FTSJ1 mRNA relative abundance in patient LCLs.

FTSJ1 mRNA is significantly reduced in LCL MM compared with a control LCL. Relative abundance of mRNA is quantified by qRT–PCR on total RNAs from each indicated cell line. Ratios are expressed in fold change of starting quantities of FTSJ1/GAPDH. Error bars represent the SD between four independent biological samples. P-values are indicated with stars, *P = 0.04; **P = 0.006; and ***P = 0.0008 (paired t test).

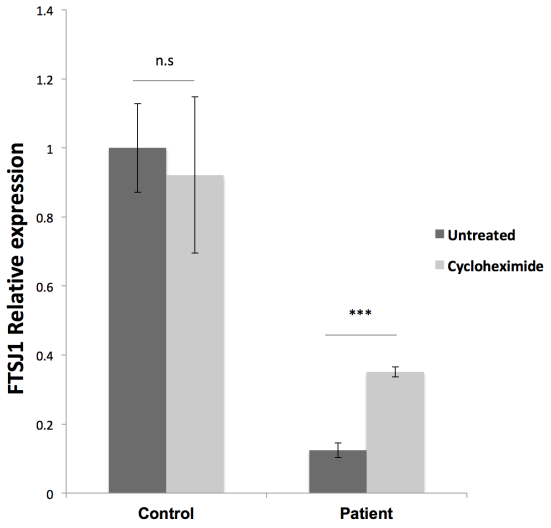

Figure S1C. FTSJ1 mRNA targeted for degradation by Nonsense-mediated mRNA Decay (NMD) in LCL-MM.

FTSJ1 mRNA is significantly down-regulated in affected patient cells (LCL-MM) when compared to control cells (LCL-25) ((B) above). Inhibition of translation by treatment of LCLs with 100 µg ml–1 cycloheximide rescued FTSJ1 mRNA from NMD, resulting in a threefold increase as analysed by qRT–PCR. Starting quantity values were normalized against GAPDH and expressed in fold change. ***P = 0.0008 (Mann–Whitney test). Error bars indicate s.d. N = 6.

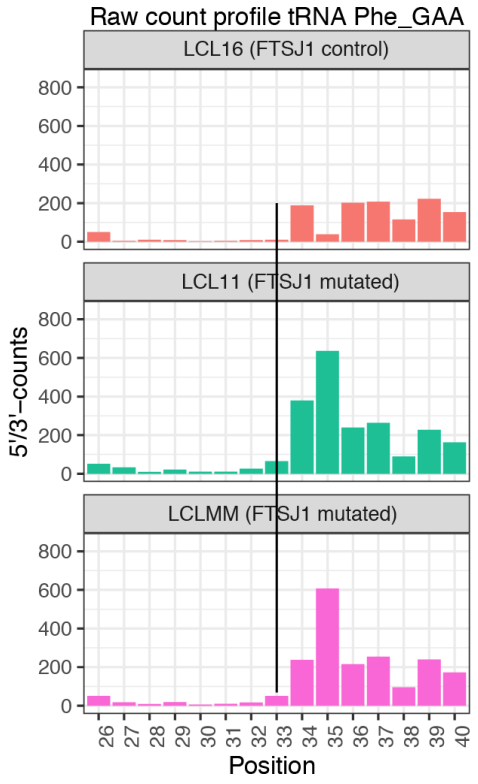

Figure S1D. FTSJ1 targets human tRNA$^{Phe(GAA)}$ at position 32.

Related to Fig 1B. RiboMethSeq analysis of tRNAPhe(GAA) modification at positions Cm32 and Gm34 alkaline fragmentation–based RiboMethSeq was performed on total RNAs extracted from indicated LCL hemizygous mutants for FTSJ1 (LCL11 and LCLMM) and control FTSJ1 (non-mutated: LCL16) as indicated. For better visualization, raw read counts are presented in a non-normalized fashion (5′/3′-counts, raw count profile). The positions of interest (Cm32) in tRNAPhe(GAA) are indicated by a black line crossing the three graphs.

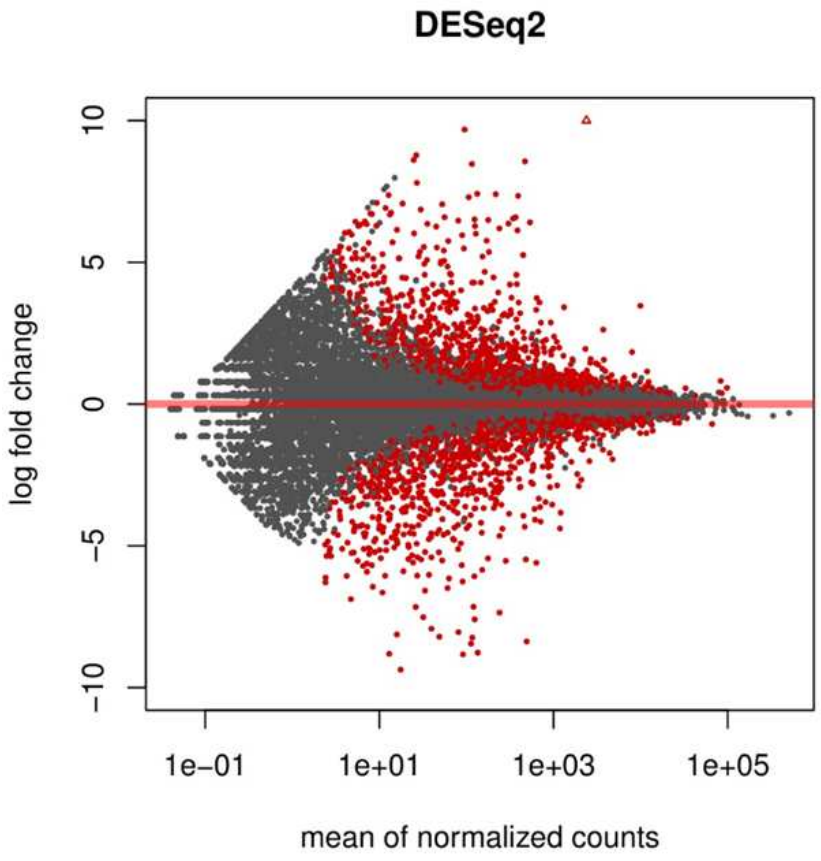

Figure S2A. FTSJ1 loss of function leads to mRNA deregulation in XLID affected individuals' LCLs.

MA plot on data from sequencing of mRNAs showing multiple deregulated mRNAs.

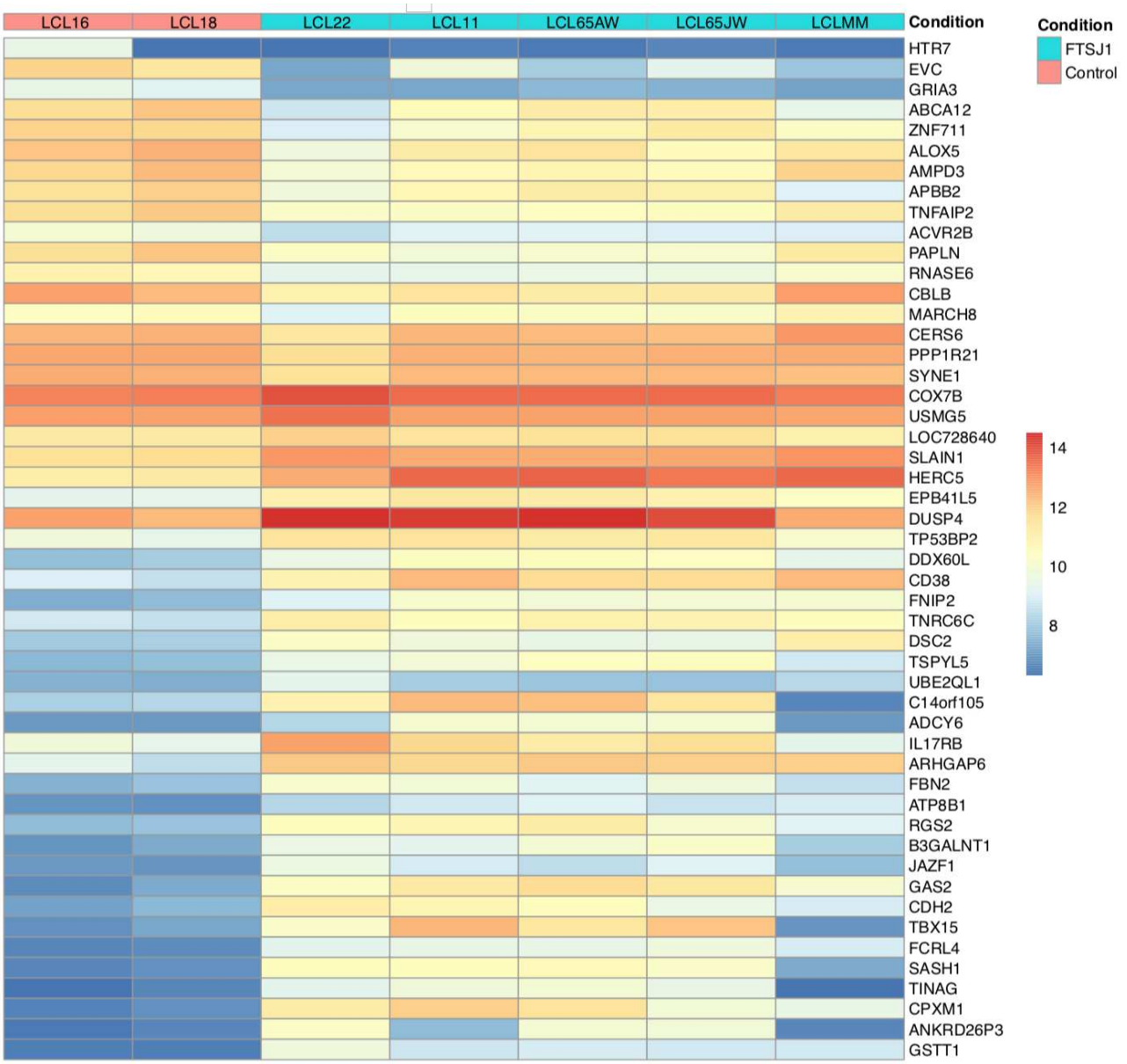

Figure S2B. FTSJ1 loss of function leads to mRNA deregulation in XLID affected individuals' LCLs

Heat map showing the top 50 deregulated mRNAs in P-values, and sorted fold change from most down-regulated to most up-regulated is represented in FTSJ1 loss of function LCLs compared with controls LCLs. Condition points to the FTSJ1 LCL status, WT (control) or mutated for the FTSJ1 gene (FTSJ1). The data come from normalized and variance-stabilizing transformed read counts using the DESeq2 package in R. Names of the LCLs are indicated in Condition lane.

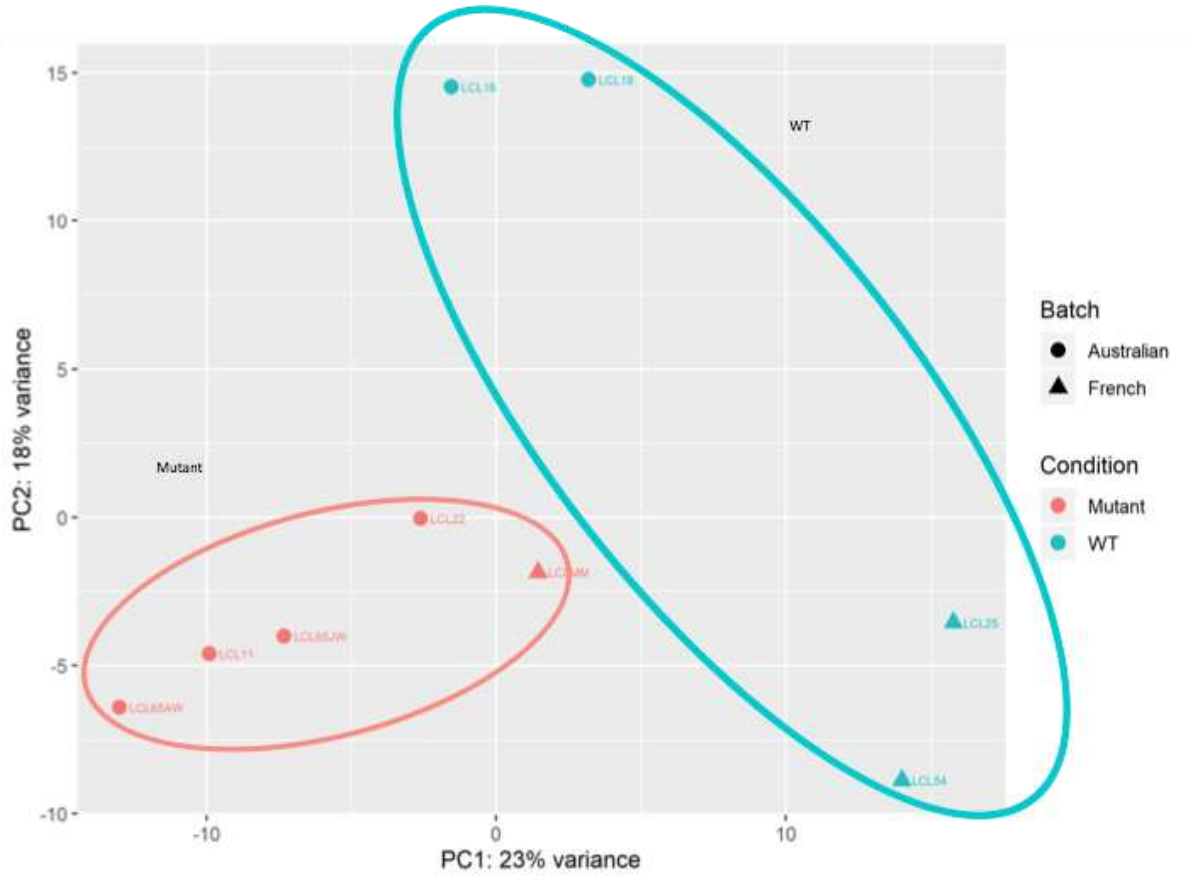

Figure S3A. FTSJ1 loss of function leads to miRNA deregulation in XLID affected individuals' cells

The principal component analysis plot shows a well-defined cluster of all LCL lines lacking FTSJ1 function that is separated from the more dispersed cluster of control lines (LCL WT for FTSJ1: WT; LCL mutant for FTSJ1: mutant).

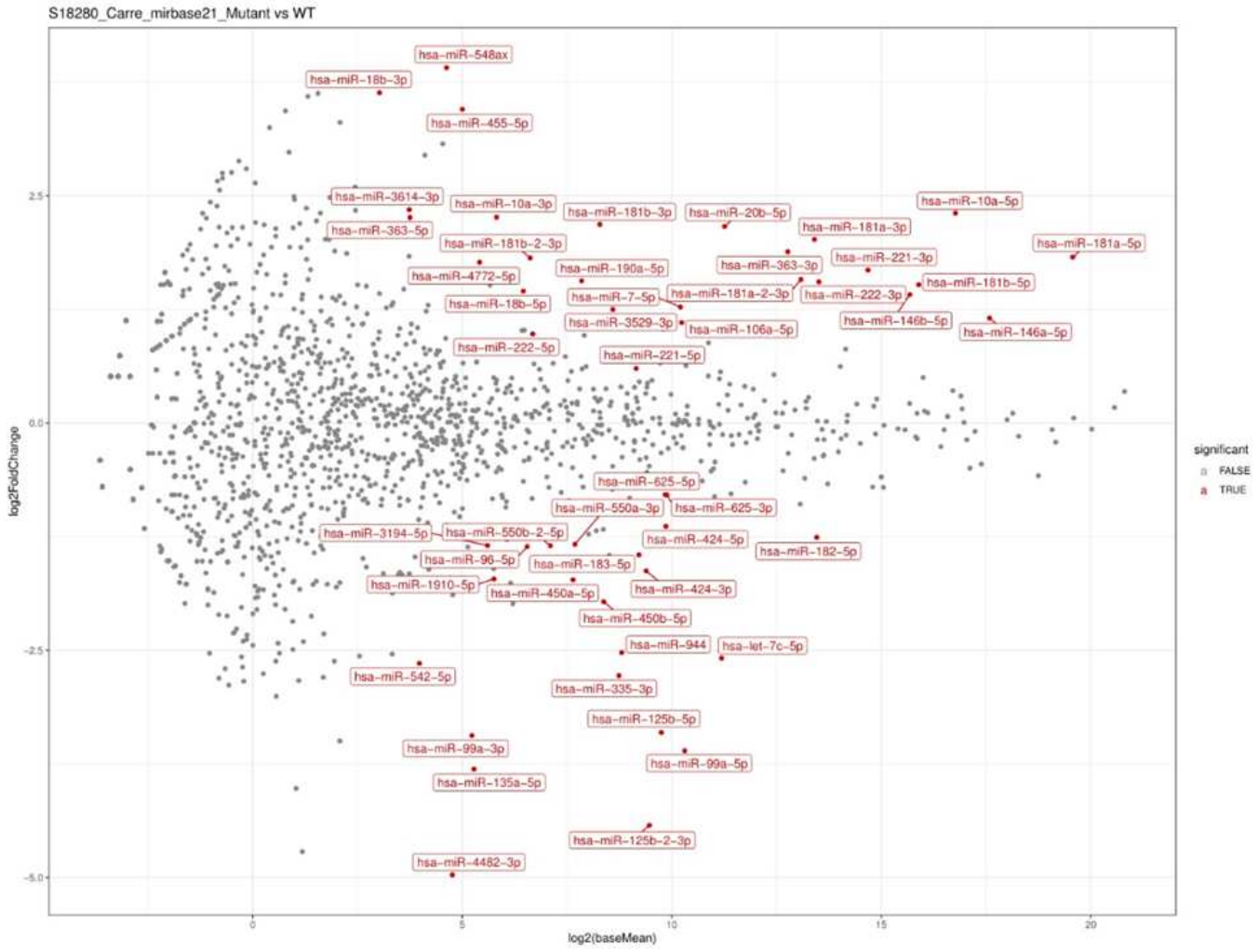

Figure S3B. FTSJ1 loss of function leads to miRNA deregulation in XLID affected individuals' LCLs

MA plot on data from sequencing of miRNAs showing multiple deregulated miRNAs (LCL WT for FTSJ1: WT; LCL mutant for FTSJ1: mutant).

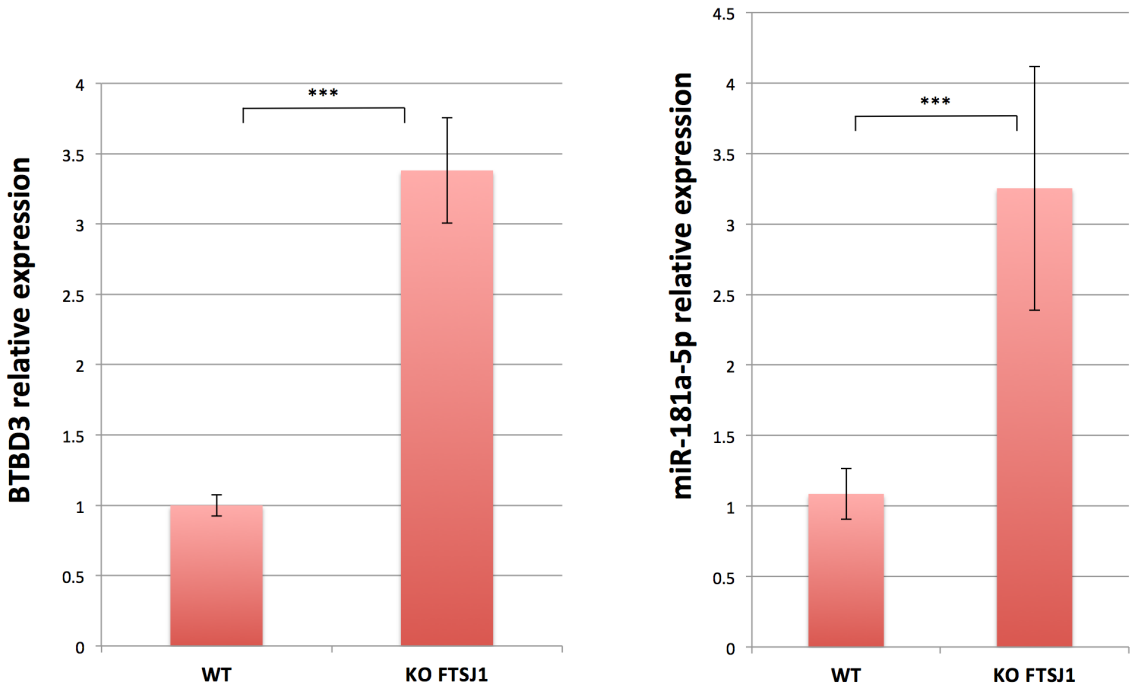

Figure S4A. *BTBD3* and *miR-181a-5p* are expressed in HeLa cells similarly to LCLs.

qRT–PCR analysis confirms expression of BTBD3 (left panel) and hsa-miR-181a-5p (right panel) in WT and FTSJ1 KO HeLa cells. Similar to what is observed in patient cells, both BTBD3 and hsa-miR-181a-5p are up-regulated in FTSJ1 KO cells. BTBD3 levels were normalized to GAPDH steady-state levels, and miR-181-a-5p levels were normalized to the small spike-in RNA UniSp6. Error bars represent the SD between three and six independent biological samples, respectively. BTBD3, ***P = 4.17 × 10−4; miR-181a-5p, ***P = 1.31 × 10−4 (paired t test).

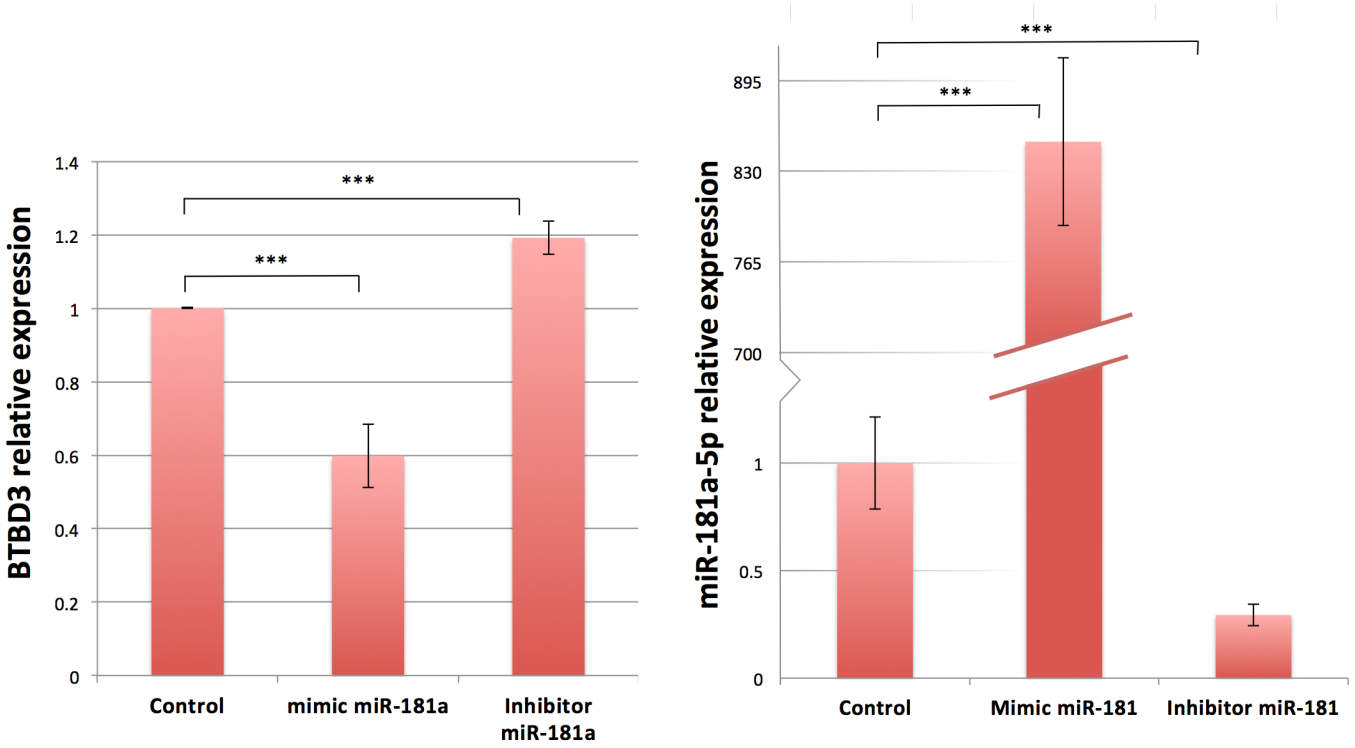

Figure S4B. *miR-181a-5p* targets *BTBD3* in HeLa cells.

Left panel: miR-181a-5p complementation in HeLa cells results in down-regulation of BTBD3 mRNA when compared to an untransfected control, as shown by relative quantification by qRT–PCR (***P = 8.55 × 10−5). Inhibition of miR-181a-5p in HeLa cells results in up-regulation of BTBD3 mRNA (***P = 1.61 × 10−4). BTBD3 levels were normalized to GAPDH. P-values are calculated with a t test on four independent biological samples. Right panel: miR-181a-5p up-regulation and down-regulation are verified by qRT–PCR to assess transfection efficiency. miR-181-a-5p levels were normalized to the small spike-in RNA UniSp6. Indicated P-values were calculated with a paired t test (untransfected control/mimic miR-181a-5p, ***P = 2.88 × 10−4; untransfected control/ inhib. miR-181a-5p, ***P = 6.37 × 10−4).

Table S1. FTSJ1 loss of function leads to miRNAs deregulation in XLID affected individuals LCLs. A list of the significantly deregulated miRNAs and their log2 fold change, p.values and adjusted p.values between FTSJ1 loss-of-function LCLs and control LCLs.

		baseMean_mutant	baseMean_wt	log2FoldChange_Mutant_vs_WT	pvalue	padj
1	**hsa-miR-20b-5p**	3987	538	2.16	1.52E-09	1.21E-06
2	**hsa-miR-222-3p**	16116	6101	1.55	1.90E-08	6.24E-06
3	**hsa-miR-548ax**	42	3	3.91	2.37E-08	6.24E-06
4	**hsa-miR-125b-2-3p**	235	1295	-4.43	6.94E-08	1.37E-05
5	**hsa-miR-221-3p**	37248	12664	1.68	2.37E-07	3.76E-05
6	**hsa-miR-335-3p**	217	690	-2.78	6.53E-07	7.92E-05
7	**hsa-miR-181b-2-3p**	142	44	1.82	7.00E-07	7.92E-05
8	**hsa-miR-99a-5p**	538	2186	-3.61	1.36E-06	0.0001
9	**hsa-miR-10a-5p**	161396	49508	2.31	2.60E-06	0.0002
10	**hsa-miR-181b-3p**	472	111	2.18	6.79E-06	0.0005
11	**hsa-miR-106a-5p**	1737	547	1.10	6.94E-06	0.0005
12	**hsa-miR-181a-2-3p**	12183	4280	1.58	1.44E-05	0.0009
13	**hsa-miR-146a-5p**	256346	121011	1.15	1.54E-05	0.0009
14	**hsa-miR-4482-3p**	2	58	-4.97	1.57E-05	0.0009
15	**hsa-miR-125b-5p**	468	1354	-3.41	1.76E-05	0.0009
16	**hsa-miR-450b-5p**	235	454	-1.97	1.83E-05	0.0009
17	**hsa-miR-424-3p**	608	750	-1.63	2.55E-05	0.0012
18	**hsa-miR-363-3p**	10299	2814	1.88	3.79E-05	0.0017
19	**hsa-let-7c-5p**	1044	3949	-2.59	4.17E-05	0.0017
20	**hsa-miR-450a-5p**	157	254	-1.73	5.17E-05	0.0020

		baseMean_mutant	baseMean_wt	log2FoldChange_Mutant_vs_WT	pvalue	padj
21	**hsa-miR-18b-5p**	131	34	1.45	8.67E-05	0.0033
22	**hsa-miR-550a-3p**	141	288	-1.33	9.04E-05	0.0033
23	**hsa-miR-181a-5p**	1097695	379340	1.82	9.61E-05	0.0033
24	**hsa-miR-550b-2-5p**	94	192	-1.35	0.0001	0.0044
25	**hsa-miR-181a-3p**	15949	4441	2.02	0.0002	0.0051
26	**hsa-miR-181b-5p**	83655	32365	1.52	0.0003	0.0100
27	**hsa-miR-183-5p**	391	848	-1.45	0.0004	0.0112
28	**hsa-miR-99a-3p**	24	55	-3.44	0.0005	0.0134
29	**hsa-miR-135a-5p**	6	80	-3.81	0.0005	0.0135
30	**hsa-miR-146b-5p**	70718	29704	1.41	0.0007	0.0190
31	**hsa-miR-542-5p**	13	19	-2.65	0.0013	0.0321
32	**hsa-miR-944**	138	833	-2.53	0.0015	0.0376
33	**hsa-miR-625-5p**	707	1186	-0.79	0.0016	0.0395
34	**hsa-miR-625-3p**	723	1220	-0.79	0.0018	0.0412
35	**hsa-miR-4772-5p**	56	26	1.77	0.0019	0.0420
36	**hsa-miR-182-5p**	8091	15213	-1.26	0.0022	0.0473

Chapter III:

A- Investigation of FTSJ1's potential functions in translation

1- FTSJ1 loss does not affect polysomes in a global manner

It was shown that FTSJ1 homolog Trm7 in yeast is affected by a 30% decrease in global translation, which translates to significantly lower polysome fraction (Pintard, Lecointe, et al. 2002). In order to evaluate the effect of FTSJ1 on translation levels, I performed a polysome profiling assay on a wild type and a patient LCL (LCL 16, and LCL 65JW respectively, see the Materials and Methods of Brazane et al. 2023 above). The polysome profiles of patient LCLs were indistinguishable from those of WT individuals, supporting that FTSJ1 lack does not affect translation at a global level (Figure 10). Although we note the presence of halfmers, stalled 40S subunits in the polysome fraction, which could be indicative of ribosomal assembly defect. Nevertheless, this result is preliminary and requires validation with proper replicates.

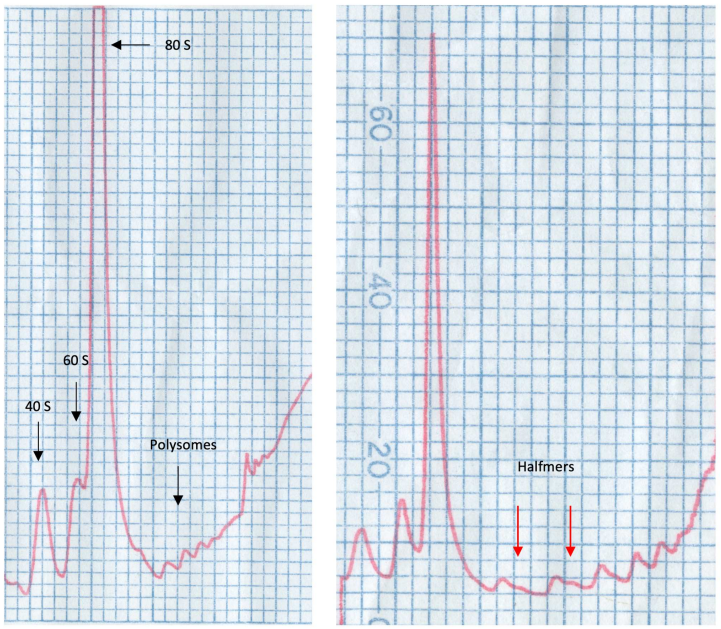

LCL 16 (WT) | LCL 65 JW (Patient)

Figure 10. Polysome profiles of WT and patient LCLs mutated in *FTSJ1*.
Polysome fractionation on a 10-40% sucrose gradient of cell extracts from a WT LCL (Left panel) and a patient LCL mutated in *FTSJ1* (Right panel). Peaks correspond to measurements of OD_{260nm} of each fraction indicated with black arrows. Halfmers are depicted with red arrows.

2- FTSJ1 involved in translation fine tuning?

The above results argue against a general translation failure upon FTSJ1 loss. In order to investigate potential translation defects or specific codon translation impairment mediated by unmodified FTSJ1 substrates at a transcriptome wide level, I performed a Ribosome profiling on LCL 16 and 65JW on three biological samples each, with the help of Dr. Isabelle Hatin at I2BC in Dr. Olivier Namy's lab. All bioinformatic analyses were performed by Hugo Arbes (Namy lab), sequencing was carried out at the EpiRNASeq Core Facility in Nancy university. An mRNA seq was performed in parallel on these same samples in order to provide information on transcript abundance. The results of the whole reads count are presented in Table 2. As shown, the libraries exhibit substantial rRNA contamination, up to 80% for some samples (Table 2). Despite the important read loss due to rRNA overrepresentation, a number of analyses were possible with the number of Ribosome Protected Footprints (RPFs) we obtained, that also show satisfactory periodicity (Refer to Appendix 2).

Samples	Total	Passing filter	rRNA	Aligned (unique)
WT.1	241,187,765	145,117,866	118,024,203	10,211,189
WT.2	227,598,466	136,844,066	120,045,988	5,439,252
WT.3	176,656,784	125,735,509	104,087,507	5,489,052
Mut.1	471,378,091	252,699,774	220,230,109	6,072,193
Mut.2	198,937,871	119,247,979	104,662,962	4,669,269
Mut.3	262,333,426	163,976,107	143,795,670	5,376,699

Table 2. Total read numbers, after quality control, rRNA mapping, and number of final reads analyzed.

Differential expression analysis (DESeq2) analysis was performed on both mRNAseq data and RPF data. The majority of differentially expressed genes are deregulated at both mRNA steady state levels (mRNA seq) and RPF levels (actively translated mRNAs) A plot of differentially expressed genes is available for download here https://drive.google.com/file/d/1IRaYa7sgLinp-KBBLqmdKrEy27hkFq3h/view?usp=sharing). However, in the absence of validation assays, it is not possible to state if deregulated transcripts are mistranslated, or their deregulation is due to reduced steady state levels. Thus, I focused on the deregulated RNAs at the translational level only. The analysis revealed over a hundred deregulated genes at the translational level upwards and downwards (Figure 11- Complete list of differentially expressed RPFs is available in Appendix 1).

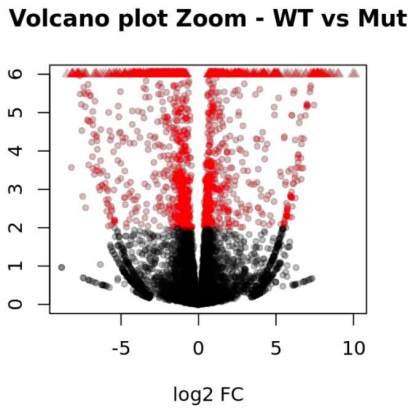

Figure 11. Representation of Ribosome protected footprints data. Volcano Plot.

Gene ontology (GO) analysis was also performed on EnrichR on all deregulated genes at the translational level with p values under 0.001. GO terms with implicated biological processes are displayed in figure 12. Interestingly, upregulated genes are significantly associated with biological processes related to RNA (Figure 12A), and downregulated genes are mostly associated with learning (Figure 12B).

Figure 12. GO analysis of differentially translated genes. (A) Biological processes of translationally up-regulated genes in FTSJ1 mutated cells. **(B)** Biological processes of translationally down-regulated genes in FTSJ1 mutated cells. GO analyses were performed on the EnrichR website.

3- Codon occupancy at the A site studies

To screen for decoding impairments on codons translated by FTSJ1 substrates, we analyzed the relative abundance of each codon at the A-site on all in-frame reads. We found that codon occupancy is significantly increased for TTT, one of the two Phenylalanine codons (Figure 13). This suggests an impairment of the decoding of TTT codons, supporting previous studies on a luciferase reporter in *FTSJ1 KO*

HEK293T cells, as well as in mouse brains mutated in *Ftsj1* (J. Li et al. 2020; Nagayoshi et al. 2021).

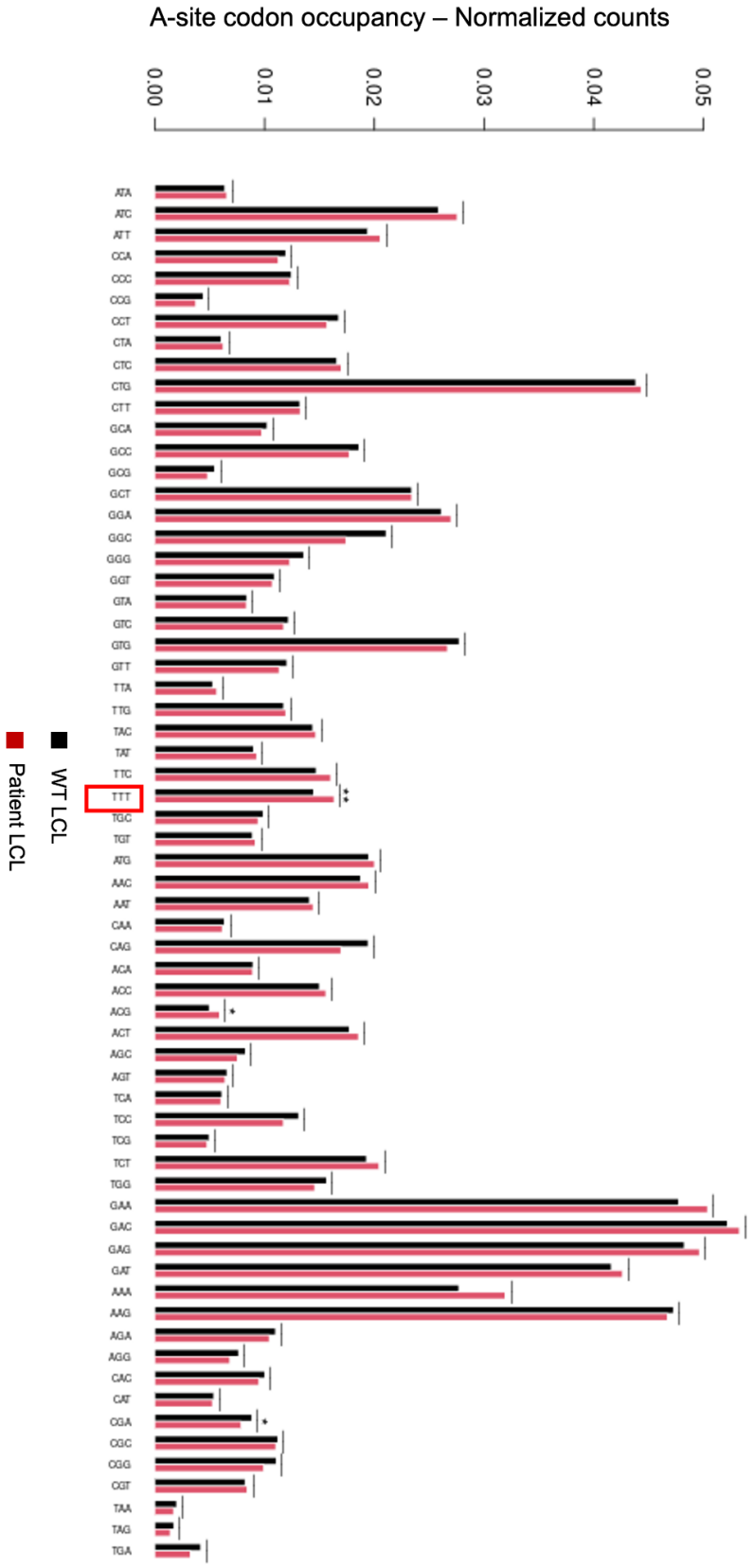

Figure 13. Ribosomal A-site codon occupancy of WT Vs Patient LCLs mutated in *FTSJ1*. A-site codon occupancy is significantly increased for TTT, a codon recognized by tRNA Phe, a substrate of FTSJ1.

We also note a decrease in CGA (Arg), as well as an increase of ACG (Thr) occupancies (Figure 13).

4- FTSJ1 involved in UGA stop codon readthrough ?

- With ribosome profiling: Two recent studies support that FTSJ1 inhibition leads to readthrough of premature UGA stop codons through Tryptophan incorporation (Trzaska et al. 2020; Carollo et al. 2023). In order to verify if such readthrough events occur on annotated terminal stop codons in FTSJ1 mutated cells, we also analyzed stop codon readthrough by examination of periodic signal on 3'UTRs. Low overall signal is observed in the 3'UTRs in all conditions, and patient cells did not exhibit an increase in periodic signal in the 3'UTR (See appendix 2). With this sequencing depth, it is thus difficult to conclude with certainty on a possible increase of terminal readthrough in mutant conditions for *FTSJ1*.

In these conditions, we focused on hAGO1, known to undergo stop codon readthrough in natural conditions, producing a larger protein isoform (Singh et al. 2019; S. Ghosh et al. 2020). Unfortunately, a low coverage of RPF on the *AGO1* CDS made it impossible to produce evidence of increased terminal stop codon readthrough in either conditions (Data not shown).

- With a readthrough biosensor: To exclude any false negative results due to low depth, I used a luciferase reporter containing : - a part of the 3' terminal sequence of *hAGO1*, - the annotated stop codon (UGA) as well as nine nucleotides upstream and nine downstream of the UGA (Dr. I. Hatin). The construct carried N-terminal β-Galactosidase followed by the AGO1 insert, and Firefly luciferase, producing bioluminesce only in the event of stop codon readthrough. Signal is normalized to β-Galactosidase activity (measured by spectrophotometry analysis at 420nm). This construct, along with an in-frame construct with no stop codon were transfected into WT HeLa cells, as well as *FTSJ1* KO Cells (Sivan et al. 2018). WT HeLa cells produced a readthrough percentage estimated to 0,08%. Unfortunately, *FTSJ1* KO

HeLa cells, like LCLs showed an insufficient rate of transfection, which prevented any possible quantification of the results *(Data not shown)*.

- With Western blot: Ghosh et al. used a polyclonal rabbit antibody specific of the 33 amino acid extension of human AGO1, called AGO1x (Lucerna-Chem, #RBP 1510). I tested this antibody by western blot on WT and Patient LCLs, but in these experimental conditions, this approach failed to discriminate between the two isoforms, even by probing the same samples with AGO1 antibody and AGO1x in parallel. AGO1 probing supposedly detecting both isoforms showed little signal overlap with AGO1x. In the absence of powerful controls, it is not possible to quantify AGO1x reliably (Figure 14).

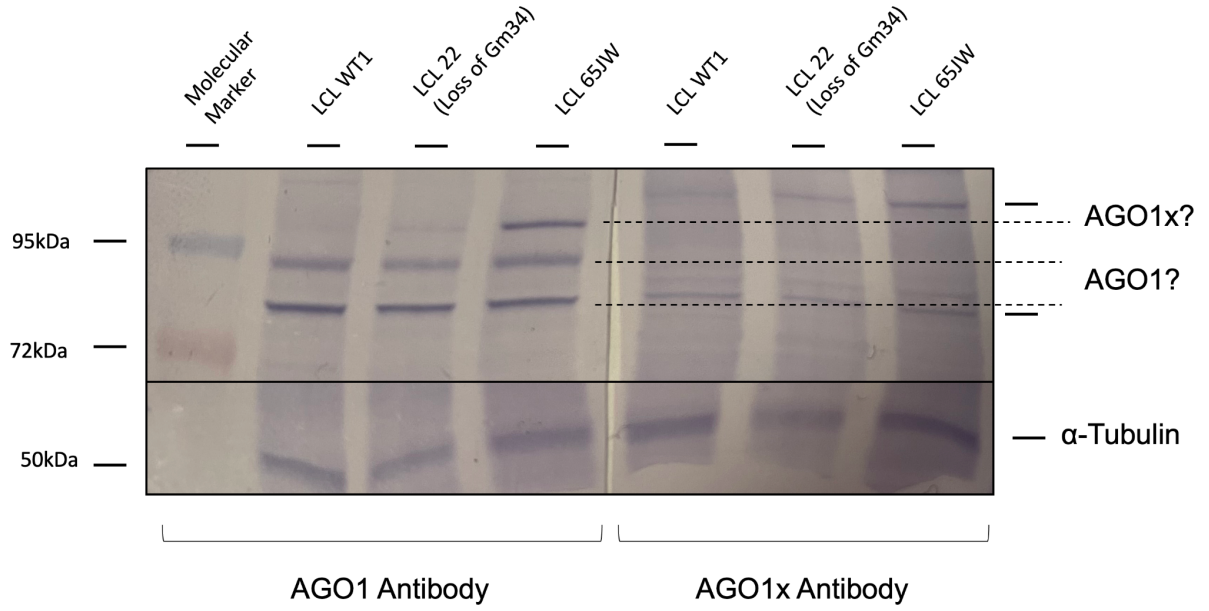

Figure 14. Immunoblot for AGO1 (Left) and AGO1x (Right) detection on a WT and two mutated LCLs after a long gel run (around 3.5 hours at 120V). Several bands are visible around the size of canonical AGO1 (97 Kda), AGO1x is 3,87 Kda bigger than AGO1.

B - Functional investigation of FTSJ1 involvement in AGO2-mediated silencing in *Drosophila*. A never (so far) ending tale…

B1- *Drosophila* AGO2 undergoes stop codon readthrough?

The beginning of our studies in *Drosophila* revealed that loss of tRNA Nm affects RNAi pathways (Angelova et al. 2020). I thus investigated the existence of AGO2 readthrough in *Drosophila* AGO2 (a homolog of hAGO1) and thus potentially producing an AGO2x protein incapable of achieving PTGS as shown for human AGO1x (Singh et al. 2019; S. Ghosh et al. 2020). To this end, I took on to construct a readthrough reporter including a part of the AGO2 CDS as well as its 3' UTR, with a Flag tag downstream of the 3'UTR (Figure 15A). I then co-transfected this construct in *Schneider 2* (S2R+ cells) together with RNAi against *CG7009*, or *LacZ* as a negative control (in the form of long dsRNAs), and screened for stop codon readthrough by Western blot. No Flag-tagged readthrough extension was detected with this method (Figure 15B). Further screening with Flag IP prior to western blot for enrichment, and later by LC-MS gave the same results (Not shown). Overall, this indicates there's probably no stop codon readthrough in *Drosophila AGO2* mRNA.

In fact, the presence of no less than three in-frame UGA stop codons in the 3'UTR extension probably would have required reading-through all three UGAs plus the annotated one in order to produce this isoform (Figure 15C).

A

B

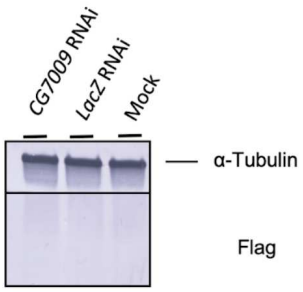

C

5′ GATCATATCATCTACTACCGAGATGGCGTGAGCGACGGCCAGTTTCCGAAAATCAAAAACGAGGAACTGAGGTGTATTAAACAA
GCCTGTGACAAGGTGGGCTGTAAACCCAAGATTTGCTGCGTGATTGTGGTGAAGCGTCATCACACTCGCTTCTTTCCCAGCGGCGA
CGTAACGACATCGAACAAGTTCAACAACGTGGACCCCGGAACCGTGGTCGATCGCACCATTGTGCATCCTAACGAGATGCAGTTCT
TCATGGTCAGCCACCAGGCCATCCAGGGCACGGCCAAGCCAACACGATACAATGTGATTGAGAACACAGGCAATCTTGACATCGAC
TTGTTGCAGCAGTTGACCTACAACCTGTGCCACATGTTCCCTCGTTGCAATCGCTCGGTTTCTTATCCGGCTCCGGCCTATTTAGC
CCATTTGGTAGCTGCTCGTGGACGCGTTTATCTGACTGGCACCAACAGGTTCCTGGATTTGAAGAAGGAGTACGCAAAGCGAACGA
TTGTCCCCGAATTCATGAAGAAAAACCCCATGTACTTTGTCTGAGCAACGTATTGAATCTTATTATTTTTTATCTTTTTTATATTA
TCACATTTCTTAAACCATATTACAAATATAAATTATGTAAAGGAGCATCTCTATTGATTCCATGATGAGCTATGATTT 3′

Figure 15. Investigation of stop codon readthrough events on AGO2 in *Drosophila* S2R+ cells. (A) Construct for AGO2 readthrough detection. (B) Anti-Flag western blot for readthrough Flag-tagged extension, on S2R+ cells c-transfected with the AGO2 construct and CG7009 dsRNA, or LacZ dsRNAs (1st and 2nd lanes respectively), or Mock (treated with transfection reagent), readthrough extension is expected to produce a 31 Kda Flag tagged peptide. (C) Sequence of the 120 Terminal codons of AGO2. The canonical stop codon is indicated in red, and the in-frame stop codons in the 3'UTR are indicated in orange. In the event of readthrough of all UGA stop codons, the peptide is predicted to stop after the last trinucleotide because of the presence of a strong UAA stop codon.

B2- AGO2 saturated with tRNA fragments?

This tale began at least 5 years ago when Dr. Dilyana Dimitrova (Former PhD student on this project) was investigating the involvement of *Drosophila* CG7009 in AGO2 mediated silencing. A 5' tRNA fragment originating from the un- Nm-modified tRNA Phe. This intriguing result led to the "saturation theory" (or *cuckoo* theory) or how the overrepresented tRFs could be overloaded as small RNAs into AGO proteins, thus reducing the binding capabilities of canonical small RNAs, hence the deregulation in RNAi pathways. Dilyana constructed a fly line with an insertion of a Flag-tagged AGO2 in chromosome II under its endogenous promoter. The presence of the endogenous AGO2 alleles was compensated by recombination of the

AGO2::Flag line with the AGO2^{414} mutant allele on the AGO2 locus in chromosome III. With these fly lines expressing a tagged AGO2 she recombined the *CG7009* ^{e02001} loss of function allele. With these flies and an identical control line with WT *CG7009* alleles, she analyzed small RNA tRFs from whole fly AGO2::Flag immunoprecipitates, first by Northern blot. When I joined the lab, I quantified small RNAs with stem-loop RT-qPCR, which ended up being inconclusive due to a low level of purified RNA that was difficult to distinguish from background contaminating RNA in negative control IPs. Another technique was necessary for improving the RNA quality and quantity as well as removing background contamination.

During the last year of my PhD I re-questioned this saturation theory through experimental supervision of Robin Hogg, a Master 2 student in the lab in order to start these experiments again with a different approach on RNA isolation and analysis. We chose to perform AGO2 RIP experiments in fly heads, as it is the most affected by loss of *CG7009 (Brazane et al. 2023)*. RIP experiments were performed on the following fly lines:

$Ago2::Flag; \frac{CG7009^{e02001}, Ago2^{414}}{CG7009^{e02001}}$: Flag tagged AGO2 mutated in CG7009, and carrying one AGO2^{414} mutated allele (Homozygous AGO2^{414} combined with CG7009^{e02001} does not produce an offspring).

$Ago2::Flag; \frac{Ago2^{414}}{TM6, TbHu}$: Flag tagged AGO2, carrying one *AGO2^{414}* mutated allele and the two WT alleles of *CG7009* as WT control for *CG7009*.

w^{1118} : Wild type *Drosophila* serving as an IP negative control.

IP is performed on head extracts with magnetic flag beads. 1% of IP is analyzed by Anti-Flag western blot, and the remaining IP undergoes RNA extraction and later shipped in 80% ethanol for AGO2 bound small RNA sequencing. The western blot analysis showed successful enrichment of AGO2::Flag (Figure 16A). A preliminary analysis of small RNA size distribution was performed by the *Fasteris* sequencing

company before sequencing on two test samples (AGO2::Flag WT and a negative flag control w^{1118}). The results show high enrichment of small RNAs, with significant peaks at 21 and 30 nucleotides (Figure 16B). AGO2 bound RNAs are normally 21 nucleotides long. The 30 nucleotide peak is predicted to correspond to a fragment of the *Drosophila* 2.5S rRNA, which is a frequent contaminant of small RNA seq libraries in *Drosophila*. This result allows first to deduce an enrichment in the expected small RNAs normally bound to AGO2, and second, that a dedicated 2.5S ribodepletion is necessary in order to prevent rRNA fragments from polluting the small RNA libraries. The sequencing is in progress at the time on three biological samples of each of the three genotypes depicted above.

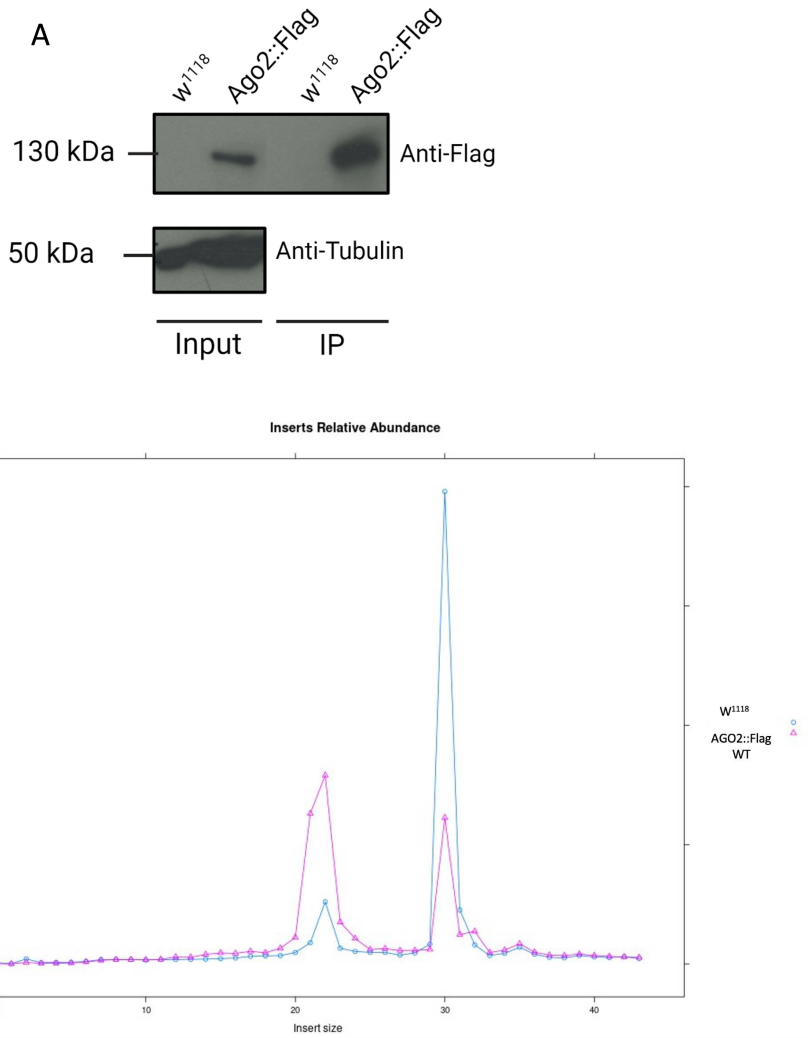

Figure 16. AGO2::Flag RIP results. (A) Western blot verification of successful immunoprecipitation of AGO2::Flag. α-tubulin is used as a loading control (*Robin Hogg*). **(B)** Profiles of W^{1118} and AGO2::Flag RNAs after Flag immunoprecipitation by fragment Analyzer. Profiles show high enrichment for small RNAs under 30 nucleotides in both samples.

Conclusions & perspectives

During my PhD I took part in studying the functions of FTSJ1, a tRNA ribose methyltransferase in the context of a neurodevelopmental disorder causing intellectual disability.

As I joined the lab, I first participated in the final stages of a research project with the goal to functionally characterize *FTSJ1* orthologs in *Drosophila melanogaster*, as well as functions in small regulatory RNA pathways. The latter point was not initially intuitively related to ribose methylation. Nonetheless, this study established a strong relationship between Nm and the three canonical small RNA pathways (mi-, si- and piRNA) using biosensors in Schneider 2 cells, but also transgenic tools in *Drosophila* animals (Angelova et al. 2020). Initially, the *automiG* sensor established a first clue about CG7009's involvement in AGO2 silencing pathways involving both the si- and miRNAs, as both these categories of small RNAs can act as guides for the silencing activity of AGO2 (Förstemann et al. 2007). Further analysis allowed the characterization of CG7009 as a tRNA *Wobble* 2'-O-methyltransferase, along with its paralog CG5220 for methylation of the neighboring nucleotide 32. Substrates of both these enzymes include $tRNA^{Phe,\ Leu,\ Trp}$ in both positions, and additional targets of CG5220 in $tRNA^{Glu,\ Gln}$ were discovered (Angelova et al. 2020).

The evolution of two methyltransferases for each position of the ACL appears unique in *Drosophila* species, and facilitates functional studies of ACL modifications separately from each other. *CG7009* was further found to act as a regulator of the siRNA-mediated viral defense, and in the somatic piRNA pathway in ovarian follicular cells (Angelova et al. 2020). However, a mechanistic link between loss of tRNA methylation and small non-coding RNA pathways is unresolved to this day. This quest has led us to propose a few hypotheses to test, notably, the saturation theory (or the *Cuckoo* theory), stating that accumulated tRFs are loaded in AGO proteins, excluding canonical small RNAs from carrying out gene regulatory functions. AGO saturation might be at the origin of the observed deregulations in said argonaute

dependant pathways. This theory is supported by many studies demonstrating the binding capabilities of tRFs to AGO proteins (Martinez, Choudury, and Slotkin 2017; Sharma et al. 2023; Kuscu et al. 2018; S. Luo et al. 2018).

The work put in by many lab members, and later myself, has been so far inconclusive. The first approach led by Dr. Dilyana Dimitrova (former PhD in the lab) included AGO immunoprecipitation experiments, followed by either RNA quantification by Northern blotting (NB). NB results did not provide reliably quantifiable data, due to low small RNA yield From IP, and difficulty to ensure equal RNA loading and signal normalization. Stem-loop RT-qPCR was further used with specific primers for the detection of tRF 5'Phe. Initially developed for miRNA quantification, this approach had been successfully used for tRF quantification (C. Chen et al. 2005; Yaping Zhang et al. 2020). This approach showed similar limitations when it comes to RNA yield, as well as additional issues, like high sensitivity to background noise, and potential mature $tRNA^{Phe}$ detection, despite the Anticodon stem loop supposedly preventing binding of the stem loop primer. Indeed, I performed stem-loop RT-qPCR on purified $tRNA^{Phe}$ which led to detection of RT products making this method unreliable for tRFs quantification under these experimental conditions. Eventually, this project re-started during my last year of PhD with a project to sequence AGO2-bound RNAs, and further analyze and quantify the potential differential loading between WT flies and *CG7009* mutants. I supervised Robin Hogg, a Master II student in the lab for the RIP experiments and RNA quantifications, which he performed successfully, and sent samples for sequencing services. The final results are currently pending at the time, but preliminary analysis of those recently obtained data are promising as tRFs are detected in those AGO2 IPs. Thus, we hope to finally get an answer as to the veracity of the saturation theory soon.

Secondly, another way to explain the deregulation of AGO2 silencing in *CG7009* mutant context was to look into the primary function of CG7009 targets in decoding during translation. Interestingly, RNA-seq on KD *CG7009* in S2 cells showed a significant downregulation of *AGO2* mRNA steady state level. Consistently, I confirmed this result by replicating the KD experiments and quantifying *AGO2* with RT-PCR in S2 cells (Angelova et al. 2020). Although transcriptional downregulation of *AGO2* could explain deregulation of AGO2-mediated silencing pathways, the mechanism leading to CG7009 regulation of *AGO2* levels is not clear. One possible explanation is that tRNA 2'-O-methylation by CG7009 allows efficient translation of *AGO2* mRNA. Thus unefficient or slow translation of CG7009-dependent codons could potentially lead to the activation of mRNA decay mechanisms like No-Go-Decay triggered by ribosome collisions, with similar outcomes for the translated mRNAs (Harigaya and Parker 2010). This hypothesis requires testing with polysome fractionation experiments followed by RT-qPCR to verify whether *AGO2* mRNA is actively translated, as well as ribosome profiling experiments, that would provide information on translationally downregulated genes, and the potential translation defects altering AGO2 or other effectors of PTGS. Mutagenesis of No-Go-Decay effectors in *CG7009 KO* context could help investigate a rescue of *AGO2* mRNA decrease. Using dedicated tools, such reporter transgenes with quantifiable protein yield could also be achieved. This same approach can also be carried out on potential candidate genes from ribosome profiling data. These approach could prove informative as there is no evidence at the moment of AGO2 protein downregulation upon *CG7009* mutation or KD, despite my attempt to use immunoblots to quantify AGO2 which failed because of low specificity of the only available batch of AGO2 antibody. These approaches would only prove valid if *FTSJ1* loss affects the decoding in a way that alters mRNA steady state levels, or by indirectly affecting regulation of other genes. However we cannot exclude the possibility of inaccurate decoding due to improper codon-anticodon interactions, or inaccurate decoding of amino acids of AGO proteins or others in *CG7009* mutants. In

fact, these alterations can alter the biology of small RNA silencing without affecting the protein steady state levels, thus only proteomic approaches can resolve this question, with emphasis on using reporter systems carrying codons recognized by FTSJ1 substrates.

With these questions left pending, the second project in human cells began, both to address the conservation of molecular phenotypes observed in *Drosophila*, but also to question their potential relevance to human disease (Brazane et al. 2023).

The second goal of my PhD was to study the transcriptome and small RNA profiles of patients derived cells, as well as investigation of FTSJ1 functions in neurogenesis and cognitive function.

We have acquired lymphoblastoid cell lines (LCLs) from patients as well as healthy individuals of similar age from hospitals in France and Australia (details in (Brazane et al. 2023). I characterized a new *FTSJ1* pathogenic variant predicted to disrupt the acceptor splice site of exon 6 (c.362-2A > T. refer to table 1 and (Brazane et al. 2023)). This variant causes a skipping of exon 6 in the final transcript (r.362_414del) leading to a shift in the reading frame, resulting in a premature stop codon (Brazane et al. 2023). *FTSJ1* mRNA steady state levels were altered by this mutation, thus suggesting it is targeted by nonsense-mediated mRNA Decay (NMD). I managed to confirm this hypothesis using a cycloheximide assay that rescues *FTSJ1* mRNA upon translation arrest, confirming that *FTSJ1* mRNA in this pathogenic variant is targeted by NMD (Refer to Figure S1C in (Brazane et al. 2023)).

Transcriptome studies revealed deregulation of 686 genes upwards and downwards. Gene ontology analysis revealed a high number of deregulated genes falling under the term of brain morphogenesis. I confirmed deregulation of a few of these genes using RT-qPCR, including *BTBD3,* a gene involved in cerebral cortex development and dendrite morphogenesis in mice (Matsui et al. 2013). Small RNA-seq analysis

revealed deregulation of a subset of miRNAs, including *miR-181a-5p*, a miRNA highly overexpressed in patient cells, as observed in small RNA-seq analysis, and confirmed by northern blot analysis performed by my co-first author Dr. Dimitrova (Figure 3C in (Brazane et al. 2023)). Leaning on a cross-analysis she performed between deregulated small RNAs and mRNAs, I performed *miR-181a-5p* complementation and inhibition experiments to confirm that *BTBD3*, a putative target of this miRNA is able to induce its regulation in human cells. Using the easily transfectable HeLa cells, I first confirmed the conservation of expression pattern of the mRNA/miRNA couple, I then confirmed that *BTBD3* is regulated by *miR-181a-5p.* However, the naturally overexpressed *miR181a-5p* in patient cells does not reduce *BTBD3* level, but instead, *BTBD3* is also overexpressed in patient cells when compared to WT LCLs. This result hints towards a regulation of BTBD3 in blood cells that is independent from the miRNA pathway. I also analyzed the regulation of another predicted mRNA/miRNA couple. The *SPARC* mRNA is found significantly downregulated in LCL patients and its putative regulator *miR-10a-5p* is found to be coincidently upregulated. The profiling of *miR-10a-5p* in HeLa cells revealed that it is not expressed sufficiently to be profiled by miRNA RT-qPCR protocol (Qiagen). This impeded complementation experiments in HeLa cells. Further investigation of this miRNA/mRNA was difficult to carry out in our experimental conditions, as LCLs transfection gave little to no results. Likewise, *FTSJ1* cDNA complementation experiments were impossible to carry out, for the same reasons both in LCLs and in *FTSJ1 KO* HeLa cells, for an unknown reason.

Importantly, we found an increased density of dendritic protrusions in dorsal telencephalon immature neurons upon treatment with FTSJ1 inhibitor DAP (Brazane et al. 2023). Although these structures do not represent mature dendritic spines to our knowledge, we propose that morphological impairments early during development might alter the fate of synaptic functions in mature neurons. Interestingly, dendritic morphology and density alterations are known to be

associated with neurodevelopmental disorders (Penzes et al. 2011; S. Lee, Zhang, and Webb 2015), including in post-mortem cerebral cortex of patients with diverse neurodevelopmental impairment, like autism spectrum disorder, and Fragile-X-syndrome, and ID (Kaufmann and Moser 2000; Geschwind and Levitt 2007; Irwin et al. 2001). These physical alterations can also be accompanied with electrophysiological changes (Yu Zhang et al. 2014).

Further investigation of the relationship between altered transcriptomes of human neural cells would provide more information as to the regulation of brain morphogenesis genes in neural tissue during development. An emphasis on *BTBD3*, and *AHNAK* could be interesting, as these two candidates are known to play an important role in neural development. Importantly, both these genes were found to be deregulated at both RNA level, and at the translational level (see Results Part III). Although a mechanistic link is lacking, the deregulation of both genes required for correct neural development could be related to dendritic spine morphology changes upon FTSJ1 inhibition. It is thus interesting to assay the expression of both these genes in a neural tissue, starting by immature neurons, and maintaining them in culture long enough to observe morphological features, as well as the transcriptomic signatures associated to those. As we previously observed a significant overexpression of *miR-181a-5p* and *miR-10a-5p* in patient LCL, it would be interesting to verify any other potential targets of this miRNA, and how they might affect gene expression.

Importantly, we also observed an overgrowth phenotype altering the morphology of neuromuscular junctions in double *CG7009;CG5220* mutant *Drosophila* larvae, consistently with previously described locomotory defects in these same mutants (Brazane et al. 2023; Angelova et al. 2020). Interestingly, golgi staining of cortical and hippocampal sections of the *Ftsj1* mouse model showed impairments in synaptic morphology, with immature filopodia-like spines rather than mature mushroom-like

spines. Accordingly, cognitive impairments are observed in these mutants (Nagayoshi et al. 2021). Interestingly, we found that all fly mutant combinations of *FTSJ1* orthologs display a significantly impaired long-term memory. Altogether these results support a conserved function for FTSJ1 in neural development and morphology, with possible roots for ID phenotypes. With the new addition of our transcriptome and translatome studies, genes implicated in the process of brain morphogenesis are associated with FTSJ1 dysfunction, but also in a similar manner in the mouse model (Brazane et al. 2023; Nagayoshi et al. 2021). Assessing the translation status in neurons could be of utility to understand the implication of tRNA methylation in these processes. Notably, local translation assays on mature neurons, dorsal organoids, or mouse hippocampal cultures could shed light as to a possible spatial translation signature leading to alteration of dendritic spine morphology and how it affects general tissue development.

This last point brings me to the last project of my PhD studies, which provided preliminary observations as to the translatome of patient LCLs. I first investigated the global translation levels with polysome profiling. I later pursued a transcriptome wide approach using ribosome profiling on a patient LCL and a control LCL from a healthy individual (See results chapter III).

Thus far, studies of FTSJ1 homologs in other organisms provided a wide picture of possible functions. In fact, polysome profiling experiments on *ΔTrm7* showed a 30% reduction in the global levels of translation, and further methionine incorporation experiments confirmed a globally reduced translation (Pintard, Lecointe, et al. 2002). Consistently, *ΔTrm7* yeast exhibited a drastic growth defect. On the other hand, studies of mammalian FTSJ1 suggested a function in translation efficiency and fidelity rather than a global effect (Nagayoshi et al. 2021; J. Li et al. 2020). Notably, studies reported effects of *FTSJ1* loss on translation termination (Trzaska et al. 2020;

Carollo et al. 2023) and UUU decoding in mice brains, as well as in human cells expressing a luciferase reporter system (Nagayoshi et al. 2021; J. Li et al. 2020).

The addition provided with our preliminary results are two fold. First, polysome profiles of patient cells did not show any drastic drop in polysomes when compared to WT LCL, as opposed to what was found in *S. cerevisiae* (Pintard, Lecointe, et al. 2002). This result points to a different function of the Trm7 family in distant organisms despite very common features like sequence identity conservation, and strong substrate overlap. Secondly, we noted the presence of halfmers in the polysome fraction. Halfmers correspond to a stalled 40S subunit awaiting a 60S subunit for ribosome assembly. Halfmers can be indicative of 60S subunit assembly defect (Moore et al. 2010). This result was obtained on two biological replicates, but needs confirmation with other methods. This observation could be unrelated to tRNA modification, but the investigation of FTSJ1 functions in translation raised an interesting question as to the possibility of other FTSJ1 substrates among rRNAs. In fact, the Trm7 family comprises a conserved Rossmann-fold structure near the catalytic pocket that accommodates RNA substrates, which was only thought to methylate tRNAs (Pintard, Lecointe, et al. 2002; Hirata et al. 2019). The E.coli ortholog *FTSJ* methylates both rRNA and tRNAs (Caldas et al. 2000; Bügl et al. 2000), however the full tRNA and rRNA substrates have not been systematically mapped, except in *S. cerevisiae* in 2017, where Chou and colleagues managed to carry out a systematic Nm mapping using RibomethSeq on several tRNA modifying enzyme mutants including *Trm7*. Surprisingly, three known Nm sites in 18S rRNA, as well as five others in the 25S rRNA were found to be significantly altered by *Trm7* mutation, with one of them appearing to be dependant on both Trm7 and its partner Trm734 (Chou et al. 2017). Our RibomedSeq experiments were performed on total RNAs from patient cells, as well as *Drosophila* mutants, with special attention to tRNAs (Angelova et al. 2020; Brazane et al. 2023), however, it is now possible in

perspective to analyze potential rRNA target on these same datasets with proper pipelines for rRNAs.

Studies showed different extent of internal Nm sites on mRNAs past the 5' cap Nm common to endogenous mRNAs (Hoernes et al. 2016; Dai et al. 2018; Hoernes et al. 2019; Elliott et al. 2019). The presence of hundreds of Nm sites in the coding regions remains controversial for many reasons, among which few studies show a high level of internal Nm sites thus far, with unclear functions for these sites and lack of functional validation (Dai et al. 2018). A preprint describing the similar results was published in BioRχiv and attributed to Spb1 rRNA methyltransferase orthologous to FTSJ3, a cap methyltransferase in mammals (Bartoli et al. 2018; Ringeard et al. 2019). Dai and colleagues point out the presence of many Nm sites in mRNAs including intronic regions with a potential to investigate novel roles for Nm in this new setting. Moreover, functions of Nm are often linked to its chemical properties, while other modifications show dynamic properties also dependent on the involvement of reader proteins, including m^6A and m^3C (Hailing Shi, Wei, and He 2019; Bohnsack et al. 2022). Thus far, only Nm "writers" are known, and no readers, or erasers are known to be involved in Nm biology. Nonetheless, mechanistic and structural properties of Nm sites in the coding regions of mRNA, appear to have disruptive functions in vivo, and in vitro as shown by studies in eukaryotic and bacterial cells, with stronger translation elongation arrest upon the presence of the modified residue in the second nucleotide of the codon (Hoernes et al. 2019, 2016; Elliott et al. 2019). Structural study of the position dependent elongation disruption seems to involve a steric clash introduced by the methyl group with the conserved A1492 in the 16S rRNA and A1492 in 18S rRNA in bacteria and eukaryotes respectively (Hoernes et al. 2019).

Based on these results, FTSJ1 is not expected to introduce any Nm sites on mRNAs, except probably in a context where Nm sites are meant to serve dynamic regulatory

functions. Therefore, the RibomethSeq data from mutated cells and *Drosophila* could be of interest in order to address this question.

RibomethSeq is so far not able to detect 3' terminal Nm in small RNAs, however, this methylation is attributed to Hen1, to prevent degradation by exonucleases (Horwich et al. 2007). Although our small RNA population analysis showed a 10% drop in miRNA levels in the *Drosophila* mutants, it cannot be attributed to a 3' terminal Nm loss, as Nm only affects siRNAs and piRNAs in *Drosophila* (Saito et al. 2007; Horwich et al. 2007).

Together with polysome profiles as a gross estimation of translation status of FTSJ1 patient cells, we performed ribosome profiling to observe potential global and specific translation alteration in the context of FTSJ1 loss. Bioinformatic analyses performed in collaboration with the Namy Lab included a differential expression analysis, as well as 5' and 3'UTR occupancy, and A-site codon occupancy. (See chapter III results).

Differential expression analysis was performed on ribosome protected footprints, as well as o,n a parallel RNA seq dataset. This allowed correlating mRNA abundance to actively translated ones. This analysis confirmed once again the deregulation in some genes we observed in our patient transcriptomes, like *ZNF711*, *AHNAK*, *BTBD3*, and *SPARC* (See the linked plot in results Chapter III). Moreover, it allowed us to identify around 100 genes deregulated only at the translational level (See appendix 1).

The gene ontology analysis showed that upregulated genes mainly associate in nucleic acid binding and processing. A few examples include POP1, a ribonuclease functioning in the RNAse P complex for tRNA 5' leader removal, as well as pre-rRNA processing. POP1 mutations cause anauxetic dysplasia, a severe skeletal development disorder (Elalaoui et al. 2016; Glazov et al. 2011). Among the upregulated genes, we also find *EXOSC8*, an exonuclease involved in rRNA

processing, and involved in pontocerebellar hypoplasia (Boczonadi et al. 2014). Importantly, we find an upregulation in genes associated with other RNA modifications, including the Dihydrouridine synthase DUSL3, the N-6 Methyladenosine transferase METTL14, as well as the cap-methyltransferase CMTR1.

Downregulated genes are mainly associated with peptidyl-tyrosine phosphorylation, a biological process involved in many signaling pathways, genes of this term include Protein Tyrosine Kinase 2 Beta (PTK2B also called PYK2), a gene involved in the MAP kinase pathway, and is responsive to calcium levels for regulation of ion channels, making it an important intermediate in neural activity regulation (Lev et al. 1995). Disorders related to PTK2B include osteoporosis and glioma (Yang et al. 2022; Loftus et al. 2009; Lipinski et al. 2006). Strikingly, the most deregulated gene, is KCNMA1, with a log2 fold change of -7,3 (padj 1,36E-07) encodes a subunit of a calcium activated Potassium channel crucial for muscle contraction, neurotransmitter release and neuronal excitability (Gonzalez-Perez and Lingle 2019). Mutations of KCNMA1 cause various neurological and muscular alterations, including epilepsy, paroxysmal Dyskinesia and intellectual disability (Z.-B. Zhang et al. 2015; Yeşil et al. 2018). Interestingly, we also found significantly downregulated genes associated with imitative and vocal learning including Huntingtin (HTT) a gene involved in various neurological alterations, such as Huntington's disease, and intellectual disability (Sapp et al. 1997; Wellington, Leavitt, and Hayden 2000; Lopes et al. 2016). We also found that Alpha-N-Acetylgalactosaminidase (NAGA) is significantly downregulated (Appendix 1). NAGA is a gene involved in Shindler disease mainly associated with neuroaxonal dystrophy (Kanzaki et al. 1989; Desnick and Wang 1990).

At the moment, there is not an apparent link between all the terms we observed and the function of FTSJ1, although many appear to be involved in RNA processing and are somehow linked to neurological disorders, however, one might speculate about a

possible involvement of the codon enrichment in this group of genes. Future analysis of the codon content of these genes could provide more insight into the biological significance of these deregulations.

Importantly, A-site codon specific analysis revealed a significant increase in TTT occupancy, one of the codons recognized by the main FTSJ1 substrate $tRNA^{Phe}$. This result is consistent with an experiment carried out by Li and colleagues testing Phe codons TTT against TTC in a luciferase reporter, which detected reduced translation efficiency only in TTT codons (J. Li et al. 2020). Consistently, Phe codons also exhibited higher A-site occupancy upon loss of murine *Ftsj1* in the nervous system (Nagayoshi et al. 2021). This increase could be indicative of ribosome stalling due to unmodified tRNAs. Interestingly, Nagayoshi and colleagues attribute ribosomal stalling to a $tRNA^{Phe}$ shortage as shown by tRNA seq analysis, associated with an accumulation of tRF 3' Phe. Similarly, northern blot analysis performed by my colleagues showed a significant increase of $tRNA^{Phe}$ fragmentation, as well as an accumulation of tRF 5' Phe (Angelova et al. 2020). Consistently, general translation defects observed in yeast are associated with $tRNA^{Phe}$, as the specific $tRNA^{Phe}$ overexpression experiment saves the growth defect (Guy et al. 2012; Guy and Phizicky 2015), and Trm7 mutant yeast shows a constitutive response to uncharged tRNAs, that is rescued with addition of charged $tRNA^{Phe}$ (Han et al. 2018). Translation analysis of our *Drosophila* mutants in the future could bring a new perspective, as it was never done in this organism, but could also facilitate the comprehension of the function of each individual ACL modification, as we have access to mutants for each one of them.

Either through tRNA shortage, tRNA decoding defects, undescribed ribosomal Nm sites alteration or tRF-mediated translation inhibition, the Trm7 family of methyltransferases appear to be involved at least in phenylalanine codon translation, especially upon G-U wobbling with cognate mRNAs.

One of the aspects related to translation that I studied during my PhD was stop codon readthrough associated with *FTSJ1* loss. Indeed, FTSJ1 inactivation leads to increased readthrough of premature UGA termination codons mediated by an unmodified $tRNA^{Trp}$ (Trzaska et al. 2020; Carollo et al. 2023). With ribosome profiling, and dedicated reporter systems in cellular models I investigated the possibility of *FTSJ1* loss to affect the proteome of patients by increasing readthrough of terminal stop codons. Readthrough can occur in natural conditions, even produce functional proteins, or antagonistic isoforms to the canonical gene product (Eswarappa et al. 2014; Singh et al. 2019). No evidence of stop codon readthrough increase was produced with the methods I used, including on a known readthrough target *hAGO1* (Singh et al. 2019; S. Ghosh et al. 2020). Likewise, the use of a readthrough sensor in *Drosophila* S2R+ cells did not produce a readthrough extended protein (See results chapter III). Although, *Drosophila* AGO2 is not known to undergo stop codon readthrough as its human counterpart *hAGO1.* These results suggest that loss of *Wobble* Nm does not increase UGA stop codon readthrough on terminal UGAs as it is the case for premature UGA stop codons. Despite UGA stop codons being the leakiest, the sequence context downstream of the stop codon might play a role in stop codon readthrough and competition of termination factors might be a lot higher on terminal stop codons.

Ribosome profiling is usually a suitable technique to investigate 3'UTR translation, however, the low sequencing depth of our libraries did not permit a observation of readthrough on *hAGO1*. We have performed a new triplicate ribosome profiling to increase the sequencing depth of our libraries and support our preliminary results, however, our overall preliminary results do not indicate any evidence of terminal stop codon readthrough in *FTSJ1* mutated LCLs.

General conclusions

Overall, mine and my colleagues' contribution brought insight into the transcriptional profiles of patient cells affected with ID, morphological features associated with those, as well as initiated a project towards the understanding of human FTSJ1 in translation, and whether this could represent an etiology for the intellectual disability associated with its loss.

Remarkable progress has been made in the field, as many studies mentioned above contributed to the understanding of the function of this modification circuitry. However, more questions piled up, as to the means of transcriptional alterations we, and others have observed. The puzzling functional involvement of small RNA silencing, the potential contribution of tRFs to AGO-mediated silencing, tRFs-mediated translation repression, and finally the contribution of translation alteration of Phe codons are still under investigation. Addressing these questions could potentially bring more insight into the role played, not only by FTSJ1 but in the numerous neurological disorders associated with the loss of RNA modifying enzymes (Pereira et al. 2018; Angelova et al. 2018; Dimitrova, Teysset, and Carré 2019; Suzuki 2021). Another frequent disease associated with RNA modification loss is cancer (Haruehanroengra et al. 2020; Begik et al. 2020). Our transcriptome studies showed a number of deregulated genes involved in various cancers (Brazane et al. 2023) including *miR-181a-5p* involved in various cancers (Indrieri et al. 2020), but other studies also pointed to functions of FTSJ1 in tumor suppression in lung cancer (He et al. 2020), as well as in P53 response in the context of hepatocellular carcinoma (Holzer et al. 2019). Although not yet clear, this study probably suggests that *FTSJ1* loss is a risk factor for the development of cancer. Coincidentally, many recent studies report a higher incidence of cancer and cancer related deaths among individuals suffering from intellectual disability (Cuypers et al. 2022; Q. Liu et al.

2021). This risk factor requires more awareness and surveillance of side pathologies among individuals with ID, particularly upon aging.

The mechanistic development of FTSJ1-related ID is still under investigation but many leads remain to be pursued based on previous findings, especially in model organisms. Indeed our study on *Drosophila* homologs allowed us to discover their involvement in small RNA silencing, which coincidentally plays an important role in regulation of local translation in neurons and glia. Heterozygous mutations of *hAGO1* are also involved in ID, suggesting an important role for miRNA mediated gene regulation in the nervous system (Schalk et al. 2022; Niu et al. 2022; Duan et al. 2023). My team will soon start a collaboration on *hAGO1* mutations and its implication in ID (in flies and humans), collaboration supported by a recently acquired ANR grant in collaboration with Dr. A. Piton (*#pAgoDE*, ANR 2023).

Finally, our preliminary results in patient cells, as well as other studies in cellular and mammalian models support a strong involvement of $tRNA^{Phe}$ in translation of TTT codons (J. Li et al. 2020; Nagayoshi et al. 2021). Li and colleagues showed by bioinformatic analyses that most genes with high TTT to TTC bias are involved in brain development. This could indicate a mistranslation of Phe codons with dramatic effects on the brain proteome during development. Moreover, most amino acids carried by FTSJ1 substrates are hydrophobic, including Phe, Leu, and Trp. This is important for membrane proteins crucial in interneuron connection and synapse formation. We hypothesize that *FTSJ1* loss could reduce, or impair translation of the cognate codons to its substrates, and thus perturb the synaptic function, membrane remodeling, ion traffic and neurotransmitter transport, inducing potential defaults in morphology and function. This of course needs to be investigated in the future with proper electrophysiological experiments (in collaboration with Dr. L. Tricoire at IBPS), combined with proper proteomic studies, and local translation experiments to

understand if amino acid misincorporation could be among the translation errors that lead to the formation of defective proteins.

Materials and methods

Foreword:

All of the materials and methods for published materials are included in a dedicated section of each article (See Results Chapter I and II). The following section includes materials and methods of unpublished experiments done for the third results chapter.

Lymphoblastoid cell lines culture

LCLs were cultured in RPMI 1640 medium with L-glutamine and sodium bicarbonate (R8758 - Sigma-Aldrich) supplemented with 10% Foetal Bovine Serum (FBS) (F7524 - Sigma-Aldrich) and 1% penicillin/streptomycin (PS) (ref. P0781; Sigma-Aldrich) at 37 °C with 5% CO2. Cells are cultured in T75 flasks, and supplemented every other day with fresh medium till confluency, and split to a third dilution every 3 days.

S2R+ cell culture

S2R+ cells were maintained at 25°C in *Schneider's Drosophila Medium* (Pan Biotech P04-91500) supplemented with 10% FBS, and 1% PS. Cells are slightly adherent but are easily homogenized with pipetting. Cells are split twice a week depending on confluency.

S2R+ transient transfection

Transfection is carried out using Effectene Transfection Reagent (Qiagen 301425) following the supplier's recommendations. 24h prior to transfection, 2.5 million cells are plated into T25 flasks in a final volume of 5mL of complete medium (S2 medium 10% FBS 1% PS. 1µg of each dsRNA (CG7009 and CG5220 or control dsRNA (LacZ) (sequences are available in Angelova et al. 2020) were diluted in DNA condensation buffer (EC) and Enhancer (both buffers are included in the kit).

Together with 1µg of readthrough plasmid for AGO2, Mock negative control cells were treated with EC buffer and Effectene transfection reagent. A mix of Effectene and EC buffer is added to the RNA/DNA mixes, homogenized, incubated 7 min at room temperature, and added dropwise onto the S2 cells. Cells are extracted 48h post transfection and assayed for Flag expression using western blot. In parallel, RNAi efficiency was assayed with RT-qPCR (as described in Brazane et al 2023).

Flag immunoprecipitation

- Cell Harvest: After transfection, cells are harvested with a 5 min centrifugation at 1000 rpm and lyzed in 100 µL of RIPA buffer (R0278 Sigma).
- Flies dissection and lysis: Flies are collected and flash frozen in 15mL falcon tubes (300 flies per sample), and stored at -80°C until the experiment takes place. Flash frozen flies are vortexed for 20 seconds, leading to separation on heads from abdomens, then passed through two successive scieves, with the first one retaining the abdomens, and the second retaining the heads. The latter are collected with a funnel into 1.5 eppendorf tubes and smashed with pestles in lysis buffer (5,8mM HEPES, 150 mM NaCL, 2 mM Mg(oAC)2, 0,1% Nonidet P40 pH 7,4 equilibrated with KOH) additionned with a protease inhibitor cocktail (5892970001 Roche). Flies are smashed three times and cleared by 3 centrifugations at 16.000 RCF 10 min, in between smashings in a total volume of 1mL added sequentially.

Cleared cell lysate is mixed with 90 µL of Flag M2 magnetic beads (M8823 Sigma) overnight at 4°C on a wheel. After IP, supernatant is eliminated, and beads are washed 3 times for 10 min on wheel with a high salt wash buffer (5,8mM HEPES, 800 mM NaCL, 2 mM Mg(oAC)2, 0,1% Nonidet P40, pH 7,4) and twice with Tris Buffered Saline 1X. 9 µL of beads are diluted in equal volume of Laemmli buffer 2X (S3401 Sigma) and denatured at 95°C for 5 min, and used for western blot. The remaining beads undergo Proteinase K treatment at 37°C for 30 min (EO0492

Thermo Scientific™) followed by RNA extraction using TRI Reagent ® (93289 Sigma) and Chloroform following the manufacturer's protocol).

Western blot

After denaturation, samples are loaded into a 4% -15% gradient polyacrylamide gel (Mini protean TGX 4561085 Bio-Rad) in a Tris Glycine SDS running buffer (25 mM Tris HCl pH 8.0, 192 mM Glycine, 0.1% SDS). Proteins are transferred onto a 22 µM PVDF membrane (Polyvinylidene difluoride) (Amersham) using Trans-blot turbo transfer system 1704150 Bio-Rad) following the MIXED MW (1.3 A constant; up to 25 V). An alternative transfer method was also used for liquid transfer with Tris-Glycine 15% Ethanol for an hour at 100V. Transfer efficiency if assessed with colored molecular marker transfer as well as a ponceau staining. Blocking is performed by immersion of the membrane in 5% dry fat Milk (Régilait écrémé) in TBS Tween (500 mM Tris-HCl pH 7.4, 150 mM NaCl, 1% Tween) during 45 minutes under shaking at room temperature. After three 5 min washed in TBST, membranes are probed with corresponding primary antibodies in solution of TBST and 3% Bovine Serum Albumin (BSA) (0332 Amresco).

Anti-FLAG (mouse Agilent, 1:5000). Anti-αTubulin (Human) (sc8035-tu02 mouse Santa Cruz Biotechnology, 1:1000). Anti-αTubulin (Drosophila) (sc23948 mouse Santa Cruz Biotechnology, 1:10.000. Anti-AGO1 (SAB 4200066 Sigma, 1:2000). Anti-AGO1x (RBP 1015 Rabbi Lucerna Chem 1:1000). After three washes, membranes are incubated with the corresponding secondary antibodies at 1:10.000 dilution: Anti-Mouse Alkaline phosphatase conjugated (AP) (S3721 Promega) or Horseradish conjugated (HRP) (4021 Promega). Anti-Rabbit AP conjugated (S3731 Promega).

After three washes detection of AP conjugated secondary antibodies is performed by addition of 200 µL of BCIP/NBT (5-Bromo-4-chloro-3-indolyl phosphate and Nitro-blue-tetrazolium (NBT)) (11681451001 Roche) in 10 mL of AP buffer (0.1M Tris

HCl pH 9.5, 0.1 M NaCl, 5 mM MgCl2). HRP conjugated membranes are revealed with a 3 min incubation with SuperSignalTM West Pico PLUS Chemiluminescent Substrate de (34580 ThermoFisher).

Polysome Profiling on Lymphoblastoid cell lines

LCLs 16 (WT) and 65JW (Patient) were harvested by centrifugation of the whole culture volume at 1200 rpm for 3 min at 4°C (75003607 Rotor; Thermo Fisher Scientific). Supernatant was eliminated and cell pellets were flash frozen and stored at -80°C, to be fractionated the next day. Polysomes were extracted from frozen pellets of 25 million of LCLs each (2 replicates for each cell line). Cells were placed on ice and lysed with 200 µL of extraction buffer (10mM Tris HCl pH7,5 , 100mM KCl, 10mM Magnesium Acetate, 1% Triton x100, 2mM DTT) additionned with 2x Protease Inhibitor Cocktail (Roche). Lysates were cleared with 5min centrifugation at 16.000 RCF at +4°C. OD measurement at 260 nm was 4.6 ; 13 ; 4.4 ; 6 in LCL 16 and 65JW extracts respectively. Lysates were loaded on a 10 - 40 % sucrose gradient, and centrifuged in a SW41 rotor for 3 hours at 39.000 rpm at +4°C. Fractions of 600 µL were collected with Teledyne ISCO.

Ribosome profiling

Over 120 million cells per biological sample were harvested by centrifugation at 1200 rpm during 3 min, then flash frozen, and stored at -80°C. Polysomes were extracted with 1 mL of extraction buffer (composition above) additionned with 2x Protease Inhibitor Cocktail and 2 units of Murine RNase Inhibitor per microliter of buffer. Lysates we cleared with a 5 min centrifugation at 16.000 RCF at +4°C.

Lysates were loaded on a 30 % sucrose cushion (saccharose 24%, 50 mM Tris-acétate pH7,6 ; 50 mM NH 4 Cl ; 12 mM MgCl 2) then centrifuged in TLA110

rotor during 90 min at 110.000 rpm at +4°C. Polysome pellets were solubilized in 500 µL of extraction buffer. Polysomes were digested with 5 units of RNase I per $OD260_{nm}$ for an hour at 25°C (AM2295 Ambion), and of 500 units of Superase-In Rnase Inhibitor (Invitrogen). RNAs were extracted by phenol at 65°C, Chloroform and precipitated by Ethanol in 0.3M Sodium acetate pH 5.2. The digested RNAs were solubilized in 75 µL of buffer. and loaded on 17 % polyacrylamide, 7 M urea in TAE 1x and migrated 6 h at 100 V. RNA oligonucleotides of 28 and 34 nucleotides are used as molecular mass markers for size selection. Fragments recovered from gel and depleted in rRNA with a Lexogen kit for human rRNA depletion. Ribosome protected footprints were quantified using fluorescent Quant-iT microRNA kit assay, and sent to the EpiRNASeq Core Facility in Nancy for Library preparation, and sequencing.

Ribosome profiling bioinformatic analyses

The ribosome profiling analysis was made using the RiboDoc tool (v0.9.0) (François et al. 2021). Its different main steps of the analysis with their corresponding programs, versions and command lines are described below. The reference genome for human alignment is Homo_sapiens.GRCh38.104 from the Ensembl database (Yates et al. 2020).

The sequencing adapters were trimmed by cutadapt v4.3 (Martin 2011) and the lengths of the RPFs was filter to keep reads from 25 to 35 nucleotides long as their expected length is around 30 nucleotides: cutadapt -e 0.125 --max-n=1 -m 25 -M 35 -a ${adapter_sequence} -o ${output.fastq} ${input.fastq} The removal of the rRNA reads was made by an alignment on the rRNA sequences by bowtie2 v2.5.1 (Langmead and Salzberg 2012) :bowtie2 -x ${index.rRNA} -U ${input.fastq} --un-gz ${output.fastq} The alignment on the genome was made with both hisat2 v2.2.1 (Kim et al. 2019) and bowtie2 v2.5.1 : hisat2 -x ${hisat2_index.genome} --no-softclip -U

${input.fastq} --un-gz ${output.fastq} -S ${output.sam_hisat2} bowtie2 -x ${bowtie2_index.genome} --end-to-end -U ${output.fastq} -S ${output.sam_bowtie2} The selection of the reads uniquely mapped on the genome was made with samtools v1.14 (H. Li et al. 2009): samtools view -F 3844 -q 1 -h -o ${output.bam} The counting of the reads corresponding to each transcript was done by htseqcount v2.0.2 (Anders, Pyl, and Huber 2015) : htseq-count -f bam -t CDS -i Parent --additional-attr Name -m intersection-strict --nonunique fraction ${input.bam} ${input.gff} > ${output.txt} The differential analysis was made with the bioconductor package DESeq2 v1.34.0 (Love, Huber, and Anders 2014). The qualitative analysis was performed on a transcriptome made from the genome with a selection of transcripts annotated as having a 5'UTR region. To study the reading frame of the Ribosome Protected Fragments (RPF), each read is represented by the coordinate corresponding to the first base of the associated ribosome's P-site. To determine where the P-site is, a P-site offset has to be defined for every read length of each sample. This step is done with the riboWaltz v1.2.0 package (Lauria et al. 2018).

AGO1 Readthrough quantification

Oligonucleotides complementary to the 18 nucleotides surrounding the canonical AGO1 stop codon were ligated to the pAC99 dual reporter plasmid, as described by (Bidou et al. 2004). Sequences of AGO1 and In-frame AGO1 (without a stop codon are as follows (TAC TTC GCT **TGA** AGG CAG AAC) and the control (TAC TTC GCT **TGG** AGG CAG AAC). Measurement of stop codon readthrough is performed by quantification of luciferase activity (Tecan), normalized by the β-galactosidase activity as an internal control as previously described (Stahl et al. 1995).

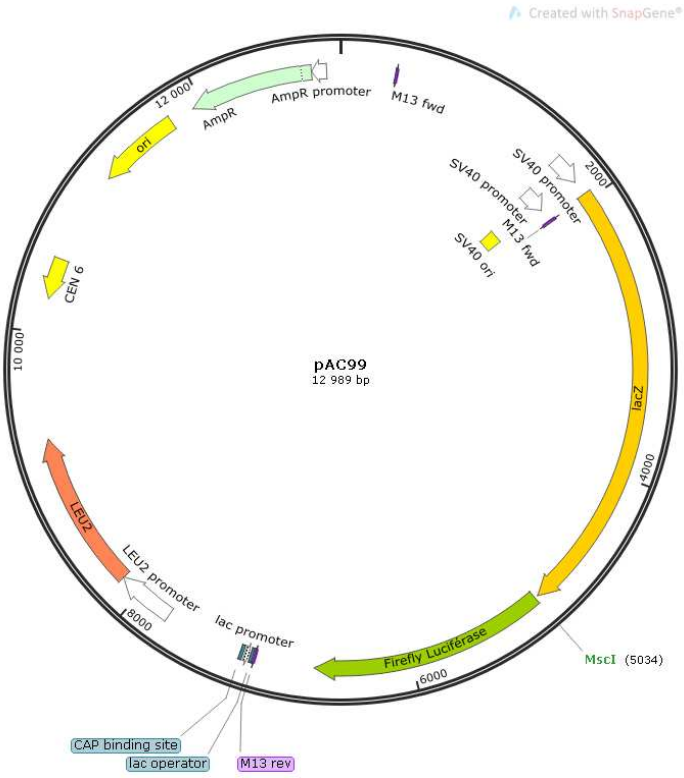

WT and *FTSJ1* KO HeLa cells were seeded into 6-well plates, and transfected the next day the reporter plasmids using the JetPei DNA transfection reagent (Polypus) following the supplier's protocol. A medium change is done after 17 hours, and cells were harvested 48h post-transfection with trypsin-EDTA (Invitrogen), and lyzed in Luciferase buffer (Tris Phosphate pH7,8 25mM (tris buffered with Phosphoric acid), Magnesium Chloride 8M, DTT 1 mM, EDTA pH8 1 mM, Triton X 100 1 %, BSA 0,1% Glycérol 15%). β-galactosidase and Firefly luciferase activities were measured as previously described (Stahl et al. 1995). Readthrough is evaluated by a ratio of luciferase to β-galactosidase activity compared to test construct, and normalized on the in-frame AGO1 construct (With TGG instead of TGA).

AGO2x readthrough sensor construction for *Drosophila* S2R+ cells

The last 120 codons of AGO2 transcript followed by its annotated stop (TGA) and the proximal 3'UTR until the next in frame strong stop codon TAA (210 nucleotides downstream of the annotated stop) were amplified from w^{1118} genomic DNA using

Phusion High-fidelity DNA polymerase (NEB), and later from cDNA with random priming (See reverse transcription protocol and PCR in Brazane et al. 2023). The following PCR primers were used, with the forward primer carrying the Kozac sequence and translation initiation codon to allow entry into the Gateway entry vector and expression of the construct in eukaryotic cells.

Forward AGO2 + Kozac: CACCATGGTGGACCCCGGAACCGTG,

Reverse AGO2: AAATCATAGCTGATCATGGAA

PCR products were purified using QIAquick Gel Extraction Kit (28706 Qiagen), and cloned into a Pentr-TOPO-D plasmid compatible with the Gateway cloning system. Entry vector was then recombined using LR Clonase II (Termofisher) into an expression vector carrying an in-frame C-terminal triple flag (pAWF), or GFP etiquette (pAWG). Reading frame maintenance was verified using sanger sequencing along the way.

References

Abbasi-Moheb, Lia, Sara Mertel, Melanie Gonsior, Leyla Nouri-Vahid, Kimia Kahrizi, Sebahattin Cirak, Dagmar Wieczorek, et al. 2012. “Mutations in NSUN2 Cause Autosomal-Recessive Intellectual Disability.” *American Journal of Human Genetics* 90 (5): 847–55.

Abou Assi, Hala, Atul K. Rangadurai, Honglue Shi, Bei Liu, Mary C. Clay, Kevin Erharter, Christoph Kreutz, Christopher L. Holley, and Hashim m. Al-Hashimi. 2020. “2′-O-Methylation Can Increase the Abundance and Lifetime of Alternative RNA Conformational States.” *Nucleic Acids Research* 48 (21): 12365–79.

Agrawal, Neema, P. V. N. Dasaradhi, Asif Mohmmed, Pawan Malhotra, Raj K. Bhatnagar, and Sunil K. Mukherjee. 2003. “RNA Interference: Biology, Mechanism, and Applications.” *Microbiology and Molecular Biology Reviews: MMBR* 67 (4): 657–85.

Aitken, Colin Echeverría, and Jon R. Lorsch. 2012. “A Mechanistic Overview of Translation Initiation in Eukaryotes.” *Nature Structural & Molecular Biology* 19 (6): 568–76.

Alexandrov, Andrei, Irina Chernyakov, Weifeng Gu, Shawna L. Hiley, Timothy R. Hughes, Elizabeth J. Grayhack, and Eric M. Phizicky. 2006. “Rapid tRNA Decay Can Result from Lack of Nonessential Modifications.” *Molecular Cell* 21 (1): 87–96.

Altwegg, M., and E. Kubli. 1979. “The Nucleotide Sequence of Phenylalanine tRNA2 of Drosophila Melanogaster: Four Isoacceptors with One Basic Sequence.” *Nucleic Acids Research* 7 (1): 93–105.

Ambros, V. 2000. “Control of Developmental Timing in Caenorhabditis Elegans.” *Current Opinion in Genetics & Development* 10 (4): 428–33.

Anderson, Paul, and Pavel Ivanov. 2014. “tRNA Fragments in Human Health and Disease.” *FEBS Letters* 588 (23): 4297–4304.

Anders, Simon, Paul Theodor Pyl, and Wolfgang Huber. 2015. “HTSeq--a Python Framework to Work with High-Throughput Sequencing Data.” *Bioinformatics* 31 (2): 166–69.

Angelova, Margarita T., Dilyana G. Dimitrova, Bruno Da Silva, Virginie Marchand, Caroline Jacquier, Cyrinne Achour, Mira Brazane, et al. 2020. “tRNA 2’-O-Methylation by a Duo of TRM7/FTSJ1 Proteins Modulates Small RNA Silencing in Drosophila.” *Nucleic Acids Research* 48 (4): 2050–72.

Angelova, Margarita T., Dilyana G. Dimitrova, Nadja Dinges, Tina Lence, Lina Worpenberg, Clément Carré, and Jean-Yves Roignant. 2018. “The Emerging Field of Epitranscriptomics in Neurodevelopmental and Neuronal Disorders.” *Frontiers in Bioengineering and Biotechnology* 6 (April): 46.

Aravin, A. A., N. M. Naumova, A. V. Tulin, V. V. Vagin, Y. M. Rozovsky, and V. A. Gvozdev. 2001. “Double-Stranded RNA-Mediated Silencing of Genomic Tandem Repeats and Transposable Elements in the D. Melanogaster Germline.” *Current Biology: CB* 11 (13): 1017–27.

Baglio, Serena Rubina, Koos Rooijers, Danijela Koppers-Lalic, Frederik J. Verweij, M. Pérez Lanzón, Nicoletta Zini, Benno Naaijkens, et al. 2015. “Human Bone Marrow- and Adipose-Mesenchymal Stem Cells Secrete Exosomes Enriched in Distinctive miRNA and tRNA Species.” *Stem Cell Research & Therapy* 6 (1): 127.

Balakin, A. G., L. Smith, and M. J. Fournier. 1996. “The RNA World of the Nucleolus: Two Major Families of Small RNAs Defined by Different Box Elements with Related Functions.” *Cell* 86 (5): 823–34.

Bartoli, Kristen M., Cassandra Schaening, Thomas M. Carlile, and Wendy V. Gilbert. 2018. “Conserved Methyltransferase Spb1 Targets mRNAs for Regulated Modification with 2′-O-Methyl Ribose.” *bioRxiv*. https://doi.org/10.1101/271916.

Batki, Julia, Jakob Schnabl, Juncheng Wang, Dominik Handler, Veselin I. Andreev, Christian E. Stieger, Maria Novatchkova, et al. 2019. “The Nascent RNA Binding Complex SFiNX Licenses piRNA-Guided Heterochromatin Formation.” *Nature Structural & Molecular Biology* 26 (8): 720–31.

Begik, Oguzhan, Morghan C. Lucas, Huanle Liu, Jose Miguel Ramirez, John S. Mattick, and Eva Maria Novoa. 2020. “Integrative Analyses of the RNA Modification Machinery Reveal Tissue- and Cancer-Specific Signatures.” *Genome Biology* 21 (1): 97.

Behm-Ansmant, Isabelle, Jan Rehwinkel, Tobias Doerks, Alexander Stark, Peer Bork, and

Elisa Izaurralde. 2006. “mRNA Degradation by miRNAs and GW182 Requires Both CCR4:NOT Deadenylase and DCP1:DCP2 Decapping Complexes.” *Genes & Development* 20 (14): 1885–98.
Bélanger, François, Janusz Stepinski, Edward Darzynkiewicz, and Jerry Pelletier. 2010. “Characterization of hMTr1, a Human Cap1 2’-O-Ribose Methyltransferase.” *The Journal of Biological Chemistry* 285 (43): 33037–44.
Bernstein, E., A. A. Caudy, S. M. Hammond, and G. J. Hannon. 2001. “Role for a Bidentate Ribonuclease in the Initiation Step of RNA Interference.” *Nature* 409 (6818): 363–66.
Betat, Heike, and Mario Mörl. 2015. “The CCA-Adding Enzyme: A Central Scrutinizer in tRNA Quality Control.” *BioEssays: News and Reviews in Molecular, Cellular and Developmental Biology* 37 (9): 975–82.
Bhaskaran, M., and M. Mohan. 2014. “MicroRNAs: History, Biogenesis, and Their Evolving Role in Animal Development and Disease.” *Veterinary Pathology* 51 (4): 759–74.
Bidou, L., I. Hatin, N. Perez, V. Allamand, J-J Panthier, and J-P Rousset. 2004. “Premature Stop Codons Involved in Muscular Dystrophies Show a Broad Spectrum of Readthrough Efficiencies in Response to Gentamicin Treatment.” *Gene Therapy* 11 (7): 619–27.
Blanchet, Sandra, David Cornu, Isabelle Hatin, Henri Grosjean, Pierre Bertin, and Olivier Namy. 2018. “Deciphering the Reading of the Genetic Code by near-Cognate tRNA.” *Proceedings of the National Academy of Sciences of the United States of America* 115 (12): 3018–23.
Blanco, Sandra, Sabine Dietmann, Joana V. Flores, Shobbir Hussain, Claudia Kutter, Peter Humphreys, Margus Lukk, et al. 2014. “Aberrant Methylation of tRNAs Links Cellular Stress to Neuro-Developmental Disorders.” *The EMBO Journal* 33 (18): 2020–39.
Boccaletto, Pietro, Filip Stefaniak, Angana Ray, Andrea Cappannini, Sunandan Mukherjee, Elżbieta Purta, Małgorzata Kurkowska, et al. 2022. “MODOMICS: A Database of RNA Modification Pathways. 2021 Update.” *Nucleic Acids Research* 50 (D1): D231–35.
Boczonadi, Veronika, Juliane S. Müller, Angela Pyle, Jennifer Munkley, Talya Dor, Jade Quartararo, Ileana Ferrero, et al. 2014. “EXOSC8 Mutations Alter mRNA Metabolism and Cause Hypomyelination with Spinal Muscular Atrophy and Cerebellar Hypoplasia.” *Nature Communications* 5 (July): 4287.
Bohmert, K., I. Camus, C. Bellini, D. Bouchez, M. Caboche, and C. Benning. 1998. “AGO1 Defines a Novel Locus of Arabidopsis Controlling Leaf Development.” *The EMBO Journal* 17 (1): 170–80.
Bohnsack, Katherine E., Nicole Kleiber, Nicolas Lemus-Diaz, and Markus T. Bohnsack. 2022. “Roles and Dynamics of 3-Methylcytidine in Cellular RNAs.” *Trends in Biochemical Sciences* 47 (7): 596–608.
Bonnet, C., M. J. Grégoire, K. Brochet, E. Raffo, B. Leheup, and P. Jonveaux. 2006. “Pure de-Novo 5 Mb Duplication at Xp11.22-p11.23 in a Male: Phenotypic and Molecular Characterization.” *Journal of Human Genetics* 51 (9): 815.
Braun, Daniela A., Jia Rao, Geraldine Mollet, David Schapiro, Marie-Claire Daugeron, Weizhen Tan, Olivier Gribouval, et al. 2017. “Mutations in KEOPS-Complex Genes Cause Nephrotic Syndrome with Primary Microcephaly.” *Nature Genetics* 49 (10): 1529–38.
Braun, Joerg E., Eric Huntzinger, Maria Fauser, and Elisa Izaurralde. 2011. “GW182 Proteins Directly Recruit Cytoplasmic Deadenylase Complexes to miRNA Targets.” *Molecular Cell* 44 (1): 120–33.
Brazane, Mira, Dilyana G. Dimitrova, Julien Pigeon, Chiara Paolantoni, Tao Ye, Virginie Marchand, Bruno Da Silva, et al. 2023. “The Ribose Methylation Enzyme FTSJ1 Has a Conserved Role in Neuron Morphology and Learning Performance.” *Life Science Alliance* 6 (4). https://doi.org/10.26508/lsa.202201877.
Brennecke, Julius, Alexei A. Aravin, Alexander Stark, Monica Dus, Manolis Kellis, Ravi Sachidanandam, and Gregory J. Hannon. 2007. “Discrete Small RNA-Generating Loci as Master Regulators of Transposon Activity in Drosophila.” *Cell* 128 (6): 1089–1103.
Brennecke, Julius, Alexander Stark, Robert B. Russell, and Stephen M. Cohen. 2005. “Principles of microRNA-Target Recognition.” *PLoS Biology* 3 (3): e85.

Bügl, H., E. B. Fauman, B. L. Staker, F. Zheng, S. R. Kushner, M. A. Saper, J. C. Bardwell, and U. Jakob. 2000. “RNA Methylation under Heat Shock Control.” *Molecular Cell* 6 (2): 349–60.

Caldas, T., E. Binet, P. Bouloc, A. Costa, J. Desgres, and G. Richarme. 2000. “The FtsJ/RrmJ Heat Shock Protein of Escherichia Coli Is a 23 S Ribosomal RNA Methyltransferase.” *The Journal of Biological Chemistry* 275 (22): 16414–19.

Cao, Thuy, Sheeja Rajasingh, Saheli Samanta, Buddhadeb Dawn, Douglas C. Bittel, and Johnson Rajasingh. 2018. “Biology and Clinical Relevance of Noncoding sno/scaRNAs.” *Trends in Cardiovascular Medicine* 28 (2): 81–90.

Carlson, B. A., S. Y. Kwon, M. Chamorro, S. Oroszlan, D. L. Hatfield, and B. J. Lee. 1999. “Transfer RNA Modification Status Influences Retroviral Ribosomal Frameshifting.” *Virology* 255 (1): 2–8.

Carollo, Pietro Salvatore, Marco Tutone, Giulia Culletta, Ignazio Fiduccia, Federica Corrao, Ivana Pibiri, Aldo Di Leonardo, et al. 2023. “Investigating the Inhibition of FTSJ1, a Tryptophan tRNA-Specific 2’-O-Methyltransferase by NV TRIDs, as a Mechanism of Readthrough in Nonsense Mutated CFTR.” *International Journal of Molecular Sciences* 24 (11). https://doi.org/10.3390/ijms24119609.

Carré, Clément, Caroline Jacquier, Anne-Laure Bougé, Fabrice de Chaumont, Corinne Besnard-Guerin, Hélène Thomassin, Josette Pidoux, et al. 2013. “AutomiG, a Biosensor to Detect Alterations in miRNA Biogenesis and in Small RNA Silencing Guided by Perfect Target Complementarity.” *PloS One* 8 (9): e74296.

Casier, Karine, Julie Autaa, Nathalie Gueguen, Valérie Delmarre, Pauline P. Marie, Stéphane Ronsseray, Clément Carré, Emilie Brasset, Laure Teysset, and Antoine Boivin. 2023. “The Histone Demethylase Kdm3 Prevents Auto-Immune piRNAs Production in Drosophila.” *Science Advances* 9 (14): eade3872.

Cavaillé, J., F. Chetouani, and J. P. Bachellerie. 1999. “The Yeast Saccharomyces Cerevisiae YDL112w ORF Encodes the Putative 2’-O-Ribose Methyltransferase Catalyzing the Formation of Gm18 in tRNAs.” *RNA* 5 (1): 66–81.

Cavaillé, J., M. Nicoloso, and J. P. Bachellerie. 1996. “Targeted Ribose Methylation of RNA in Vivo Directed by Tailored Antisense RNA Guides.” *Nature* 383 (6602): 732–35.

Cenik, Elif Sarinay, and Phillip D. Zamore. 2011. “Argonaute Proteins.” *Current Biology: CB* 21 (12): R446–49.

Cesaro, Bianca, Marco Tarullo, and Alessandro Fatica. 2023. “Regulation of Gene Expression by m6Am RNA Modification.” *International Journal of Molecular Sciences* 24 (3). https://doi.org/10.3390/ijms24032277.

Chalker, Douglas L., and Meng-Chao Yao. 2011. “DNA Elimination in Ciliates: Transposon Domestication and Genome Surveillance.” *Annual Review of Genetics* 45 (September): 227–46.

Chan, Clarence W., Bhaskar Chetnani, and Alfonso Mondragón. 2013. “Structure and Function of the T-Loop Structural Motif in Noncoding RNAs.” *Wiley Interdisciplinary Reviews. RNA* 4 (5): 507–22.

Chen, Caifu, Dana A. Ridzon, Adam J. Broomer, Zhaohui Zhou, Danny H. Lee, Julie T. Nguyen, Maura Barbisin, et al. 2005. “Real-Time Quantification of microRNAs by Stem-Loop RT-PCR.” *Nucleic Acids Research* 33 (20): e179.

Chen, Xuemei. 2010. “Small RNAs - Secrets and Surprises of the Genome.” *The Plant Journal: For Cell and Molecular Biology* 61 (6): 941–58.

Chen, Yu, and Deyin Guo. 2016. “Molecular Mechanisms of Coronavirus RNA Capping and Methylation.” *Virologica Sinica* 31 (1): 3–11.

Chernyakov, Irina, Joseph M. Whipple, Lakmal Kotelawala, Elizabeth J. Grayhack, and Eric M. Phizicky. 2008. “Degradation of Several Hypomodified Mature tRNA Species in Saccharomyces Cerevisiae Is Mediated by Met22 and the 5’-3' Exonucleases Rat1 and Xrn1.” *Genes & Development* 22 (10): 1369–80.

Chou, Hsin-Jung, Elisa Donnard, H. Tobias Gustafsson, Manuel Garber, and Oliver J. Rando. 2017. “Transcriptome-Wide Analysis of Roles for tRNA Modifications in Translational Regulation.” *Molecular Cell* 68 (5): 978–92.e4.

Cobb, Matthew. 2017. “60 Years Ago, Francis Crick Changed the Logic of Biology.” *PLoS Biology* 15 (9): e2003243.
Cohn, Waldo E., and Elliot Volkin. 1951. “Nucleoside-5′-Phosphates from Ribonucleic Acid.” *Nature* 167 (4247): 483–84.
Cole, Christian, Andrew Sobala, Cheng Lu, Shawn R. Thatcher, Andrew Bowman, John W. S. Brown, Pamela J. Green, Geoffrey J. Barton, and Gyorgy Hutvagner. 2009. “Filtering of Deep Sequencing Data Reveals the Existence of Abundant Dicer-Dependent Small RNAs Derived from tRNAs.” *RNA* 15 (12): 2147–60.
Costa, Bruno, Marco Li Calzi, Mauricio Castellano, Valentina Blanco, Ernesto Cuevasanta, Irene Litvan, Pavel Ivanov, Kenneth Witwer, Alfonso Cayota, and Juan Pablo Tosar. 2023. “Nicked tRNAs Are Stable Reservoirs of tRNA Halves in Cells and Biofluids.” *Proceedings of the National Academy of Sciences of the United States of America* 120 (4): e2216330120.
Cuypers, Maarten, Bianca W. M. Schalk, Anne J. N. Boonman, Jenneken Naaldenberg, and Geraline L. Leusink. 2022. “Cancer-Related Mortality among People with Intellectual Disabilities: A Nationwide Population-Based Cohort Study.” *Cancer* 128 (6): 1267–74.
Czech, Benjamin, Colin D. Malone, Rui Zhou, Alexander Stark, Catherine Schlingeheyde, Monica Dus, Norbert Perrimon, et al. 2008. “An Endogenous Small Interfering RNA Pathway in Drosophila.” *Nature* 453 (7196): 798–802.
Dabrowski, Maciej, Zuzanna Bukowy-Bieryllo, and Ewa Zietkiewicz. 2015. “Translational Readthrough Potential of Natural Termination Codons in Eucaryotes--The Impact of RNA Sequence.” *RNA Biology* 12 (9): 950–58.
Daily, D. K., H. H. Ardinger, and G. E. Holmes. 2000. “Identification and Evaluation of Mental Retardation.” *American Family Physician* 61 (4): 1059–67, 1070.
Dai, Qing, Sharon Moshitch-Moshkovitz, Dali Han, Nitzan Kol, Ninette Amariglio, Gideon Rechavi, Dan Dominissini, and Chuan He. 2018. “Corrigendum: Nm-Seq Maps 2’-O-Methylation Sites in Human mRNA with Base Precision.” *Nature Methods* 15 (3): 226–27.
Dalluge, J. J., T. Hashizume, A. E. Sopchik, J. A. McCloskey, and D. R. Davis. 1996. “Conformational Flexibility in RNA: The Role of Dihydrouridine.” *Nucleic Acids Research* 24 (6): 1073–79.
Davis, F. F., and F. W. Allen. 1957. “Ribonucleic Acids from Yeast Which Contain a Fifth Nucleotide.” *The Journal of Biological Chemistry* 227 (2): 907–15.
Deng, Junfang, Ryan N. Ptashkin, Yu Chen, Zhi Cheng, Guangliang Liu, Thien Phan, Xiaoling Deng, et al. 2015. “Respiratory Syncytial Virus Utilizes a tRNA Fragment to Suppress Antiviral Responses Through a Novel Targeting Mechanism.” *Molecular Therapy: The Journal of the American Society of Gene Therapy* 23 (10): 1622–29.
Denli, Ahmet M., Bastiaan B. J. Tops, Ronald H. A. Plasterk, René F. Ketting, and Gregory J. Hannon. 2004. “Processing of Primary microRNAs by the Microprocessor Complex.” *Nature* 432 (7014): 231–35.
Desnick, R. J., and A. M. Wang. 1990. “Schindler Disease: An Inherited Neuroaxonal Dystrophy due to Alpha-N-Acetylgalactosaminidase Deficiency.” *Journal of Inherited Metabolic Disease* 13 (4): 549–59.
Dever, Thomas E., Jonathan D. Dinman, and Rachel Green. 2018. “Translation Elongation and Recoding in Eukaryotes.” *Cold Spring Harbor Perspectives in Biology* 10 (8). https://doi.org/10.1101/cshperspect.a032649.
Di Fazio, Arianna, Margarita Schlackow, Sheng Kai Pong, Adele Alagia, and Monika Gullerova. 2022. “Dicer Dependent tRNA Derived Small RNAs Promote Nascent RNA Silencing.” *Nucleic Acids Research* 50 (3): 1734–52.
Dimitrova, Dilyana G., Laure Teysset, and Clément Carré. 2019. “RNA 2’-O-Methylation (Nm) Modification in Human Diseases.” *Genes* 10 (2). https://doi.org/10.3390/genes10020117.
Duan, Ye, Li Li, Ganesh Prabhakar Panzade, Amélie Piton, Anna Zinovyeva, and Victor Ambros. 2023. “Modeling Neurodevelopmental Disorder-Associated hAGO1 Mutations in C. Elegans Argonaute ALG-1.” *bioRxiv*. https://doi.org/10.1101/2023.04.06.535748.
Dubrovsky, Edward B., Veronica A. Dubrovskaya, Louis Levinger, Steffen Schiffer, and Anita

Marchfelder. 2004. “Drosophila RNase Z Processes Mitochondrial and Nuclear Pre-tRNA 3’ Ends in Vivo.” *Nucleic Acids Research* 32 (1): 255–62.
Durdevic, Zeljko, Mehrpouya Balaghy Mobin, Katharina Hanna, Frank Lyko, and Matthias Schaefer. 2013. “The RNA Methyltransferase Dnmt2 Is Required for Efficient Dicer-2-Dependent siRNA Pathway Activity in Drosophila.” *Cell Reports* 4 (5): 931–37.
Durdevic, Zeljko, and Matthias Schaefer. 2013. “tRNA Modifications: Necessary for Correct tRNA-Derived Fragments during the Recovery from Stress?” *BioEssays: News and Reviews in Molecular, Cellular and Developmental Biology* 35 (4): 323–27.
Edvardson, Simon, Laurence Prunetti, Aiman Arraf, Drago Haas, Jo Marie Bacusmo, Jennifer F. Hu, Asas Ta-Shma, Peter C. Dedon, Valérie de Crécy-Lagard, and Orly Elpeleg. 2017. “tRNA N6-Adenosine Threonylcarbamoyltransferase Defect due to KAE1/TCS3 (OSGEP) Mutation Manifest by Neurodegeneration and Renal Tubulopathy.” *European Journal of Human Genetics: EJHG* 25 (5): 545–51.
Elalaoui, Siham Chafai, Fatima Zahra Laarabi, Maria Mansouri, Nidal Alaoui Mrani, Gen Nishimura, and Abdelaziz Sefiani. 2016. “Further Evidence of POP1 Mutations as the Cause of Anauxetic Dysplasia.” *American Journal of Medical Genetics. Part A* 170 (9): 2462–65.
Elbashir, S. M., W. Lendeckel, and T. Tuschl. 2001. “RNA Interference Is Mediated by 21- and 22-Nucleotide RNAs.” *Genes & Development* 15 (2): 188–200.
El-Hattab, A. W., J. Bournat, P. A. Eng, J. B. S. Wu, B. A. Walker, P. Stankiewicz, S. W. Cheung, and C. W. Brown. 2011. “Microduplication of Xp11.23p11.3 with Effects on Cognition, Behavior, and Craniofacial Development.” *Clinical Genetics* 79 (6): 531–38.
Elkayam, Elad, Claus-D Kuhn, Ante Tocilj, Astrid D. Haase, Emily M. Greene, Gregory J. Hannon, and Leemor Joshua-Tor. 2012. “The Structure of Human Argonaute-2 in Complex with miR-20a.” *Cell* 150 (1): 100–110.
Elliott, Brittany A., Hsiang-Ting Ho, Srivathsan V. Ranganathan, Sweta Vangaveti, Olga Ilkayeva, Hala Abou Assi, Alex K. Choi, Paul F. Agris, and Christopher L. Holley. 2019. “Modification of Messenger RNA by 2’-O-Methylation Regulates Gene Expression in Vivo.” *Nature Communications* 10 (1): 3401.
El Yacoubi, Basma, Benjamin Lyons, Yulien Cruz, Robert Reddy, Brian Nordin, Fabio Agnelli, James R. Williamson, Paul Schimmel, Manal A. Swairjo, and Valérie de Crécy-Lagard. 2009. “The Universal YrdC/Sua5 Family Is Required for the Formation of Threonylcarbamoyladenosine in tRNA.” *Nucleic Acids Research* 37 (9): 2894–2909.
Ender, Christine, and Gunter Meister. 2010. “Argonaute Proteins at a Glance.” *Journal of Cell Science* 123 (Pt 11): 1819–23.
Eswarappa, Sandeepa M., Alka A. Potdar, William J. Koch, Yi Fan, Kommireddy Vasu, Daniel Lindner, Belinda Willard, Linda M. Graham, Paul E. DiCorleto, and Paul L. Fox. 2014. “Programmed Translational Readthrough Generates Antiangiogenic VEGF-Ax.” *Cell* 157 (7): 1605–18.
Fabry, Martin H., Federica A. Falconio, Fadwa Joud, Emily K. Lythgoe, Benjamin Czech, and Gregory J. Hannon. 2021. “Maternally Inherited piRNAs Direct Transient Heterochromatin Formation at Active Transposons during Early Drosophila Embryogenesis.” *eLife* 10 (July). https://doi.org/10.7554/eLife.68573.
Farkas, W. R. 1980. “Effect of Diet on the Queuosine Family of tRNAs of Germ-Free Mice.” *The Journal of Biological Chemistry* 255 (14): 6832–35.
Feder, Marcin, Jakub Pas, Lucjan S. Wyrwicz, and Janusz M. Bujnicki. 2003. “Molecular Phylogenetics of the RrmJ/fibrillarin Superfamily of Ribose 2’-O-Methyltransferases.” *Gene* 302 (1-2): 129–38.
Fire, A., D. Albertson, S. W. Harrison, and D. G. Moerman. 1991. “Production of Antisense RNA Leads to Effective and Specific Inhibition of Gene Expression in C. Elegans Muscle.” *Development* 113 (2): 503–14.
Fire, A., S. Xu, M. K. Montgomery, S. A. Kostas, S. E. Driver, and C. C. Mello. 1998. “Potent and Specific Genetic Interference by Double-Stranded RNA in Caenorhabditis Elegans.” *Nature* 391 (6669): 806–11.
Förstemann, Klaus, Michael D. Horwich, Liangmeng Wee, Yukihide Tomari, and Phillip D.

Zamore. 2007. “Drosophila microRNAs Are Sorted into Functionally Distinct Argonaute Complexes after Production by Dicer-1.” *Cell* 130 (2): 287–97.
François, Pauline, Hugo Arbes, Stéphane Demais, Agnès Baudin-Baillieu, and Olivier Namy. 2021. “RiboDoc: A Docker-Based Package for Ribosome Profiling Analysis.” *Computational and Structural Biotechnology Journal* 19 (May): 2851–60.
Freude, Kristine, Kirsten Hoffmann, Lars-Riff Jensen, Martin B. Delatycki, Vincent des Portes, Bettina Moser, Ben Hamel, et al. 2004. “Mutations in the FTSJ1 Gene Coding for a Novel S-Adenosylmethionine-Binding Protein Cause Nonsyndromic X-Linked Mental Retardation.” *American Journal of Human Genetics* 75 (2): 305–9.
Froyen, Guy, Marijke Bauters, Jackie Boyle, Hilde Van Esch, Karen Govaerts, Hans van Bokhoven, Hans-Hilger Ropers, et al. 2007. “Loss of SLC38A5 and FTSJ1 at Xp11.23 in Three Brothers with Non-Syndromic Mental Retardation due to a Microdeletion in an Unstable Genomic Region.” *Human Genetics* 121 (5): 539–47.
Fu, Hanjiang, Junjun Feng, Qin Liu, Fang Sun, Yi Tie, Jie Zhu, Ruiyun Xing, Zhixian Sun, and Xiaofei Zheng. 2009. “Stress Induces tRNA Cleavage by Angiogenin in Mammalian Cells.” *FEBS Letters* 583 (2): 437–42.
Funk, Holly M., Daisy J. DiVita, Hannah E. Sizemore, Kendal Wehrle, Catherine L. W. Miller, Morgan E. Fraley, Alex K. Mullins, Adrian R. Guy, Eric M. Phizicky, and Michael P. Guy. 2022. “Identification of a Trm732 Motif Required for 2’-O-Methylation of the tRNA Anticodon Loop by Trm7.” *ACS Omega* 7 (16): 13667–75.
Gerber, Janina L., Sandra Köhler, and Jirka Peschek. 2022. “Eukaryotic tRNA Splicing - One Goal, Two Strategies, Many Players.” *Biological Chemistry* 403 (8-9): 765–78.
Geschwind, Daniel H., and Pat Levitt. 2007. “Autism Spectrum Disorders: Developmental Disconnection Syndromes.” *Current Opinion in Neurobiology* 17 (1): 103–11.
Ghildiyal, Megha, Hervé Seitz, Michael D. Horwich, Chengjian Li, Tingting Du, Soohyun Lee, Jia Xu, et al. 2008. “Endogenous siRNAs Derived from Transposons and mRNAs in Drosophila Somatic Cells.” *Science* 320 (5879): 1077–81.
Ghildiyal, Megha, and Phillip D. Zamore. 2009. “Small Silencing RNAs: An Expanding Universe.” *Nature Reviews. Genetics* 10 (2): 94–108.
Ghosh, Agnidipta, and Christopher D. Lima. 2010. “Enzymology of RNA Cap Synthesis.” *Wiley Interdisciplinary Reviews. RNA* 1 (1): 152–72.
Ghosh, Souvik, Joao C. Guimaraes, Manuela Lanzafame, Alexander Schmidt, Afzal Pasha Syed, Beatrice Dimitriades, Anastasiya Börsch, et al. 2020. “Prevention of dsRNA-Induced Interferon Signaling by AGO1x Is Linked to Breast Cancer Cell Proliferation.” *The EMBO Journal* 39 (18): e103922.
Glasser, A. L., C. el Adlouni, G. Keith, E. Sochacka, A. Malkiewicz, M. Santos, M. F. Tuite, and J. Desgrès. 1992. “Presence and Coding Properties of 2’-O-Methyl-5-Carbamoylmethyluridine (ncm5Um) in the Wobble Position of the Anticodon of tRNA(Leu) (U*AA) from Brewer's Yeast.” *FEBS Letters* 314 (3): 381–85.
Glazov, Evgeny A., Andreas Zankl, Marina Donskoi, Tony J. Kenna, Gethin P. Thomas, Graeme R. Clark, Emma L. Duncan, and Matthew A. Brown. 2011. “Whole-Exome Re-Sequencing in a Family Quartet Identifies POP1 Mutations as the Cause of a Novel Skeletal Dysplasia.” *PLoS Genetics* 7 (3): e1002027.
Gong, Pingyuan, Jing Li, Ling Dai, Kejin Zhang, Zijian Zheng, Xiaocai Gao, and Fuchang Zhang. 2008. “Genetic Variations in FTSJ1 Influence Cognitive Ability in Young Males in the Chinese Han Population.” *Journal of Neurogenetics* 22 (4): 277–87.
Gonzalez-Perez, Vivian, and Christopher J. Lingle. 2019. “Regulation of BK Channels by Beta and Gamma Subunits.” *Annual Review of Physiology* 81 (February): 113–37.
Graille, Marc. 2022. “Division of Labor in Epitranscriptomics: What Have We Learnt from the Structures of Eukaryotic and Viral Multimeric RNA Methyltransferases?” *Wiley Interdisciplinary Reviews. RNA* 13 (1): e1673.
Green, Eric D., James D. Watson, and Francis S. Collins. 2015. “Human Genome Project: Twenty-Five Years of Big Biology.” *Nature* 526 (7571): 29–31.
Greer, C. L., C. L. Peebles, P. Gegenheimer, and J. Abelson. 1983. “Mechanism of Action of a Yeast RNA Ligase in tRNA Splicing.” *Cell* 32 (2): 537–46.

Grosjean, Henri. 2015. “RNA Modification: The Golden Period 1995-2015.” *RNA* 21 (4): 625–26.
Grosjean, Henri, Gérard Keith, and Louis Droogmans. 2004. “Detection and Quantification of Modified Nucleotides in RNA Using Thin-Layer Chromatography.” *Methods in Molecular Biology* 265: 357–91.
Guy, Michael P., and Eric M. Phizicky. 2015. “Conservation of an Intricate Circuit for Crucial Modifications of the tRNAPhe Anticodon Loop in Eukaryotes.” *RNA* 21 (1): 61–74.
Guy, Michael P., Brandon M. Podyma, Melanie A. Preston, Hussam H. Shaheen, Kady L. Krivos, Patrick A. Limbach, Anita K. Hopper, and Eric M. Phizicky. 2012. “Yeast Trm7 Interacts with Distinct Proteins for Critical Modifications of the tRNAPhe Anticodon Loop.” *RNA* 18 (10): 1921–33.
Guy, Michael P., Marie Shaw, Catherine L. Weiner, Lynne Hobson, Zornitza Stark, Katherine Rose, Vera M. Kalscheuer, Jozef Gecz, and Eric M. Phizicky. 2015. “Defects in tRNA Anticodon Loop 2’-O-Methylation Are Implicated in Nonsyndromic X-Linked Intellectual Disability due to Mutations in FTSJ1.” *Human Mutation* 36 (12): 1176–87.
Hamilton, A. J., and D. C. Baulcombe. 1999. “A Species of Small Antisense RNA in Posttranscriptional Gene Silencing in Plants.” *Science*.
Han, Lu, Michael P. Guy, Yoshiko Kon, and Eric M. Phizicky. 2018. “Lack of 2’-O-Methylation in the tRNA Anticodon Loop of Two Phylogenetically Distant Yeast Species Activates the General Amino Acid Control Pathway.” *PLoS Genetics* 14 (3): e1007288.
Hardt, W. D., J. Schlegl, V. A. Erdmann, and R. K. Hartmann. 1993. “Role of the D Arm and the Anticodon Arm in tRNA Recognition by Eubacterial and Eukaryotic RNase P Enzymes.” *Biochemistry* 32 (48): 13046–53.
Harigaya, Yuriko, and Roy Parker. 2010. “No-Go Decay: A Quality Control Mechanism for RNA in Translation.” *Wiley Interdisciplinary Reviews. RNA* 1 (1): 132–41.
Haruehanroengra, Phensinee, Ya Ying Zheng, Yubin Zhou, Yun Huang, and Jia Sheng. 2020. “RNA Modifications and Cancer.” *RNA Biology* 17 (11): 1560–75.
Haussecker, Dirk, Yong Huang, Ashley Lau, Poornima Parameswaran, Andrew Z. Fire, and Mark A. Kay. 2010. “Human tRNA-Derived Small RNAs in the Global Regulation of RNA Silencing.” *RNA* 16 (4): 673–95.
Hellen, Christopher U. T. 2018. “Translation Termination and Ribosome Recycling in Eukaryotes.” *Cold Spring Harbor Perspectives in Biology* 10 (10). https://doi.org/10.1101/cshperspect.a032656.
He, Qihan, Lin Yang, Kaiping Gao, Peikun Ding, Qianqian Chen, Juan Xiong, Wenhan Yang, et al. 2020. “Correction: FTSJ1 Regulates tRNA 2’-O-Methyladenosine Modification and Suppresses the Malignancy of NSCLC via Inhibiting DRAM1 Expression.” *Cell Death & Disease* 11 (6): 418.
Hinnebusch, Alan G. 2011. “Molecular Mechanism of Scanning and Start Codon Selection in Eukaryotes.” *Microbiology and Molecular Biology Reviews: MMBR* 75 (3): 434–67, first page of table of contents.
Hirata, Akira, Keisuke Okada, Kazuaki Yoshii, Hiroyuki Shiraishi, Shinya Saijo, Kento Yonezawa, Nobutaka Shimizu, and Hiroyuki Hori. 2019. “Structure of tRNA Methyltransferase Complex of Trm7 and Trm734 Reveals a Novel Binding Interface for tRNA Recognition.” *Nucleic Acids Research* 47 (20): 10942–55.
Höck, Julia, and Gunter Meister. 2008. “The Argonaute Protein Family.” *Genome Biology* 9 (2): 210.
Hoernes, Thomas Philipp, Nina Clementi, Klaus Faserl, Heidelinde Glasner, Kathrin Breuker, Herbert Lindner, Alexander Hüttenhofer, and Matthias David Erlacher. 2016. “Nucleotide Modifications within Bacterial Messenger RNAs Regulate Their Translation and Are Able to Rewire the Genetic Code.” *Nucleic Acids Research* 44 (2): 852–62.
Hoernes, Thomas Philipp, and Matthias David Erlacher. 2017. “Translating the Epitranscriptome.” *Wiley Interdisciplinary Reviews. RNA* 8 (1). https://doi.org/10.1002/wrna.1375.
Hoernes, Thomas Philipp, David Heimdörfer, Daniel Köstner, Klaus Faserl, Felix Nußbaumer, Raphael Plangger, Christoph Kreutz, Herbert Lindner, and Matthias David Erlacher.

2019. “Eukaryotic Translation Elongation Is Modulated by Single Natural Nucleotide Derivatives in the Coding Sequences of mRNAs.” *Genes* 10 (2). https://doi.org/10.3390/genes10020084.
Holzer, Kerstin, Alessandro Ori, Amy Cooke, Daniel Dauch, Elisabeth Drucker, Philip Riemenschneider, Amparo Andres-Pons, et al. 2019. “Nucleoporin Nup155 Is Part of the p53 Network in Liver Cancer.” *Nature Communications* 10 (1): 2147.
Honda, Shozo, Shin Hayashi, Issei Imoto, Jun Toyama, Hitoshi Okazawa, Eiji Nakagawa, Yu-Ichi Goto, and Johji Inazawa. 2010. “Copy-Number Variations on the X Chromosome in Japanese Patients with Mental Retardation Detected by Array-Based Comparative Genomic Hybridization Analysis.” *Journal of Human Genetics* 55 (9): 590–99.
Hopper, Anita K., Dave A. Pai, and David R. Engelke. 2010. “Cellular Dynamics of tRNAs and Their Genes.” *FEBS Letters* 584 (2): 310–17.
Horwich, Michael D., Chengjian Li, Christian Matranga, Vasily Vagin, Gwen Farley, Peng Wang, and Phillip D. Zamore. 2007. “The Drosophila RNA Methyltransferase, DmHen1, Modifies Germline piRNAs and Single-Stranded siRNAs in RISC.” *Current Biology: CB* 17 (14): 1265–72.
Hou, Ya-Ming. 2010. “CCA Addition to tRNA: Implications for tRNA Quality Control.” *IUBMB Life* 62 (4): 251–60.
Hsu, Phillip J., Qili Fei, Qing Dai, Hailing Shi, Dan Dominissini, Lijia Ma, and Chuan He. 2019. “Single Base Resolution Mapping of 2’-O-Methylation Sites in Human mRNA and in 3' Terminal Ends of Small RNAs.” *Methods* 156 (March): 85–90.
Huang, Zheng-Hao, Yu-Ping Du, Jing-Tao Wen, Bing-Feng Lu, and Yang Zhao. 2022. “snoRNAs: Functions and Mechanisms in Biological Processes, and Roles in Tumor Pathophysiology.” *Cell Death Discovery* 8 (1): 259.
Hutvágner, G., J. McLachlan, A. E. Pasquinelli, E. Bálint, T. Tuschl, and P. D. Zamore. 2001. “A Cellular Function for the RNA-Interference Enzyme Dicer in the Maturation of the Let-7 Small Temporal RNA.” *Science* 293 (5531): 834–38.
Hutvagner, Gyorgy, and Martin J. Simard. 2008. “Argonaute Proteins: Key Players in RNA Silencing.” *Nature Reviews. Molecular Cell Biology* 9 (1): 22–32.
Incarnato, Danny, Francesca Anselmi, Edoardo Morandi, Francesco Neri, Mara Maldotti, Stefania Rapelli, Caterina Parlato, Giulia Basile, and Salvatore Oliviero. 2017. “High-Throughput Single-Base Resolution Mapping of RNA 2´-O-Methylated Residues.” *Nucleic Acids Research* 45 (3): 1433–41.
Indrieri, Alessia, Sabrina Carrella, Pietro Carotenuto, Sandro Banfi, and Brunella Franco. 2020. “The Pervasive Role of the miR-181 Family in Development, Neurodegeneration, and Cancer.” *International Journal of Molecular Sciences* 21 (6). https://doi.org/10.3390/ijms21062092.
Ipsaro, Jonathan J., Paul A. O’Brien, Shibani Bhattacharya, Arthur G. Palmer 3rd, and Leemor Joshua-Tor. 2021. “Asterix/Gtsf1 Links tRNAs and piRNA Silencing of Retrotransposons.” *Cell Reports* 34 (13): 108914.
Irwin, S. A., B. Patel, M. Idupulapati, J. B. Harris, R. A. Crisostomo, B. P. Larsen, F. Kooy, et al. 2001. “Abnormal Dendritic Spine Characteristics in the Temporal and Visual Cortices of Patients with Fragile-X Syndrome: A Quantitative Examination.” *American Journal of Medical Genetics* 98 (2): 161–67.
Ishimura, Ryuta, Gabor Nagy, Ivan Dotu, Huihao Zhou, Xiang-Lei Yang, Paul Schimmel, Satoru Senju, Yasuharu Nishimura, Jeffrey H. Chuang, and Susan L. Ackerman. 2014. “RNA Function. Ribosome Stalling Induced by Mutation of a CNS-Specific tRNA Causes Neurodegeneration.” *Science* 345 (6195): 455–59.
Ivanov, Pavel. 2015. “Emerging Roles of tRNA-Derived Fragments in Viral Infections: The Case of Respiratory Syncytial Virus.” *Molecular Therapy: The Journal of the American Society of Gene Therapy*. Elsevier.
Ivanov, Pavel, Mohamed M. Emara, Judit Villen, Steven P. Gygi, and Paul Anderson. 2011. “Angiogenin-Induced tRNA Fragments Inhibit Translation Initiation.” *Molecular Cell* 43 (4): 613–23.
Izant, J. G., and H. Weintraub. 1984. “Inhibition of Thymidine Kinase Gene Expression by

Anti-Sense RNA: A Molecular Approach to Genetic Analysis." *Cell* 36 (4): 1007–15.
Jády, B. E., and T. Kiss. 2001. "A Small Nucleolar Guide RNA Functions Both in 2'-O-Ribose Methylation and Pseudouridylation of the U5 Spliceosomal RNA." *The EMBO Journal* 20 (3): 541–51.
Jansen, Sandra, Lisenka E. L. M. Vissers, and Bert B. A. de Vries. 2023. "The Genetics of Intellectual Disability." *Brain Sciences* 13 (2). https://doi.org/10.3390/brainsci13020231.
Jensen, Lars R., Lillian Garrett, Sabine M. Hölter, Birgit Rathkolb, Ildikó Rácz, Thure Adler, Cornelia Prehn, et al. 2019. "A Mouse Model for Intellectual Disability Caused by Mutations in the X-Linked 2'-O-methyltransferase Ftsj1 Gene." *Biochimica et Biophysica Acta, Molecular Basis of Disease* 1865 (9): 2083–93.
Kanzaki, T., M. Yokota, N. Mizuno, Y. Matsumoto, and Y. Hirabayashi. 1989. "Novel Lysosomal Glycoaminoacid Storage Disease with Angiokeratoma Corporis Diffusum." *The Lancet* 1 (8643): 875–77.
Kaufmann, W. E., and H. W. Moser. 2000. "Dendritic Anomalies in Disorders Associated with Mental Retardation." *Cerebral Cortex* 10 (10): 981–91.
Kawarada, Layla, Takeo Suzuki, Takayuki Ohira, Shoji Hirata, Kenjyo Miyauchi, and Tsutomu Suzuki. 2017. "ALKBH1 Is an RNA Dioxygenase Responsible for Cytoplasmic and Mitochondrial tRNA Modifications." *Nucleic Acids Research* 45 (12): 7401–15.
Kazimierczyk, Marek, Marta Wojnicka, Ewa Biała, Paulina Żydowicz-Machtel, Barbara Imiołczyk, Tomasz Ostrowski, Anna Kurzyńska-Kokorniak, and Jan Wrzesinski. 2022. "Characteristics of Transfer RNA-Derived Fragments Expressed during Human Renal Cell Development: The Role of Dicer in tRF Biogenesis." *International Journal of Molecular Sciences* 23 (7). https://doi.org/10.3390/ijms23073644.
Keam, Simon P., Andrew Sobala, Sara Ten Have, and Gyorgy Hutvagner. 2017. "tRNA-Derived RNA Fragments Associate with Human Multisynthetase Complex (MSC) and Modulate Ribosomal Protein Translation." *Journal of Proteome Research* 16 (2): 413–20.
Kennerdell, J. R., and R. W. Carthew. 1998. "Use of dsRNA-Mediated Genetic Interference to Demonstrate That Frizzled and Frizzled 2 Act in the Wingless Pathway." *Cell* 95 (7): 1017–26.
Kerr, B., G. Turner, J. Mulley, A. Gedeon, and M. Partington. 1991. "Non-Specific X Linked Mental Retardation." *Journal of Medical Genetics* 28 (6): 378–82.
Ketting, R. F., S. E. Fischer, E. Bernstein, T. Sijen, G. J. Hannon, and R. H. Plasterk. 2001. "Dicer Functions in RNA Interference and in Synthesis of Small RNA Involved in Developmental Timing in C. Elegans." *Genes & Development* 15 (20): 2654–59.
Kim, Daehwan, Joseph M. Paggi, Chanhee Park, Christopher Bennett, and Steven L. Salzberg. 2019. "Graph-Based Genome Alignment and Genotyping with HISAT2 and HISAT-Genotype." *Nature Biotechnology* 37 (8): 907–15.
Kiss-László, Z., Y. Henry, J. P. Bachellerie, M. Caizergues-Ferrer, and T. Kiss. 1996. "Site-Specific Ribose Methylation of Preribosomal RNA: A Novel Function for Small Nucleolar RNAs." *Cell* 85 (7): 1077–88.
Komarov, Pavel A., Olesya Sokolova, Natalia Akulenko, Emilie Brasset, Silke Jensen, and Alla Kalmykova. 2020. "Epigenetic Requirements for Triggering Heterochromatinization and Piwi-Interacting RNA Production from Transgenes in the Drosophila Germline." *Cells* 9 (4). https://doi.org/10.3390/cells9040922.
Konevega, Andrey L., Natalia G. Soboleva, Valentin I. Makhno, Yuri P. Semenkov, Wolfgang Wintermeyer, Marina V. Rodnina, and Vladimir I. Katunin. 2004. "Purine Bases at Position 37 of tRNA Stabilize Codon-Anticodon Interaction in the Ribosomal A Site by Stacking and Mg2+-Dependent Interactions." *RNA* 10 (1): 90–101.
Koopal, Balwina, Sumanth K. Mutte, and Daan C. Swarts. 2023. "A Long Look at Short Prokaryotic Argonautes." *Trends in Cell Biology* 33 (7): 605–18.
Kotelawala, Lakmal, Elizabeth J. Grayhack, and Eric M. Phizicky. 2008. "Identification of Yeast tRNA Um(44) 2'-O-Methyltransferase (Trm44) and Demonstration of a Trm44 Role in Sustaining Levels of Specific tRNA(Ser) Species." *RNA* 14 (1): 158–69.
Krol, A. R. van der, L. A. Mur, M. Beld, J. N. Mol, and A. R. Stuitje. 1990. "Flavonoid Genes in

Petunia: Addition of a Limited Number of Gene Copies May Lead to a Suppression of Gene Expression." *The Plant Cell* 2 (4): 291–99.
Kroupova, Alena, Fabian Ackle, Igor Asanović, Stefan Weitzer, Franziska M. Boneberg, Marco Faini, Alexander Leitner, et al. 2021. "Molecular Architecture of the Human tRNA Ligase Complex." *eLife* 10 (December). https://doi.org/10.7554/eLife.71656.
Kuchino, Y., E. Borek, D. Grunberger, J. F. Mushinski, and S. Nishimura. 1982. "Changes of Post-Transcriptional Modification of Wye Base in Tumor-Specific tRNAPhe." *Nucleic Acids Research* 10 (20): 6421–32.
Kuscu, Canan, Pankaj Kumar, Manjari Kiran, Zhangli Su, Asrar Malik, and Anindya Dutta. 2018. "tRNA Fragments (tRFs) Guide Ago to Regulate Gene Expression Post-Transcriptionally in a Dicer-Independent Manner." *RNA* 24 (8): 1093–1105.
Kuzmenko, Anton, Anastasiya Oguienko, Daria Esyunina, Denis Yudin, Mayya Petrova, Alina Kudinova, Olga Maslova, et al. 2020. "DNA Targeting and Interference by a Bacterial Argonaute Nuclease." *Nature* 587 (7835): 632–37.
Lafontaine, D. L., C. Bousquet-Antonelli, Y. Henry, M. Caizergues-Ferrer, and D. Tollervey. 1998. "The Box H + ACA snoRNAs Carry Cbf5p, the Putative rRNA Pseudouridine Synthase." *Genes & Development* 12 (4): 527–37.
Lagos-Quintana, Mariana, Reinhard Rauhut, Jutta Meyer, Arndt Borkhardt, and Thomas Tuschl. 2003. "New microRNAs from Mouse and Human." *RNA* 9 (2): 175–79.
Lalande, Stéphanie, Rémy Merret, Thalia Salinas-Giegé, and Laurence Drouard. 2020. "Arabidopsis tRNA-Derived Fragments as Potential Modulators of Translation." *RNA Biology* 17 (8): 1137–48.
Langmead, Ben, and Steven L. Salzberg. 2012. "Fast Gapped-Read Alignment with Bowtie 2." *Nature Methods* 9 (4): 357–59.
Lauria, Fabio, Toma Tebaldi, Paola Bernabò, Ewout J. N. Groen, Thomas H. Gillingwater, and Gabriella Viero. 2018. "riboWaltz: Optimization of Ribosome P-Site Positioning in Ribosome Profiling Data." *PLoS Computational Biology* 14 (8): e1006169.
Lee, R. C., R. L. Feinbaum, and V. Ambros. 1993. "The C. Elegans Heterochronic Gene Lin-4 Encodes Small RNAs with Antisense Complementarity to Lin-14." *Cell* 75 (5): 843–54.
Lee, Stacey, Huaye Zhang, and Donna J. Webb. 2015. "Dendritic Spine Morphology and Dynamics in Health and Disease." *Cell Health and Cytoskeleton* 7 (June): 121–31.
Lee, Suzanne R., and Kathleen Collins. 2005. "Starvation-Induced Cleavage of the tRNA Anticodon Loop in Tetrahymena Thermophila*." *The Journal of Biological Chemistry* 280 (52): 42744–49.
Lee, Yong Sun, Yoshiyuki Shibata, Ankit Malhotra, and Anindya Dutta. 2009. "A Novel Class of Small RNAs: tRNA-Derived RNA Fragments (tRFs)." *Genes & Development* 23 (22): 2639–49.
Lee, Yoontae, Chiyoung Ahn, Jinju Han, Hyounjeong Choi, Jaekwang Kim, Jeongbin Yim, Junho Lee, et al. 2003. "The Nuclear RNase III Drosha Initiates microRNA Processing." *Nature* 425 (6956): 415–19.
Lee, Yoontae, Kipyoung Jeon, Jun-Tae Lee, Sunyoung Kim, and V. Narry Kim. 2002. "MicroRNA Maturation: Stepwise Processing and Subcellular Localization." *The EMBO Journal* 21 (17): 4663–70.
Lev, S., H. Moreno, R. Martinez, P. Canoll, E. Peles, J. M. Musacchio, G. D. Plowman, B. Rudy, and J. Schlessinger. 1995. "Protein Tyrosine Kinase PYK2 Involved in Ca(2+)-Induced Regulation of Ion Channel and MAP Kinase Functions." *Nature* 376 (6543): 737–45.
Lewis, Benjamin P., I-Hung Shih, Matthew W. Jones-Rhoades, David P. Bartel, and Christopher B. Burge. 2003. "Prediction of Mammalian microRNA Targets." *Cell* 115 (7): 787–98.
Li, Guoping, Aidan C. Manning, Alex Bagi, Xinyu Yang, Priyanka Gokulnath, Michail Spanos, Jonathan Howard, et al. 2022. "Distinct Stress-Dependent Signatures of Cellular and Extracellular tRNA-Derived Small RNAs." *Advancement of Science* 9 (17): e2200829.
Li, Heng, Bob Handsaker, Alec Wysoker, Tim Fennell, Jue Ruan, Nils Homer, Gabor Marth,

Goncalo Abecasis, Richard Durbin, and 1000 Genome Project Data Processing Subgroup. 2009. “The Sequence Alignment/Map Format and SAMtools.” *Bioinformatics* 25 (16): 2078–79.

Li, Jing, Yan-Nan Wang, Bei-Si Xu, Ya-Ping Liu, Mi Zhou, Tao Long, Hao Li, et al. 2020. “Intellectual Disability-Associated Gene ftsj1 Is Responsible for 2′-O-Methylation of Specific tRNAs.” *EMBO Reports* 21 (8): e50095.

Lipinski, Christopher A., Nhan L. Tran, Andrea Dooley, Yuan-Ping Pang, Carole Rohl, Jean Kloss, Zhongbo Yang, et al. 2006. “Critical Role of the FERM Domain in Pyk2 Stimulated Glioma Cell Migration.” *Biochemical and Biophysical Research Communications* 349 (3): 939–47.

Liu, Jidong, Michelle A. Carmell, Fabiola V. Rivas, Carolyn G. Marsden, J. Michael Thomson, Ji-Joon Song, Scott M. Hammond, Leemor Joshua-Tor, and Gregory J. Hannon. 2004. “Argonaute2 Is the Catalytic Engine of Mammalian RNAi.” *Science* 305 (5689): 1437–41.

Liu, Qianwei, Hans-Olov Adami, Abraham Reichenberg, Alexander Kolevzon, Fang Fang, and Sven Sandin. 2021. “Cancer Risk in Individuals with Intellectual Disability in Sweden: A Population-Based Cohort Study.” *PLoS Medicine* 18 (10): e1003840.

Liu, Xiang, Feng Jiang, Savitha Kalidas, Dean Smith, and Qinghua Liu. 2006. “Dicer-2 and R2D2 Coordinately Bind siRNA to Promote Assembly of the siRISC Complexes.” *RNA* 12 (8): 1514–20.

Loftus, Joseph C., Zhongbo Yang, Nhan L. Tran, Jean Kloss, Carole Viso, Michael E. Berens, and Christopher A. Lipinski. 2009. “The Pyk2 FERM Domain as a Target to Inhibit Glioma Migration.” *Molecular Cancer Therapeutics* 8 (6): 1505–14.

Lopes, Fátima, Mafalda Barbosa, Adam Ameur, Gabriela Soares, Joaquim de Sá, Ana Isabel Dias, Guiomar Oliveira, et al. 2016. “Identification of Novel Genetic Causes of Rett Syndrome-like Phenotypes.” *Journal of Medical Genetics* 53 (3): 190–99.

Lorenz, Christian, Christina E. Lünse, and Mario Mörl. 2017. “tRNA Modifications: Impact on Structure and Thermal Adaptation.” *Biomolecules* 7 (2). https://doi.org/10.3390/biom7020035.

Love, Michael I., Wolfgang Huber, and Simon Anders. 2014. “Moderated Estimation of Fold Change and Dispersion for RNA-Seq Data with DESeq2.” *Genome Biology* 15 (12): 550.

Lucas, Morghan C., Leszek P. Pryszcz, Rebeca Medina, Ivan Milenkovic, Noelia Camacho, Virginie Marchand, Yuri Motorin, Lluís Ribas de Pouplana, and Eva Maria Novoa. 2023. “Quantitative Analysis of tRNA Abundance and Modifications by Nanopore RNA Sequencing.” *Nature Biotechnology*, April. https://doi.org/10.1038/s41587-023-01743-6.

Luo, Shiqi, Feng He, Junjie Luo, Shengqian Dou, Yirong Wang, Annan Guo, and Jian Lu. 2018. “Drosophila tsRNAs Preferentially Suppress General Translation Machinery via Antisense Pairing and Participate in Cellular Starvation Response.” *Nucleic Acids Research* 46 (10): 5250–68.

Luo, Yicheng, Peng He, Nivedita Kanrar, Katalin Fejes Toth, and Alexei A. Aravin. 2022. “Maternally Inherited siRNAs Initiate piRNA Cluster Formation.” *bioRxiv*. https://doi.org/10.1101/2022.02.08.479612.

Magee, Rogan, and Isidore Rigoutsos. 2020. “On the Expanding Roles of tRNA Fragments in Modulating Cell Behavior.” *Nucleic Acids Research* 48 (17): 9433–48.

Maillard, P. V., C. Ciaudo, A. Marchais, Y. Li, F. Jay, S. W. Ding, and Olivier Voinnet. 2013. “Antiviral RNA Interference in Mammalian Cells.” *Science* 342 (6155): 235–38.

Makarova, Kira S., Yuri I. Wolf, John van der Oost, and Eugene V. Koonin. 2009. “Prokaryotic Homologs of Argonaute Proteins Are Predicted to Function as Key Components of a Novel System of Defense against Mobile Genetic Elements.” *Biology Direct* 4 (August): 29.

Marchand, Virginie, Florence Blanloeil-Oillo, Mark Helm, and Yuri Motorin. 2016. “Illumina-Based RiboMethSeq Approach for Mapping of 2’-O-Me Residues in RNA.” *Nucleic Acids Research* 44 (16): e135.

Marquet, R., C. Isel, C. Ehresmann, and B. Ehresmann. 1995. “tRNAs as Primer of Reverse Transcriptases.” *Biochimie* 77 (1-2): 113–24.

Martinez, German, Sarah G. Choudury, and R. Keith Slotkin. 2017. “tRNA-Derived Small

RNAs Target Transposable Element Transcripts." *Nucleic Acids Research* 45 (9): 5142–52.
Martin, Marcel. 2011. "Cutadapt Removes Adapter Sequences from High-Throughput Sequencing Reads." *EMBnet.journal* 17 (1): 10–12.
Matranga, Christian, Yukihide Tomari, Chanseok Shin, David P. Bartel, and Phillip D. Zamore. 2005. "Passenger-Strand Cleavage Facilitates Assembly of siRNA into Ago2-Containing RNAi Enzyme Complexes." *Cell* 123 (4): 607–20.
Matsui, Asuka, May Tran, Aya C. Yoshida, Satomi S. Kikuchi, Mami U, Masaharu Ogawa, and Tomomi Shimogori. 2013. "BTBD3 Controls Dendrite Orientation toward Active Axons in Mammalian Neocortex." *Science* 342 (6162): 1114–18.
Maulik, Pallab K., Maya N. Mascarenhas, Colin D. Mathers, Tarun Dua, and Shekhar Saxena. 2011. "Prevalence of Intellectual Disability: A Meta-Analysis of Population-Based Studies." *Research in Developmental Disabilities* 32 (2): 419–36.
Maute, Roy L., Christof Schneider, Pavel Sumazin, Antony Holmes, Andrea Califano, Katia Basso, and Riccardo Dalla-Favera. 2013. "tRNA-Derived microRNA Modulates Proliferation and the DNA Damage Response and Is down-Regulated in B Cell Lymphoma." *Proceedings of the National Academy of Sciences of the United States of America* 110 (4): 1404–9.
Meister, Gunter, Markus Landthaler, Agnieszka Patkaniowska, Yair Dorsett, Grace Teng, and Thomas Tuschl. 2004. "Human Argonaute2 Mediates RNA Cleavage Targeted by miRNAs and siRNAs." *Molecular Cell* 15 (2): 185–97.
Mohn, Fabio, Grzegorz Sienski, Dominik Handler, and Julius Brennecke. 2014. "The Rhino-Deadlock-Cutoff Complex Licenses Noncanonical Transcription of Dual-Strand piRNA Clusters in Drosophila." *Cell* 157 (6): 1364–79.
Moore, Joseph B., 4th, Jason E. Farrar, Robert J. Arceci, Johnson M. Liu, and Steven R. Ellis. 2010. "Distinct Ribosome Maturation Defects in Yeast Models of Diamond-Blackfan Anemia and Shwachman-Diamond Syndrome." *Haematologica* 95 (1): 57–64.
Motorin, Yuri, and Virginie Marchand. 2018. "Detection and Analysis of RNA Ribose 2'-O-Methylations: Challenges and Solutions." *Genes* 9 (12). https://doi.org/10.3390/genes9120642.
Murphy, Frank V., 4th, Venki Ramakrishnan, Andrzej Malkiewicz, and Paul F. Agris. 2004. "The Role of Modifications in Codon Discrimination by tRNA(Lys)UUU." *Nature Structural & Molecular Biology* 11 (12): 1186–91.
Nagayoshi, Y., T. Chujo, S. Hirata, H. Nakatsuka, C-W Chen, M. Takakura, K. Miyauchi, et al. 2021. "Loss of Ftsj1 Perturbs Codon-Specific Translation Efficiency in the Brain and Is Associated with X-Linked Intellectual Disability." *Science Advances* 7 (13). https://doi.org/10.1126/sciadv.abf3072.
Nakanishi, Kotaro. 2022. "Anatomy of Four Human Argonaute Proteins." *Nucleic Acids Research* 50 (12): 6618–38.
Nakanishi, Kotaro, and Osamu Nureki. 2005. "Recent Progress of Structural Biology of tRNA Processing and Modification." *Molecules and Cells* 19 (2): 157–66.
Napoli, C., C. Lemieux, and R. Jorgensen. 1990. "Introduction of a Chimeric Chalcone Synthase Gene into Petunia Results in Reversible Co-Suppression of Homologous Genes in Trans." *The Plant Cell* 2 (4): 279–89.
Nechooshtan, Gal, Dinar Yunusov, Kenneth Chang, and Thomas R. Gingeras. 2020. "Processing by RNase 1 Forms tRNA Halves and Distinct Y RNA Fragments in the Extracellular Environment." *Nucleic Acids Research* 48 (14): 8035–49.
Nellen, W., and C. Lichtenstein. 1993. "What Makes an mRNA Anti-Sense-Itive?" *Trends in Biochemical Sciences* 18 (11): 419–23.
Nicoloso, M., L. H. Qu, B. Michot, and J. P. Bachellerie. 1996. "Intron-Encoded, Antisense Small Nucleolar RNAs: The Characterization of Nine Novel Species Points to Their Direct Role as Guides for the 2'-O-Ribose Methylation of rRNAs." *Journal of Molecular Biology* 260 (2): 178–95.
Nishimasu, Hiroshi, Hirotsugu Ishizu, Kuniaki Saito, Satoshi Fukuhara, Miharu K. Kamatani, Luc Bonnefond, Naoki Matsumoto, et al. 2012. "Structure and Function of Zucchini

Endoribonuclease in piRNA Biogenesis." *Nature* 491 (7423): 284–87.
Niu, Yue, Qiaoqiao Qian, Juan Li, Pan Gong, Xianru Jiao, Xiao Mao, Bo Xiao, Lili Long, and Zhixian Yang. 2022. "De Novo Variants in AGO1 Recapitulate a Heterogeneous Neurodevelopmental Disorder Phenotype." *Clinical Genetics* 101 (4): 459–65.
Noma, Akiko, Yohei Kirino, Yoshiho Ikeuchi, and Tsutomu Suzuki. 2006. "Biosynthesis of Wybutosine, a Hyper-Modified Nucleoside in Eukaryotic Phenylalanine tRNA." *The EMBO Journal* 25 (10): 2142–54.
Okamura, Katsutomo, Akira Ishizuka, Haruhiko Siomi, and Mikiko C. Siomi. 2004. "Distinct Roles for Argonaute Proteins in Small RNA-Directed RNA Cleavage Pathways." *Genes & Development* 18 (14): 1655–66.
Olina, A. V., A. V. Kulbachinskiy, A. A. Aravin, and D. M. Esyunina. 2018. "Argonaute Proteins and Mechanisms of RNA Interference in Eukaryotes and Prokaryotes." *Biochemistry. Biokhimiia* 83 (5): 483–97.
Ontiveros, R. Jordan, Julian Stoute, and Kathy Fange Liu. 2019. "The Chemical Diversity of RNA Modifications." *Biochemical Journal* 476 (8): 1227–45.
Pandey, Kush Kumar, Deeksha Madhry, Y. S. Ravi Kumar, Shivani Malvankar, Leena Sapra, Rupesh K. Srivastava, Sankar Bhattacharyya, and Bhupendra Verma. 2021. "Regulatory Roles of tRNA-Derived RNA Fragments in Human Pathophysiology." *Molecular Therapy. Nucleic Acids* 26 (December): 161–73.
Pan, Tao. 2018. "Modifications and Functional Genomics of Human Transfer RNA." *Cell Research* 28 (4): 395–404.
Pan, Yu, Tong-Meng Yan, Jing-Rong Wang, and Zhi-Hong Jiang. 2021. "The Nature of the Modification at Position 37 of tRNAPhe Correlates with Acquired Taxol Resistance." *Nucleic Acids Research* 49 (1): 38–52.
Paushkin, Sergey V., Meenal Patel, Bansri S. Furia, Stuart W. Peltz, and Christopher R. Trotta. 2004. "Identification of a Human Endonuclease Complex Reveals a Link between tRNA Splicing and Pre-mRNA 3' End Formation." *Cell* 117 (3): 311–21.
Peixoto, Paul, Pierre-François Cartron, Aurélien A. Serandour, and Eric Hervouet. 2020. "From 1957 to Nowadays: A Brief History of Epigenetics." *International Journal of Molecular Sciences* 21 (20). https://doi.org/10.3390/ijms21207571.
Penzes, Peter, Michael E. Cahill, Kelly A. Jones, Jon-Eric VanLeeuwen, and Kevin M. Woolfrey. 2011. "Dendritic Spine Pathology in Neuropsychiatric Disorders." *Nature Neuroscience* 14 (3): 285–93.
Pereira, Marisa, Stephany Francisco, Ana Sofia Varanda, Mafalda Santos, Manuel A. S. Santos, and Ana Raquel Soares. 2018. "Impact of tRNA Modifications and tRNA-Modifying Enzymes on Proteostasis and Human Disease." *International Journal of Molecular Sciences* 19 (12). https://doi.org/10.3390/ijms19123738.
Peters, Lasse, and Gunter Meister. 2007. "Argonaute Proteins: Mediators of RNA Silencing." *Molecular Cell* 26 (5): 611–23.
Pintard, Lionel, Janusz M. Bujnicki, Bruno Lapeyre, and Claire Bonnerot. 2002. "MRM2 Encodes a Novel Yeast Mitochondrial 21S rRNA Methyltransferase." *The EMBO Journal* 21 (5): 1139–47.
Pintard, Lionel, François Lecointe, Janusz M. Bujnicki, Claire Bonnerot, Henri Grosjean, and Bruno Lapeyre. 2002. "Trm7p Catalyses the Formation of Two 2'-O-Methylriboses in Yeast tRNA Anticodon Loop." *The EMBO Journal* 21 (7): 1811–20.
Poirier, Enzo Z., Michael D. Buck, Probir Chakravarty, Joana Carvalho, Bruno Frederico, Ana Cardoso, Lyn Healy, Rachel Ulferts, Rupert Beale, and Caetano Reis e Sousa. 2021. "An Isoform of Dicer Protects Mammalian Stem Cells against Multiple RNA Viruses." *Science* 373 (6551): 231–36.
Polack, Fernando P., Stephen J. Thomas, Nicholas Kitchin, Judith Absalon, Alejandra Gurtman, Stephen Lockhart, John L. Perez, et al. 2020. "Safety and Efficacy of the BNT162b2 mRNA Covid-19 Vaccine." *The New England Journal of Medicine* 383 (27): 2603–15.
Pratt, Ashley J., and Ian J. MacRae. 2009. "The RNA-Induced Silencing Complex: A Versatile Gene-Silencing Machine." *The Journal of Biological Chemistry* 284 (27): 17897–901.

Preall, Jonathan B., and Erik J. Sontheimer. 2005. “RNAi: RISC Gets Loaded.” *Cell*.
Ramser, J., B. Winnepenninckx, C. Lenski, V. Errijgers, M. Platzer, C. E. Schwartz, A. Meindl, and R. F. Kooy. 2004. “A Splice Site Mutation in the Methyltransferase Gene FTSJ1 in Xp11.23 Is Associated with Non-Syndromic Mental Retardation in a Large Belgian Family (MRX9).” *Journal of Medical Genetics* 41 (9): 679–83.
Raymond, F. L. 2006. “X Linked Mental Retardation: A Clinical Guide.” *Journal of Medical Genetics* 43 (3): 193–200.
Rehwinkel, Jan, Isabelle Behm-Ansmant, David Gatfield, and Elisa Izaurralde. 2005. “A Crucial Role for GW182 and the DCP1:DCP2 Decapping Complex in miRNA-Mediated Gene Silencing.” *RNA* 11 (11): 1640–47.
Reinhart, B. J., F. J. Slack, M. Basson, A. E. Pasquinelli, J. C. Bettinger, A. E. Rougvie, H. R. Horvitz, and G. Ruvkun. 2000. “The 21-Nucleotide Let-7 RNA Regulates Developmental Timing in Caenorhabditis Elegans.” *Nature* 403 (6772): 901–6.
Renieri, A., C. Pescucci, I. Longo, F. Ariani, F. Mari, and I. Meloni. 2005. “Non-Syndromic X-Linked Mental Retardation: From a Molecular to a Clinical Point of View.” *Journal of Cellular Physiology* 204 (1): 8–20.
Reyniers, J. P., J. R. Pleasants, B. S. Wostmann, J. R. Katze, and W. R. Farkas. 1981. “Administration of Exogenous Queuine Is Essential for the Biosynthesis of the Queuosine-Containing Transfer RNAs in the Mouse.” *The Journal of Biological Chemistry* 256 (22): 11591–94.
Ringeard, Mathieu, Virginie Marchand, Etienne Decroly, Yuri Motorin, and Yamina Bennasser. 2019. “FTSJ3 Is an RNA 2’-O-Methyltransferase Recruited by HIV to Avoid Innate Immune Sensing.” *Nature* 565 (7740): 500–504.
Robertus, J. D., J. E. Ladner, J. T. Finch, D. Rhodes, R. S. Brown, B. F. Clark, and A. Klug. 1974. “Structure of Yeast Phenylalanine tRNA at 3 A Resolution.” *Nature* 250 (467): 546–51.
Rodriguez, Antony, Sam Griffiths-Jones, Jennifer L. Ashurst, and Allan Bradley. 2004. “Identification of Mammalian microRNA Host Genes and Transcription Units.” *Genome Research* 14 (10A): 1902–10.
Rosselló-Tortella, Margalida, Pere Llinàs-Arias, Yuriko Sakaguchi, Kenjyo Miyauchi, Veronica Davalos, Fernando Setien, Maria E. Calleja-Cervantes, et al. 2020. “Epigenetic Loss of the Transfer RNA-Modifying Enzyme TYW2 Induces Ribosome Frameshifts in Colon Cancer.” *Proceedings of the National Academy of Sciences of the United States of America* 117 (34): 20785–93.
Ruby, J. Graham, Calvin H. Jan, and David P. Bartel. 2007. “Intronic microRNA Precursors That Bypass Drosha Processing.” *Nature* 448 (7149): 83–86.
Saito, Kuniaki, Kazumichi M. Nishida, Tomoko Mori, Yoshinori Kawamura, Keita Miyoshi, Tomoko Nagami, Haruhiko Siomi, and Mikiko C. Siomi. 2006. “Specific Association of Piwi with rasiRNAs Derived from Retrotransposon and Heterochromatic Regions in the Drosophila Genome.” *Genes & Development* 20 (16): 2214–22.
Saito, Kuniaki, Yuriko Sakaguchi, Takeo Suzuki, Tsutomu Suzuki, Haruhiko Siomi, and Mikiko C. Siomi. 2007. “Pimet, the Drosophila Homolog of HEN1, Mediates 2’-O-Methylation of Piwi- Interacting RNAs at Their 3' Ends.” *Genes & Development* 21 (13): 1603–8.
Sakaguchi, Asami, Yukio Yamashita, Tomohiro Ishii, Tomoko Uehara, Kenjiro Kosaki, Takao Takahashi, and Toshiki Takenouchi. 2019. “Further Evidence of a Causal Association between AGO1, a Critical Regulator of microRNA Formation, and Intellectual Disability/autism Spectrum Disorder.” *European Journal of Medical Genetics* 62 (6): 103537.
Sapp, E., C. Schwarz, K. Chase, P. G. Bhide, A. B. Young, J. Penney, J. P. Vonsattel, N. Aronin, and M. DiFiglia. 1997. “Huntingtin Localization in Brains of Normal and Huntington’s Disease Patients.” *Annals of Neurology* 42 (4): 604–12.
Sarot, Emeline, Geneviève Payen-Groschêne, Alain Bucheton, and Alain Pélisson. 2004. “Evidence for a Piwi-Dependent RNA Silencing of the Gypsy Endogenous Retrovirus by the Drosophila Melanogaster Flamenco Gene.” *Genetics* 166 (3): 1313–21.
Saxena, S. K., S. M. Rybak, R. T. Davey Jr, R. J. Youle, and E. J. Ackerman. 1992.

"Angiogenin Is a Cytotoxic, tRNA-Specific Ribonuclease in the RNase A Superfamily." *The Journal of Biological Chemistry* 267 (30): 21982–86.
Schaefer, Matthias, Tim Pollex, Katharina Hanna, Francesca Tuorto, Madeleine Meusburger, Mark Helm, and Frank Lyko. 2010. "RNA Methylation by Dnmt2 Protects Transfer RNAs against Stress-Induced Cleavage." *Genes & Development* 24 (15): 1590–95.
Schalk, Audrey, Margot A. Cousin, Nikita R. Dsouza, Thomas D. Challman, Karen E. Wain, Zoe Powis, Kelly Minks, et al. 2022. "De Novo Coding Variants in the AGO1 Gene Cause a Neurodevelopmental Disorder with Intellectual Disability." *Journal of Medical Genetics* 59 (10): 965–75.
Schirle, Nicole T., and Ian J. MacRae. 2012. "The Crystal Structure of Human Argonaute2." *Science* 336 (6084): 1037–40.
Schorn, Andrea J., Michael J. Gutbrod, Chantal LeBlanc, and Rob Martienssen. 2017. "LTR-Retrotransposon Control by tRNA-Derived Small RNAs." *Cell* 170 (1): 61–71.e11.
Schorn, Andrea J., and Rob Martienssen. 2018. "Tie-Break: Host and Retrotransposons Play tRNA." *Trends in Cell Biology* 28 (10): 793–806.
Sekulovski, Samoil, Pascal Devant, Silvia Panizza, Tasos Gogakos, Anda Pitiriciu, Katharina Heitmeier, Ewan Phillip Ramsay, et al. 2021. "Assembly Defects of Human tRNA Splicing Endonuclease Contribute to Impaired Pre-tRNA Processing in Pontocerebellar Hypoplasia." *Nature Communications* 12 (1): 5610.
Sharma, Manu, Hanbang Zhang, Gretchen Ehrenkaufer, and Upinder Singh. 2023. "Stress Response in Entamoeba Histolytica Is Associated with Robust Processing of tRNA to tRNA Halves." *mBio* 14 (2): e0345022.
Shigematsu, Megumi, and Yohei Kirino. 2015. "tRNA-Derived Short Non-Coding RNA as Interacting Partners of Argonaute Proteins." *Gene Regulation and Systems Biology* 9 (September): 27–33.
Shi, Hailing, Jiangbo Wei, and Chuan He. 2019. "Where, When, and How: Context-Dependent Functions of RNA Methylation Writers, Readers, and Erasers." *Molecular Cell* 74 (4): 640–50.
Shi, H., and P. B. Moore. 2000. "The Crystal Structure of Yeast Phenylalanine tRNA at 1.93 A Resolution: A Classic Structure Revisited." *RNA* 6 (8): 1091–1105.
Singh, Anumeha, Lekha E. Manjunath, Pradipta Kundu, Sarthak Sahoo, Arpan Das, Harikumar R. Suma, Paul L. Fox, and Sandeep M. Eswarappa. 2019. "Let-7a-Regulated Translational Readthrough of Mammalian AGO1 Generates a microRNA Pathway Inhibitor." *The EMBO Journal* 38 (16): e100727.
Sivan, Gilad, Shira G. Glushakow-Smith, George C. Katsafanas, Jeffrey L. Americo, and Bernard Moss. 2018. "Human Host Range Restriction of the Vaccinia Virus C7/K1 Double Deletion Mutant Is Mediated by an Atypical Mode of Translation Inhibition." *Journal of Virology* 92 (23). https://doi.org/10.1128/JVI.01329-18.
Sloan, Katherine E., Ahmed S. Warda, Sunny Sharma, Karl-Dieter Entian, Denis L. J. Lafontaine, and Markus T. Bohnsack. 2017. "Tuning the Ribosome: The Influence of rRNA Modification on Eukaryotic Ribosome Biogenesis and Function." *RNA Biology* 14 (9): 1138–52.
Smardon, A., J. M. Spoerke, S. C. Stacey, M. E. Klein, N. Mackin, and E. M. Maine. 2000. "EGO-1 Is Related to RNA-Directed RNA Polymerase and Functions in Germ-Line Development and RNA Interference in C. Elegans." *Current Biology: CB* 10 (4): 169–78.
Srinivasan, Madhusudhan, Preeti Mehta, Yao Yu, Evelyn Prugar, Eugene V. Koonin, A. Wali Karzai, and Rolf Sternglanz. 2011. "The Highly Conserved KEOPS/EKC Complex Is Essential for a Universal tRNA Modification, t6A." *The EMBO Journal* 30 (5): 873–81.
Srinivasan, Sundaramoorthy, Adrian Gabriel Torres, and Lluís Ribas de Pouplana. 2021. "Inosine in Biology and Disease." *Genes* 12 (4). https://doi.org/10.3390/genes12040600.
Stahl, G., L. Bidou, J. P. Rousset, and M. Cassan. 1995. "Versatile Vectors to Study Recoding: Conservation of Rules between Yeast and Mammalian Cells." *Nucleic Acids Research* 23 (9): 1557–60.
Suzuki, Tsutomu. 2021. "The Expanding World of tRNA Modifications and Their Disease Relevance." *Nature Reviews. Molecular Cell Biology* 22 (6): 375–92.

Swarts, Daan C., Matthijs M. Jore, Edze R. Westra, Yifan Zhu, Jorijn H. Janssen, Ambrosius P. Snijders, Yanli Wang, et al. 2014. “DNA-Guided DNA Interference by a Prokaryotic Argonaute.” *Nature* 507 (7491): 258–61.

Swarts, Daan C., Kira Makarova, Yanli Wang, Kotaro Nakanishi, René F. Ketting, Eugene V. Koonin, Dinshaw J. Patel, and John van der Oost. 2014. “The Evolutionary Journey of Argonaute Proteins.” *Nature Structural & Molecular Biology* 21 (9): 743–53.

Tabara, H., M. Sarkissian, W. G. Kelly, J. Fleenor, A. Grishok, L. Timmons, A. Fire, and C. C. Mello. 1999. “The Rde-1 Gene, RNA Interference, and Transposon Silencing in C. Elegans.” *Cell* 99 (2): 123–32.

Takano, Kyoko, Eiji Nakagawa, Ken Inoue, Fumiaki Kamada, Shigeo Kure, Yu-Ichi Goto, and Japanese Mental Retardation Consortium. 2008. “A Loss-of-Function Mutation in the FTSJ1 Gene Causes Nonsyndromic X-Linked Mental Retardation in a Japanese Family.” *American Journal of Medical Genetics. Part B, Neuropsychiatric Genetics: The Official Publication of the International Society of Psychiatric Genetics* 147B (4): 479–84.

Tat, Trinh To, Patricia A. Maroney, Sangpen Chamnongpol, Jeff Coller, and Timothy W. Nilsen. 2016. “Cotranslational microRNA Mediated Messenger RNA Destabilization.” *eLife* 5 (April). https://doi.org/10.7554/eLife.12880.

Thompson, Debrah M., Cheng Lu, Pamela J. Green, and Roy Parker. 2008. “tRNA Cleavage Is a Conserved Response to Oxidative Stress in Eukaryotes.” *RNA* 14 (10): 2095–2103.

Thüring, Kathrin, Katharina Schmid, Patrick Keller, and Mark Helm. 2016. “Analysis of RNA Modifications by Liquid Chromatography-Tandem Mass Spectrometry.” *Methods* 107 (September): 48–56.

Tomari, Yukihide, Tingting Du, and Phillip D. Zamore. 2007. “Sorting of Drosophila Small Silencing RNAs.” *Cell* 130 (2): 299–308.

Torri, Alessandro, Johannes Jaeger, Thomas Pradeu, and Maria-Carla Saleh. 2022. “The Origin of RNA Interference: Adaptive or Neutral Evolution?” *PLoS Biology* 20 (6): e3001715.

Tosar, Juan Pablo, and Alfonso Cayota. 2020. “Extracellular tRNAs and tRNA-Derived Fragments.” *RNA Biology* 17 (8): 1149–67.

Trzaska, Carole, Séverine Amand, Christine Bailly, Catherine Leroy, Virginie Marchand, Evelyne Duvernois-Berthet, Jean-Michel Saliou, et al. 2020. “2,6-Diaminopurine as a Highly Potent Corrector of UGA Nonsense Mutations.” *Nature Communications* 11 (1): 1509.

Tuorto, Francesca, Reinhard Liebers, Tanja Musch, Matthias Schaefer, Sarah Hofmann, Stefanie Kellner, Michaela Frye, Mark Helm, Georg Stoecklin, and Frank Lyko. 2012. “RNA Cytosine Methylation by Dnmt2 and NSun2 Promotes tRNA Stability and Protein Synthesis.” *Nature Structural & Molecular Biology* 19 (9): 900–905.

Tuorto, Francesca, and Frank Lyko. 2016. “Genome Recoding by tRNA Modifications.” *Open Biology* 6 (12). https://doi.org/10.1098/rsob.160287.

Vagin, Vasily V., Alla Sigova, Chengjian Li, Hervé Seitz, Vladimir Gvozdev, and Phillip D. Zamore. 2006. “A Distinct Small RNA Pathway Silences Selfish Genetic Elements in the Germline.” *Science* 313 (5785): 320–24.

Valadon, Charlène, and Olivier Namy. 2021. “The Importance of the Epi-Transcriptome in Translation Fidelity.” *Non-Coding RNA* 7 (3). https://doi.org/10.3390/ncrna7030051.

Vanssay, Augustin de, Anne-Laure Bougé, Antoine Boivin, Catherine Hermant, Laure Teysset, Valérie Delmarre, Christophe Antoniewski, and Stéphane Ronsseray. 2012. “Paramutation in Drosophila Linked to Emergence of a piRNA-Producing Locus.” *Nature* 490 (7418): 112–15.

Vitali, Patrice, and Tamás Kiss. 2019. “Cooperative 2’-O-Methylation of the Wobble Cytidine of Human Elongator tRNAMet(CAT) by a Nucleolar and a Cajal Body-Specific Box C/D RNP.” *Genes & Development* 33 (13-14): 741–46.

Vodovar, Nicolas, and Maria-Carla Saleh. 2012. “Chapter 1 - Of Insects and Viruses: The Role of Small RNAs in Insect Defence.” In *Advances in Insect Physiology*, edited by Elizabeth L. Jockusch, 42:1–36. Academic Press.

Waas, William F., Zhanna Druzina, Melanie Hanan, and Paul Schimmel. 2007. “Role of a

tRNA Base Modification and Its Precursors in Frameshifting in Eukaryotes." *The Journal of Biological Chemistry* 282 (36): 26026–34.
Wang, Nan, Shuang Qu, Wu Sun, Ziyi Zeng, Hongwei Liang, Chen-Yu Zhang, Xi Chen, and Ke Zen. 2018. "Direct Quantification of 3' Terminal 2'-O-Methylation of Small RNAs by RT-qPCR." *RNA* 24 (11): 1520–29.
Wang, Rongyue, Tingying Lei, Fang Fu, Ru Li, Xiangyi Jing, Xin Yang, Juan Liu, Dongzhi Li, and Can Liao. 2019. "Application of Chromosome Microarray Analysis in Patients with Unexplained Developmental Delay/intellectual Disability in South China." *Pediatrics and Neonatology* 60 (1): 35–42.
Wang, Xiaoyun, Zaneta Matuszek, Yong Huang, Marc Parisien, Qing Dai, Wesley Clark, Michael H. Schwartz, and Tao Pan. 2018. "Queuosine Modification Protects Cognate tRNAs against Ribonuclease Cleavage." *RNA* 24 (10): 1305–13.
Wellington, C. L., B. R. Leavitt, and M. R. Hayden. 2000. "Huntington Disease: New Insights on the Role of Huntingtin Cleavage." *Journal of Neural Transmission. Supplementum*, no. 58: 1–17.
Werner, Maria, Elzbieta Purta, Katarzyna H. Kaminska, Iwona A. Cymerman, David A. Campbell, Bidyottam Mittra, Jesse R. Zamudio, Nancy R. Sturm, Jacek Jaworski, and Janusz M. Bujnicki. 2011. "2'-O-Ribose Methylation of cap2 in Human: Function and Evolution in a Horizontally Mobile Family." *Nucleic Acids Research* 39 (11): 4756–68.
Wilkinson, Martha L., Sharon M. Crary, Jane E. Jackman, Elizabeth J. Grayhack, and Eric M. Phizicky. 2007. "The 2'-O-Methyltransferase Responsible for Modification of Yeast tRNA at Position 4." *RNA* 13 (3): 404–13.
Willkomm, Sarah, Adrian Zander, Alexander Gust, and Dina Grohmann. 2015. "A Prokaryotic Twist on Argonaute Function." *Life* 5 (1): 538–53.
Xie, Meng, and Bin Yu. 2015. "siRNA-Directed DNA Methylation in Plants." *Current Genomics* 16 (1): 23–31.
Xie, Yaoyao, Lipeng Yao, Xiuchong Yu, Yao Ruan, Zhe Li, and Junming Guo. 2020. "Action Mechanisms and Research Methods of tRNA-Derived Small RNAs." *Signal Transduction and Targeted Therapy* 5 (1): 109.
Xu, Benjin, Ling Liu, and Guangtao Song. 2021. "Functions and Regulation of Translation Elongation Factors." *Frontiers in Molecular Biosciences* 8: 816398.
Yamasaki, Satoshi, Pavel Ivanov, Guo-Fu Hu, and Paul Anderson. 2009. "Angiogenin Cleaves tRNA and Promotes Stress-Induced Translational Repression." *The Journal of Cell Biology* 185 (1): 35–42.
Yang, Huiliang, Lijun Wang, Christian Shigley, and Wentian Yang. 2022. "Protein Tyrosine Phosphatases in Skeletal Development and Diseases." *Bone Research* 10 (1): 10.
Yates, Andrew D., Premanand Achuthan, Wasiu Akanni, James Allen, Jamie Allen, Jorge Alvarez-Jarreta, M. Ridwan Amode, et al. 2020. "Ensembl 2020." *Nucleic Acids Research* 48 (D1): D682–88.
Ye, Keqiong, Ru Jia, Jinzhong Lin, Minghua Ju, Jin Peng, Anbi Xu, and Liman Zhang. 2009. "Structural Organization of Box C/D RNA-Guided RNA Methyltransferase." *Proceedings of the National Academy of Sciences of the United States of America* 106 (33): 13808–13.
Yeşil, Gözde, Ayşe Aralaşmak, Enes Akyüz, Dilara İçağasıoğlu, Türkan Uygur Şahin, and Yavuz Bayram. 2018. "Expanding the Phenotype of Homozygous KCNMA1 Mutations; Dyskinesia, Epilepsy, Intellectual Disability, Cerebellar and Corticospinal Tract Atrophy." *Balkan Medical Journal* 35 (4): 336–39.
Yildirim, Ilyas, Elzbieta Kierzek, Ryszard Kierzek, and George C. Schatz. 2014. "Interplay of LNA and 2'-O-Methyl RNA in the Structure and Thermodynamics of RNA Hybrid Systems: A Molecular Dynamics Study Using the Revised AMBER Force Field and Comparison with Experimental Results." *The Journal of Physical Chemistry. B* 118 (49): 14177–87.
Yi, Rui, Yi Qin, Ian G. Macara, and Bryan R. Cullen. 2003. "Exportin-5 Mediates the Nuclear Export of Pre-microRNAs and Short Hairpin RNAs." *Genes & Development* 17 (24): 3011–16.

Yoshihisa, Tohru, Kaori Yunoki-Esaki, Chie Ohshima, Nobuyuki Tanaka, and Toshiya Endo. 2003. “Possibility of Cytoplasmic Pre-tRNA Splicing: The Yeast tRNA Splicing Endonuclease Mainly Localizes on the Mitochondria.” *Molecular Biology of the Cell* 14 (8): 3266–79.

Yuan, Ya, Jiamei Li, Zhi He, Xiaolan Fan, Xueping Mao, Mingyao Yang, and Deying Yang. 2021. “tRNA-Derived Fragments as New Hallmarks of Aging and Age-Related Diseases.” *Aging and Disease* 12 (5): 1304–22.

Yudelevich, A. 1971. “Specific Cleavage of an Escherichia Coli Leucine Transfer RNA Following Bacteriophage T4 Infection.” *Journal of Molecular Biology* 60 (1): 21–29.

Yue, D., N. Maizels, and A. M. Weiner. 1996. “CCA-Adding Enzymes and poly(A) Polymerases Are All Members of the Same Nucleotidyltransferase Superfamily: Characterization of the CCA-Adding Enzyme from the Archaeal Hyperthermophile Sulfolobus Shibatae.” *RNA* 2 (9): 895–908.

Zamore, P. D., T. Tuschl, P. A. Sharp, and D. P. Bartel. 2000. “RNAi: Double-Stranded RNA Directs the ATP-Dependent Cleavage of mRNA at 21 to 23 Nucleotide Intervals.” *Cell* 101 (1): 25–33.

Zaremba, Mindaugas, Donata Dakineviciene, Edvardas Golovinas, Evelina Zagorskaitė, Edvinas Stankunas, Anna Lopatina, Rotem Sorek, et al. 2022. “Short Prokaryotic Argonautes Provide Defence against Incoming Mobile Genetic Elements through NAD+ Depletion.” *Nature Microbiology* 7 (11): 1857–69.

Zhang, Yaping, Qin Deng, Longxiang Tu, Dan Lv, and Dewu Liu. 2020. “tRNA-derived Small RNAs: A Novel Class of Small RNAs in Human Hypertrophic Scar Fibroblasts.” *International Journal of Molecular Medicine* 45 (1): 115–30.

Zhang, Yu, Audrey Bonnan, Guillaume Bony, Isabelle Ferezou, Susanna Pietropaolo, Melanie Ginger, Nathalie Sans, et al. 2014. “Dendritic Channelopathies Contribute to Neocortical and Sensory Hyperexcitability in Fmr1(-/y) Mice.” *Nature Neuroscience* 17 (12): 1701–9.

Zhang, Zhong-Bin, Mao-Qiang Tian, Kai Gao, Yu-Wu Jiang, and Ye Wu. 2015. “De Novo KCNMA1 Mutations in Children with Early-Onset Paroxysmal Dyskinesia and Developmental Delay.” *Movement Disorders: Official Journal of the Movement Disorder Society* 30 (9): 1290–92.

Zhu, Yinzhou, Stephan P. Pirnie, and Gordon G. Carmichael. 2017. “High-Throughput and Site-Specific Identification of 2’-O-Methylation Sites Using Ribose Oxidation Sequencing (RibOxi-Seq).” *RNA* 23 (8): 1303–14.

Appendix 1

mRNA seq						RiboSeq					
ID_rna	Mean WT	Average Mut.	baseMean_rna	log2FoldChange	padj_rna	ID_ribo	Mean WT	Mean Mut	baseMean_ribo	log2FoldChange	padj_ribo
ABCF1	2 257	3 471	2810,357805	0,195445821	4,04E-01	ABCF1	523	644	578,6194183	0,637532211	3,32E-03
AC010197.2	6 905	11 259	8702,814648	0,227148454	9,69E-02	AC010197.2	1 368	1 515	1435,324109	0,465486813	1,47E-03
ADAM17	677	746	698,7848586	-0,356880244	2,74E-01	ADAM17	275	115	185,911472	-0,964395689	7,80E-03
AFG3L2	975	1 705	1285,125819	0,345444965	1,48E-01	AFG3L2	471	538	499,7626927	0,508612895	7,36E-03
APH1B	333	318	320,2528827	-0,59586352	2,02E-01	APH1B	172	55	100,24982	-1,241473586	2,74E-03
ARMCX3	876	1 486	1125,909649	0,284029627	2,60E-01	ARMCX3	234	297	264,8357485	0,66475508	5,53E-04
ASB2	552	463	492,4629112	-0,852878389	6,17E-01	ASB2	205	31	96,57930513	-2,210273647	6,02E-04
ATP2B4	229	259	238,7157158	-0,314515727	6,41E-01	ATP2B4	80	8	35,23039455	-2,77197299	5,03E-05
ATP5F1A	13 089	21 527	16575,31296	0,240249896	1,84E-01	ATP5F1A	5 346	5 665	5447,124255	0,420168222	6,32E-04
BAZ1A	2 565	4 262	3321,922362	0,299039281	1,33E-01	BAZ1A	582	698	636,8298765	0,618973607	4,03E-03
BPGM	843	1 241	1013,363563	0,10101584	6,78E-01	BPGM	80	117	99,87911674	0,868292425	6,79E-03
BUD31	2 272	3 998	2982,407041	0,333069198	9,46E-02	BUD31	437	549	489,0952298	0,663317252	2,26E-03
C19orf53	4 112	5 234	4614,139819	-0,103125527	7,03E-01	C19orf53	708	386	521,9865549	-0,555450567	1,46E-03
CAD	1 434	2 446	1880,919969	0,330966511	3,09E-01	CAD	1 576	1 851	1685,977304	0,590040251	3,04E-05
CCSER1	8 954	11 317	10035,73723	-0,105518022	7,48E-01	CCSER1	27	3	12,47686733	-2,729034045	3,22E-03
CD2AP	1 809	3 258	2395,5134	0,361053964	1,04E-01	CD2AP	383	455	415,1163831	0,59404329	1,24E-03
CD40	2 654	3 294	2906,77645	-0,163447492	6,84E-01	CD40	590	247	374,5671833	-0,870275941	3,84E-03
CD80	1 365	1 669	1479,295728	-0,198987198	5,66E-01	CD80	338	146	227,6462212	-0,894619796	1,28E-05
CDC25A	893	1 246	1070,398529	0,08525823	8,64E-01	CDC25A	117	152	134,5273987	0,692455123	6,67E-03
CDC6	1 404	2 472	1899,653718	0,407935054	1,38E-01	CDC6	266	367	319,879017	0,806407306	2,20E-04
CELF1	1 979	3 179	2508,945129	0,242635715	1,38E-01	CELF1	488	524	499,0853173	0,451206989	7,87E-03
CERKL	553	1 131	789,6359009	0,536064817	1,71E-01	CERKL	0	14	7,682332563	6,53342055	7,23E-05
CLPTM1	1 774	2 204	1953,176911	-0,159931857	5,58E-01	CLPTM1	656	304	460,3903459	-0,842424429	6,94E-03
CLSPN	1 226	2 169	1669,433379	0,423086833	1,97E-01	CLSPN	467	647	557,2567808	0,821954113	9,44E-06
CLSTN3	696	731	708,1121562	-0,403964166	2,76E-01	CLSTN3	331	139	219,2548423	-0,908852453	7,75E-04
CMTR1	1 175	2 372	1660,410804	0,522508183	8,29E-02	CMTR1	527	583	543,8031962	0,491842523	3,42E-03
COPS9	2 041	2 201	2122,624737	-0,342711012	1,50E-01	COPS9	350	143	233,1630079	-0,977212275	3,00E-06
CPNE1	4 797	7 038	5744,927419	0,087663022	6,27E-01	CPNE1	733	905	807,6943419	0,637145787	5,69E-04
CPSF6	2 247	3 241	2687,787084	0,082863336	7,13E-01	CPSF6	705	801	749,0912175	0,508047973	2,84E-03
DCAF1	1 354	1 999	1644,222261	0,125562985	6,33E-01	DCAF1	633	676	645,4391205	0,444691598	4,92E-03
DHX15	3 973	6 441	5072,166158	0,259238517	2,57E-01	DHX15	1 902	2 071	1963,361139	0,473222222	5,61E-03
DIP2B	1 239	2 174	1630,250497	0,341255394	1,33E-01	DIP2B	521	604	552,9295909	0,565368085	6,84E-04
DIPK1A	13 178	14 655	13825,35375	-0,31412095	1,59E-01	DIPK1A	84	26	51,8417633	-1,400686182	5,62E-03
DNAJC15	2 209	2 479	2326,690945	-0,297535974	2,04E-01	DNAJC15	468	229	322,2027221	-0,671924417	6,83E-04
DPAGT1	844	913	874,9187781	-0,352052747	2,80E-01	DPAGT1	364	164	250,554561	-0,871629161	9,66E-03

DTL	1 810	3 225	2455,447814	0,415663221	7,13E-02	DTL	583	779	677,2186615	0,768342141	1,34E-08
DUS3L	299	525	397,8312625	0,369127064	1,19E-01	DUS3L	101	150	124,5414557	0,907358686	1,78E-03
EFNA5	700	495	609,3406903	-0,958781458	4,19E-01	EFNA5	208	61	116,9929682	-1,314757699	5,84E-04
EFR3A	1 560	2 885	2112,205586	0,417762795	1,20E-01	EFR3A	467	565	513,8068247	0,616924469	2,13E-04
EIF3C	37	85	58,11004446	0,748062778	1,21E-01	EIF3C	612	712	652,0294089	0,565928846	4,76E-04
ENO1	29 039	47 964	37675,12828	0,302014899	1,72E-01	ENO1	16 706	17 128	16401,3977	0,408005166	6,47E-03
ESCO2	1 001	1 746	1341,088866	0,384875235	1,37E-01	ESCO2	394	528	455,9310563	0,799963733	6,52E-05
EXOSC8	1 295	1 996	1606,632715	0,181267109	5,30E-01	EXOSC8	521	574	535,4533924	0,521704612	6,63E-03
FAM107B	11 289	12 766	11608,51507	-0,369642451	3,24E-01	FAM107B	880	354	573,2184674	-0,935131308	3,61E-05
FEN1	1 426	2 271	1827,176597	0,269592956	3,94E-01	FEN1	585	667	612,1792026	0,530081645	3,40E-03
FHL2	365	556	444,4849933	0,136384363	7,72E-01	FHL2	19	43	31,34648806	1,428089611	9,72E-03
FUS	4 656	7 923	6196,525398	0,367282957	2,42E-01	FUS	1 524	1 664	1586,052599	0,431142749	7,77E-03
G3BP2	3 345	4 410	3824,713657	-0,043973799	9,05E-01	G3BP2	1 383	1 452	1404,21477	0,390216265	5,85E-03
GNL3L	1 032	1 407	1202,145946	0,00451986	9,90E-01	GNL3L	375	428	394,7819614	0,521034675	5,05E-03
GNS	954	1 036	972,6967797	-0,397251471	4,31E-01	GNS	441	180	290,8248901	-0,980195596	2,04E-03
GPR15	4 643	6 982	5497,07577	0,059316545	9,23E-01	GPR15	2 333	782	1476,841607	-1,297345483	8,65E-07
GSDMB	102	106	102,8048627	-0,436669993	2,63E-01	GSDMB	10	0	4,258107986	-5,396842163	6,46E-03
GSN	229	413	306,9292936	0,387523932	1,38E-01	GSN	71	122	96,74642592	1,137971226	2,49E-04
GTPBP4	2 613	3 742	3148,940893	0,106306326	7,56E-01	GTPBP4	963	1 029	982,1493694	0,445900921	3,63E-03
H2AC16	9	24	15,20810466	0,842908508	5,85E-01	H2AC16	1 142	1 620	1378,330001	0,805434178	6,62E-06
H2AC17	24	45	32,86084623	0,438789225	5,61E-01	H2AC17	4 990	5 800	5337,115309	0,555685076	7,49E-04
H2AC18	4	10	7,093219378	0,843302262	6,28E-01	H2AC18	458	645	557,1657906	0,821028594	4,63E-07
H2AC8	40	108	68,17188631	0,929335126	8,19E-02	H2AC8	5 316	5 834	5483,878719	0,452218566	3,88E-03
H2BC6	95	140	113,8504647	0,090309728	9,10E-01	H2BC6	218	422	331,5546203	1,184347709	9,03E-04
H3C7	14	18	14,98356348	-0,296558623	8,53E-01	H3C7	5 448	7 522	6436,347467	0,818388297	4,73E-09
H3C8	41	79	58,01101912	0,510881123	4,75E-01	H3C8	4 203	4 654	4370,438331	0,480229794	2,90E-04
H4C13	2	3	2,441271088	0,144785855	9,77E-01	H4C13	321	132	221,2301777	-1,031043205	6,29E-04
H4C5	20	46	30,70042863	0,671722928	4,84E-01	H4C5	7 820	10 461	9242,737479	0,701522871	2,02E-04
H4C6	6	13	8,696152111	0,577904751	7,35E-01	H4C6	1 289	1 627	1455,066368	0,661971384	1,61E-08
HEATR5B	826	853	831,8857107	-0,439504827	9,11E-02	HEATR5B	479	248	343,6226712	-0,599808477	1,48E-03
HERC1	1 302	1 394	1332,109817	-0,389323259	2,41E-01	HERC1	1 039	555	751,8716439	-0,543424523	6,29E-04
HIF1A	1 873	3 329	2469,059884	0,348565942	9,63E-02	HIF1A	825	940	878,9690201	0,509898344	5,98E-04
HLA-DMA	2 881	3 494	3108,947948	-0,21410378	4,07E-01	HLA-DMA	1 432	590	940,836462	-0,962240674	3,41E-08
HLTF	670	1 294	928,2377776	0,471154662	8,13E-02	HLTF	291	376	336,333088	0,659305495	2,13E-03
HNRNPAB	5 649	7 701	6726,303942	0,068534591	9,06E-01	HNRNPAB	1 700	1 749	1698,524428	0,377896665	5,01E-03
HTT	4 409	4 599	4476,846712	-0,416808538	7,62E-02	HTT	2 203	1 186	1599,366795	-0,539440854	4,80E-05
HYAL3	162	202	178,7273342	-0,149281455	6,88E-01	HYAL3	10	0	4,168666406	-5,36401061	7,26E-03

IKZF2	3 410	6 106	4500,47459	0,353739788	1,29E-01	IKZF2	610	641	612,4247002	0,426709311	9,56E-03
IQSEC1	1 264	2 199	1656,569856	0,331013109	1,47E-01	IQSEC1	230	308	264,4712627	0,77536726	5,87E-04
IST1	2 103	3 215	2559,154867	0,133260633	5,25E-01	IST1	378	443	403,38705	0,574572058	2,26E-03
KCNMA1	313	349	326,9550905	-0,2986135	6,54E-01	KCNMA1	73	0	31,33149165	-7,304922531	1,36E-07
KLHL24	287	275	270,5491159	-0,667458131	3,04E-01	KLHL24	137	38	78,1581642	-1,475644	2,05E-05
LARS2	656	1 076	842,3325573	0,274451572	3,24E-01	LARS2	252	299	274,2334144	0,573290702	8,63E-03
LDHA	17 609	32 414	24544,15807	0,480958095	1,21E-01	LDHA	6 257	9 049	7721,944333	0,859282831	1,05E-08
LDHB	25 488	41 745	32190,51285	0,232627767	8,75E-02	LDHB	7 293	7 959	7572,504671	0,447886462	2,95E-04
LGMN	613	648	617,5975237	-0,424956221	4,48E-01	LGMN	402	156	249,6113957	-0,961116901	3,37E-04
LMBRD1	841	1 115	941,5704932	-0,103461549	8,25E-01	LMBRD1	563	258	393,3822801	-0,851657997	1,95E-03
LOXL2	26	55	36,05974738	0,491000898	6,41E-01	LOXL2	2	39	20,45564265	4,63209895	5,02E-03
LTBP1	11	15	12,51229368	-0,075866589	9,68E-01	LTBP1	0	7	3,750666673	5,50364326	8,64E-03
MACROD2	2 036	1 694	1888,709095	-0,70631213	5,33E-01	MACROD2	220	49	111,5843655	-1,690805387	2,29E-04
MARS2	738	1 347	1013,650867	0,447061058	6,67E-02	MARS2	286	348	315,2355763	0,604154762	1,25E-03
MCM10	643	1 170	886,228323	0,452970267	1,06E-01	MCM10	363	488	422,5394405	0,78153394	6,45E-06
MEAF6	1 654	1 986	1789,203435	-0,209119151	4,50E-01	MEAF6	256	126	182,091904	-0,724165467	7,15E-03
MERTK	105	216	153,9815086	0,603827633	5,12E-02	MERTK	7	28	18,59969752	2,359303144	5,93E-04
METTL14	627	962	767,3753478	0,149641424	5,35E-01	METTL14	202	237	218,8448327	0,558436971	9,42E-03
MIF	5 621	7 291	6372,31196	-0,075637155	8,30E-01	MIF	2 809	1 608	2096,220432	-0,471102755	2,66E-04
MINPP1	491	474	483,9099341	-0,51428624	1,09E-01	MINPP1	168	76	118,0871355	-0,865796266	8,33E-03
MSH6	1 468	2 351	1863,214445	0,245960716	2,87E-01	MSH6	1 206	1 379	1280,417591	0,550115589	7,13E-04
MTG2	547	899	703,9652706	0,278266594	2,48E-01	MTG2	90	163	128,4552894	1,141451461	5,00E-04
MYC	1 901	3 040	2372,091405	0,200200039	5,02E-01	MYC	1 092	1 225	1147,490668	0,468992517	4,10E-03
NAGA	1 203	1 330	1253,869915	-0,336336544	2,84E-01	NAGA	262	100	174,3660841	-1,139654286	2,41E-03
NDUFA1	3 237	3 821	3496,064443	-0,21903801	1,89E-01	NDUFA1	2 871	1 554	2096,240772	-0,553311589	2,66E-04
NDUFA7	1 188	1 612	1372,484657	-0,017447298	9,61E-01	NDUFA7	263	111	170,5184438	-0,87227645	2,79E-03
NEK7	1 298	1 382	1311,572214	-0,426135635	1,70E-01	NEK7	160	71	107,6634715	-0,81282711	4,93E-03
NQO1	716	1 021	864,7596848	0,102191701	8,50E-01	NQO1	259	330	294,910784	0,64431232	8,66E-03
NUP88	3 050	4 784	3772,852059	0,175612721	3,21E-01	NUP88	651	736	691,4637245	0,492395708	2,31E-03
PACS1	3 749	4 807	4141,095917	-0,1446106	6,11E-01	PACS1	475	241	332,2664445	-0,598828621	3,79E-03
PARP9	2 011	2 400	2137,975094	-0,258188977	4,88E-01	PARP9	781	358	524,8938644	-0,756903579	1,54E-05
PBK	921	1 350	1119,749977	0,123459326	7,21E-01	PBK	343	411	374,8398913	0,596772353	3,51E-03
PCDHGB5	50	40	45,76314214	-0,788742054	1,36E-01	PCDHGB5	2	25	14,19262801	4,150805787	2,67E-05
PCNT	834	1 548	1129,847846	0,415245293	8,80E-02	PCNT	366	454	406,9454573	0,637546937	5,14E-03
PDE12	696	930	806,4948147	-0,010974494	9,78E-01	PDE12	278	321	296,6017179	0,542353282	3,97E-03
PFAS	992	1 774	1349,715481	0,422379925	1,48E-01	PFAS	746	966	853,7948192	0,690496624	1,19E-05
PIGM	96	116	104,3954755	-0,195223162	6,59E-01	PIGM	89	35	58,29040164	-1,071822526	8,72E-03

PIGU	608	631	615,5006282	-0,433131646	1,29E-01	PIGU	164	64	108,9907128	-1,065303045	2,01E-03
PJA2	1 964	3 326	2512,126279	0,27165293	3,51E-01	PJA2	674	729	690,6386881	0,446363377	2,55E-03
PLEC	716	887	790,6342016	-0,147832772	6,28E-01	PLEC	545	292	393,7376202	-0,571699531	6,01E-03
PLXNB2	3 244	3 196	3202,903262	-0,508810121	1,26E-01	PLXNB2	1 236	506	793,8527386	-0,933017809	3,90E-05
POLA1	1 442	2 402	1856,791755	0,283339128	1,23E-01	POLA1	641	794	712,6746905	0,683259478	4,96E-04
POLD3	1 024	1 742	1344,758973	0,334623461	9,90E-02	POLD3	178	234	204,9296387	0,720234911	1,31E-03
POP1	641	1 178	888,4514254	0,471436959	7,90E-02	POP1	282	362	319,9174554	0,718648714	1,29E-03
PSME2	4 713	7 340	5921,170483	0,219425443	3,94E-01	PSME2	1 310	1 478	1394,266731	0,483059051	4,33E-03
PTK2B	3 880	4 093	3950,615143	-0,404073582	1,18E-01	PTK2B	1 238	626	876,9000067	-0,636462324	5,36E-06
RAPGEF1	3 979	4 932	4324,338685	-0,192462267	5,78E-01	RAPGEF1	554	261	372,0999538	-0,698576329	3,00E-03
RBM39	3 614	5 736	4529,641097	0,212767506	1,12E-01	RBM39	686	877	788,2200191	0,660043384	4,13E-03
RETSAT	866	924	880,9637933	-0,410359641	1,75E-01	RETSAT	230	98	157,2779237	-0,967644116	3,73E-03
RFWD3	1 859	2 832	2295,995091	0,170570022	4,98E-01	RFWD3	426	485	449,0326593	0,525114711	3,19E-03
RHBDD3	396	449	421,5982069	-0,265653451	2,79E-01	RHBDD3	48	13	28,23372024	-1,53932377	3,87E-03
RHOF	2 191	2 505	2334,260647	-0,258388944	1,08E-01	RHOF	309	146	213,7041524	-0,755594909	5,01E-03
RIF1	1 292	2 088	1642,475188	0,249581999	2,25E-01	RIF1	810	958	880,141501	0,599365853	7,77E-04
RIPK3	233	206	222,0955335	-0,623563664	6,48E-02	RIPK3	90	28	51,51268415	-1,292182468	5,99E-03
RNF213	3 531	7 048	5018,852035	0,53861914	5,56E-02	RNF213	3 339	4 264	3751,525347	0,73162453	1,91E-06
RPL31	29 579	32 664	30926,66804	-0,323551118	6,79E-02	RPL31	1 027	211	547,1863698	-1,899041243	2,18E-07
RPRD1B	797	1 448	1061,200966	0,373898635	1,50E-01	RPRD1B	206	259	228,3319924	0,684101813	2,17E-03
S100A13	74	162	110,8677624	0,645842089	1,21E-01	S100A13	15	47	31,47753486	1,909960454	1,35E-03
S100A2	15	29	21,29210117	0,578535526	5,54E-01	S100A2	3	47	24,91623906	4,05165794	1,52E-03
SDE2	239	451	326,2649915	0,433462836	1,24E-01	SDE2	146	197	169,0750135	0,780006765	8,76E-04
SEMA7A	2 899	3 249	3028,724626	-0,318533169	4,71E-01	SEMA7A	1 062	469	723,9854899	-0,883692658	7,41E-03
SERINC1	1 703	2 132	1856,657744	-0,185162913	6,32E-01	SERINC1	736	366	530,3159903	-0,760126736	8,98E-03
SERINC3	1 930	2 381	2084,31362	-0,213270573	6,25E-01	SERINC3	483	215	337,3229431	-0,9229815	2,41E-03
SIDT2	668	684	668,917049	-0,454960024	1,95E-01	SIDT2	138	49	85,06651755	-1,11541969	6,02E-03
SLC1A4	3 043	3 184	3021,050943	-0,496915296	3,28E-01	SLC1A4	717	320	496,9663019	-0,914031279	9,16E-03
SLC4A5	413	423	411,5591948	-0,489841352	3,12E-01	SLC4A5	24	1	12,172343	-4,976028588	2,87E-03
SMC1A	2 548	4 089	3223,781141	0,236515145	4,29E-01	SMC1A	1 134	1 378	1251,85625	0,572919619	4,95E-03
SMDT1	2 499	3 250	2804,465838	-0,103488501	7,23E-01	SMDT1	269	139	191,6741666	-0,599184234	8,74E-03
SPCS1	5 937	7 308	6471,491758	-0,190899957	4,21E-01	SPCS1	1 285	603	883,517679	-0,724077948	3,40E-03
SPG11	1 822	2 502	2073,291703	-0,055047553	9,04E-01	SPG11	1 068	624	807,3118361	-0,43099413	8,25E-03
SPN	2 782	3 027	2858,864669	-0,374031484	3,38E-01	SPN	2 011	1 008	1421,154172	-0,690180763	9,44E-03
SRA1	1 746	2 679	2149,98668	0,163880931	3,34E-01	SRA1	275	366	321,0549352	0,718288501	5,26E-04
STRA6	47	37	42,33322392	-0,827234053	1,17E-01	STRA6	9	0	4,306238614	-5,400940321	6,51E-03
STX11	1 088	1 895	1413,051225	0,311739311	1,35E-01	STX11	118	161	138,0267404	0,774991559	8,86E-03

SUSD1	413	444	419,2673197	-0,410044239	1,94E-01	SUSD1	124	45	76,0765499	-1,072234494	3,43E-03
SVIL	177	282	222,1274252	0,219817938	4,66E-01	SVIL	1	29	16,4589287	4,902220423	6,27E-06
TCERG1	1 951	2 955	2421,139225	0,182786459	5,33E-01	TCERG1	476	554	514,2333847	0,551581094	1,55E-03
TEP1	1 339	1 465	1366,095803	-0,398228888	2,99E-01	TEP1	766	416	563,1167844	-0,564265864	6,49E-04
TLE5	14 341	19 699	16706,18228	0,008815613	9,81E-01	TLE5	853	468	620,9553397	-0,522829384	3,13E-03
TMEM138	677	666	682,0348667	-0,442130679	9,50E-02	TMEM138	86	28	53,05478688	-1,335935742	6,49E-04
TMEM205	614	622	615,1874631	-0,460020976	7,05E-02	TMEM205	247	98	163,0780022	-1,050584547	3,40E-04
TMPO	4 315	6 270	5182,639504	0,097231487	7,02E-01	TMPO	1 168	1 273	1205,390914	0,457473798	4,00E-03
TNFRSF13C	2 504	2 572	2492,864923	-0,476126544	9,17E-02	TNFRSF13C	219	80	137,2686768	-1,115754274	2,78E-04
TPI1	6 263	8 553	7338,947681	0,023097567	9,55E-01	TPI1	3 549	4 046	3760,705209	0,51811302	1,64E-03
TRIM5	2 896	4 997	3751,298873	0,304415001	1,47E-01	TRIM5	596	647	604,4475463	0,4868595	7,43E-03
UBE4A	1 538	1 598	1571,139959	-0,398826225	5,69E-02	UBE4A	389	184	273,7848424	-0,778602098	4,36E-03
UCP2	5 591	6 663	6020,267465	-0,225954431	3,45E-01	UCP2	1 194	441	714,6153375	-0,979749329	2,90E-03
USP1	2 461	4 084	3135,6658	0,255287245	1,82E-01	USP1	457	521	487,3968485	0,524936176	3,79E-03
USP39	1 500	2 173	1801,972878	0,094684584	7,36E-01	USP39	332	392	359,6583785	0,553189085	4,67E-03
WEE1	706	974	818,9064297	-0,001298558	9,98E-01	WEE1	198	260	229,3256233	0,734721845	3,04E-03
WSB1	1 604	2 442	1947,324864	0,128156604	5,31E-01	WSB1	282	366	321,4200857	0,762331867	2,78E-04
XYLT1	342	328	332,8957612	-0,559419694	1,59E-01	XYLT1	51	5	26,30997271	-2,967822013	3,39E-05
YPEL5	1 346	1 522	1377,088441	-0,376065642	4,71E-01	YPEL5	333	135	212,4646316	-0,933408182	9,59E-04
YTHDC2	635	978	781,5279183	0,16401992	4,66E-01	YTHDC2	294	369	328,3014177	0,692730624	1,87E-04
ZBTB38	3 968	4 539	4116,33811	-0,346949057	3,88E-01	ZBTB38	697	337	485,6251766	-0,709856372	4,26E-06
ZDHHC24	379	426	391,3087353	-0,358672317	4,42E-01	ZDHHC24	93	20	46,7223836	-1,725846273	5,43E-03
ZMAT3	5 593	6 100	5773,510509	-0,354485915	1,23E-01	ZMAT3	567	280	395,3146577	-0,658744415	5,20E-03

Appendix 2

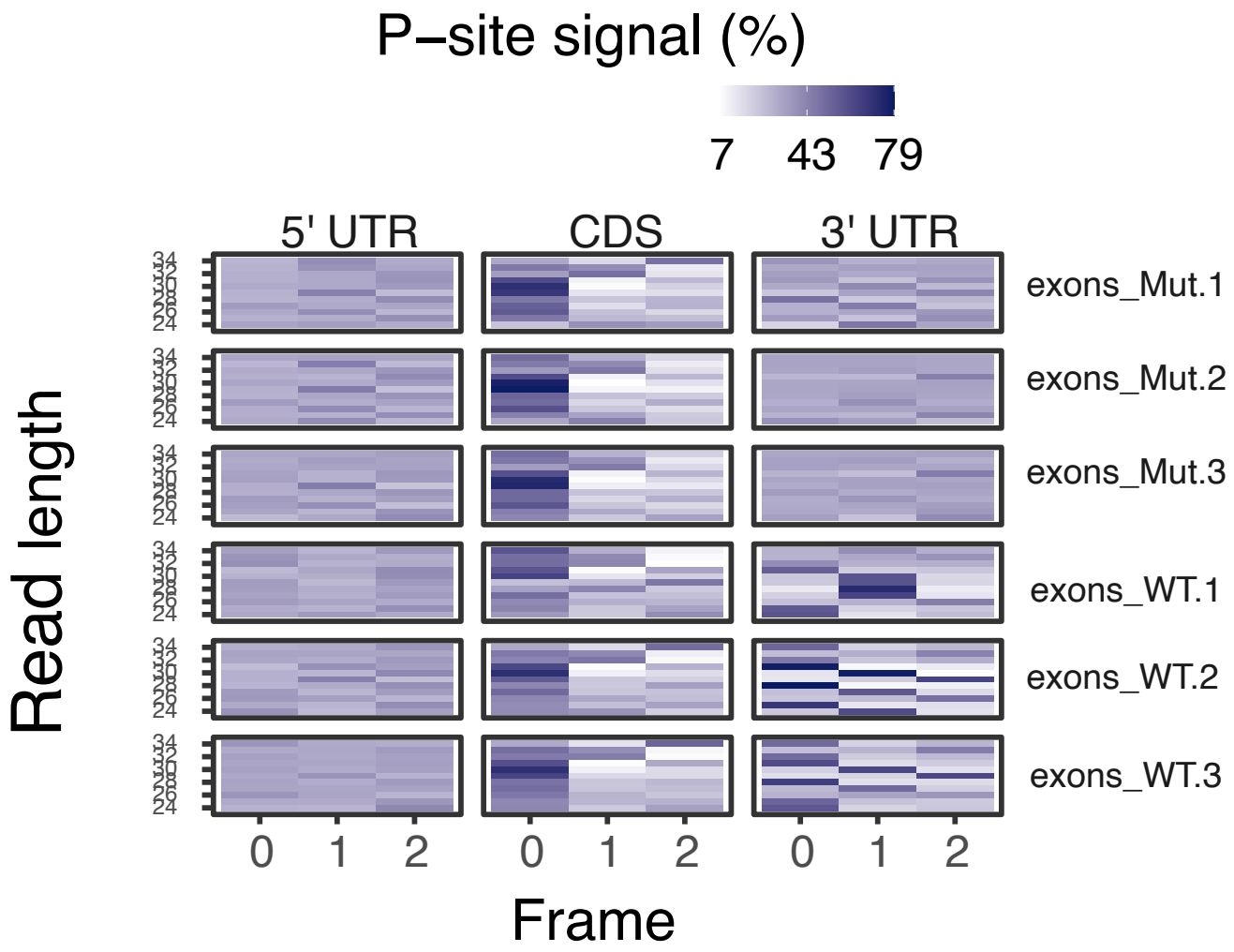

Ribosome Profiling on three biological samples of WT and FTSJ1 mutated LCLs
CDS and UTR coverage of 24-34 reads

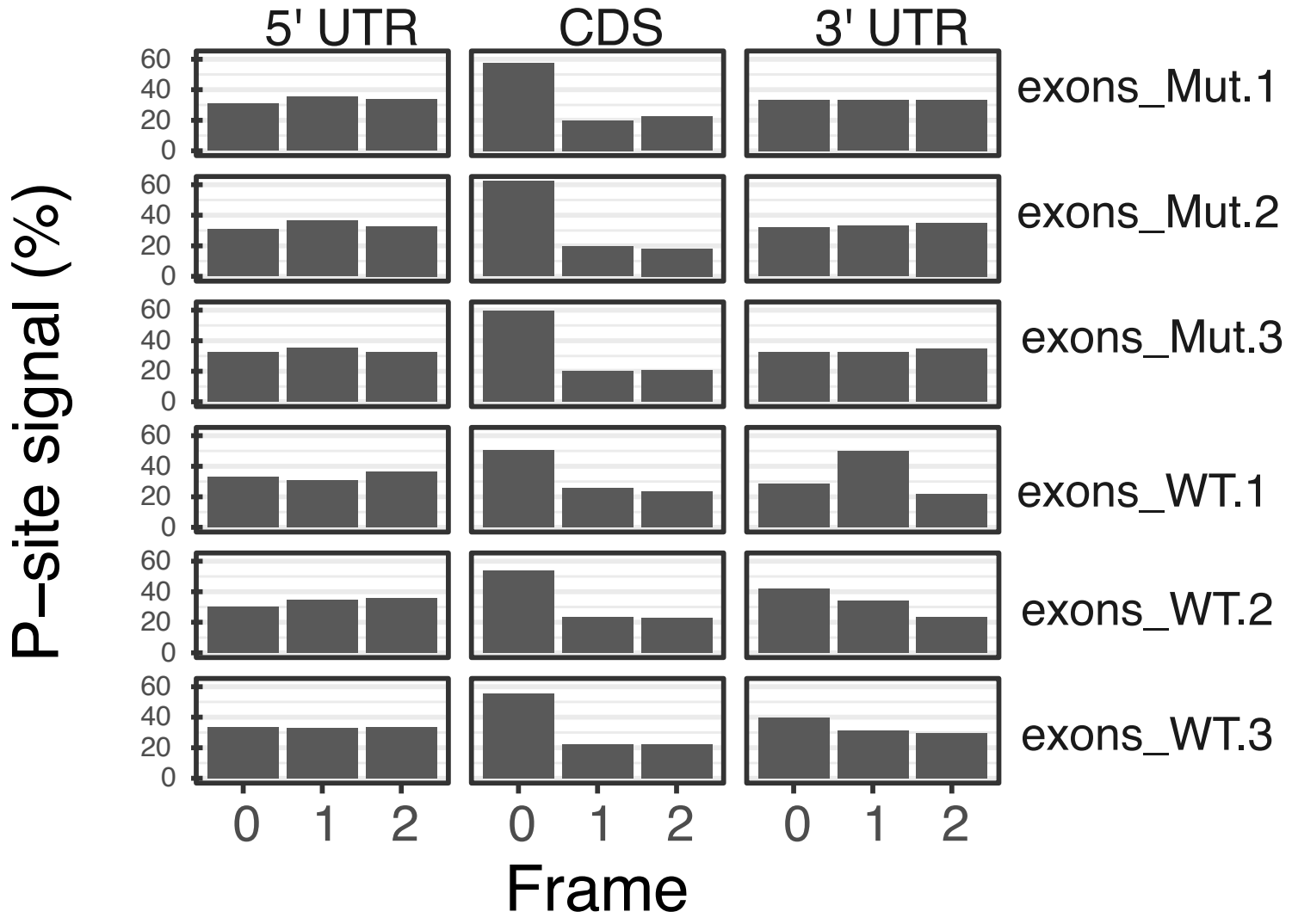

Ribosome Profiling on three biological samples of WT and FTSJ1 mutated LCLs
CDS and UTR coverage. CDS reads shows codon periodicity